

UNIVERSITY OF KENT AT CANTERBURY

A KINETIC AND THERMODYNAMIC INVESTIGATION OF

SOME AQUEOUS DYE-SURFACTANT SYSTEMS

*by*

*Neal Charles White*

*A thesis submitted in partial fulfilment of the  
requirement for the degree of Doctor of Philosophy*

Faculty of Natural Sciences  
University Chemical Laboratories

Canterbury 1972-75

## ACKNOWLEDGEMENTS

I wish to thank my supervisor, Dr. Brian H. Robinson, for his guidance and help throughout the research programme. His patient reading and commenting on the text are very much appreciated. I should also like to thank Dr. Alan D. James for many helpful discussions.

I am grateful to the members of the mechanical and electronic workshops without whose skill this project would not have been possible.

My thanks to Miss D. Paine for her excellent typing of this thesis and to Mr. A.J. Fassam who took the photographs shown in Chapter 2.

Finally, my thanks are due to the Science Research Council for financial support during the period 1972-75 and to the University of Kent for the facilities of the laboratories.

## ABSTRACT

A Joule heating temperature-jump relaxation spectrometer has been designed and constructed. The fastest heating time of the instrument is approximately  $0.2\mu\text{s}$ , which enables reactions with half lives greater than  $0.5\mu\text{s}$  to be followed. To ensure maximum flexibility three easily interchangeable capacitors are fitted ( $0.01$ ,  $0.02$  and  $0.05\mu\text{F}$ ). The maximum temperature rise ( $0.05\mu\text{F}$  capacitor,  $40\text{kV}$  discharge) is  $6.5\text{K}$ . Concentration changes may be monitored by observing changes in fluorescence, absorbance and light-scattering. An existing small volume stopped-flow instrument has been modified to enable the observation of changes in light-scattering and fluorescence. A data capture system has been developed to facilitate the rapid and accurate determination of kinetic parameters.

The thermodynamics and kinetics of the interaction between acridine-type dyes and anionic surfactants have been investigated. The dyes used have distinctly different absorption and fluorescence characteristics below and above the CMC. They may, therefore, be used to determine the CMC of anionic surfactants.

Below the CMC of the surfactant, a time-dependent association of dye and surfactant is observed which leads to the growth of large aggregates. The strength of this interaction increases sharply with increasing hydrocarbon chain-length of the surfactant, and with the tendency of the dye to self-associate in aqueous solution. A mutually induced aggregation mechanism is proposed.

Above the CMC of the surfactant the dyes are absorbed by the micelles. Evidence is presented which establishes that the dyes are incorporated into the hydrocarbon region (palisade layer) of the micelle, and not simply held at the surface by electrostatic forces.

The kinetics of dye absorption have been studied by the stopped-flow method utilising fluorescence and absorbance detection. The rate of absorption for a given dye reaches a limiting value for high surfactant concentrations i.e. for a micellar surfactant dye ratio (M/D) greater than  $\sim 10^2$ . The limiting rate of absorption is found to decrease as the hydrocarbon chain length of the surfactant increases. The limiting rate is found to be dependent to some extent on ionic strength, pH, and co-solvent e.g. methanol, but is little affected by small additions (0.01 mole fraction) of potential impurities e.g. dodecanol. For a given micelle the process of dye absorption is very sensitive to the geometric shape of the acridine dyes, subtle structural changes resulting in large kinetic effects. Dyes having the same geometry are found to be absorbed at very similar rates.

The mechanism proposed for the absorption is a two-step process involving a very rapid (diffusion-controlled) absorption of the dye onto the micelle surface followed by a slow absorption or "intercalation" into an energetically more favourable site in the palisade layer of the micelle.

## CONTENTS

ABSTRACT	I
<u>CHAPTER 1 - GENERAL INTRODUCTION</u>	1
1.1 Classification of Colloid Systems.	1
1.2 General Properties of Micellar Systems.	1
1.3 Thermodynamics of the Monomer-Micelle Equilibrium.	6
1.3.1 Introduction.	6
1.3.2 The Multiple-Equilibrium Approach.	7
1.3.3 The Phase-Separation Approach.	8
1.3.4 Contributions to the Overall Free-Energy of Micelle Formation.	10
1.3.5 The Hydrophobic Contribution.	10
1.3.6 The Electrostatic Contribution.	14
1.3.7 The Enthalpy and Entropy of Micelle Formation.	16
1.4 Dynamics of Micelle Processes.	20
1.4.1 Introduction.	20
1.4.2 The Fast Relaxation Process (I).	21
1.4.3 The Slow Relaxation Process (II) and Overall Kinetic Models.	26
1.5 Uses and Industrial Importance of Micellar Systems.	31
<u>CHAPTER 2 - DESCRIPTION OF APPARATUS AND GENERAL EXPERIMENTAL         PROCEDURE</u>	37
2.1 Introduction.	37
2.2 Abbreviations.	37
2.3 Materials.	37

2.4	Purification of Materials.	37
2.4.1	Acridine Orange.	37
2.4.2	Acriflavine.	42
2.4.3	Atebrine.	42
2.4.4	Malachite Green.	42
2.4.5	Methylene Blue.	42
2.4.6	Proflavine.	43
2.4.7	Pyronine G.	43
2.4.8	Rhodamine 6G.	43
2.4.9	Surfactants.	44
2.5	Preparation of Solutions.	45
2.6	Spectrophotometers.	45
2.7	Measurement of pH.	46
2.8	Description of the Temperature-Jump Apparatus.	46
2.8.1	Introduction.	46
2.8.2	High Voltage Discharge Unit.	49
2.8.3	Optical Arrangement.	52
2.8.4	The Temperature-Jump Cell.	54
2.8.5	Photomultiplier Heads.	56
2.8.6	Photometric Control Unit.	58
2.8.7	Absorption Measurements.	59
2.8.8	Fluorescence Measurements.	64
2.8.9	Determination of the Absorption Path-Length ( $l_{TS}$ ) and the Temperature-rise of the Cell.	65
2.8.10	Evaluation of the Performance of the Temperature-Jump Instrument.	71
2.9	Description of the Stopped-Flow Instrument.	77
2.9.1	Introduction.	77
2.9.2	Modifications.	78

2.9.3	Determination of the Effective Path-Length of the Quartz Observation Chamber.	80
2.9.4	The Relationship between Absorption Photomultiplier Voltage and Concentration Changes.	83
2.9.5	The Relationship between Emission Photomultiplier Voltage and Concentration Changes.	86
2.9.6	Determination of the "Dead-time" of the Stopped-Flow Instrument.	89
2.9.7	Determination of Mixing Efficiency.	90
2.10	Derivation of Relaxation Expressions.	91
2.10.1	Single-Step Association-Dissociation Equilibrium.	91
2.10.2	Consecutive Multi-Step Equilibrium.	93
2.10.3	Relaxation Amplitudes.	97
2.11	The Stopped-Flow Method.	99
2.12	The Transient Recorder and Paper Tape Punch.	100
2.12.1	Introduction.	100
2.12.2	The Transient Recorder and Paper Tape Punch.	100
 <u>CHAPTER 3 - A COOPERATIVE MODEL FOR MICELLE FORMATION</u>		107
3.1	Introduction.	107
3.2	Step-wise Self-association Models.	109
3.2.1	Non-cooperative Step-wise Self-association.	110
3.2.2	Step-wise Association Model with Slowly Varying Equilibrium Constants.	111
3.2.3	The Infinite Cooperativity Model of Kresheck et al.	115
3.2.4	General Cooperative Model for Micelle Formation.	117
3.2.5	Mathematical Treatment of the Cooperative Model.	121

<u>CHAPTER 4 - DETERMINATION OF CRITICAL MICELLE CONCENTRATIONS BY</u>	
<u>THE DYE-PROBE TECHNIQUE</u>	
4.1	Introduction. 138
4.2	Spectrophotometric Determinations of CMC's. 139
4.3	Fluorimetric Determination of CMC's. 154
4.4	Determination of the CMC of Anionic Surfactants by Non-Acridine Dyes. 163
4.5	General Conclusions. 166
 <u>CHAPTER 5 - KINETIC INVESTIGATION OF THE INTERACTION BETWEEN</u>	
<u>ACRIDINE DYES AND ANIONIC SURFACTANTS BELOW THE</u>	
<u>CRITICAL MICELLE CONCENTRATION</u>	
5.1	Introduction. 171
5.2	Experimental. 173
5.2.1	Stopped-flow Kinetics. 173
5.2.2	Manual Mix Kinetics. 173
5.2.3	Temperature-Jump Kinetics. 174
5.3	Results. 174
5.3.1	Effect of Dye Concentration and Structure. 174
5.3.2	Effect of Surfactant Concentration and Chain-Length. 175
5.4	Mechanism. 185
5.4.1	The Fast Process I 185
5.4.2	The Slow Aging Process and Dissolution Kinetics. 193
5.5	Temperature-Jump Investigation of Pre-CMC Dye-Surfactant Solutions. 195
5.5.1	Results. 195
5.5.2	Discussion. 198

<u>CHAPTER 6 - THE INTERACTION OF CATIONIC DYES WITH ANIONIC MICELLES</u>	202
6.1 Introduction	202
6.2 Experimental Conditions.	206
6.2.1 Direct Interaction of Dye and Micelle above the CMC.	206
6.2.2 Ionic-Strength Jump Experiments.	207
6.2.3 Temperature-Jump Experiments.	207
6.3 The Interaction of Dye with Sodium-n-alkyl Sulphate Micelles.	208
6.3.1 The Effect of Variation in Dye Structure.	208
6.3.2 The Effect of pH.	216
6.3.3 The Influence of Ionic Strength.	219
6.3.4 Addition of Cosolvent and Potential Impurities.	221
6.3.5 Variation in Surfactant Chain-Length and Head Group.	226
6.3.6 Discussion of the Activation Parameters.	232
6.3.7 Proposed Mechanism of Dye Absorption.	242
6.3.8 Interaction of Non-Acridine Dyes with Micelles.	249
6.4 Ionic Strength-Jump.	251
6.4.1 Results.	251
6.4.2 Mechanism.	255
6.4.2.1 Absorption of a Dye-Surfactant Monomer.	256
6.4.2.2 Dye-induced Micelle Formation.	257
6.4.3 Dye Concentration Dependence	260
6.5 Temperature-Jump Experiments.	262
6.5.1 Results.	262
6.5.2 Discussion.	266
6.6 General Conclusions and Suggestions for Further Work.	266
<u>APPENDIX I</u>	AII
<u>APPENDIX II</u>	AIII

CHAPTER 1

GENERAL INTRODUCTION

## CHAPTER 1

### GENERAL INTRODUCTION

#### 1.1 Classification of Colloid Systems

Colloid science is concerned with systems which contain components which have dimensions within the range 1 to 100nm, i.e. systems containing large molecules e.g. synthetic and biopolymers, small particles e.g. metal sols, or aggregate species e.g. micelles.

Colloids find many applications in industry: plastics, rubber, paint, detergents, foodstuffs, drugs and heterogeneous catalysis are a few examples. The vast range of industrial processes which are based on colloid systems emphasise the importance of a sound practical and theoretical understanding of colloid phenomena.

Colloidal systems may be grouped into three general classifications:

(1) Colloidal dispersions: These are thermodynamically unstable owing to their high surface free energy and are irreversible systems in the sense that they are not easily reconstituted after phase separation.

(2) True solutions of macromolecules: These are thermodynamically stable and reversible in the sense that they are easily reconstituted after separation of solute from solvent.

(3) Association colloids (Micelles), which are thermodynamically stable.

This thesis will be concerned exclusively with the group three colloids (micelles in aqueous media).

#### 1.2 General Properties of Micellar Systems

The characteristic property which distinguishes micelles

from other colloidal systems is that the associated units of the former, the micelles, are in dynamic association-dissociation equilibrium with the monomer units. The monomers are molecules usually of low molecular weight (<500), which exhibit a property known as amphipathy. This term was introduced by G.S. Hartley<sup>(1)</sup> to describe the sympathy of one part of the molecule for water, hydrophilicity, and the antipathy of another part for water, hydrophobicity. Molecules which show this property are known as amphiphiles, surfactants or tensides. Throughout this thesis the term surfactant will be used. The hydrophilic part, or head-group, of the molecule may be ionic, zwitterionic or non-ionic. The hydrophobic part, or tail-group, is usually a hydrocarbon chain. Examples are shown in figure 1.2.1.

The physical properties of very dilute aqueous surfactant solutions do not differ significantly from those of non-surfactants, in that close to ideal behaviour is observed. As the concentration of surfactant is increased, a dramatic and abrupt change in various physical properties is observed. A diagrammatic representation depicting changes in several physical properties for one ionic surfactant (sodium dodecyl sulphate, SDS) is shown in figure 1.2.2. The properties plotted are those of refractive index ( $\eta$ ), density ( $\rho$ ), turbidity ( $\tau$ ), molar conductivity ( $\lambda$ ), osmotic pressure ( $\pi$ ) and surface tension ( $\sigma$ ). These sudden changes in physical properties have been attributed to the reversible association of typically 20 to 100 monomers to form molecular aggregates, micelles. For ionic surfactant systems, the micelle surface charge is partially neutralised by counter ion binding. The concentration at which the abrupt changes occur, actually a small but finite range of surfactant concentration, is called the Critical Micelle Concentration, CMC. Figure 1.2.1 contains CMC values for a number of different classes of surfactants in water. It must be noted that the

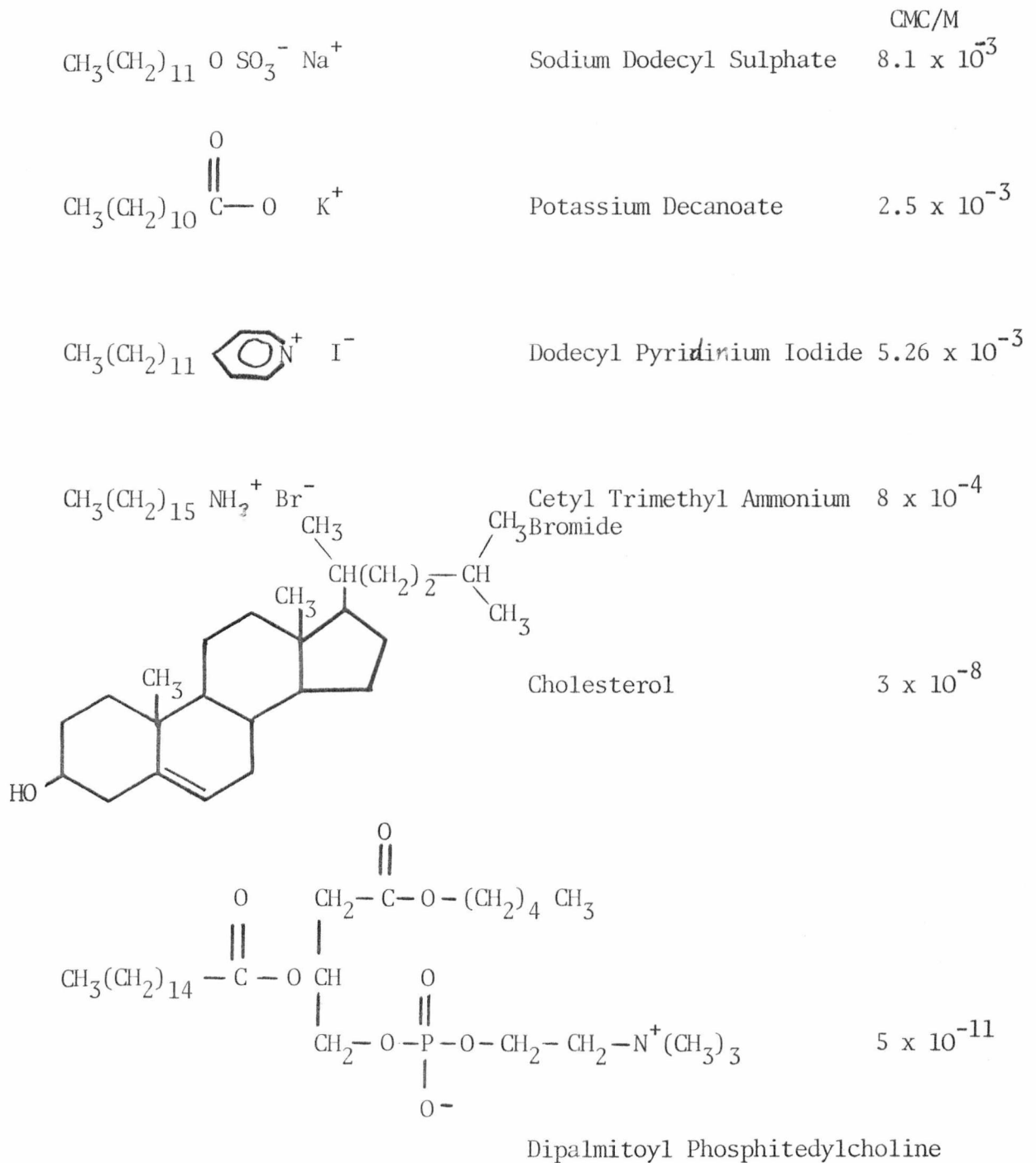


FIGURE 1.2.1

SOME TYPICAL SURFACTANTS AND THEIR CMC'S IN AQUEOUS SOLUTION

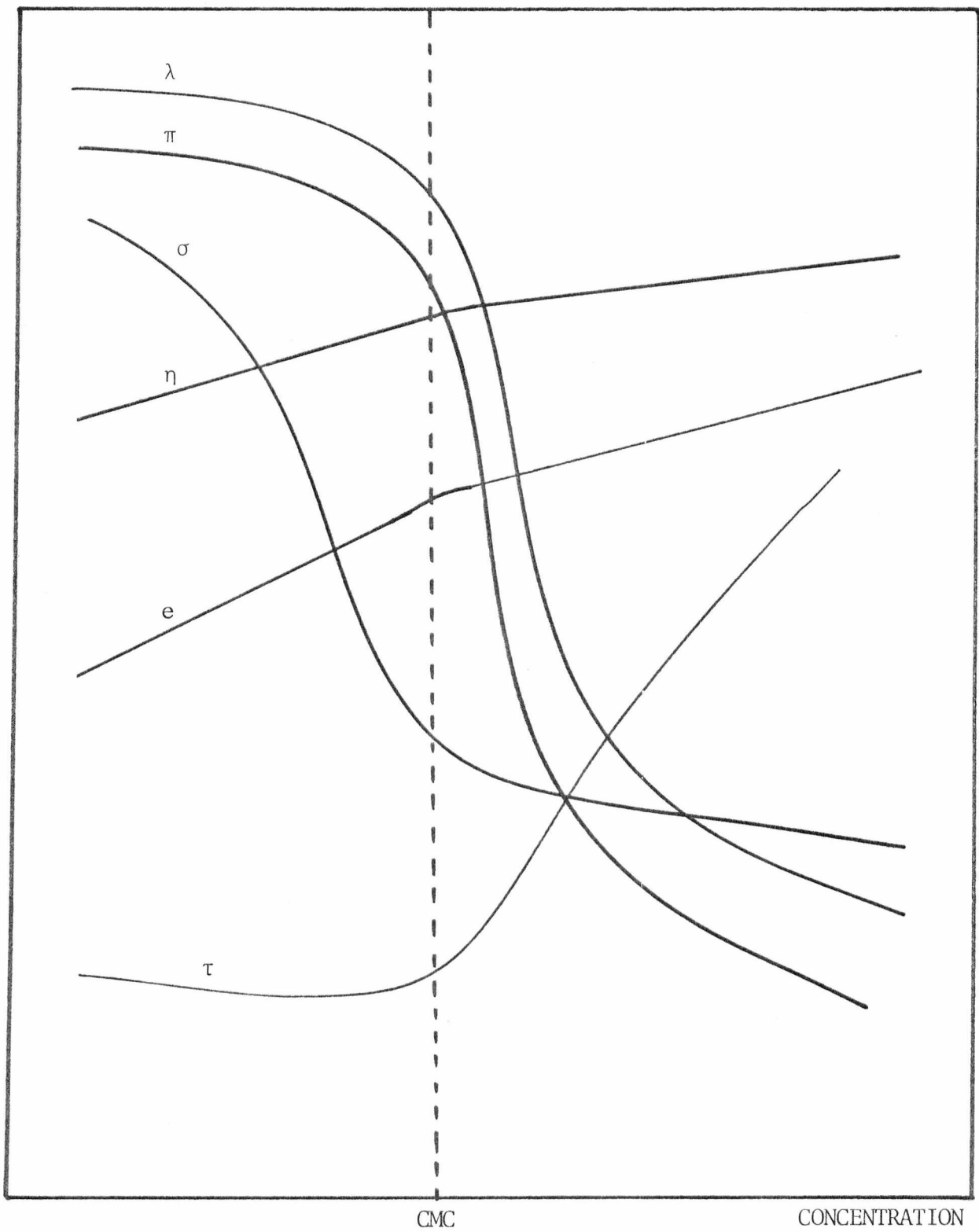


FIGURE 1.2.2

TYPICAL VARIATIONS IN THE PHYSICAL PROPERTIES OF SURFACTANTS SHOWING  
THE CMC

CMC values cover an extremely wide range of concentrations depending on the nature of the surfactant. The physical properties mentioned above and many others may be used to determine the CMCs<sup>(2)</sup> of surfactants and to provide information regarding the size and structure of the micelles.

The interpretation of the abrupt changes in physical properties has led to a fairly detailed structural picture of the micelle. For many systems the micelle appears to be approximately spherical of 1-3nm radius, with the hydrophilic head-groups at the surface. The hydrocarbon chains are usually thought to be fairly flexible, so that the hydrocarbon micelle core is effectively a small volume of liquid hydrocarbon. However, the viscosity of the hydrocarbon micelle interior has been found experimentally to be greater than for pure liquid<sup>(5)</sup> hydrocarbon of the same chain-length. This has been attributed to the high internal pressure of the micelle core, which leads to a severe restriction on the mobility of the hydrocarbon chains. Ionic micelles have large surface potentials, for SDS it is -132mV<sup>(4)</sup>, and generally 50-70% of the counter ions are bound within the Stern layer. A diagrammatic representation of a micelle is shown in figure 1.2.3.

The CMCs for a given class of surfactants e.g. sodium n-alkyl sulphates  $C_nH_{2n+1}OSO_3^- Na^+$ , are found to decrease as the hydrocarbon chain-length is increased, while the head-group type and counter ion (providing it has the same charge) do not affect the CMC to any great extent<sup>(5)</sup>. The amount of added electrolyte also drastically changes the CMC, which decreases as the added ionic strength is increased<sup>(6)</sup>. The mean aggregation number,  $z$ , also increases with added ionic strength<sup>(6)</sup>. The variation in the CMC for a given homologous series of surfactants with those factors mentioned above (and many others) has been extensively documented<sup>(5)</sup>. Some of the thermodynamic factors which determine the

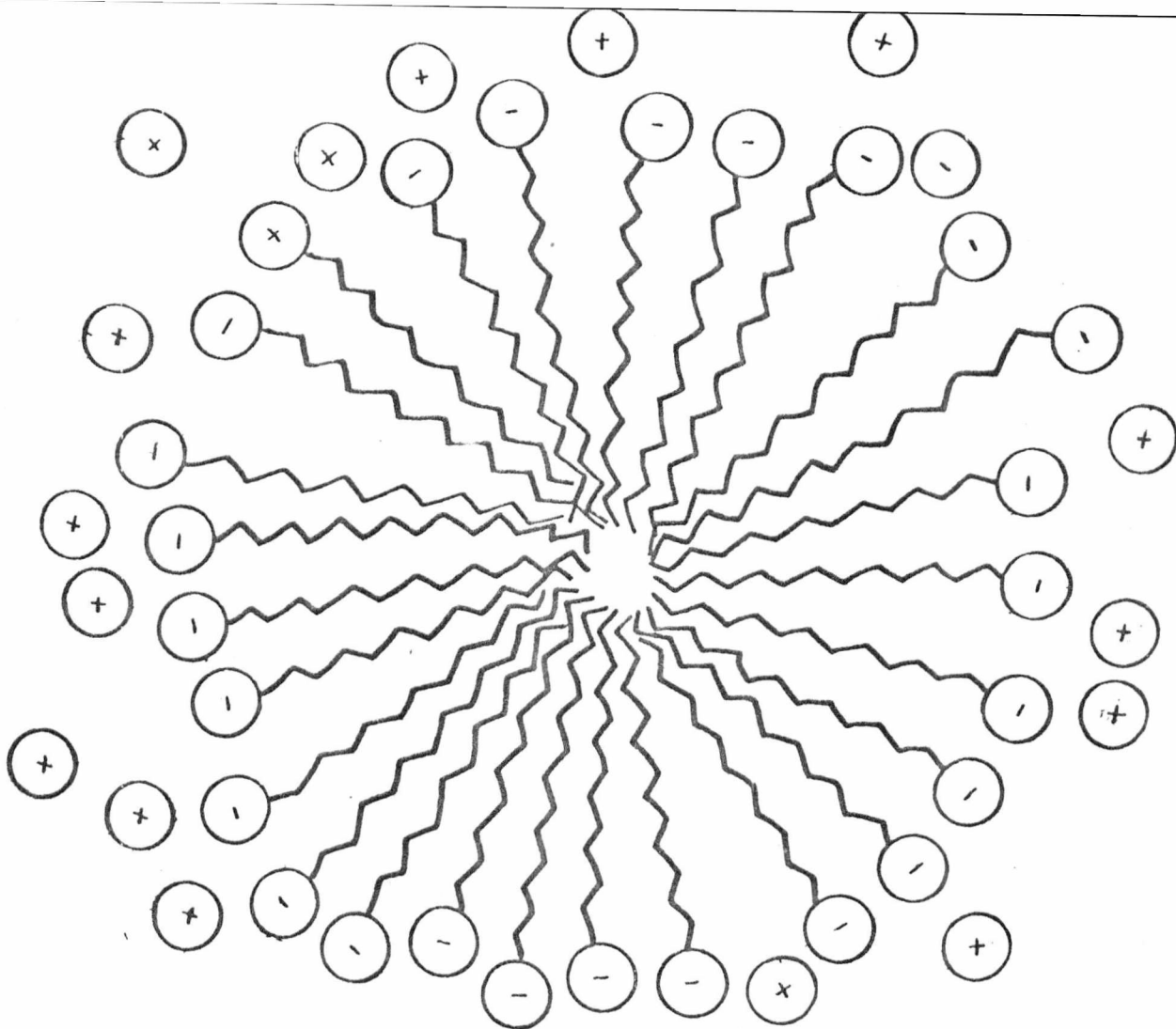


FIGURE 1.2.3

SCHEMATIC DIAGRAM OF A MICELLE

CMC values are considered in the following section.

1.3 Thermodynamics of the Monomer-Micelle Equilibrium

1.3.1 Introduction

There are two main approaches which may be used to interpret the thermodynamics of the monomer-micelle equilibrium. One description of the process is in terms of a dynamic equilibrium<sup>(7)</sup> between monomers, (A) and micelles, (M) based on the Law of Mass Action. The other approach considers micelle formation, or, micellisation, in terms of a phase-separation model<sup>(8)</sup>. It will be shown that both approaches oversimplify the real situation, since assumptions have to be made regarding the size distribution of the micelles. Hall and Pethica<sup>(9)</sup> have attempted to overcome this drawback by the application of Hills<sup>(10)</sup>

small system thermodynamics to micellar systems. In this approach each micelle is regarded as an independent small system in equilibrium with monomer surfactant. This last model is discussed in considerable detail elsewhere<sup>(9)</sup>.

### 1.3.2 The Multiple-Equilibrium Approach<sup>(7,9,10)</sup>

A simplified multiple-equilibrium approach can provide a simple, thermodynamic formulation of micellisation which is rigorous for monodisperse systems. For such a monodisperse micelle (M) in equilibrium with monomers (A) we have:



neglecting any effect of counterion binding.

The overall molar equilibrium constant for micelle formation ( $K'_m$ ), neglecting activity coefficients, is expressed by:

$$K' = \frac{[M_z]}{[A]^z} \quad (1.3.2.2)$$

It is useful to express concentrations in mole fraction units so that the free energies obtained are in unitary units<sup>(11)</sup>. Let  $x_A$  represent the mole fraction of monomer in bulk solution and  $x_m$  the mole fraction of surfactant monomer contained in each micelle. Hence,

$$K = \frac{x_m}{z(x_A)^z} \quad (1.3.2.3)$$

Thermodynamic calculations based on equation (1.3.2.3) are now straightforward.  $\Delta G_m^0$ , the free energy of transfer of one monomer to the micellar state is given by

$$z\Delta G_m^0 = -RT \ln K \quad (1.3.2.4)$$

The equation for representing micelle formation then becomes

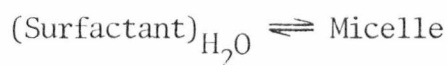
$$\ln x_m = -\frac{z\Delta G_m^0}{RT} + z \ln x_A + \ln z \quad (1.3.2.5)$$

Throughout thermodynamic ideality is assumed, but this is not a serious limitation. Any non-ideality of the monomer is corrected for by replacing the mole fraction  $x_A$ , by the activity. The ideality of the micellar species is not assumed unless  $K$  or  $\Delta G_m^0$  are held constant and independent of all variables except  $z$ . In fact,  $\Delta G_m^0$  will be a function of many variables such as ionic strength. For the rigorous case,  $\Delta G_m^0$  will depend on the micelle aggregation number, and for a polydisperse system the thermodynamics will be much more complex. Since most calculations are performed at low micellar concentrations the effect of inter-micelle interactions will be small. A concentration dependent term could be introduced to account for such interactions.

### 1.3.3 The Phase-Separation Approach<sup>(8)</sup>

Micelles, in this treatment, are considered to be a separate phase, the phase-separation occurring at the CMC.

The process may be represented in the following way:



The micelle is then a separate phase and has an activity of 1. The equilibrium constant for the formation of the separate micelle phase is given by:

$$K_m = [\text{Surfactant}]_{\text{H}_2\text{O}} \quad (1.3.3.1)$$

$$K_m = \text{CMC} \quad (1.3.3.2)$$

Neglecting all effects due to counterion binding the thermodynamic parameters  $\Delta G_m^0$  and  $\Delta H_m^0$  are given by

$$\Delta G_m^0 = -RT \ln \text{CMC} \quad (1.3.3.3)$$

$$\text{and } \Delta H_m^0 = \frac{RT^2 d \ln \text{CMC}}{dT} \quad (1.3.3.4)$$

The phase-separation approach is not acceptable on experimental grounds, since the CMC is not a discontinuity but occurs over a small but finite range of concentrations. Also, micelles are generally small, certainly smaller than many enzymes and so do not constitute a true phase.

The fundamental difference between the multiple-equilibrium and phase-separation approaches is that the former model states that the monomer activity must increase (however slowly) above the CMC and in the phase-separation approach it must remain constant. Surface tension<sup>(12)</sup> and dialysis<sup>(13)</sup> measurements on extremely pure surfactants have shown that an increase in monomer activity does in fact occur above the CMC.

The phase-separation description of micelle formation therefore seems inappropriate, although its intrinsic simplicity has wide appeal. Any realistic thermodynamic description of micelle formation should, therefore, be based on a multiple-equilibrium scheme, and the implications of this model will be considered further in Chapter 3.

#### 1.3.4 Contributions to the Overall Free Energy of Micelle Formation

When considering ionic (e.g. sodium n-alkyl sulphate) surfactants, it is necessary to separate the overall free energy of micellisation, ( $\Delta G_m^0$ ), into the negative contribution arising from the hydrophobic interaction ( $\Delta G_{\text{hyd}}^0$ ), and the positive contribution arising from the repulsive Coulombic potential associated with the charged head-groups ( $\Delta G_{\text{el}}^0$ ).

$$\Delta G_m^0 = \Delta G_{\text{hyd}}^0 + \Delta G_{\text{el}}^0 \quad (1.3.4.1)$$

#### 1.3.5 The Hydrophobic Contribution

A factor of fundamental importance in the estimation of  $\Delta G_{\text{hyd}}^0$  is the extent to which water penetrates the micelle. It is possible to estimate this unfavourable contribution to micelle formation from a consideration of the possible hydrocarbon chain surface area which is in contact with water. Calculations based on a model in which the hydrocarbon chains are closely packed, perpendicular to the core surface and in an infinite bilayer, will result in zero contact area between the hydrocarbon chains and water. A surface area per chain (S) of  $0.2\text{nm}^2$  is determined<sup>(14,15)</sup>. Obviously, this is an unrealistic model, but it represents the lowest limit for the value of S.

Further theoretical calculations based on either spherical or ellipsoidal micelles provide a better estimate of S<sup>(14,15)</sup>. The volume and surface area of spherical or ellipsoidal micelles is easily calculated. The radius, r, or minor axis,  $b_0$ , is equal to the extended chain length,  $l_{\text{max}}$ , of the monomer. The volume of the alkyl chain is easily calculated from an empirical relationship derived from the X-ray data of Reiss-Hlusson et al<sup>(16)</sup>. From the volume of a single alkyl chain and the volume of a micelle consisting of surfactants of the same

chain length,  $n$ , the maximum aggregation number,  $z$ , and the surface area per chain,  $S$ , can be found.

The volume, surface area and maximum aggregation number will depend on the chain-length, for example if  $n=12$  the maximum value of  $z$  for a spherical micelle is 56. Any estimate which allows for water penetration will reduce  $n$  to an effective chain length ( $n'$ ) and this will drastically reduce the maximum aggregation number, for example if  $n'=10$ ,  $z$  will have a maximum value of only 40. The experimental determinations of  $z$  are much larger, but the introduction of slight elliptical character to the micelle greatly increases the maximum values of  $z$ . Table 1.3.5.1.

It can be seen from table 1.3.5.1 that for ellipsoidal micelles the ratio of semi-major ( $a_0$ ) to semi-minor ( $b_0$ ) axes has a small effect on  $S$ , and the choice of  $n$  is by far the most critical factor. It is possible to obtain values of  $S$  from the experimental determination of the aggregation number only.  $S$  is found to decrease with increasing aggregation number and tends to a limiting value of  $\sim 0.45\text{nm}^2$  which corresponds to the surface area per chain of cylindrical micelles.

Table 1.3.4.1 shows that the values of  $S$  calculated from the spherical and ellipsoidal micelle models are much greater than the theoretical value for close-packed hydrocarbon chains, and indicates the possibility for some water penetration between the hydrocarbon chains. Direct experimental evidence supporting the penetration of water into the micelle to a depth of a few carbon atoms has been obtained from X-ray scattering<sup>(17)</sup> and NMR measurements<sup>(18-20)</sup>. These results have been re-evaluated and criticised by Stigter<sup>(21)</sup>. The conclusions reached from his investigation relating the change in CMC for a given hydrocarbon chain-length to the specific head group electrostatic potential at the micelle surface, are that the hydrocarbon-water interface is 0.04-0.12nm (0.4-1.2Å) from the  $\alpha$ -carbon atoms. This study

TABLE 1.3.5.1

MAXIMUM AGGREGATION NUMBER (z) AND SURFACE AREA PER CHAIN (S) FOR  
SPHERICAL AND ELLIPSOIDAL MICELLES

n	10		12		15	
	z	$S_{nm}^2$	z	$S_{nm}^2$	z	$S_{nm}^2$
Sphere, $r=l_{max}$	40	0.82	56	0.78	84	0.76
Ellipsoids $b_o=l_{max}$						
Prolate, $a_o/b_o$ 1.25	50	0.77	70	0.70	95	0.66
1.50	60	0.74	84	0.65	126	0.60
2.0	70	0.70	111	0.60	167	0.52

infers that there is no penetration of water between the hydrocarbon chains.

In conclusion the evidence regarding the penetration of water between hydrocarbon chains seems to be contradictory and no clear understanding of this fundamental problem is available at the present time.

The free energy of contact between water and hydrocarbon chains has been shown to follow simple rules. The transfer of an n-alkyl chain from water to a liquid hydrocarbon results in a free energy of transfer which includes a contribution of  $-8790 \text{ Jmole}^{-1}$  per  $\text{CH}_3$  group and  $-3558 \text{ Jmole}^{-1}$  per  $\text{CH}_2$  group<sup>(14)</sup>. The free energy of transfer of a hydrocarbon can be related to the surface area in contact with water; the free energy of transfer is  $-10.5 \text{ kJmole}^{-1}$  per  $\text{nm}^2$  of hydrocarbon removed from contact with water<sup>(22)</sup>.

These results may be applied to the transfer of alkyl chains from water to the micelle interior. However, as already stated, the hydrocarbon chains in the micelle are more constrained than in bulk hydrocarbon. Wishna has shown that this extra constraint may have a significant effect on the free energy of transfer<sup>(23)</sup>. A positive contribution of approximately  $400\text{-}1000 \text{ Jmole}^{-1}$  per  $\text{CH}_2$  unit is taken to be a reasonable estimate.

These empirical arguments suggest a separation of  $\Delta G_{\text{hyd}}^0$  into two factors, a constant term, independent of micelle size and a term which is dependent on micelle size representing the contact area of the hydrocarbon chains with water.

An appropriate expression is<sup>(15)</sup>

$$\Delta G_{\text{hyd}}^0 = -8372 - 2930(n_c - 1) + 10500(S - 0.21) \text{ Jmole}^{-1} \quad (1.3.5.1)$$

where S is the surface area per chain at the distance of closest approach

of water (for sodium dodecyl sulphate  $\sim 0.7\text{nm}^2$ ) and  $0.21\text{nm}^2$  is the area representing no water penetration.

For  $n=12$ ,

$$\underline{\Delta G_{\text{hyd}}^{\text{O}}} = -33.07\text{kJmole}^{-1}$$

Although the penetration of water into the micelle is of fundamental importance in an understanding of micelle structure, it is seen that for most micelles its contribution to the overall free energy is small. For sodium dodecyl sulphate it is approximately  $3\text{kJmole}^{-1}$ . However, for sodium hexyl sulphate,  $n=6$ , the contribution is much larger, approximately  $6\text{kJmole}^{-1}$  in a total hydrophobic contribution of  $23\text{kJmole}^{-1}$ . But even for this extreme case, (sodium hexyl sulphate has a CMC of  $\sim 0.4\text{M}$  and is the last in the homologous series which forms micelles), the contribution is approximately 25% of the hydrophobic contribution.

### 1.3.6 The Electrostatic Contribution

The electrostatic repulsive potential ( $\Delta G_{\text{el}}^{\text{O}}$ ) in equation 1.3.1.1 can be empirically represented by

$$\Delta G_{\text{el}}^{\text{O}} = \alpha/r \quad (1.3.6.1)$$

$r$  is the distance of separation between head groups, and  $\alpha$  is a constant which contains contributions from both the repulsive potential between the head groups and an attractive potential with counterions.

The electrostatic contribution to the overall free energy is expected to be very dependent on the particular head groups of the surfactant and local environmental conditions e.g. ionic strength. It will be independent of alkyl chain-length.

The equation (1.3.6.1) is purely empirical and no mechanism for

the repulsive interaction can be deduced from its form. Tanford<sup>(14,15)</sup> has shown that expressions similar to those derived by Debye and Hückel for the work of charging a sphere radius  $r_o$ , with  $m$  charges may be used to calculate  $\Delta G_{e1}^O$ .

$$\Delta G_{e1}^O = \frac{2\pi \epsilon^2 N r_o (1+Ka_i)}{DR (1+Kr_o + Ka_i)} \quad (1.3.6.2)$$

where  $a_i$  is the average radius of mobile ions in the surrounding electrolyte,  $\epsilon$  is the electronic charge,  $D$  is the dielectric constant of the medium,  $R$  is the surface area per charge at the surface of the micelle and  $K$  is the Debye-Hückel parameter proportional to the square root of the ionic strength.

One method which may be employed to obtain values of  $\Delta G_{e1}^O$ , which avoids the need to derive a suitable theoretical expression, is to make use of the experimental data from pressure-area curves for surfactants at a hydrocarbon-water interface. Data is, however, difficult to obtain and must be corrected for surface curvature before application to micellar systems. A typical value obtained from such experiments for sodium dodecyl sulphate is  $11.7 \text{ kJmole}^{-1}$ <sup>(24)</sup> at zero ionic strength.

The total free energy of micelle formation for sodium dodecyl sulphate is therefore

$$\begin{aligned} \Delta G_m^O &= -33.07 + 11.7 \text{ kJmole}^{-1} \\ &= \underline{\underline{-21.37 \text{ kJmole}^{-1}}} \end{aligned}$$

The hydrophobic contribution greatly outweighs the electrostatic contribution and micelle formation is expected to take place. For ionic and non-ionic surfactants of the same chain-length,  $\Delta G_{\text{hyd}}^O$  will be the same and the difference in the CMC values is a consequence of the electrostatic contribution. In general, non-ionic surfactants have

CMC values a factor of ~4 lower than ionic surfactants of the same chain-length, i.e.  $\Delta G_{\text{ionic}}^{\circ} - \Delta G_{\text{non-ionic}}^{\circ} = \Delta \Delta G^{\circ} = \Delta G_{\text{el}}^{\circ} = -RT \ln \frac{\text{CMC}_{\text{ionic}}}{\text{CMC}_{\text{non-ionic}}}$ .

To enable a better understanding of the process of micelle formation and the driving forces responsible, it is necessary to establish the relative importance of contributions from the enthalpy and entropy of micelle formation to the overall free energy of the process. These contributions will be considered in the following section.

### 1.3.7 The Enthalpy and Entropy of Micelle Formation

Only a small number of measurements of the enthalpy of micellisation ( $\Delta H_{\text{m}}^{\circ}$ ) have been reported. Until recently<sup>(25)</sup> micelle formation was regarded essentially as an interfacial energy effect, analogous with the coalescence of oil drops in water. Since interfacial free energy has a large enthalpy component, micelle formation is expected to be highly exothermic. In fact, experimental determinations of  $\Delta H_{\text{m}}^{\circ}$ , from the temperature dependence of the CMC<sup>(26-28)</sup> and direct calorimetric methods<sup>(29-34)</sup> show that  $\Delta H_{\text{m}}^{\circ}$  is usually numerically small (less than  $4 \text{ kJmole}^{-1}$ ) see table 1.3.7.1. The enthalpy change is temperature dependent in all cases, the heat capacity of micellisation, ( $\Delta C_{\text{pm}}^{\circ}$ ) being between  $200\text{-}400 \text{ Jmole}^{-1}\text{K}^{-1}$  for all surfactants investigated.

Since  $\Delta H_{\text{m}}^{\circ}$  is small, micelle formation is primarily an entropy driven process. There are two main sources of the positive entropy contribution ( $\Delta S_{\text{m}}^{\circ}$ ). The most important arises from the destruction of the organised water around the hydrocarbon chains. These structured regions (the rather inappropriate term "Ice-bergs" has been introduced to describe them)<sup>(35)</sup> are not permanent, static regions of water, but dynamic associations of water molecules with the hydrocarbon chains, in which bound water is exchanged with the bulk solvent. This "binding" of water by the monomeric surfactant molecules below the CMC, results in a loss

TABLE 1.3.7.1

VALUES OF  $\Delta H_m^0$  OF SODIUM DODECYL SULPHATE, IN AQUEOUS SOLUTION

METHOD	TEMP/K	$\Delta H_m^0/\text{Jmole}^{-1}$	REFERENCE
CALORIMETRIC	297	$-1046 \pm 1046$	29
TEMP. DEPENDENCE OF CMC	278	+3348	26
	298	+2511	
	318	-7953	
CALORIMETRIC	298	+4186	30
TEMP. DEPENDENCE OF CMC	273	+1674	28
	298	-416	
	303	-2093	
TEMP. DEPENDENCE OF CMC	293-313	-1674	27
CALORIMETRIC	299.8	-1884	31
	313.2	-9210	
CALORIMETRIC	276	+1461 $\pm$ 58 )	33
	278	+364 $\pm$ 63 } )	
	303	-2553 $\pm$ 79 )	

of translational and rotational entropy. Micelle formation involves desolvation which results in the destruction of these ordered regions and a consequent increase in the entropy of the system. It should be noted that for ionic micelles  $\Delta S_m^O$  is smaller than the entropy change for the transfer of a hydrocarbon chain of the same length from water to liquid hydrocarbon. Hence, the association of the head groups during micelle formation is associated with a negative entropy change. The high surface potential causes an increase in the hydration of the head groups.

Thought to be of secondary importance is the supposed increase in "flexibility" of the hydrocarbon chains on their transfer from an aqueous to a micellar environment. Precise experimental information is difficult to obtain, but Aranow and Witten<sup>(36)</sup> have discussed on a theoretical basis the change in internal torsional oscillations of the surfactant in water to hindered internal rotation in the micelle. Relatively large entropy changes are predicted. It is, however, unclear how well this model represents the state of the hydrocarbon chains in aqueous and micellar environments.

The relative contributions of the factors discussed to the overall free energy of micelle formation for some surfactants are given in table 1.3.7.2.

A recent kinetic investigation<sup>(37)</sup> of micelle formation has shown that the micelle is formed via a nucleus of 6-10 monomers.  $\Delta H$  for the formation of this nucleus is large and endothermic. The addition of monomers to this nucleus results in a small and exothermic and hence the overall enthalpy of formation is small.

TABLE 1.3.7.2

RELATIVE CONTRIBUTIONS TO THE FREE ENERGY OF  
MICELLISATION AT 298K

SURFACTANT	$\Delta G_n^0/\text{kJmole}^{-1}$	$\Delta G_{\text{hyd}}^0/\text{kJmole}^{-1}$	$\Delta G_{\text{el}}^0/\text{kJmole}^{-1}$	$\Delta H_m^0/\text{kJmole}^{-1}$	$T\Delta S^0/\text{kJmole}^{-1}$	$10^3\text{CMC/M}$
SDS	-21.5	-33.07	+11.7	+0.4	+21	8.0
DTAB <sup>(37)</sup>	-17.2	~28	~11	-1.33	+15.9	16.0

DTAB is Dodecyl trimethyl ammonium bromide

## 1.4 Dynamics of Micelle Processes

### 1.4.1 Introduction

The dynamic aspects of micellar systems have only been investigated during the past decade, although many papers concerned with the equilibrium properties of micelles have been published since the 1930's. The key dynamic processes associated with micelles occur over very short times ( $<1s$ ), outside the range of classical techniques. Following the development of relaxation methods (both single-step and stationary) the rapid micelle processes can now be studied.

Since 1965 the dynamics of micelle processes have been investigated by nearly all the fast reaction techniques available including:- stopped-flow<sup>(37,38)</sup>, temperature-jump<sup>(39)</sup>, pressure-jump<sup>(40)</sup>, and ultrasonic absorption<sup>(41)</sup>. Also, NMR<sup>(42)</sup> and ESR<sup>(43)</sup> methods have been applied to the study of the dynamic behaviour of micelles from a different viewpoint.

The single perturbation relaxation methods involve the sudden, external perturbation of the system into a non-equilibrium state; the process of attaining equilibrium (relaxation) under the new conditions is then observed. In order to achieve a relaxation the following conditions must be met:- (i) the system must be at equilibrium before the perturbation is applied, (ii) the process under investigation must have an enthalpy change for temperature-jump, a volume change for pressure-jump or a dipole change for E field-jump if a perturbation (and subsequent relaxation) of the system is to be observed. The stopped-flow method is not subject to these conditions.

For ultrasonic methods the system is perturbed by the continuous irradiation of sound waves. The system is therefore subjected to a variable frequency periodic fluctuation in pressure and temperature, and so the concentrations will vary periodically with the sound absorption in the correct frequency range but with a phase-lag. The system under

investigation must have a volume or enthalpy change associated with it, if sound absorption is to take place. By measuring the sound absorption at several frequencies, the characteristic relaxation time(s) for the system can be obtained.

The application of these essentially similar techniques has produced very different apparent rate constants which have been assigned to the same process:- that of micelle association-dissociation. This has, until recently, caused a great deal of confusion over the analysis of the raw kinetic data. This state of affairs has retarded the development of a dynamic picture of micelles.

#### 1.4.2 The Fast Relaxation Process (I)

The ultrasonic absorption method has shown that a very fast relaxation process I exists in ionic micellar systems<sup>(42)</sup>. Yasunaga et al<sup>(44)</sup> initially attributed this relaxation to the association-dissociation process of counterions at the micelle surface. Extensive measurements by Graber et al<sup>(45)</sup> and Wyn-Jones et al<sup>(37,46,47)</sup> have shown that this relaxation process is, in fact, independent of the type of counterion but dependent on the alkyl chain-length. Also the measured volume change for process I is too large for counterion binding; it is, for instance, much larger than for the equivalent process of counterion binding to linear polyelectrolytes<sup>(45)</sup>.

However, another possible origin of the relaxation process is the exchange of water to and from the micelle surface. The relaxation time is, therefore, expected to be dependent on the water structure close to the micelle surface. The addition of  $\text{Li}^+$  and  $\text{Na}^+$  which alter the water structure near the micelle surface do not effect the observed relaxation time. Water exchange is therefore discounted as the relaxation process observed<sup>(44)</sup>.

The observed relaxation process I is now thought by nearly all workers to be the diffusion-controlled exchange of monomer surfactant between bulk solution and the micelles.



The assignment of the rapid relaxation process I as an exchange is consistent with NMR results and ESR data on the rate of exchange of spin labelled surfactant ions between bulk solution and micelles. In an NMR experiment the monomeric and micellar species produce a time averaged spectrum in which individual signals are no broader than signals obtained when monomers are present alone. The absence of line-broadening indicates that any process which occurs in the system is fast on the NMR timescale i.e. mean residence time of a monomer in the micelle is less than  $\sim 10^{-4}$  sec.<sup>(48)</sup>. The ESR experiments, in which some surfactant monomers are labelled with a radical e.g. nitroxide, also indicate the mean residence time of a monomer in the micelle is  $\sim 10^{-4}$  sec.<sup>(49)</sup>.

A further possibility consistent with the observed relaxation data is the exchange of end surfactant ions to and from pre-micelle aggregates which may exist close to the CMC.

The application of temperature-jump<sup>(39,50,54)</sup>, pressure-jump<sup>(40)</sup> and stopped-flow<sup>(38)</sup> techniques to the study of micelle dynamics has shown the existence of a "slow" relaxation process (II) which occurs in the millisecond time range. In common with process I the slow relaxation is apparently characterised and analysed as a single relaxation time. This slow relaxation has also been attributed by several workers<sup>(50,51)</sup> to the exchange process, in particular the loss of a monomer from a stable micelle which is the rate-determining step in the breakdown of the complete micelle.

This situation in which two relaxations, which differ by up to

three orders of magnitude, have been assigned to the same chemical process is clearly not acceptable. An attempt has been made by Muller<sup>(52)</sup> to reconcile the difference in relaxation times. Muller pointed out that the slow relaxation II was not detected by NMR, and went on to examine the differences in the various relaxation techniques. He showed that the "large perturbation" of the temperature-jump method would not allow linearisation of the rate equations, i.e. the relaxation time should depend on the amplitude of the perturbation. Muller therefore concluded that the slow process II was in fact the complete dissolution of the micelles. Recently, Hoffmann et al<sup>(37,53)</sup> have determined the relaxation time as a function of the size of the perturbation (by temperature-jump and stopped-flow, Tondre personal communication). A very small dependence of relaxation time on the amplitude of the perturbation was observed. Although the reason for the differences in relaxation times put forward by Muller may be incorrect, the concept of a slow complete breakdown of the micelle (dissolution) has been accepted. The kinetic equations for the process will be discussed in the next section.

Nakagawa<sup>(54)</sup> has recently reviewed the kinetic results obtained for micellar solutions by various relaxation, NMR and ESR methods. The model he proposed is similar to that of Muller in that two relaxation processes were postulated.

- (i) an exchange process (rapid)
- (ii) a readjustment of micelle size and aggregation number (slow)

Process (ii) involves the change in micelle concentration aggregation number and size distribution. Figure 1.4.2.1.

We may consider the relaxation processes with the aid of the micelle distribution curve figure 1.4.2.1. Muller assumes that one or more monomer ions dissociate from the micelles state 1  $\rightarrow$  2. This is

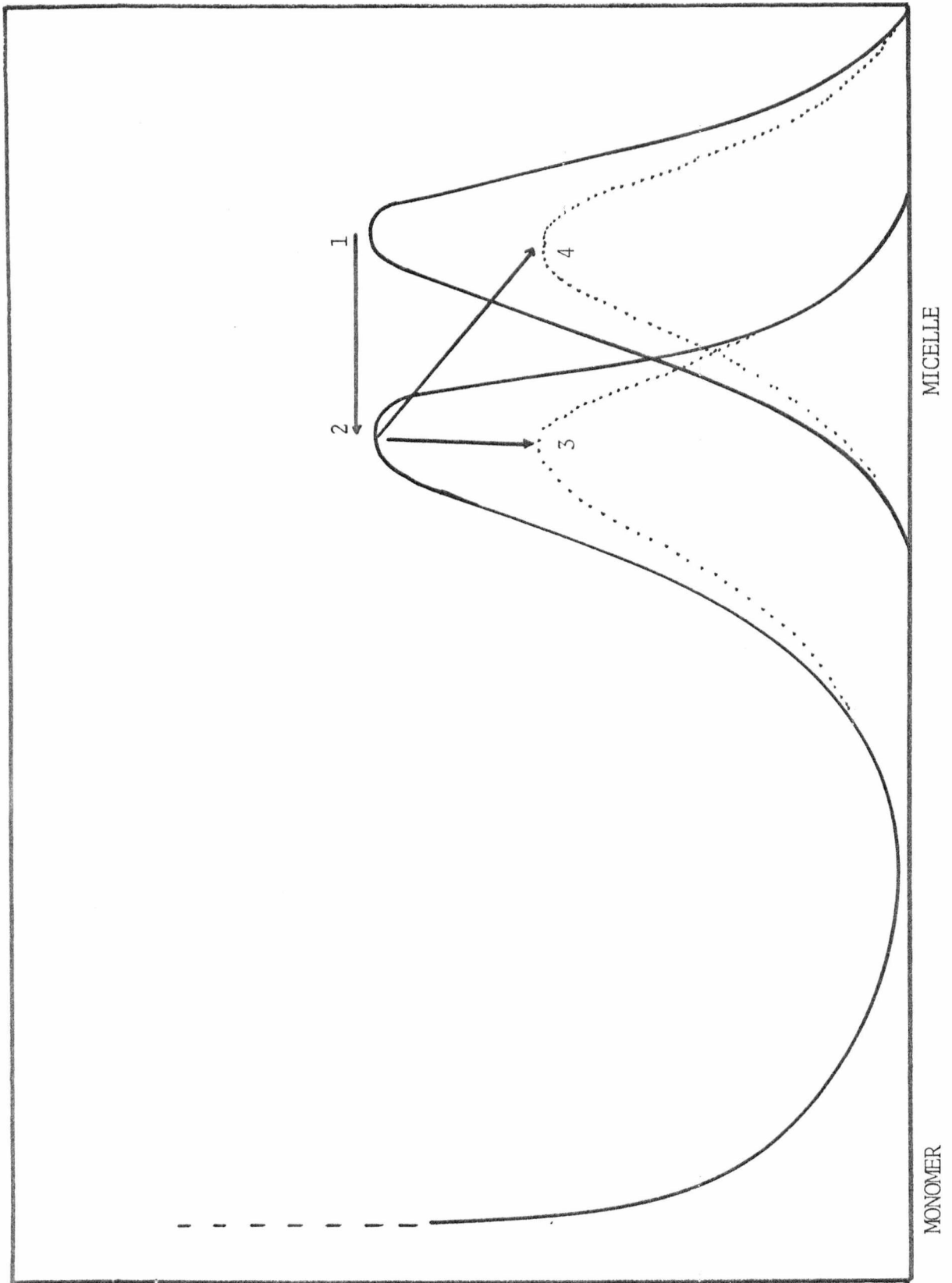


FIGURE 1.4.2.1

DISTRIBUTION CURVE FOR MICELLE/MONOMER DURING A TEMPERATURE-JUMP

the exchange process I. A few micelles then dissociate completely represented by  $2 \rightarrow 3$ . Muller<sup>(52)</sup> suggests that both processes are detectable by relaxation methods but only process I will be detected by the NMR method.

Nakagawa<sup>(54)</sup> assumes process I occurs, but assumes the slow process II to be represented by  $2 \rightarrow 4$  in figure 1.4.2.1 and calls this a "self-adjustment of micelle distribution until final equilibrium is reached". Moreover, he asserts that this process will not be detectable except by light-scattering. He therefore attempts to analyse all the data so far collected by an exchange mechanism. This is clearly invalid since measurements on sodium dodecyl sulphate by light scattering temperature-jump<sup>(51)</sup> and pressure-jump with conductivity detection<sup>(40)</sup> yield the same relaxation times.

The analysis developed by Nakagawa for the exchange process is, however, of interest. He assumes that the rate at which monomer surfactant enters an existing micelle is proportional to the surface area of the micelle and the concentration of monomers. The importance of the micelle surface area is also considered by Wyn-Jones et al<sup>(47)</sup>.

The expression for the reciprocal relaxation time derived by Nakagawa is

$$1/\tau_I = k_{21} \left( b + \frac{C_A^0 - \text{CMC}}{\text{CMC}} \right) \quad (1.4.2.2)$$

where  $b$  is a constant equal to  $1/3$ ,  $1$  or  $2$  depending on the exact proportionality assumed between surface area and rate.

The assumption that the exchange rate is proportional to the surface area of micelle is a reasonable one. The effects of such factors as surface potential on the rate could be included provided that the dependence of  $k_{21}$  on the parameter and the dependence of the parameter on the aggregation, is known.

Equation (1.4.2.2) predicts a linear dependence of  $1/\tau_I$  with total concentration, which has been observed experimentally<sup>(47)</sup>. Hoffmann et al<sup>(37,53)</sup> have shown slight upward curvature of the plots of  $1/\tau_I$  against  $C_A^0$ . The explanation for this behaviour is that the concentration is high and the polydispersity of the micelles at high concentrations affect the exchange kinetics.

Wyn-Jones et al<sup>(47)</sup> have developed a model based on the Langmuir absorption theory. The derived relaxation expression is

$$1/\tau_I = k_{12} a_o((1-\alpha)/\alpha)C_A^0 - k_{21} a^o \quad (1.4.2.3)$$

where  $a^o$  is the surface area covered by one mole of monomer in the micelle;  $\alpha$  is the fraction of the total micelle surface covered by monomers.

The model of Hoffmann et al<sup>(37,55)</sup> is a complete treatment of the fast and slow relaxation processes on the basis of the theory of heat conduction and will be discussed in section 1.4.3.

#### 1.4.3 The Slow Relaxation Process (II)

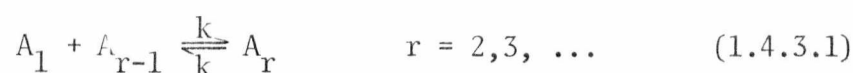
The only complete treatment of the slow relaxation process is given by Hoffmann et al and the same theory is used to derive the relaxation expressions for both the fast and slow relaxations.

The theory of micelle dynamics based on the theory of heat conduction was developed by Aniansson and Wall<sup>(37,53)</sup>. The approach is based on the similarity between the rate expressions for a series of bimolecular equilibria and heat conduction. Aniansson and Wall<sup>(55)</sup> pointed out that the kinetic process may be visualised as a system of "two large metal blocks" connected by a thin wire; "one block"

corresponding to the monomers and oligomers and the other to the stable micelles. The two relaxations were then seen to be (1) the fast relaxation as an initial rapid adjustment of micelle and (2) the slow relaxation as a pseudo-stationary flow from one "block" to the other.

The assumption was made that the aggregation number  $r$  was a continuous function and the relaxation times  $\tau_I$  and  $\tau_{II}$  could be obtained.

The overall process may be represented by



where  $A_r$  is an aggregate containing  $r$  monomers.

The attainment of equilibrium following a perturbation will involve the movement of excess populations on the distribution curve from one region to a region consistent with the new equilibrium conditions. According to equation (1.4.3.1), this will occur in steps which are small compared to the distance in aggregation *space* generally covered i.e. the process will have the appearance of a flow.

A consequence of the theory is that diffusion through the narrow tube connecting the two "blocks" (monomers and micelles) will be very much slower than the equalisation at each end. These two processes will be coupled since each one will result in a net production or consumption of monomers. But since one process is very much more rapid than the other, they may be treated as decoupled equilibria.

The relaxation expression derived by this method<sup>(37,53)</sup> is given by

$$1/\tau_I = \frac{k_{21}}{\sigma^2} + \frac{k_{21}}{z} a(1-C_0) \quad (1.4.3.2)$$

where  $\sigma$  is the width of the distribution curve  $\approx 10$

$a$  is  $(C_A^0 - \bar{A}_1)/\bar{A}_1$

$\bar{A}_1$  is the equilibrium concentration of monomers = CMC

$C_0$  is the average relative deviation from equilibrium of the micelles generally  $<1\%$

$z$  is the average micelle aggregation number.

$1/\tau_I$  is therefore a linear function of  $C_A^0$  (experimentally observed) with a slope of  $k_{21}/z$ . Since  $z$  is known from light scattering measurements  $k_{21}$  can be calculated and hence  $\sigma$  from the intercept. This plot therefore leads to an experimental estimate of  $\sigma$  for the first time.

Process I is represented by path I in figure 1.4.3.1 i.e. no net change in micelle concentration but a change in average aggregation number.

These techniques suggest relaxation times of the order of one microsecond for exchange of  $C_{12}$  alkyl-chain ionic surfactants. The ultrasonic method shows that the relaxation time increases rapidly with increasing surfactant chain-length<sup>(46)</sup>. The exchange process is assumed to be diffusion controlled and rates of the order of  $10^9 \text{ l mole}^{-1} \text{ sec.}^{-1}$  are observed<sup>(37)</sup>. It is, however, not clear why such a process should approach the diffusion-controlled limit. Ionic micelles are highly charged species and have high internal microviscosity<sup>(3)</sup>. The entering monomer must, therefore, experience considerable charge repulsion. The entrance of the monomer will also lead to considerable local reorientation of the existing hydrocarbon-chains. Both these effects should operate to decrease the rate below the diffusion-controlled limit.

Since the micelle is fairly open at the surface<sup>(14,15)</sup>, an incoming monomer may not experience significant steric-hindrance in the early stages. On the assumption that little or no water is present in the outer regions of the micelle (see section 1.3.5<sup>(17-21)</sup>) it may be possible for the monomer to reach a stage (at the diffusion-controlled rate) where the hydrophobic (favourable) contribution outweighs the electrostatic repulsion. The monomer has then reached a "point of no

return" and must complete its entrance into the micelle. The completion of the entrance may be aided by some form of "hydrophobic suction" which drags the monomer into the micelle.

The increasing relaxation time with increasing chain-length is consistent with the decreasing surface area per head group with increasing chain-length and indicates that the entrance of monomer is not entirely diffusion-controlled.

The slow relaxation or "pseudo-stationary flow" may be represented on a micelle distribution curve as process 2→3. (Figure 1.4.2.1).

The relaxation expression derived by Aniansson and Wall<sup>(37,54,55,56)</sup> is given by

$$1/\tau_{II} \approx \frac{z^2}{\bar{A}_1} \frac{1}{R} \left( \frac{1}{1 + \sigma^2/za} \right) \quad (1.4.3.3)$$

where  $R = \sum_{r_1+1}^{r_2} \frac{1}{k_{21,r} \bar{A}_r}$

Since  $z$  is of the order of 60 small changes in  $z$  will produce large changes in the number of micelles. It has also been shown that if the narrow tube is short

$$R = \frac{l}{k_{21,s} \bar{A}_s}$$

where  $s$  is the aggregation number at the minimum value of  $\bar{A}_s$  (of the order of 6-10);  $l$  is the effective length of the tube.

The rate of distribution is characterised by the value of  $R$

$$\left( = \sum_{r_1+1}^{r_2} \frac{1}{k_{21,r} \bar{A}_r} = \frac{l}{k_{21,r} \bar{A}_r} \right)$$

The enthalpy of the exchange process (obtained from a plot of  $1/\tau_I$  against  $1/T_K$ ) is exothermic. Since the overall enthalpy of micelle

formation  $\Delta H_m$  is small (section 1.3.7) there must be a process which has a large endothermic enthalpy. The temperature dependence of  $1/\tau_{II}$  leads to such an endothermic enthalpy for the formation of the aggregate at the distribution minimum. Micelle formation-dissolution is therefore considered to operate via a nucleus of surfactant molecules which may at high temperatures be as small as two. (See Chapter 3).

The present picture of micelle dynamics is one in which monomer surfactant is in rapid exchange equilibrium between micelles and bulk solution. This exchange process is dependent on the total surfactant concentration and occurs in the microsecond time range. The micelles also dissociate in the millisecond to second time range. Considerable progress has been made in the attempt to account for the observed variations in rate with (i) surfactant concentration, (ii) counter-ion type, (iii) ionic strength and (iv) surfactant chain length.

Further studies on the effects of impurities e.g. long chain alcohols, and the interaction of dyes with micelles are in progress in an attempt to further amplify the picture and widen our knowledge concerning micelle processes in real situations e.g. in micellar catalysis, detergent cleaning action, release of drugs administered in micellar form etc. It is hoped that these studies will enable a clearer understanding of the effects of additives, such as drugs, on the stability of micelles. This knowledge may be of great importance in understanding the dynamic processes which occur at the cell membrane surface and such properties as membrane stability, permeability and transport of drugs across membranes.

### 1.5 Uses and Industrial Importance of Micellar Systems

The use of pharmaceutical substances which have only a limited solubility in water has presented problems to the formulation and administration of drugs in suitable forms. The large scale introduction of surface-active substances and the discovery of the phenomena of micellar solubilisation has led to the extensive use of surface-active substances in the pharmaceutical industry. Water-insoluble bactericides, vitamins, steroids, essential oils and antibiotics have been formulated in micellar systems, thus facilitating their use in medicine.

Micellar solutions have been used to facilitate the extraction of crude drugs from plants. For example, anionic detergents have been used to solubilise alkaloids<sup>(56)</sup> and Tween 20 has been used in the extraction of Belladonna<sup>(57)</sup>.

The phospholipids of the body form aggregates in solution which are now considered to be micelles. The nature of the micelles formed by lecithin and lysolecithin may be spherical, helical or folded-laminar types. The main factor which determines the micellar shape is the stereochemistry of the individual phospholipid molecules. The interpretation of solubilisation by these components requires an understanding of phospholipid micellisation, and this is also important in the explanation of the transport of drugs across membranes. Studies have suggested<sup>(58)</sup> that phospholipid bi-layers may momentarily micellise when in contact with increased  $\text{Ca}^{2+}$  concentration, which may suggest a mechanism for the transport of drugs through the pores formed.

Micelles provide environments which are quite different from aqueous solution. Reactions which occur within the micellar environments may be quite different from those which occur in aqueous solution. Reactions between ions are especially influenced by the presence of ionic surfactants both above and below the CMC<sup>(59)</sup>. For example, the

alkaline-fading of positively charged triphenylmethane dyes e.g. crystal violet is accelerated by cationic micelles and greatly reduced by anionic micelles<sup>(60)</sup>. In this case it is thought that the dye are adsorbed/absorbed by the anionic micelles which then present a considerable charge barrier to the hydroxyl ions. The pH in the region of the micelle is known to depend on the surface charge size and polarity.<sup>(61)</sup> Anionic micelles repel hydroxyl ions and the pH at the micelle surface may be up to 2pH units lower than in bulk solution. Cationic micelles on the other hand attract hydroxyl ions and form ones of high hydroxyl ion concentration and negative charge which will attract the positively charged dye. A vast range of surfactant types exist and it may be possible to provide micellar systems which will be tailor-made to catalyse or inhibit industrially important processes and promote novel syntheses.

It can be seen that micellar systems not only have intrinsic scientific appeal and are interesting systems for study, but are useful in many important industrial and medical situations. It must be stressed that in most cases it is the phenomena of solubilisation and the absorption of molecules into micelles which play the dominant roles in determining the mode of action. It is for these reasons that the work described in this thesis was undertaken.

## REFERENCES

- (1) G.S. Hartley, Aqueous Solutions of Paraffin Chain Salts, (Hermann et Cie, Paris, 1936).
- (2) K. Shinoda, T. Nakagawa, B. Tamamushi and T. Isemura, Colloidal Surfactants, (Academic Press, New York, 1963).
- (3) M. Shinitzky, A.C. Dianoux, C. Gitler and G. Weber, *Biochem.*, 1971, 10, 2106.
- (4) D. Stigter and K.J. Mysels, *J. Phys. Chem.*, 1955, 59, 45.
- (5) P. Mukerjee and K.J. Mysels, Critical Micelle Concentrations of Aqueous Surfactant Systems, (National Bureau of Standards 36, Washington, 1971).
- (6) M.F. Emerson and A. Holtzer, *J. Phys. Chem.*, 1967, 71, 1898.
- (7) J.M. Corkill, J.F. Goodman, T. Walker and T. Wyer, *Proc. Roy. Soc.*, 1969, A312, 243.
- (8) G. Stainsby and A.E. Alexander, *Trans. Faraday Soc.*, 1950, 46, 587.
- (9) D.G. Hall and B.A. Pethica, Non-Ionic Surfactants, ed. M.J. Schick (Marcel Dekker Inc., New York, 1967), Chapter 16.
- (10) T.L. Hill, Thermodynamics of Small Systems, Vol.2 (W.A. Benjamin Inc., New York, 1964).
- (11) R.W. Gurney, Ionic Processes in Solution, (Dover, New York, 1962)-
- (12) P.H. Elworthy and K.J. Mysels, *J. Colloid Sci.*, 1966, 21, 331.
- (13) K.J. Mysels, P. Mukerjee and M. Abu-Hamdiyak, *J. Physic. Chem.*, 1963, 67, 1943.
- (14) C. Tanford, The Hydrophobic Effect, (Wiley-Interscience, New York, 1974).
- (15) C. Tanford, *J. Phys. Chem.*, 1974, 78, 2469.
- (16) F. Reiss-Husson and V. Luzzati, *J. Phys. Chem.*, 1964, 68, 3504.
- (17) F. Reiss-Husson and V. Luzzati, *J. Colloid Interface Sci.*, 1966, 21, 534.

- (18) N. Muller and R.H. Birkhahn, *J. Phys. Chem.*, 1967, 71, 957.
- (19) N. Muller and H. Simsohn, *J. Phys. Chem.*, 1971, 75, 942.
- (20) N. Muller and R.H. Birkhahn, *J. Phys. Chem.*, 1968, 72, 583.
- (21) D. Stigter, *J. Phys. Chem.*, 1974, 78, 2480.
- (22) R.B. Hermann, *J. Phys. Chem.*, 1972, 76, 2754.
- (23) A. Wishna, *J. Phys. Chem.*, 1963, 67, 2079.
- (24) I. Reich, *J. Phys. Chem.*, 1956, 60, 257.
- (25) B.D. Flockhart and A.R. Ubbelohde, *J. Colloid Sci.*, 1953, 8, 428.
- (26) E.D. Goddard and G.C. Benson, *Canad. J. Chem.*, 1957, 35, 986.
- (27) E. Matijevic and B.A. Pethica, *Trans. Faraday Soc.*, 1958, 54, 587.
- (28) B.D. Flockhart, *J. Colloid Sci.*, 1961, 16, 484.
- (29) E.D. Goddard and B.A. Pethica, *J. Chem. Soc.*, 1951, 2659.
- (30) E.D. Goddard and G.C. Benson, *Trans. Faraday Soc.*, 1956, 52, 409.
- (31) L. Benjamin, *J. Phys. Chem.*, 1964, 68, 3575.
- (32) J.M. Corkill, J.F. Goodman and J.R. Tate, *Trans. Faraday Soc.*, 1964, 60, 996.
- (33) G. Pilcher, M.N. Jones, L. Espada and H.A. Skinner, *J. Chem. Thermodyn.*, 1969, 1, 381.
- (34) M.N. Jones, G. Pilcher and L. Espada, *J. Chem. Thermodyn.*, 1970, 2, 333.
- (35) H.S. Frank and M.W. Evans, *J. Phys. Chem.*, 1945, 13, 507.
- (36) R.H. Aranow and L. Witten, *J. Phys. Chem.*, 1960, 64, 1643.
- (37) E.A.G. Aniansson, S.N. Wall, M. Alingron, H. Hoffmann, I. Kielmann, W. Ulbricht, R. Zana, J. Lang and C. Tondre, *J. Phys. Chem.*, 1976, 80, 905.
- (38) J. Lang and E.M. Eyring, *J. Polymer Sci.*, 1972, A-2 10, 89.
- (39) B.C. Bennion, L.K.J. Tong, L.P. Holmes and E.M. Eyring, *J. Phys. Chem.*, 1969, 73, 3288.
- (40) T. Yasunaga, S. Fujic and M. Miura, *J. Colloid Interface Sci.*,

1969, 30, 399.

- (41) K. Takeda and T. Yasunaga, *J. Colloid Interface Sci.*, 1972, 40, 127.
- (42) T. Nakagawa and K. Tori, *Kolloid-Z-Z Polym.*, 1964, 194, 43.
- (43) K.K. Fox, *Trans. Faraday Soc.*, 1971, 67, 2802.
- (44) T. Yasunaga, H. Oguri and M. Miura, *J. Colloid Interface Sci.*, 1967, 23, 352.
- (45) E. Graber, J. Lang and R. Zana, *Kolloid-Z-Z Polym.*, 1970, 238, 470.
- (46) P.J. Sams, E. Wyn-Jones and J. Rassing, *Chem. Phys. Lett.*, 1972, 12, 233.
- (47) J. Rassing, P.J. Sams and E. Wyn-Jones, *J. Chem. Soc. Faraday II*, 1974,
- (48) N. Muller and F.E. Platko, *J. Phys. Chem.*, 1971, 75, 547.
- (49) N.M. Atherton and S.J. Strach, *J. Chem. Soc. Faraday Trans. II*, 1972, 68, 374.
- (50) G.C. Kresheck, E. Hamsori, G. Davenport and H.A. Scheraga, *J. Amer. Chem. Soc.*, 1966, 88, 246.
- (51) B.C. Bennion and E.M. Eyring, *J. Colloid Interface Sci.*, 1970, 32, 286.
- (52) N. Muller, *J. Phys. Chem.*, 1972, 76, 3017.
- (53) J. Lang, C. Tondre, R. Zana, R. Bauer, H. Hoffmann and W. Ulbricht, *J. Phys. Chem.*, 1975, 79, 276.
- (54) T. Nakagawa, *Colloid Polymer Sci.*, 1974, 252, 56.
- (55) E.A.G. Aniansson and S.N. Wall, *J. Phys. Chem.*, 1974, 78, 1024.
- (56) E. Brachmann-Hansen, *J. Amer. Pharm. Assoc.*, 1954, 43, 27.
- (57) W.J. Bulter and G.A. Wiese, *J. Amer. Pharm. Assoc.*, 1953, 42, 382.
- (58) D. Chapman and R.B. Leslie, Molecular Biophysics (Oliver & Boyd, 1967).
- (59) E.F. Fendler and J.H. Fendler, *Prog. Phys. Org. Chem.*, 1970, 8, 271.
- (60) E.P.J. Pagnstree and E. Grunwald, *J. Amer. Chem. Soc.*, 1959, 81, 4540.
- (61) G.S. Hartley and J.W. Row, *Trans. Faraday Soc.*, 1940, 36, 101.

C H A P T E R 2

DESCRIPTION OF APPARATUS AND GENERAL EXPERIMENTAL PROCEDURE

## CHAPTER 2

### DESCRIPTION OF APPARATUS AND GENERAL EXPERIMENTAL PROCEDURE

#### 2.1 Introduction

In this chapter the equipment, experimental procedures and apparatus relating to the kinetic measurements are described.

#### 2.2 Abbreviations

A number of abbreviations are used throughout the text. These abbreviations and, where appropriate, the corresponding structural formulae, are given in table 2.2.1.

#### 2.3 Materials

Details of the suppliers and grades of the chemicals are given in table 2.3.1.

#### 2.4 Purification of Materials

##### 2.4.1 Acridine Orange (AO)

Acridine orange was dissolved in triply distilled water and 1M sodium hydroxide was added slowly with shaking, a yellow precipitate (neutral dye) formed which was filtered, washed with water and dried at 393K<sup>(1)</sup>.

	C	H	N
Elemental analysis % Calculated	76.05	7.16	15.85
(as neutral dye) % Found	75.9	7.01	15.73

TABLE 2.2.1

ABBREVIATIONS AND STRUCTURAL FORMULAE OF COMPOUNDS USED

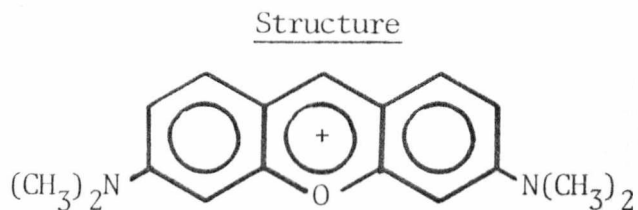
<u>Compound</u>	<u>Abbreviation</u>	<u>Structure</u>
Acridine Orange	AO <sup>+</sup>	
Acriflavine	AF <sup>+</sup>	
Atebrine	AB <sup>2+</sup>	
Malachite Green	MG <sup>+</sup>	
Methylene Blue	MB <sup>+</sup>	
Proflavine	PF <sup>+</sup>	

TABLE 2.2.1 (cont.)

Compound                      Abbreviation

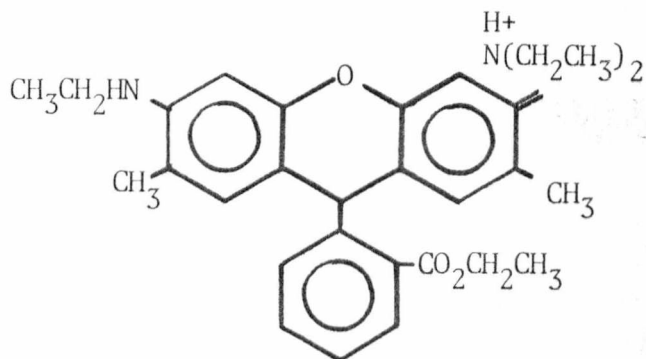
Pyronine G

PYG<sup>+</sup>

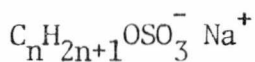


Rhodamine 6G

RhG<sup>+</sup>



n-alkyl sodium sulphates



n

1    methyl

SMeS

8    octyl

SOS

10   decyl

SDeS

12   dodecyl

SDS

14   tetradecyl

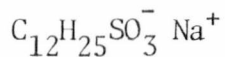
STS

16   hexadecyl

SHDS

sodium dodecyl sulphate

SDSn



sodium dodecyl benzene sulphate

SDBSn

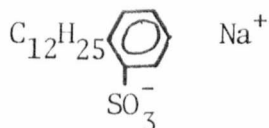


TABLE 2.3.1

SUPPLIER AND GRADE OF REAGENTS USED

<u>Reagent</u>	<u>Supplier</u>	<u>Grade</u>
Acridine Orange	Fisons	
Acriflavine	Fisons	
Atebrine	Fisons	
t-Butanol	Fisons	A.R.
Diethyl ether	Fisons	A.R.
Dioxane	Fisons	S.L.R.
Dodecan-1-ol	Fisons	Specially pure
Ethan-1-ol	Fisons	A.R.
Isopropyl alcohol	Fisons	A.R.
Malachite Green	Fisons	
Methanol	Fisons	A.R.
Methylene Blue	Fisons	
Proflavine	Fisons	
Pyrorine G	Fluka	
Rhodamine 6G	Fisons	
Sodium Chloride	Fisons	
Sodium Decyl Sulphate	Cambrian	>99%
Sodium Dodecyl Sulphate	Fisons	
Sodium Dodecyl Benzene Sulphonate	Phaltz & Bauer	
Sodium Dodecyl Sulphonate	Cambrian	>99%
Sodium Hexadecyl Sulphate	Cambrian	>99%
Sodium Hydroxide	Fisons	A.R.
Sodium Methyl Sulphate	Fisons	S.L.R.

TABLE 2.3.1 (cont.)

<u>Reagent</u>	<u>Supplier</u>	<u>Grade</u>
Sodium Perchlorate	Fisons	S.L.R.
Sodium Tetradecyl Sulphate	Cambrian	>99%

#### 2.4.2 Acriflavine (AF)

Acriflavine was shaken with a small excess of sodium hydroxide, left overnight at 273K, filtered, brought to pH=7 with hydrochloric acid and evaporated to dryness. The product was recrystallised twice from methanol, twice from triply distilled water and dried at 393K<sup>(2)</sup>.

		C	H	N
Elemental analysis	% Calculated	64.86	5.40	16.22
(as the hydrochloride)	% Found	64.80	5.42	16.17

#### 2.4.3 Atebrine (AB)

Atebrine was dissolved in hot triply distilled water and hydrochloric acid was added. The solution was filtered and allowed to cool. The product was filtered off and recrystallised from triply distilled water, dried at 373K and stored over silica gel<sup>(3)</sup>.

		C	H	N
Elemental analysis	% Calculated	63.3	7.12	9.64
(as the hydrochloride)	% Found	63.0	7.10	9.60

#### 2.4.4 Malachite Green (MG)

Malachite green was recrystallised from triply distilled water three times<sup>(4)</sup>.

		C	H	N
Elemental analysis	% Calculated	75.7	6.85	7.68
(as the chloride)	% Found	75.1	6.95	7.61

#### 2.4.5 Methylene Blue (MB)

Methylene blue was recrystallised three times from water and ethanol and dried at 393K<sup>(5)</sup>.

		C	H	N
Elemental analysis	% Calculated	60.0	5.61	13.1
(as the chloride)	% Found	59.85	5.63	13.0

#### 2.4.6 Proflavine (PF)

Proflavine was recrystallised three times from triply distilled water and dried at 393K<sup>(6)</sup>.

		C	H	N
Elemental analysis	% Calculated	56.80	4.00	15.23
(as the hemisulphate)	% Found	56.68	3.83	15.10

#### 2.4.7 Pyronine G (PYG)

Pyronine G was dissolved in methanol, filtered precipitated with ether and dried at 373K<sup>(7)</sup>.

		C	H	N
Elemental analysis	% Calculated	67.3	6.29	9.2
(as the chloride)	% Found	67.1	6.30	9.0

#### 2.4.8 Rhodamine 6G (RhG)

Rhodamine 6G was recrystallised from triply distilled water three times and dried at 383K<sup>(8)</sup>.

		C	H	N
Elemental analysis	% Calculated	69.9	6.26	6.23
	% Found	69.1	6.13	5.91

The purity of the dyes was also checked by comparison with literature values of the extinction coefficients. The spectral characteristics of the dyes used are shown in table 2.4.1.

TABLE 2.4.1

SPECTRAL CHARACTERISTICS OF DYES USED

Spectra were recorded in unbuffered triply distilled water (pH 6-7); temperature 298K.

Dye <sup>+</sup>	$\lambda_{\max}/\text{nm}$	$10^{-3}\epsilon/\text{dm}^3\text{Mole}^{-1}\text{cm}^{-1}$	$\lambda_{\text{em}}/\text{nm}$
AO	492	55	526
AF	452	47	510
AB*	425	10	502
MG	620	83	
MB	656	81	710
PF	444	41	510
PYG	550	46	570
Rh6G	530	80	580

$\lambda_{\text{em}}$  is the wavelength of maximum fluorescence intensity

$\epsilon$  is the extinction coefficient at  $\lambda_{\max}$  (for  $10^{-5}\text{M}$  dye)

\* AB<sup>2+</sup>

2.4.9 Surfactants

The alkyl sulphates and sodium dodecyl sulphonate were greater than 99% pure and were extracted with ether for 36 hours, dried and kept over silica gel<sup>(9)</sup>.

The sodium o-dodecyl benzene sulphonate was dissolved in ether and extracted several times in a separatory-funnel with water. The aqueous layer was evaporated to dryness. The essentially pure sodium o-dodecyl benzene sulphonate was then recrystallised from anhydrous ethanol<sup>(10)</sup>.

Elemental Analysis:

$C_nH_{2n+1}SO_4^-Na^+$	% Calculated			% Found		
	C	H	S	C	H	S
n						
8	41.38	7.32	13.8	41.01	7.20	13.73
10	46.15	8.10	12.31	45.91	8.00	12.11
12	50.00	8.68	11.11	49.53	8.73	10.96
14	53.16	9.18	10.13	52.31	9.11	10.00
16	55.81	9.59	9.30	55.20	9.41	9.21
$C_{12}H_{25}SO_3^-Na^+$	52.94	9.19	11.76	52.41	9.01	11.81
$C_{12}H_{25}C_6H_5SO_3^-Na^+$	62.07	8.33	9.19	61.31	8.21	9.23

## 2.5 Preparation of Solutions

Triply distilled water was used for the preparation of all aqueous solutions.

Stock dye solutions were made up in aluminium foil covered polyethylene bottles, to minimise the effects of adsorption and photodecomposition. Dye solutions were stored at 277K and were found to be stable for many months.

Stock surfactant solutions were kept for no more than three days in order to minimise any effects of hydrolysis<sup>(11)</sup>.

## 2.6 Spectrophotometers

The UV/visible spectra of solutions were recorded on either a Pye-Unicam SP8000 spectrophotometer, or a Penkin-Elmer 402 machine. The absolute accuracy obtainable with both these machines is  $\pm 0.003$  optical

density units. The temperature of the thermostat tanks for these machines was controlled by a thermistor device designed by members of the Electronics Workshop of this Laboratory. The temperature could be controlled to within  $\pm 0.05\text{K}$  in the range 273-323K.

## 2.7 Measurement of pH

The pH meter (Radiometer model PHM26) was equipped with G202B glass and K401 and K901 reference electrodes. The pH standards employed were 0.05M potassium hydrogen phthalate (pH  $4.000 \pm 0.002$ ), 0.05M potassium phosphate monobasic sodium hydroxide buffer (pH  $7.00 \pm 0.02$ ), and sodium tetraborate (pH  $9.180 \pm 0.002$ ) at 298K.

## 2.8 Description of the Temperature-Jump Apparatus

### 2.8.1 Introduction

The temperature-jump technique is the most common of the "single-step" perturbation relaxation methods<sup>(12)</sup>. Relaxation methods involve the perturbation of a chemical equilibrium such that the rate of approach to the new equilibrium state is linearly dependent on the displacement. The reciprocal of the proportionality factor is called the relaxation time,  $\tau$ . The other methods of single step perturbation are pressure-jump and electric field jump. Perturbation of a chemical equilibrium can also be effected by a periodic variation of the external forcing parameters e.g. NMR, ESR, dielectric and acoustic absorptions.

The method is based on the temperature dependence of the equilibrium constant K for the reaction under study:

$$\frac{d}{dT} (\ln K) = \frac{\Delta H^{\circ}}{RT^2} \quad (2.8.1.1)$$

where R is the gas constant and  $\Delta H^{\circ}$  is the standard enthalpy change.

If  $\Delta H^{\circ} \neq 0$ , a rapidly applied temperature rise  $\Delta T$  will cause a displacement in the equilibrium and the chemical reactants will relax to the new equilibrium conditions, defined by  $K(T+\Delta T)$ . If  $\Delta H^{\circ}$  is positive the shift will be towards the production of more products; if  $\Delta H^{\circ}$  is negative the shift will be towards the production of more reactants. The relaxation time,  $\tau$ , will be independent of the direction of the displacement of the initial equilibrium.

Systems with  $\Delta H^{\circ} \neq 0$  may react in one of three ways to the temperature perturbation:

- (1) if the reaction is very slow no change in the initial equilibrium will occur and essentially no change in the absorbance will be observed on the time scale of the experiment, curve 1, figure 2.8.1.1;
- (2) if the reaction is very rapid, the new equilibrium will be set up almost instantaneously and the absorbance change will follow the rate of the physical perturbation, curve 2, figure 2.8.1.1;
- (3) if the reaction proceeds at an intermediate rate, the chemical re-equilibration will be observed taking place, curve 3, figure 2.8.1.1.

If the displacement is small, then the reaction transient follows an exponential, irrespective of the order of the reaction. The transient exponential is described by the equation  $A = A_0 e^{-t/\tau}$ , where  $A$  is the absorbance difference between the new equilibrium and that at time  $t$ , and  $\tau$  is the aforementioned relaxation time.

The most important feature of the relaxation method is that the experimental parameters used to monitor the transient concentration

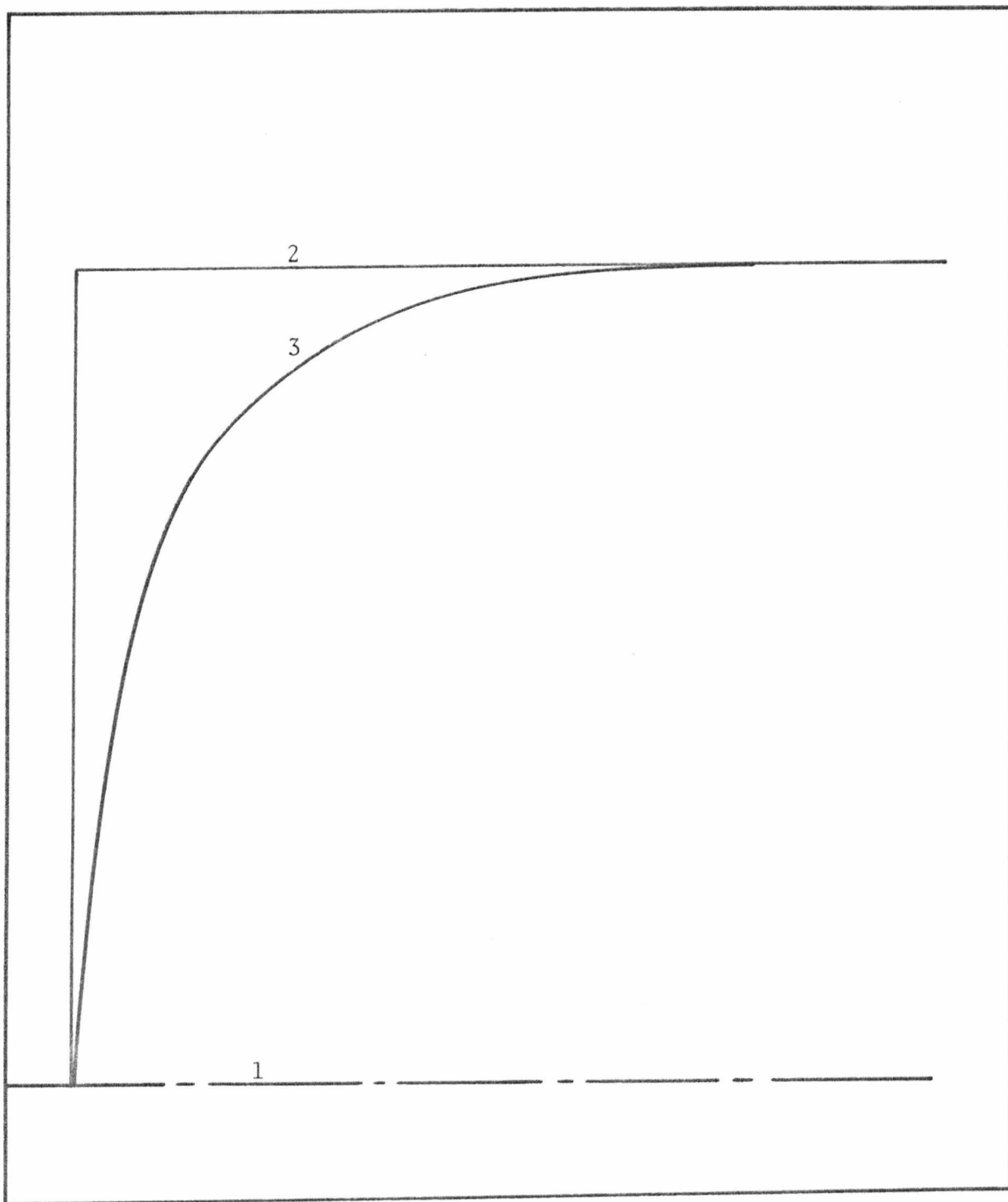


FIGURE 2.8.1.1

RESPONSE OF A CHEMICAL EQUILIBRIUM TO A RAPID TEMPERATURE PERTURBATION

changes in the system are a sum of exponential decay curves (relaxation times). Each relaxation time,  $\tau_i$ , is a function of all the rate constants of the chemical system and is a function of the reactant concentrations. A particular  $\tau$  value will usually have a dependence on only a limited set of rate constants, the others being negligible in comparison.

The relaxation times are characteristic of the chemical system and are independent of the mode of the perturbation.

A general description of relaxation methods will be found in references (12)-(14).

The temperature-jump relaxation spectrometer described here was designed and constructed in consultation with the Mechanical Workshops of this Laboratory.

The instrument described in this work produces a temperature rise in the chemical system by the discharging of a high-voltage capacitor through the solution which contains an inert electrolyte (e.g. NaCl). The instrument has been designed to produce a 1-5K temperature rise in 0.5-5 $\mu$ S. Detection of transient concentration changes is by fluorescence, absorbance and light-scattering.

### 2.8.2 High Voltage Discharge Unit

In a temperature-jump experiment the temperature rise in the sample solution is required such that the heating time is less than  $\tau_{\text{CHEM}}/10$ , where  $\tau_{\text{CHEM}}$  is the chemical relaxation time. The heating time ( $\tau_{\text{H}}$ ) for a capacitor discharge (C) through a conducting solution (resistance R) is given by the relationship  $\tau_{\text{H}} \sim \frac{1}{2}RC$ . The heating time can, therefore, be reduced in either of two ways:

(i) By decreasing the cell resistance (reduced electrode separation,

increased electrode area or the addition of inert electrolyte).

(ii) By decreasing the value of the discharge capacitor.

Since there may be experimental disadvantages in increasing the ionic strength, the most simple method which will reduce the heating time is to reduce the value of the capacitor, which also reduces the magnitude of the temperature rise ( $\Delta T$ ), since  $\Delta T \propto C$  for a fixed discharge voltage. The apparatus has three easily interchangeable capacitors, the values of which are 0.05, 0.02 and 0.01 $\mu$ F. For a cell resistance of 100 $\Omega$  ( $I \sim 0.1$ ) the heating times are 2.5, 1.0 and 0.5 $\mu$ sec. respectively.

The capacitors, capacitor charging and trigger unit were supplied by Hartley Measurements Ltd., Hartley Whitney, Berks. The maximum voltage which may be discharged through the cell is 40kV.

A schematic diagram of the high-voltage supply, spark-gap and trigger unit is shown in figure 2.8.2.1. In this design both the cell electrodes are at earth potential until the spark-gap is triggered. This arrangement is much safer than the normal configuration in which one electrode is held at the discharge voltage until triggering. The design employed here ensures that the capacitor cannot be charged unless the cell is in position. The equipment also has a "dump switch" which allows residual charge to be quickly and safely discharged to earth.

The spark-gap is a simple triggered unit with the trigger electrode at the centre of the cathode. The discharge voltage may be pre-set and varied from 15 to 40kV. The spark-gap is triggered by a 300V pulse which, when fed through the pulse transformer, produces a 30kV triggering "kick" for the spark-gap. The spark-gap may be triggered manually or automatically and in a repetitive mode when the capacitor has been

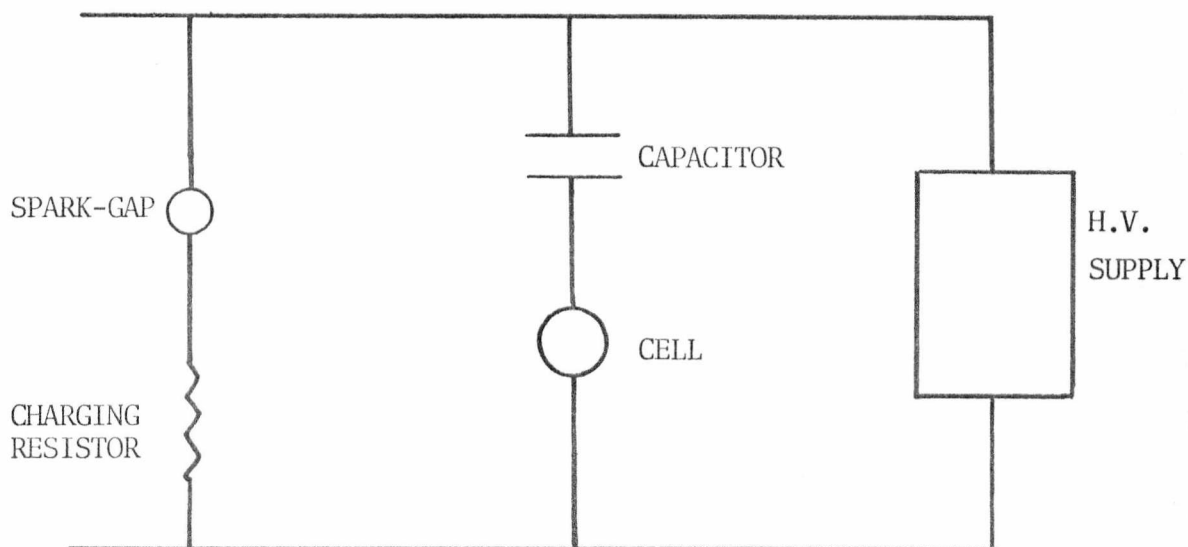


FIGURE 2.8.2.4

CIRCUIT DIAGRAM FOR H.V. SUPPLY & SPARK-GAP

charged to a pre-set voltage.

When the system is used in the repetitive mode, the time interval between discharges may be varied from 0.2 to 60 seconds. This allows solutions to be "jumped" many times in rapid succession. The resulting transients would be recorded and processed by a signal-averaging unit. This procedure will improve the signal-to-noise ratio (the signal-to-noise ratio is improved by a factor of  $\sqrt{N}$ , where  $N$  is the number of measurements). Application of signal-averaging will be useful when the observation of small, noisy transient changes is necessary.

The rapid repetitive "jumping" of a solution will lead to heating of the solution and consequently a gradual change in the observed transients. The repetitive mode would be most useful when very short heating times ( $\sim 0.1 \mu\text{sec.}$ ) are required. The small capacitor necessary to achieve these short heating times will mean that the temperature-jump will be very small ( $\Delta T \sim 0.1\text{K}$ ). Approximately ten jumps may be used before any significant heating of the solution (total temperature rise  $< 1\text{K}$ ) occurs.

In order to employ the repetitive mode without heating the sample solution, a closed circuit flow-through cell would need to be designed. With such a cell any size temperature-jump may be used providing the sample solution can be cooled to the initial temperature before it enters the cell again. This arrangement would allow rapid repetitive jumping of the solution, with a jump repetition rate of 5 per second, 100 jumps could be achieved in just over 20 seconds, and the signal-to-noise ratio would be improved by a factor of  $\sim 10$ .

### 2.8.3 Optical Arrangement

The optical arrangement of the instrument is as shown in figure 2.8.3.1. The light source used is the 100 watt Mercury arc lamp (HBO 100w/2) of Hanovia Inc., New Jersey, N.Y. Pure xenon (Hanovia) and tungsten 50 watt pre-focus projector lamp Al 17 supplied by Woton, West Germany. The light is focused onto the fixed aperture slit of a UV/Vis high intensity grating monochromator (Bausch and Lomb, 33-86-97), which has an aperture ratio of approximately 1:2 and a dispersion of  $3.3\text{nm mm}^{-1}$ , giving a bandpass of 10nm for an exit slit width of 3mm. The lamp power supply was constructed by the Electronics Workshop of this Laboratory (ripple less than 0.05%). The design is similar to that used in the Göttingen Messanlagen, Studiengesellschaft temperature-jump instrument<sup>(15)</sup>.

The lamp and monochromator are rigidly mounted on a track which allows horizontal movement to facilitate focusing. Vertical movement of the lamp and monochromator is achieved by screw-in supports which may be locked at any desired height. The exit end of the monochromator is attached to the cell housing by a tightly fitting split collar which reduces the effects of vibration.

The monochromator exit slit is focused at the centre of the sample

cell (A) by a collimating/focusing pair of lenses (B,CC') focal length 50 and 100mm respectively. The collimating lens (B) may be axially adjusted to correct for chromatic aberation at the focus. The light transmitted through the cell is refocused onto the absorption photo-multiplier (RCAIP28) by a plano-convex collecting lens (D) mounted in the cell holder, focal length 25mm. Facility is provided to replace this lens by a concave parabolic mirror in order to increase the light intensity in the sample cell if fluorescence is to be measured without simultaneous measurements of absorbance.

The fluorescent light emitted at  $90^{\circ}$  (in the horizontal plane) to the excitation beam is focused by collecting lenses (E,F) focal length 25mm onto the fluorescence photomultipliers, (RCAIP21), after passing through a 50mm by 25mm rectangular interference filter (e.g. Jena Veril Verlauf S60 400-700nm) or a 50mm by 25mm rectangular cut-off filter (e.g. Oriel G-770).

At present the lenses are made of glass (Ealing Beck Ltd.) but

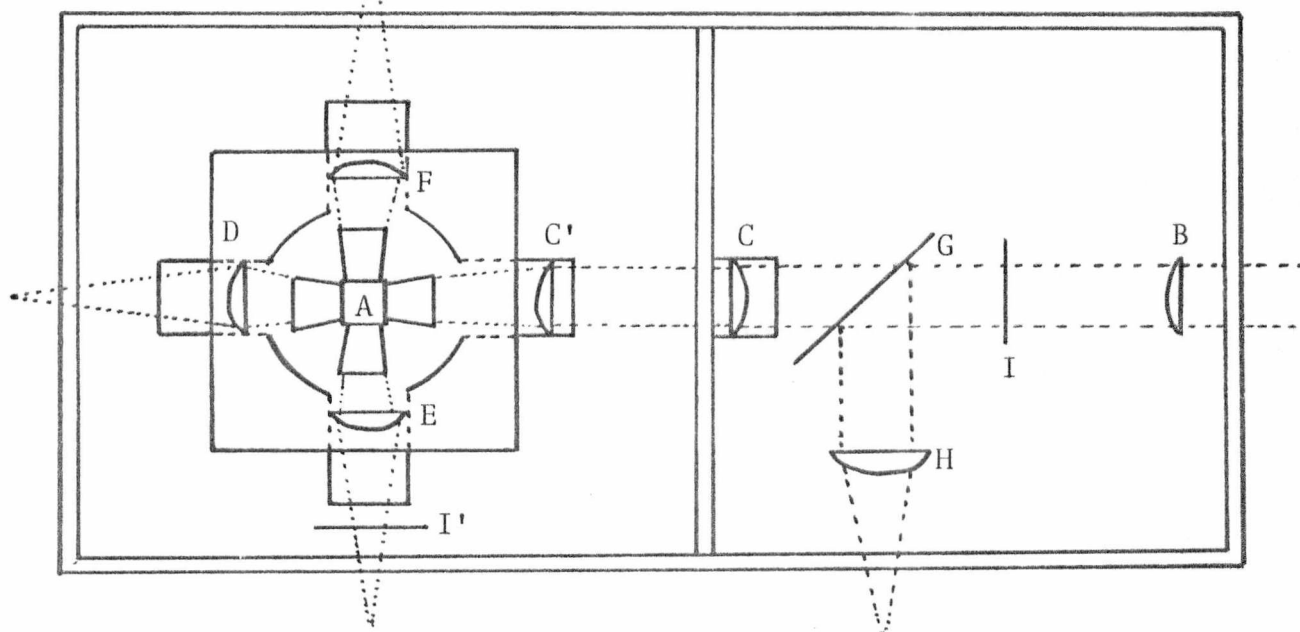


FIGURE 2.8.3.1

OPTICAL ARRANGEMENT OF THE TEMPERATURE-JUMP DETECTION SYSTEM

these could easily be replaced by fused silica lenses to allow operation in the UV region of the spectrum when required.

Part of the excitation light beam is deflected by a fused silica beam splitter (G) (Grubb and Parsons, England), (97% transmittance, 3% reflectance) and focused by a lens (H) onto a reference photomultiplier (RCAIP28).

For measurements of transient changes in polarisation of fluorescence a polariser (I) is inserted in the excitation light beam before the collimating lens. The analyser (I') is inserted between the cell holder and one of the fluorescence photomultipliers. Both polariser and analyser can be rotated through  $360^{\circ} \pm 0.1^{\circ}$  and locked in any position (Ealing Beck No. 22-9161).

Except for the monochromator/light source unit, all the optical components are contained in an aluminium matt-black painted light-tight compartment approximately 300mm x 200mm x 200mm to which the photomultipliers are attached by light-tight aluminium flanges. All the lenses and filters are easily replaced and adapted. The whole optical system is mounted on an optical bench to ensure stability and vibration-free operation.

The lamp and optical components are aligned so that the excitation beam passes through the centre of the temperature-jump cell.

The beam is sufficiently far removed from the electrodes that transient changes at the electrode surfaces do not interfere with the detection of transient optical changes.

A mechanically operated shutter is provided to prevent excessive and damaging illumination of the sample solution and photomultipliers.

#### 2.8.4 The Temperature-Jump Cell

The temperature-jump cell coupled to the optical system described

in the previous section, has been designed to comply with the following requirements

- (i) maximum light throughput,
  - (ii) absence of self-fluorescence and optical strain effects in the cell window materials,
  - (iii) small sample volume,
- and (iv) uniform solution heating.

The temperature-jump cell is similar to that used in the Göttingen Messanlagen Studiengesellschaft temperature-jump instrument<sup>(15)</sup>.

The cell body is machined completely from black Dynal (polyacetal resin). The volume of heated sample liquid is approximately  $1.5\text{cm}^3$  and the total cell liquid volume is approximately  $3\text{cm}^3$ . The absorption path length ( $l$ ) determined by a spectrophotometric method (section 2.8.9) is found to be  $7.35 \pm 0.1\text{mm}$ . The four quartz conical section windows with optically flat faces have an inner diameter of  $6.0\text{mm}$ , and an included angle of  $31^\circ$ .

An enhancement in fluorescence light output could, however, be obtained by fitting emission windows with a larger included angle (up to  $60^\circ$ ) and the outer faces spherically ground.

The electrodes are made of gold capped steel and are designed to produce a "clean" discharge through the solution.

The lower electrode although removable for cleaning, can be firmly fixed in the cell body, and the upper electrode can be removed while the cell is still in the holder. The cell is aligned in the holder by a pin in the holder which fits into a hole in the cell body. The cell is then connected to the high tension lead by a push-fit socket.

The cell is fitted in a square ( $90\text{mm} \times 90\text{mm}$ ) section holder which is thermostatted by means of circulating water through channels drilled

in the holder. The temperature of the thermostat bath for the instrument was controlled by a thermistor device designed by members of the Electronics Workshop of this Laboratory. The temperature could be controlled to  $\pm 0.1^{\circ}\text{C}$  in the range 283-318K.

The temperature of the test solution is monitored by means of a Comark 1604 electronic thermometer. The Cr/Al thermocouple can be placed directly into the test solution through a small (2mm diameter) hole in the top electrode body. The time required to re-establish the initial temperature after a 2K temperature-jump is approximately 3 minutes.

#### 2.8.5 Photomultiplier Heads

To obtain the optimum signal-to-noise ratio for a photomultiplier, the highest possible light levels must be employed, within the region where the photomultiplier response is linear. There are two main sources of noise.

(i) Shot noise. That is the statistical fluctuation of electron emission, caused by the random arrival of photons at the photo cathode. This is the major component of noise in times shorter than 0.1m.sec. In general, the signal-to-noise ratio (S/N) for a photometric detection circuit may be given by equation (2.8.5.1)<sup>(16)</sup>,

$$S/N \propto (\delta I/I) \cdot I_0 \quad (2.8.5.1)$$

where  $I_0$  is the incident light intensity and  $\delta I/I$  is the relative change in light intensity. It can be seen that increasing the incident light intensity,  $I_0$  will increase the signal-to-noise ratio, (see section 2.8.7 for further details).

(ii) Ripple from the monitoring lamp power supply and physical movements of the source can produce interfering noise at longer times

(>0.1 msec.)

For the optical arrangement described here, the photocathode current for the RCAIP28 photomultipliers used for absorption and reference light detection, ranges from  $1 \times 10^{-4}$  to  $1 \times 10^{-7}$  A, whilst that for the RCAIP21 photomultipliers used for fluorescence detection ranges from  $1 \times 10^{-4}$  to  $1 \times 10^{-8}$  A. For maximum efficiency and ease of operation, the photomultipliers are used with dynode-switching circuits (designed by Dr. C.J. Wilson of this Laboratory), the absorption photomultipliers with 4 to 7 dynodes and the fluorescence photomultipliers with 6 to 9 dynodes. The dynode-switching circuits are incorporated directly into the photomultiplier housings and the output is fed to the photometric control unit smoothing circuits by short low loss coaxial cable (capacitance  $50 \text{ pF m}^{-1}$ ).

In order to obtain a fast response time for the detection circuit, the anode load resistance of the photomultipliers is fixed at  $10 \text{ k}\Omega$ . This, together with the capacitance of the coaxial cable and dynode-switching circuit  $\sim 50 \text{ pF}$ , gives a calculated response time of approximately 500 nsec. The response time was accurately measured using a square light pulse obtained from a light emitting diode by switching it with the square-wave voltage generator (4V) from the oscilloscope. The resulting modified voltage-pulse produced at the photomultiplier anode was displayed on the oscilloscope, and the response time calculated. The response time was found to be approximately 600 nsec.

The photomultipliers are powered by a Brandenberg 475R photomultiplier supply. They are shielded with mu-metal to minimise electrostatic/magnetic pick-up from the high-voltage discharge. A further necessary precaution to reduce electrostatic/magnetic pick-up is to electrically isolate the photomultipliers from the light-tight compartment. This is achieved by fixing the photomultiplier heads to the compartment by nylon bolts and earthing the photomultiplier at the oscilloscope or transient recorder.

Since the anode saturation current of the photomultiplier is approximately 1mA and the anode load resistance is 10k $\Omega$ , the measured signal corresponding to saturation (the onset of non-linear response to optical changes) is 10V. In practice, the measured signal is kept below 5V (maximum anode current 500 $\mu$ A) which prevents damage to the photomultipliers. Since noise is introduced as each dynode is added to the chain, the optimum working conditions are high voltage and the smallest possible number of active dynodes which will give a good signal.

The shutter fitted to the light-tight compartment is kept closed except during signal measurement and temperature-jumps to ensure (i) that solutions are not photo-decomposed and (ii) that exposure of the photomultipliers to high anode currents is kept to a minimum.

#### 2.8.6 Photometric Control Unit

The photometric control unit is arranged in the form of an analog computer<sup>(17)</sup> (figure 2.8.6.1). There are four input channels, two fluorescence, one absorbance and a reference. A, B, C and D respectively. Each input signal is processed via an input amplifier with continuously adjustable gain controls in order to set a normalised signal. The input offsets for channels A, B and C are normally switched off, but they can be used for dark current or stray light compensation.

The two main amplifiers R and S have switchable gains of 1, 2 and 5, and can be switched to a number of input signals. The summation amplifier S can select signals A,  $(A+B)/2$ ,  $(A/2)+B$ , B or D, the offset control can be connected to the reference input D or switched off. The differential amplifier R can select signals A, B or  $\pm(A-B)$ , the offset can be connected to D or the output of the summation amplifier.

The output of the amplifiers can be divided R/S and also R/D and S/D. The output stage consists of a rise time filter which enables

smoothing time constants from 1 μsec. to 5 msec. to be used. This time constant must be set at least five times shorter than the relaxation time to be measured. A delay mode, to cancel the effects of the instantaneous fluorescence change which accompanies the temperature rise or fast relaxation processes in multistep relaxation mechanisms is provided by the transient recorder (see details in section 2.10).

In order to normalise signals and control amplitudes, a voltmeter is provided which allows the voltage at various points marked with a square in figure 2.8.6.1 in the circuit to be measured.

The complete temperature-jump instrument is shown in photographs 2.8.1 and 2.8.2.

### 2.8.7 Absorption Measurements

The absorbance  $A$  of a sample at a given wavelength  $\lambda$  is given by

$$A = l \sum_{i=1}^n C_i \epsilon_i \quad (2.8.7.1)$$

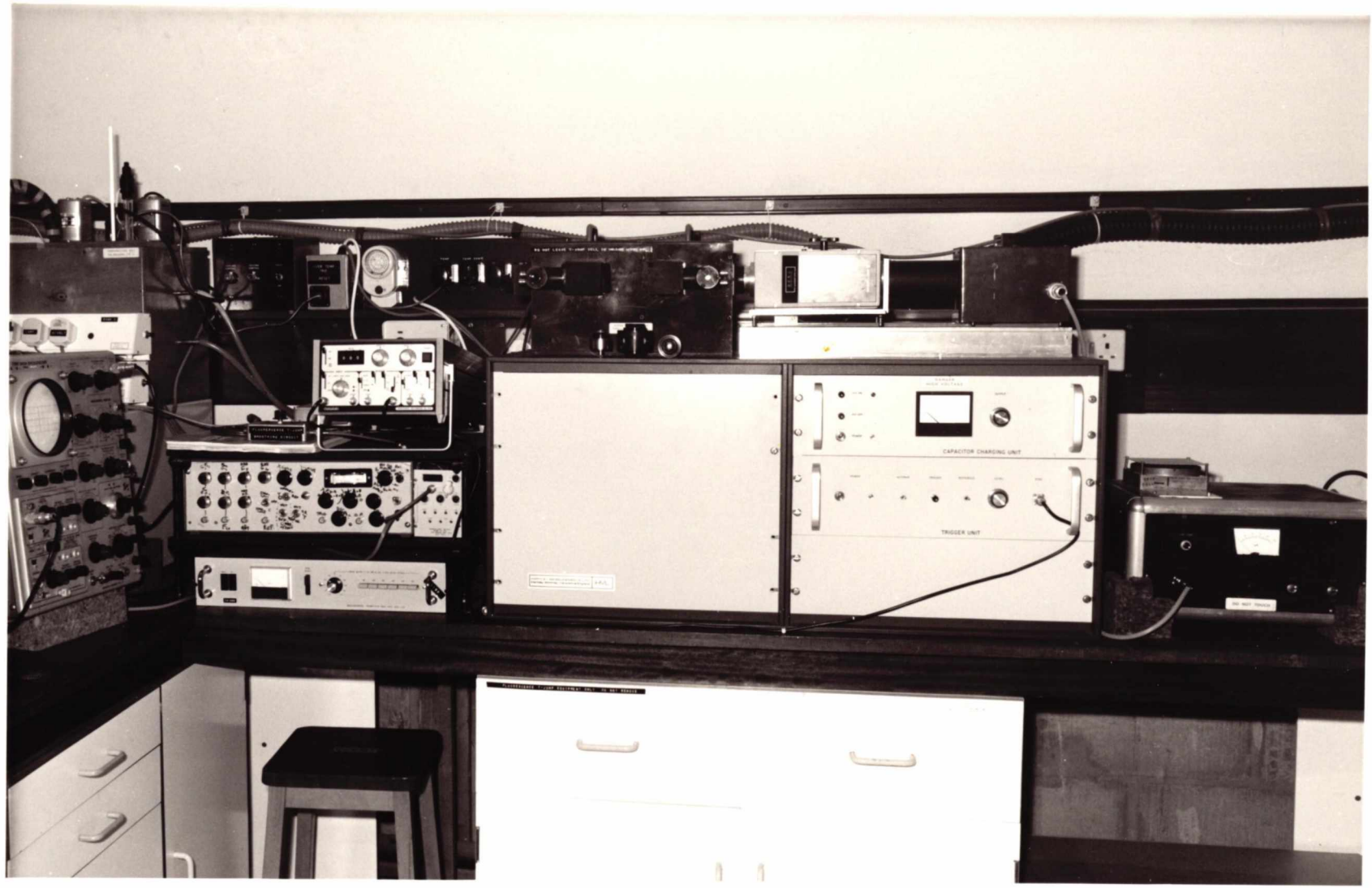
where  $l$  is the absorption path length of the sample cell  $C_i$  and  $\epsilon_i$  are the concentration and molar extinction coefficient of species  $i$ .

If  $I_0$  is the incident light intensity, the Beer-Lambert Law gives the intensity of the transmitted light  $I$  (see figure 2.8.7.1),

$$I = I_0 10^{-A} \quad (2.8.7.2)$$

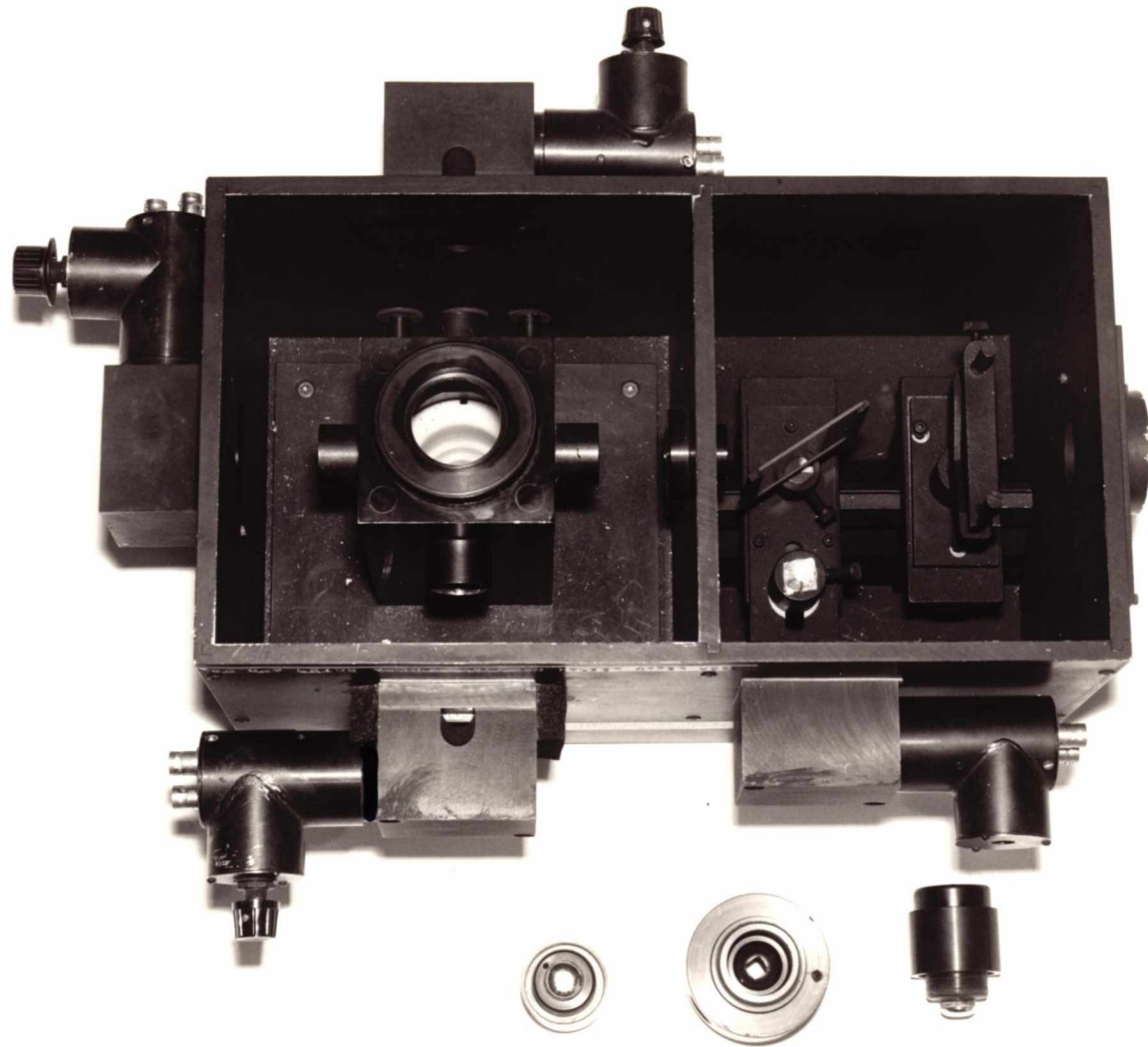
Now, if  $V_0^A$  is the measured photomultiplier signal with water in the cell,  $V_i^A$  and  $V_f^A$  are the signals before and after a temperature-jump perturbation, then the change in absorbance  $\Delta A$  is given by

$$\Delta I/I = \Delta A = \log_{10} V_0^A / V_i^A - \log_{10} V_0^A / V_f^A \quad (2.8.7.3)$$



09

PHOTOGRAPH 2.8.1 : THE TEMPERATURE-JUMP SPECTROMETER



PHOTOGRAPH 2.8.2 : THE TEMPERATURE-JUMP CELL HOLDER AND DETECTION UNIT

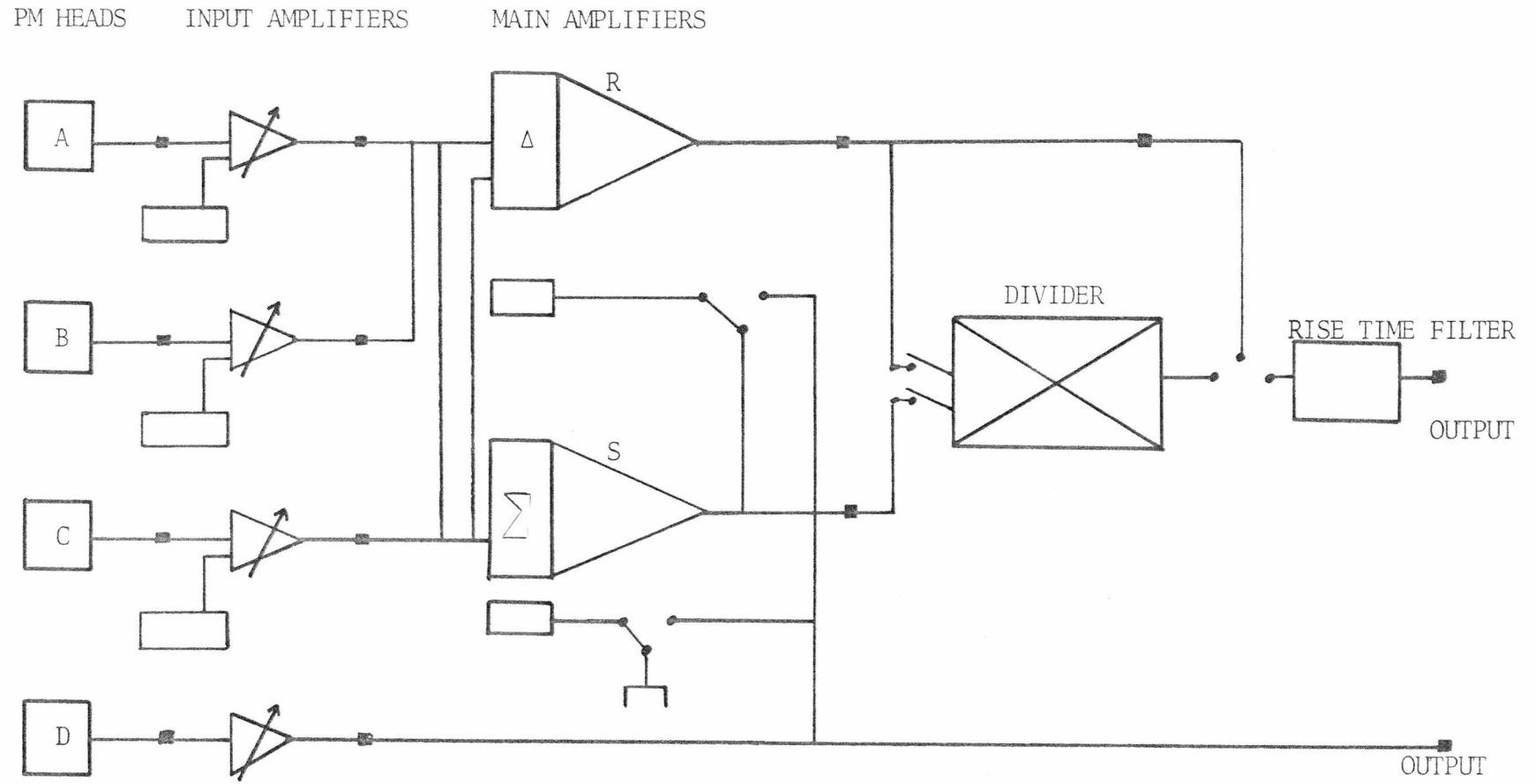


FIGURE 2.8.6.1

PHOTOMETRIC DETECTION CIRCUIT

$$\Delta A = \log_{10} V_f^A / V_i^A \quad (2.8.7.4)$$

Since  $V_f^A = V_i^A \pm \Delta V^A$  equation (2.8.7.4) may be written

$$\Delta A = \log_{10}(1 + \Delta V^A / V_i^A) = 1/2.303 \ln(1 + \Delta V^A / V_i^A) \quad (2.8.7.5)$$

If the percentage signal change is small i.e.  $\Delta V^A / V_i^A < 5\%$ , then we can consider the first term of the expansion of  $\ln(1 + \Delta V^A / V_i^A)$

$$\therefore \Delta A = 1/2.303 \Delta V^A / V_i^A \quad (2.8.7.6)$$

$$\text{or } \Delta V^A = 2.303 \Delta A \cdot V_i^A \quad (2.8.7.7)$$

For absorption measurements the absorption photomultiplier is connected to input channel C. The signal is then processed through amplifier R or S with the offset control set to reference channel D.

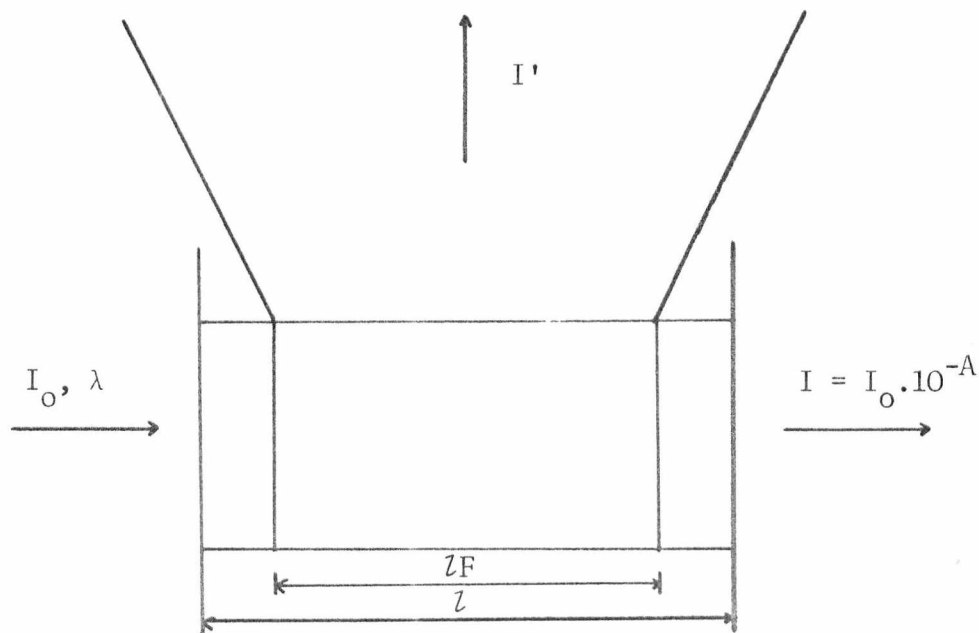


FIGURE 2.8.7.1

TRANSMITTED AND EMITTED LIGHT INTENSITIES

Since the noise in photomultipliers is primarily shot noise, the signal-to-noise ratio  $(S/N)^A$  for absorbance is given by<sup>(12,16)</sup>:

$$(S/N)^A = (\Delta I/I)(2\tau_D I B(\lambda)/P)^{\frac{1}{2}} \quad (2.8.7.8)$$

where  $\tau_D$  is the detector rise time,  $B(\lambda)$  is the photo sensitivity at wavelength  $\lambda$  and  $P$  is a noise factor which takes into account the noise due to secondary emission at the dynode surfaces.

Substituting for  $I$  from equation (2.8.7.2)

$$(S/N)^A = \left(\frac{\Delta A}{A}\right) A 10^{-A/2} (2\tau_D I_0 B(\lambda)/P)^{\frac{1}{2}} \quad (2.8.7.9)$$

### 2.8.8 Fluorescence Measurements

The total fluorescence over all angles  $I^F$  of a sample at excitation and emission wavelengths  $\lambda_{ex}$ ,  $\lambda_{em}$  respectively is given by<sup>(17)</sup>

$$I^F = 2.303 \sum_{i=1}^n C_i \epsilon_i \phi_i \quad (2.8.8.1)$$

where  $\phi_i$  is the quantum yield of species  $i$ .

The measured fluorescence intensity  $F$  of a sample is dependent on the path length  $l^F$ , the spherical angle of fluorescence  $\alpha$ , the incident light  $F_0$  and the absorbance of the solution over the path length  $l^F$ ,  $A^F$ .

$$F = F_0 e^{-A/2} \cdot \left( \frac{\sinh A^F/2}{A^F/2} \right) \frac{2}{4\pi} - l^F I^F \quad (2.8.8.2)$$

The relative fluorescence change  $\Delta F/F$  following a temperature-jump perturbation is given by

$$\Delta F/F = \Delta V^F/V^F = \Delta I^F/I^F - (l/2 - (l^F) \cdot A/12) \partial A - \left( \frac{\partial \ln I^F}{\partial T} \right) \partial T \quad C_1 - C_n \quad (2.8.8.3)$$

where  $V^F$  is the initial signal at the photomultiplier and  $\Delta V^F$  is the signal change.

The first and second terms represent the chemical contributions. The second term reflects the "inner-filter effect" at wavelength  $\lambda_{ex}$ . The third term represents the instantaneous change in the quantum yield with temperature, this must be separated from the chemical relaxation process.

For fluorescence measurements the output from both fluorescence photomultipliers are normally fed into channels A and B. The signals are equalised, summed in amplifier S to give  $(A+B)/2$ . The combination of both signals increase the overall signal-to-noise ratio. Offset S is set to reference channel D.

Analogous to equation (2.8.7.8) the signal-to-noise ratio for fluorescence  $(S/N)^F$  is given by

$$(S/N)^F = (\Delta F/F) (2\tau_D F B(\lambda)/P)^{1/2} \quad (2.8.8.4)$$

### 2.8.9 Determination of the Absorption Path Length ( $l_{TJ}$ ) and Temperature Rise of the Cell

For accurate amplitude analysis the path length of the temperature-jump cell must be known, also the temperature rise for a given discharge voltage must be accurately determined.

The path length of the cell was determined using a solution of acridine orange approximately  $2 \times 10^{-5} M$  containing  $2.0 \times 10^{-1} M$  sodium chloride. The spectrum of this solution is shown in figure 2.8.9.1.

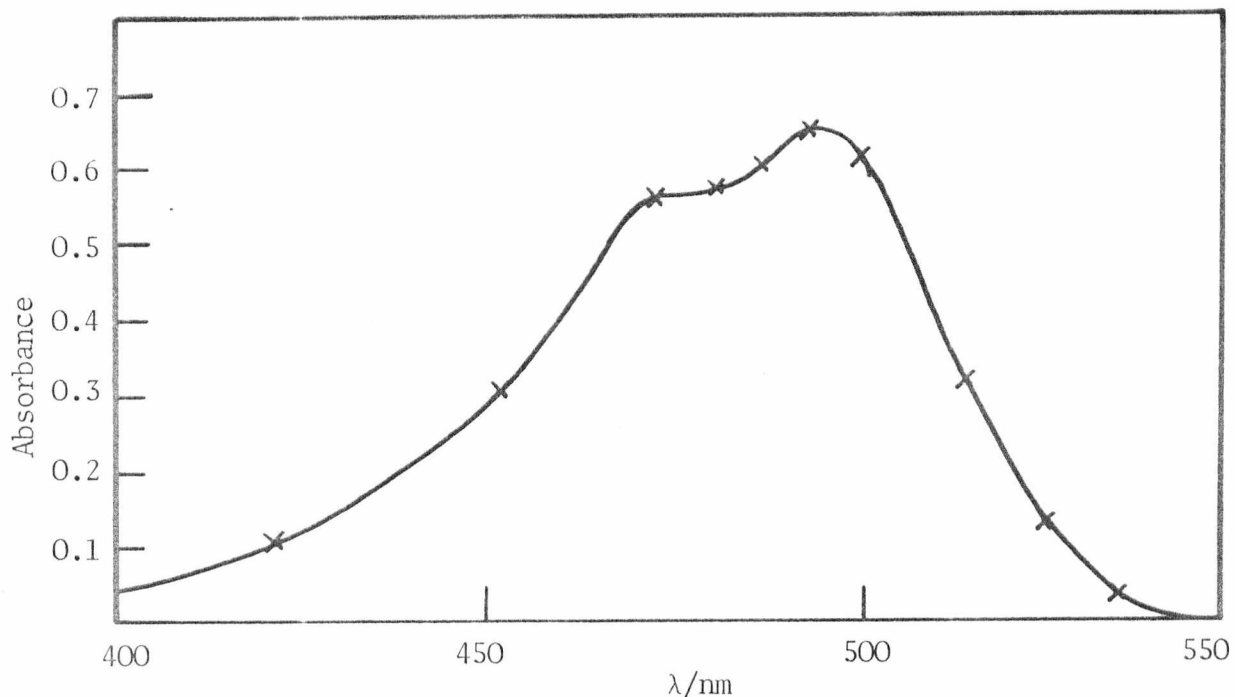


FIGURE 2.8.9.1

SPECTRUM OF ACRIDINE ORANGE USED IN THE PATH LENGTH DETERMINATION

The transmitted light falling on the absorption photomultiplier gives a signal  $V_0$  volts when water is in the cell.  $V_0$  is measured at various wavelengths between 400 and 550 nm. This will take account of the wavelength-dependent sensitivity of the photomultiplier surface and the wavelength-dependent intensity of the lamp. The transmitted light with acridine orange in the cell  $V$  is then measured at the same wavelengths. The calculated absorbance  $\log_{10} V_0/V (A_{TJ})$  is then compared with the absorbance determined in the spectrophotometer ( $A_{SP}$ ). The results are shown in table 2.8.9.1.

It can be seen that the values determined are wavelength dependent, this is because of the bandpass of the optical system (exit slit width 3mm, bandpass ~10nm). From the area of the curve to the positive and negative side of the mean wavelength, values between 470 and 500nm should give values close to the true path length. The very inaccurate values obtained at the either extreme of the wavelength range may also be due to the very low absorbance of the test solution i.e. small inaccuracies

in the determination of  $V$  will greatly effect the absorbance measured.

TABLE 2.8.9.1

ABSORPTION PATH LENGTH DETERMINATION OF THE TEMPERATURE JUMP CELL

Temp. 298.2K; Test solution  $2 \times 10^{-5} \text{M. AO}^+ / 2.0 \times 10^{-1} \text{M. NaCl}$

$\lambda_{\text{nm}}$	$A_{\text{SP}}$	<u>SIGNAL</u>		$A_{\text{TJ}}$	$l_{\text{TJ}}/\text{mm}$
		Water $V_0/\text{volts}$	$\text{AO}^+ V/\text{volts}$		
400	0.05	0.80	0.65	0.08	16.0
410	0.07	0.88	0.78	0.04	7.0
420	0.11	1.30	0.88	0.17	15.0
450	0.31	1.65	0.90	0.26	8.5
470	0.56	2.01	0.76	0.42	7.5
480	0.58	2.05	0.74	0.43	7.4
490	0.63	2.10	0.72	0.42	7.3
500	0.57	2.20	0.83	0.42	7.2
510	0.31	2.35	1.40	0.28	9.0
520	0.11	2.65	2.00	0.11	10.0
530	0.04	2.80	2.61	0.03	8.5
550	0.0	3.0	3.0	0.0	10.0

Mean of values for which the slit width error is small =  $7.35 \pm 0.1 \text{mm}$

As shown in the path length determination, the bandpass of the excitation beam can seriously affect the calculated value of  $l_{\text{TJ}}$ , it will also seriously affect the measured amplitude of any relaxation process. For the determination of activation parameters from relaxation amplitudes, the amplitude must be known at zero-slit-width. This must be separately determined for each system under study. To determine the temperature rise in the cell, ( $\Delta T$ ), the absorbance change with temperature of a test solution in the spectrophotometer is compared with the

absorbance change in the temperature-jump cell for a given discharge voltage ( $V_{DIS}$ ). Since the amplitude is dependent on the bandpass of the optical system, the amplitude must be determined at zero-slit width if an accurate measure of the temperature rise is to be achieved.

The absorbance change ( $\Delta A$ ) at 580nm for a solution of cresol red, approximately  $3 \times 10^{-5} M$  (pH = 7.8, 0.15M sodium nitrate,  $1 \times 10^{-1} M$  tris buffer) is found to be 0.00980 optical density units  $K^{-1}$  (figure 2.8.9.2). This solution is then subjected to a temperature-jump of various magnitudes. The jumps are repeated at three different slit-width combinations (5.36/3.0, 2.68/1.56 and 1.34/0.75mm). The amplitudes observed ( $\Delta V_O^A$ ) are measured to an accuracy of  $\pm 2mV$  by enlarging the photographic traces onto graph paper. A plot of amplitudes versus slit width is made and the amplitude is extrapolated to zero-slit width ( $\Delta V_O^A$ ) (figure 2.8.9.3). All the amplitudes are normalised to an input signal  $V^A$  of 4.3 volts.

The relation between observed amplitude  $\Delta V_O$ , input signal  $V$ , path length  $l_{TJ}$  and absorbance change  $\Delta A$  is given by equation 2.8.9.1 (see section 2.8.7 for derivation of equation 2.8.9.1)

$$\Delta V_O^A = 2.303 V^A \cdot l_{TJ} \cdot \Delta A \quad (2.8.9.1)$$

For  $V^A = 4.3$  volts

$$l = 0.73 \text{ cm.} \quad \Delta V_O^A = 7.17 \Delta A$$

i.e. 10mV = 0.0014 Optical density units.

The absorbance change in the temperature jump cell  $\Delta A_{TJ}$  is simply related to  $\Delta A$ ;  $\Delta A_{TJ} = l_{TJ} \Delta A$ .

Therefore, for the cresol red system:

$$\Delta A_{TJ} = l_{TJ} \times 0.0098 \text{ for } \Delta T = 1K$$

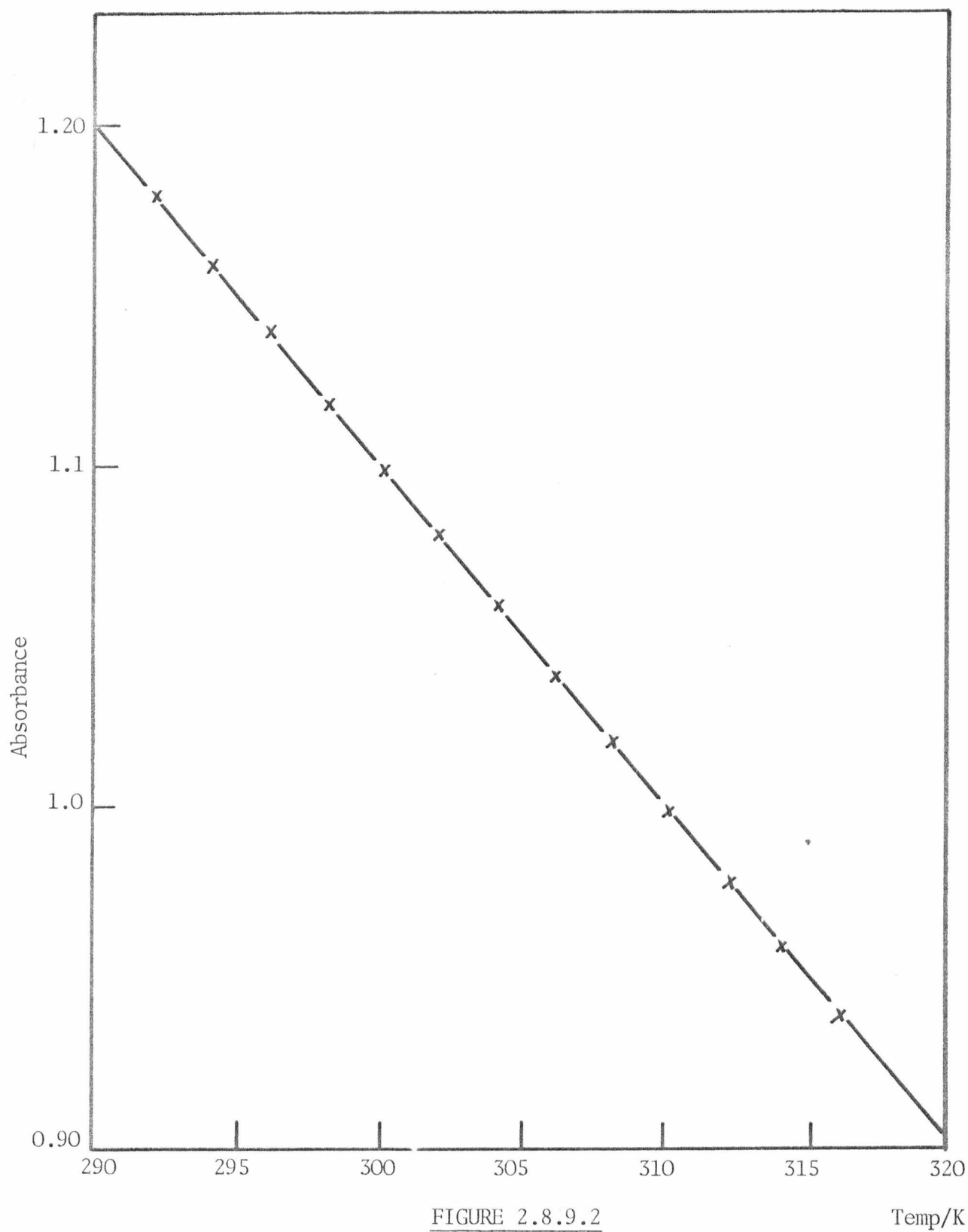


FIGURE 2.8.9.2

Temp/K

DETERMINATION OF THE TEMPERATURE COEFFICIENT OF THE ABSORBANCE OF CRESOL RED

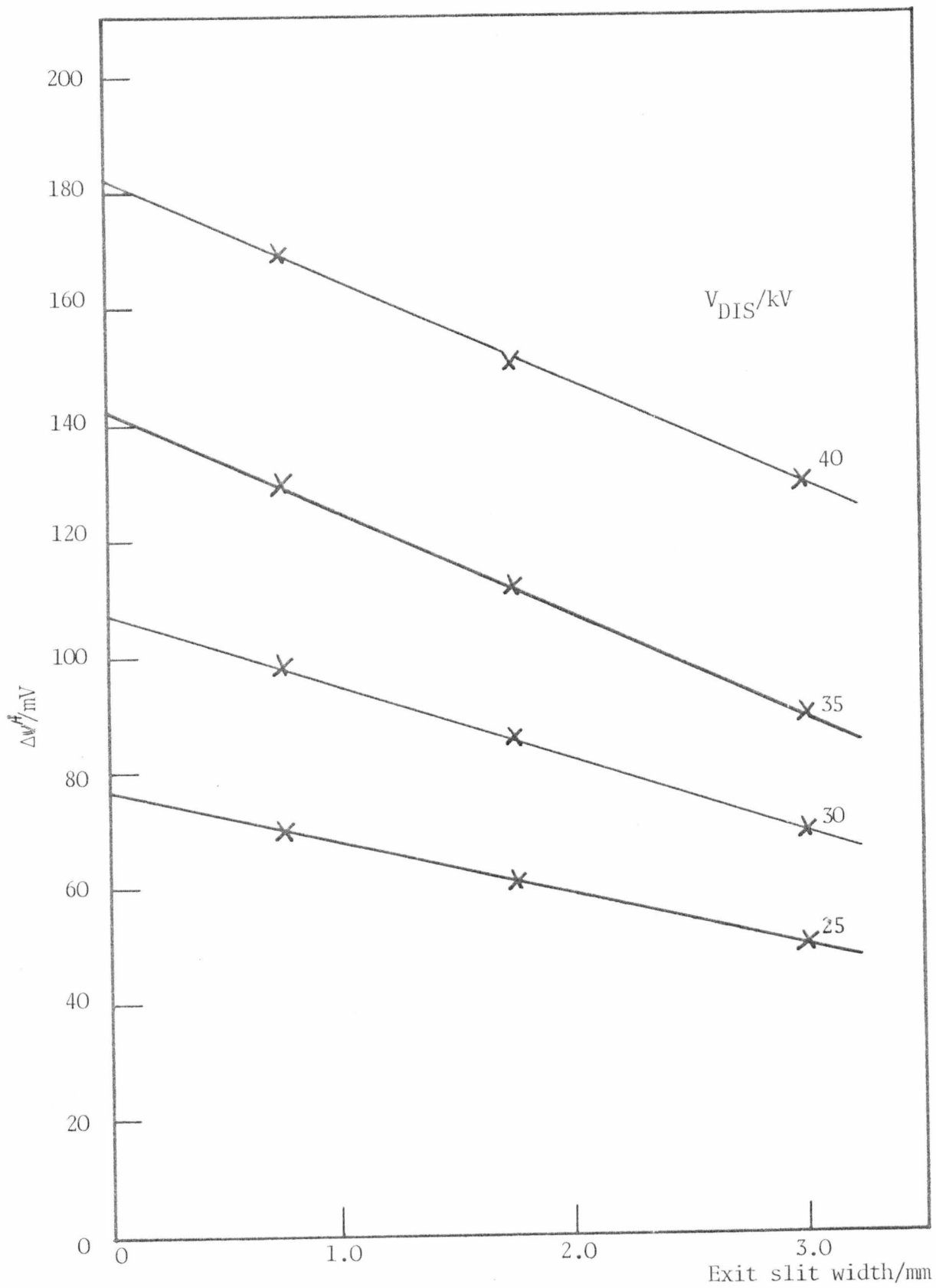


FIGURE 2.8.9.3

DETERMINATION OF SIGNAL AMPLITUDE AT ZERO-SLIT WIDTH

$$\therefore \Delta V_O = 7.17 \times 0.73 \times 0.0098 \times 10^3$$

$$\underline{\Delta V_O = 70\text{mV K}^{-1}}$$

The temperature rise of a solution for a given discharge voltage is therefore simple to calculate. The results are shown in figure 2.8.9.4.

The mass of sample heated may be calculated from the relationship

$$\frac{1}{2} CV_{\text{DIS}}^2 = M C_p \Delta T$$

C = capacitor  
M = mass of sample  
C<sub>p</sub> = specific heat of water

For V = 30x10<sup>3</sup> volts, C = 0.02μF, ΔT = 1.5K

$$\frac{1}{2} \times 0.02 \times 10^{-6} \times (30)^2 \times 10^6 = M \times 4.18 \times 1.5$$

$$9 = 6.27M$$

$$\underline{M = 1.43\text{g}}$$

#### 2.8.10 Evaluation of the Performance of the Temperature-Jump

##### Instrument

Two systems have been chosen to evaluate the performance of the temperature-jump instrument. The interaction between the dye proflavine and Calf-Thymus DNA is well characterised and has been studied by absorbance and fluorescence temperature-jump spectrometry<sup>(17,18)</sup>. This system has a characteristic relaxation time in the millisecond region. The second test system used in the dimerisation of acridine orange in aqueous solution<sup>(19)</sup>. The characteristic relaxation time is of the order of 10-20μsec. and allows an estimation of the quality of the machine for the observation of very rapid processes.

A detailed account of the wavelength dependence of the absorption signal-to-noise ratio will not be given, except to say that in the range 350-700nm it is greater than 10<sup>3</sup>, and at the maximum efficiency

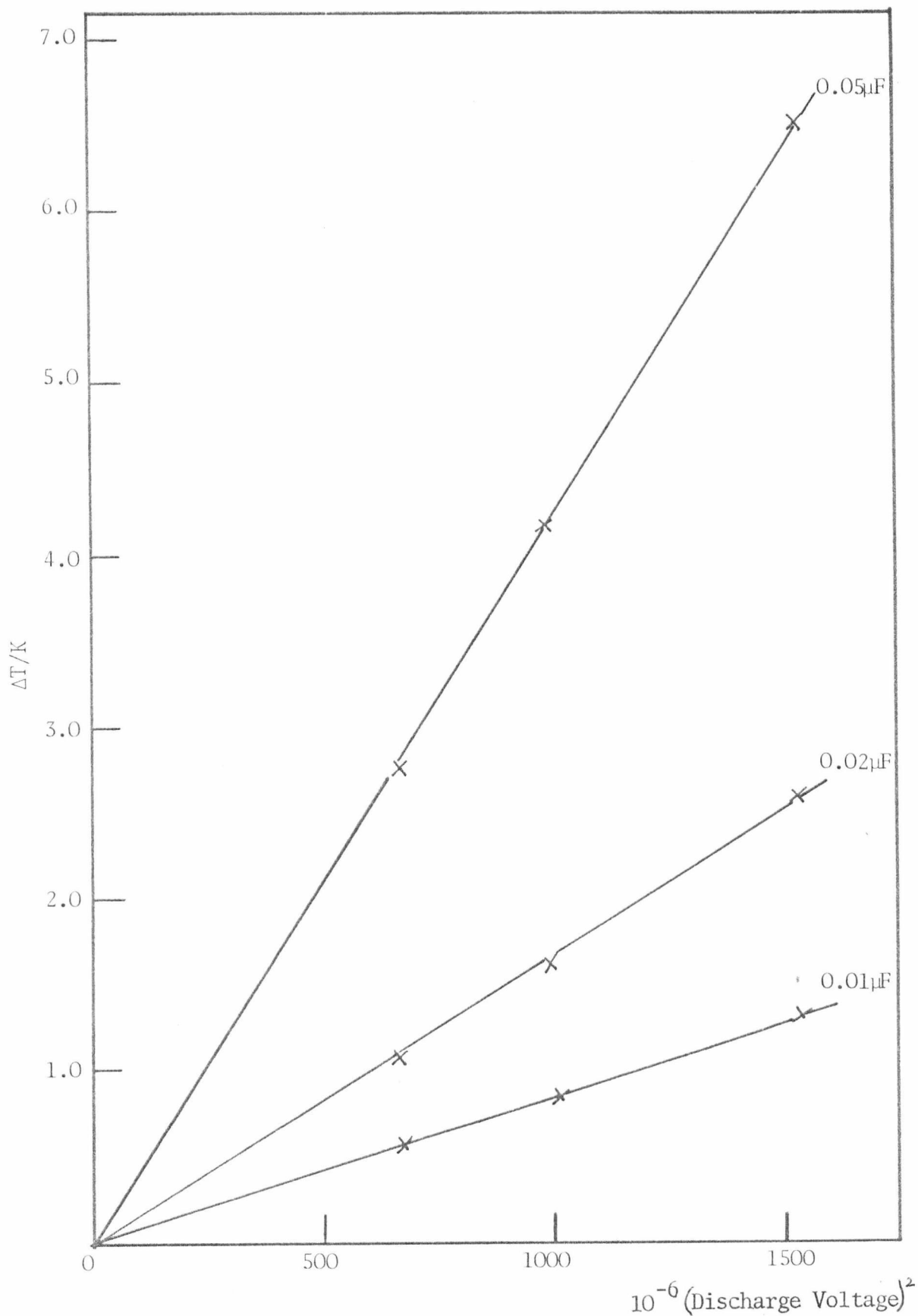


FIGURE 2.8.9.4

DETERMINATION OF THE TEMPERATURE RISE IN THE T-JUMP CELL

of the lamp (50 watt tungsten), monochromator and photomultiplier (~500nm) it is close to  $10^4$  (for a bandwidth of 1MHz).

The wavelength dependence of the fluorescence signal-to-noise ratio is more difficult to measure, since it would require a wide range of fluorescent species to cover a range of wavelengths. For the proflavine/DNA system  $\lambda_{ex}$  444nm,  $\lambda_{em}$  all wavelengths above 490nm, it is approximately 150.

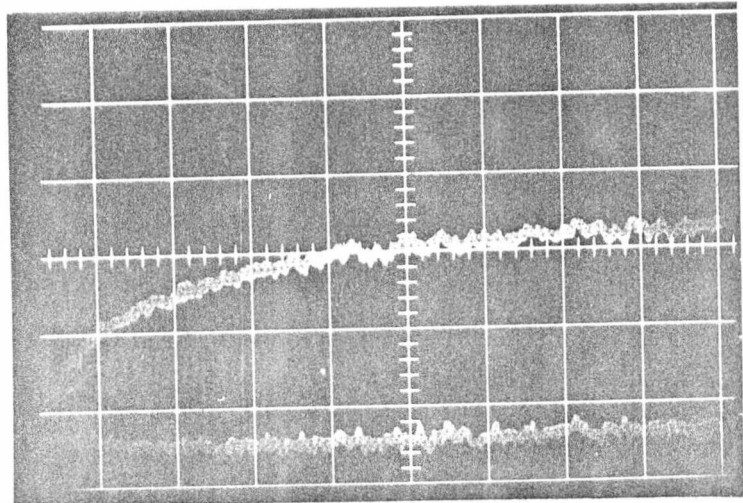
Although often quoted the signal-to-noise ratio in itself does not give any real indication of the quality of the traces which may be obtained. The quality of the traces, overall sensitivity and accuracy which may be obtained depend on the signal change-to-noise ratio,  $\Delta V/N$ .

The proflavine/DNA system has been used to assess absorption and fluorescence performance of the temperature-jump instrument in the millisecond time region. The experimental conditions were as follows.

Proflavine concentration  $3 \times 10^{-6} M$ , Calf-Thymus DNA (molecular weight  $2 \times 10^7$ ) sufficient to give a phosphate-to-dye ratio (P/D) of 20,  $< 0.5 mM$  EDTA,  $0.03 M$  K-phosphate buffer,  $pH = 7.3$ ,  $0.1 K Cl$ , final temperature  $298.2 K$ .

The light source was the 50 watt tungsten lamp, excitation wavelength 444nm. The total fluorescence above 490nm was observed using a cut-off filter (Oriel G770-475). For absorbance measurements the photomultiplier was operated at 500 volts with 5 active dynodes (total signal 4.5 volts). Fluorescence measurements were made using one photomultiplier operated at 800V with 8 active dynodes (total signal 1.5 volts, scattered light, water only in cell, 50mV). A temperature rise of 1.5K was achieved by the discharge of the  $0.02 \mu F$  capacitor at 30kV. Monochromator exit slit 3mm.

Sample traces are shown in figures 2.8.10.1 a-c. The bandwidth of the detection system is  $30 \mu S$ , for absorbance and fluorescence measurements.



(a)  $\text{PF}^+$ /DNA A

$$[\text{PF}^+] = 3 \times 10^{-6} \text{M}$$

$$P/D = 20$$

$$\mu = 0.1 (\text{KCl}),$$

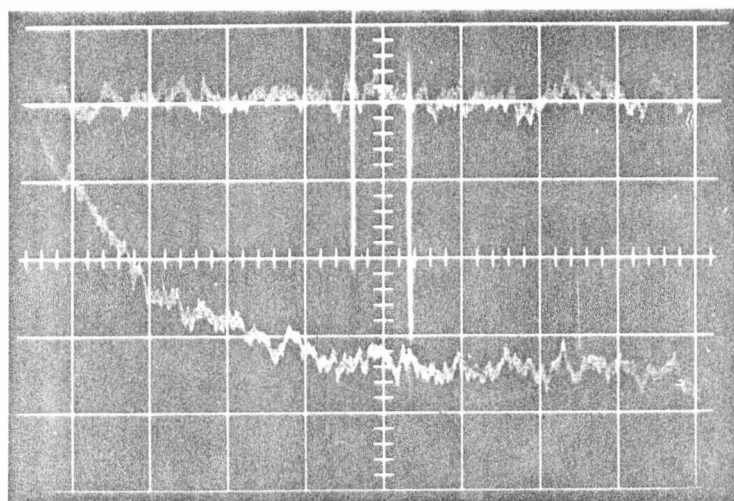
$$\text{pH} = 7.3,$$

$$V^0 = 4.2 \text{V}.$$

$$\lambda = 444 \text{nm}, 500 \mu\text{s}/5 \text{mV}$$

$$\text{Temp. } 298.2 \text{K}$$

$$\Delta A = 0.05\%$$



(b)  $\text{PF}^+$ /DNA F

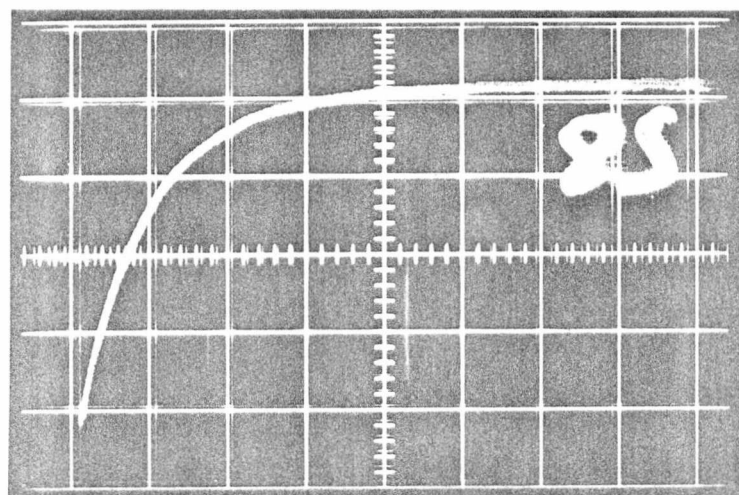
$$\lambda_{\text{ex}} = 444 \text{nm}, \lambda_{\text{em}} > 475 \text{nm}$$

$$V^0 = 1.5 \text{V}$$

$$500 \mu\text{s}/10 \text{mV}$$

$$\text{Temp. } 298.2 \text{K}$$

$$\Delta F = 0.25\%$$



(c)  $\text{AO}^+$  A

$$[\text{AO}^+] = 1 \times 10^{-5} \text{M}$$

$$\mu = 0.1 (\text{NaCl}),$$

$$\text{pH} \approx 7,$$

$$V^0 = 4.2 \text{V}.$$

$$\lambda = 492 \text{nm}, 20 \mu\text{s}/10 \text{mV}$$

$$\text{Temp. } 298.2 \text{K}$$

$$\Delta A = 0.20\%$$

FIGURE 2.8.10.1  
TYPICAL TEMPERATURE-JUMP TRANSIENTS

The absorbance signal-change-to-noise ratio is approximately 20, and for fluorescence it is approximately 10.

The absorbance change is 6mV in 4.5 volts, a transmittance change of 0.15%, and corresponds to a change in absorbance of the solution of 0.0008. The change in fluorescence intensity is approximately 1.5%. The measured relaxation-time is in good agreement with the published values<sup>(17,18)</sup>. Rigler et al quote a relaxation time of  $0.9 \pm 0.05$  msec., the result obtained in this work is  $0.97 \pm 0.1$  msec.

Under the present operating conditions with the proflavine/DNA system, the temperature-jump instrument compares very favourably with the commercial instruments currently available. Small increases in the overall sensitivity may be achieved if a more powerful light source is used, but further improvements are unlikely to be achieved.

Very few instruments with fluorescence detection have been reported<sup>(17,20,21)</sup> and even fewer experimental traces have been published, which makes comparison between instruments difficult. However, the instrument reported by Rigler et al seems to have the best published performance to date. Using the same test system as that employed here, but with a temperature-jump 3.3 times as large the fluorescence signal change-to-noise ratio is  $\approx 100$ . This is  $\approx 3$  times better than that reported here, (allowing for the difference in the size of the temperature-jump).

The dimerisation of acridine orange was used to test the operation of the instrument in the  $\mu$ sec. time region. The experimental conditions were as follows:

Acridine orange concentration  $1 \times 10^{-5}$  M, 0.1 NaCl, final temperature 298.2K.

The light source was the 50 watt tungsten lamp, the observation

wavelength was 492nm. The absorbance photomultiplier was operated at 600 volts with 6 active dynodes (total signal 4.5 volts). A temperature-jump of 1.5K was achieved by the discharge of the 0.2 $\mu$ F capacitor at 30kV. Monochromator exit slit 3mm.

A sample trace is shown in figure 2.8.10.1 d. The bandwidth of the detection system is 1 $\mu$ S. The absorbance signal-change-to-noise ratio is approximately 30.

The absorbance change is 35mV in 4.5 volts a transmittance change of 0.77% and corresponds to a change in absorbance of the solution of 0.049. The measured relaxation time is in good agreement with the published values. Robinson et al<sup>(19)</sup> quote a relaxation time of 14 $\mu$ S, the result obtained in this test is 14.1 $\mu$ S $\pm$ 1.5.

Under the present operating conditions with the acridine orange system, the temperature-jump instrument compares very favourably with the commercial instruments currently available.

The longest relaxation time which can be measured is determined by how rapidly cooling of the solution after the temperature jump will cause convection currents which will affect the measured signal. This time may be determined as follows. A system with a relaxation time of less than 10ms is subjected to a temperature-jump. The change in absorbance is measured on a long time base ( $\geq$ 0.1s). The deviation of the observed trace from the horizontal (following the rapid relaxation) will give an indication of the maximum time before cooling affect the trace. Using the acridine orange system in this instrument this time is  $\sim$ 0.5s i.e. the longest relaxation time which may be accurately determined is  $\sim$ 0.4s.

The overall fluorescence signal-change-to-noise ratio of our instrument would be improved by: (see equations 2.8.8.2,4)

- (1) using a more powerful light source e.g. a xenon or mercury arc lamp;

- (2) employing both fluorescence photomultipliers in parallel (increase  $(\Delta V^F/N)^F$  by  $\sim 2$ );
- (3) improvement of the optical system, mainly by using fish-eye conical windows in the temperature jump cell;
- (4) increasing the size of the temperature-jump.

Increasing the light intensity would bring about the largest improvement in  $(\Delta V^F/N)^F$ . For the proflavine/DNA system discussed above, excitation by the 436nm line of a 100 watt mercury arc lamp will increase the fluorescence signal by a factor of  $\sim 5$ . This allows a reduction in the number of active dynodes employed and a reduction in the photomultiplier voltage to be made. This results in an increase in the signal-change-to-noise ratio of  $\sim 3$ .

## 2.9 Description of the Stopped-Flow Instrument

### 2.9.1 Introduction

The stopped-flow instrument employed in the course of this work has been largely described<sup>(22)</sup>. A block diagram of the instrument is shown in figure 2.9.1.1.

Several modifications have been made to the basic design in the course of this work. The instrument has been adapted for observation of fluorescence and light-scattering changes, and several minor design faults, which became apparent with prolonged operation over several years, have been eliminated.

The previously undetermined machine parameters, path length and dead-time have been measured.

### 2.9.2 Modifications

The major change necessary to adopt the existing instrument to enable the detection of fluorescence and light-scattering changes has been to fit flexible quartz fibre-optic light-guides (Schott, Jena, Mainz, W.Germany) A and B in figure 2.9.1.1. These 0.5m light guides have an optical aperture (diameter) of 2mm and a transmittance decrease of 20%/m. The light guide A transmits the light output from a light source (C) and a Bausch and Lomb (excitation) High Intensity UV/Vis 33-86-79 monochromator (D) to the observation cell of the stopped-flow instrument (E). Each end is rigidly fixed to monochromator (D) and and detection block (F) respectively. This arrangement considerably reduces the effects of vibration on stopping the flow. The absorption photomultiplier (G) (RCAIP28) is fitted with a dynode switching circuit (1-4 active dynodes), and the load resistance is 100k $\Omega$ .

The other quartz light-guide (B) is rigidly fixed into the vertical iris of the detection block, so that emission is at 90<sup>0</sup>, to the excitation beam; the other end is connected to the entrance slit of a second Bausch and Lomb (emission) High Intensity UV/Vis 33-86-79 monochromator (H). Since fluorescent light intensities are usually very low, the emission photomultiplier (I), (RCAIP28), is fitted with a dynode switching circuit (7-9 active dynodes), the load resistance is again 100k $\Omega$ . For both absorbance and fluorescence photomultipliers, the dynode switching circuit, together with an RC smoothing circuit (0.1, 1, 2, 5 & 10m. Sec. time constants), are housed in a box fitted directly to the photomultiplier (J,K).

The original drive syringes (Summit 1cm<sup>3</sup>) were found to be prone to leakage, due to poorly machined pistons and non-circular syringe barrels. There was also an alignment problem since tip and barrel were out of line. They have been replaced by 1cm<sup>3</sup> gas-tight precision syringes (Precision

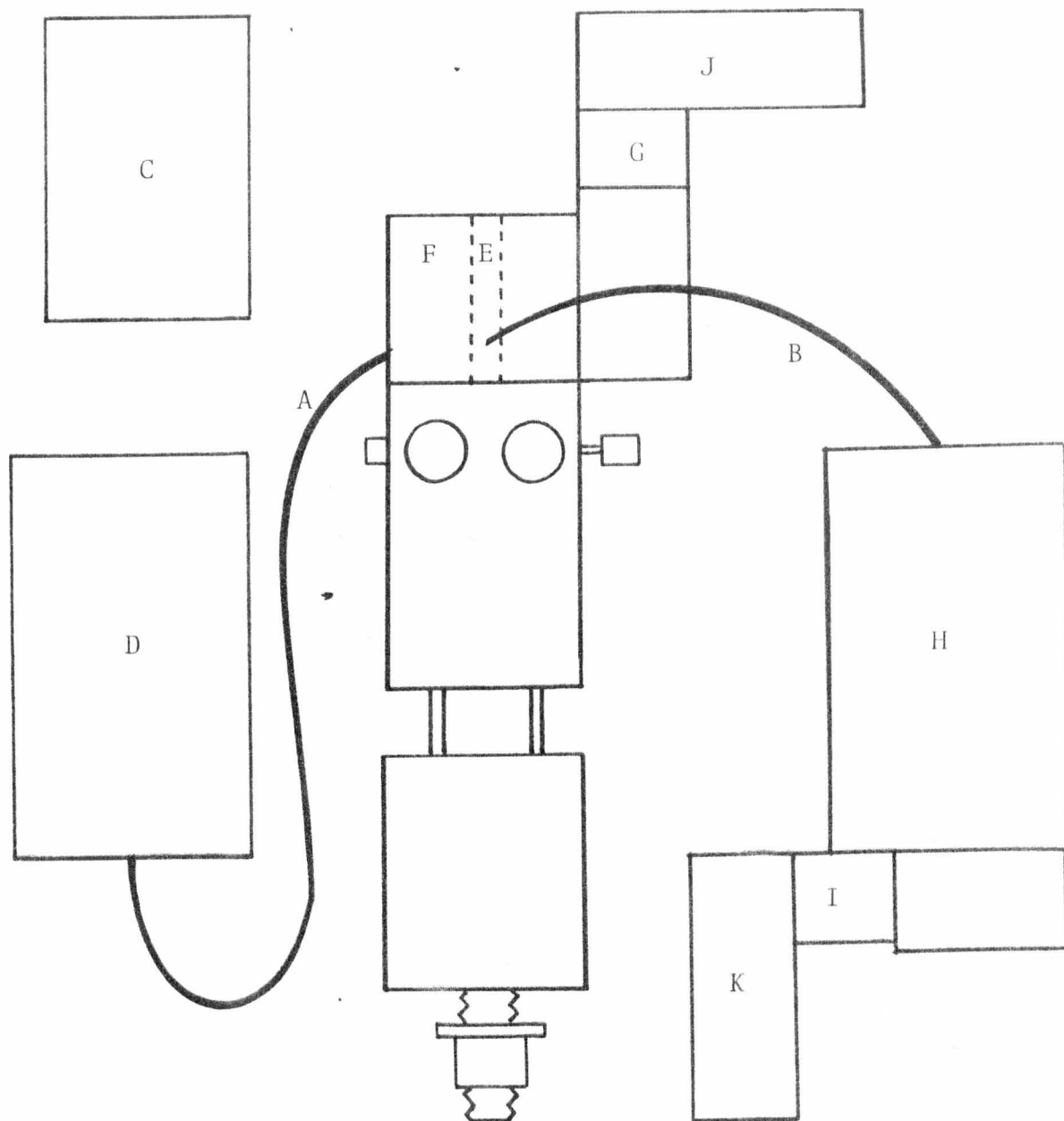


FIGURE 2.9.1.1

BLOCK DIAGRAM OF THE STOPPED FLOW INSTRUMENT

Sampling Corporation, Baton Rouge, Louisiana, U.S.A.). These also ensure that equal volumes of reagent solutions are delivered from each syringe.

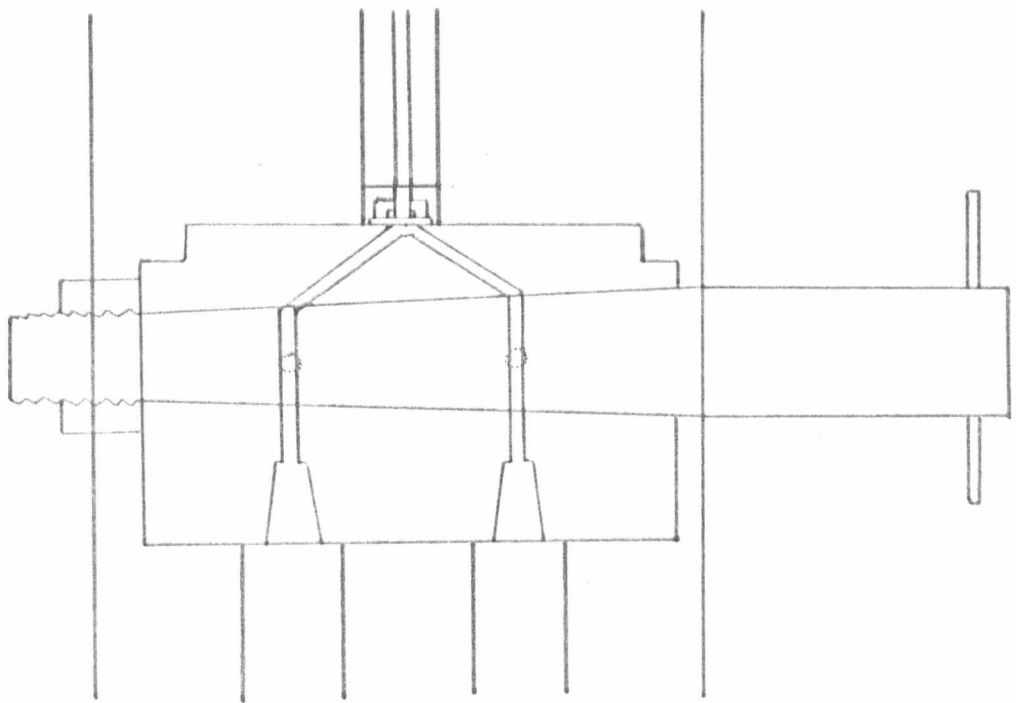
It is known that the volume of solution delivered per run does not affect the transients unless it falls below a critical value when pre-back diffusion may effect the value of the observed rate<sup>(23)</sup>. For this apparatus this volume is approximately 75 $\mu$ l per syringe. In practice, the usual volume delivered is greater than 100 $\mu$ l. This ensures that both the transient time constants and amplitudes are not distorted by insufficient clearing out of aged solution from the mixer-observation chamber region.

After continuous use for some years the original three-way central control adjustable tapered Teflon tap in figure 2.9.2.1 a, began to leak. The manufacture of new tap Ke-F block combinations did not solve the problem, which was thought to be due to the poor quality of the new batch of Ke-F supplied which resulted in rapid deformation of its machined shape. Mr. P. Smith of the Mechanical Workshops, U.K.C., of this laboratory designed a new "push-pull" type control tap in stainless steel shown in figure 2.9.2.1 b. This new control tap has proved to be very successful in operation.

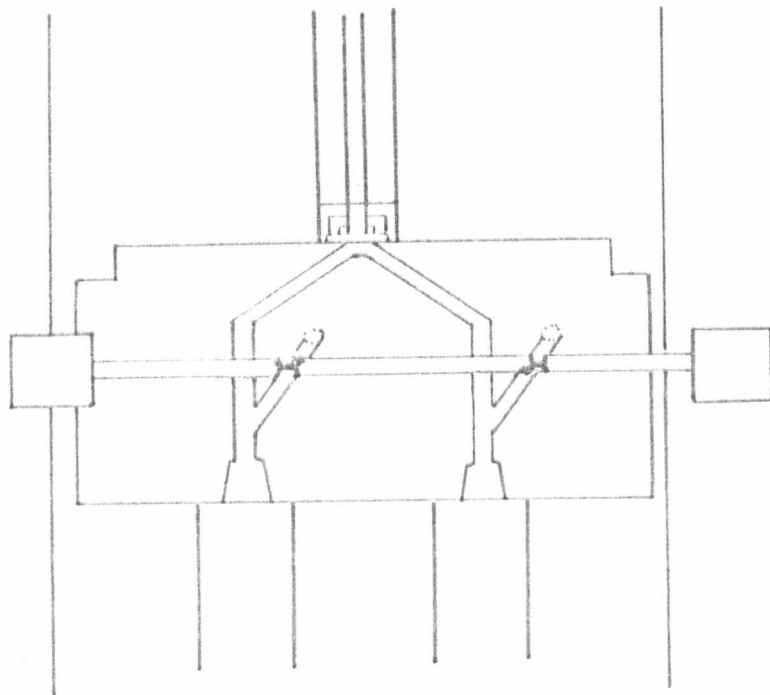
### 2.9.3 Determination of the Effective Path Length of the Quartz Observation Chamber

Since the observation chamber is cylindrical only an "effective" path length can be measured.

The light intensity falling on the photomultiplier should be zero when the observation chamber is filled with a completely opaque solution, unless some light is scattered around the observation chamber. This may be checked by filling the observation chamber with a concentrated



a. ORIGINAL THREE-WAY TEFLON TAP



b. NEW "PUSH-PULL" TYPE TAP

FIGURE 2.9.2.1

solution (0.1M) of potassium permanganate in water which has a very high visible absorbance. The photomultiplier voltage was then <0.001V.

The absorbance  $A^*$  of a solution in the observation chamber of the apparatus is related to the observed photomultiplier signal (volts) by equation (2.9.3.1) in which  $V_0$  is the photomultiplier signal when water is in the observation chamber,  $V$  is the signal when an absorbing species is present, and  $V'$  represents the light which by-passes the observation chamber.

In general,

$$A^* = \log_{10} \left[ \frac{(V_0 - V')}{(V - V')} \right] \quad (2.9.3.1)$$

If,  $V' \approx 0$   $A^* = \log_{10}(V_0/V)$  (2.9.3.2)

By definition, if the path length is  $l$ (cm), the concentration  $C$ (M) and the extinction coefficient  $\epsilon$ ( $M^{-1}cm^{-1}$ )

$$A = l \sum_i (\epsilon_i C_i) \quad (2.9.3.3)$$

Hence, the absorbance ( $A$ ) measured in the spectrophotometer cell of length  $l$ (1cm) is related to the absorbance  $A^*$  measured in the stopped-flow observation chamber of length  $l^*$  by the equation

$$A^*/A = l^*/l \quad (2.9.3.4)$$

From equation (2.9.3.2) and (2.9.3.4)

$$A = (l/l^*)A^* = (l/l^*) \log(V_0/V) \quad (2.9.3.5)$$

$$A l^* = \log_{10}(V_0/V) \quad (2.9.3.6)$$

Hence, by plotting  $\log_{10}(V_0/V)$  against  $A$  for a given wavelength,

TABLE 2.9.3.1

ABSORPTION PATH LENGTH DETERMINATION FOR THE  
OBSERVATION CELL OF THE STOPPED-FLOW APPARATUS

Temp. 298(±0.2)K;  $\lambda = 540\text{nm}$  for measurements of A and V

Solution	A	Signal V/volts	$\text{Log}_{10}(V^0/V)$
Water	-	4.1( $V^0$ )	
$\text{kMnO}_4$	-	0.001	
1	1.20	2.30	0.250
2	1.00	2.61	0.196
3	0.81	2.85	0.157
4	0.60	3.05	0.127
5	0.29	3.25	0.100
6	0.22	3.60	0.057

the effective path length of the observation chamber can be determined from the slope.

Results for the stopped-flow apparatus are shown in figure 2.9.3.1 and table 2.9.3.1. The effective path length is found to be  $2.0 \pm 0.1\text{mm}$ .

2.9.4 The Relationship between Absorption Photomultiplier Voltage  
and Concentration Changes

The relationship between transmitted light intensity (input signal to the oscilloscope)  $V^A$ , measured signal change  $\Delta V^A$  and the absorbance of the solution is shown below.

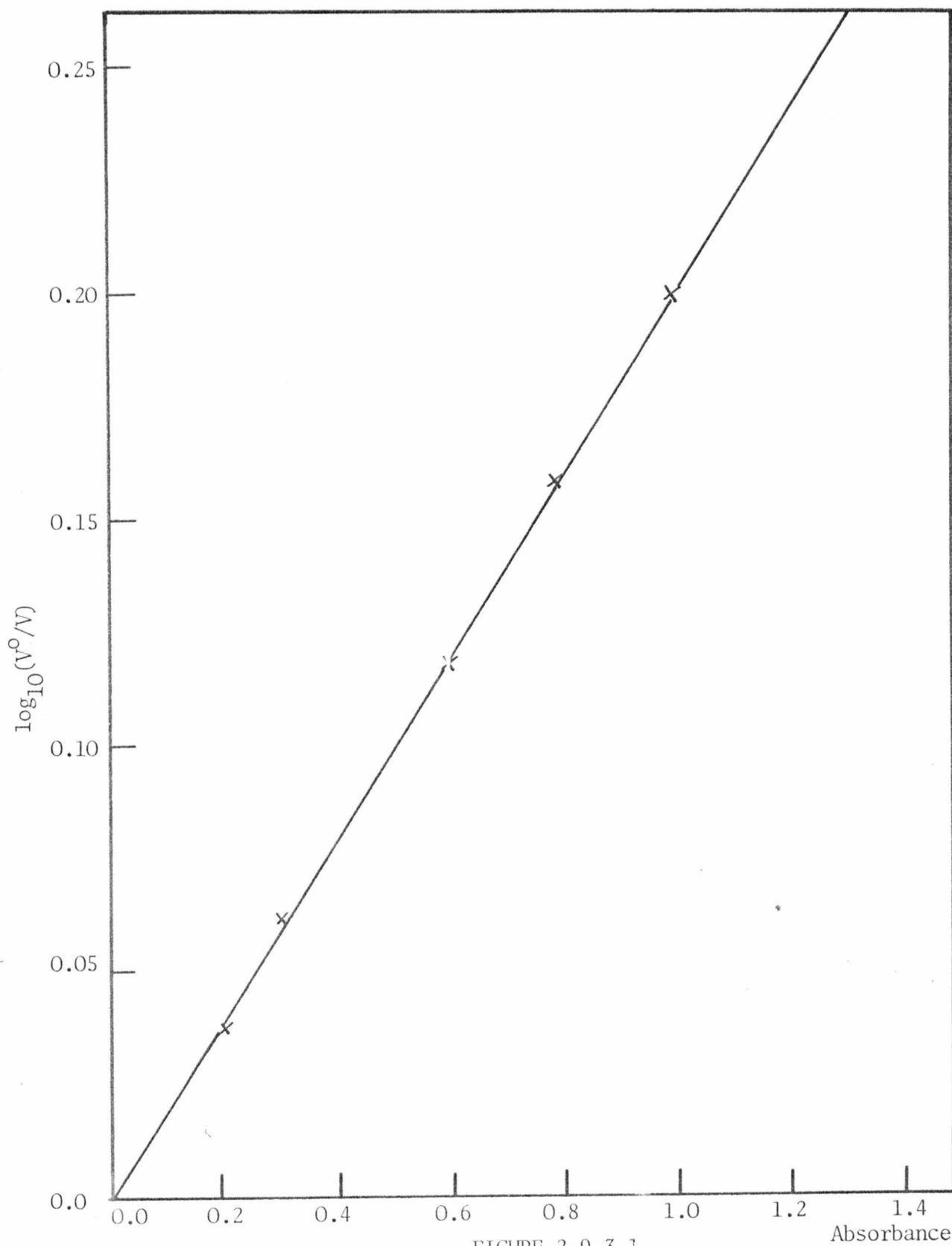


FIGURE 2.9.3.1

PLOT OF  $\log_{10}(V^0/V)$  vs Absorbance FOR THE DETERMINATION OF PATH LENGTH OF THE STOPPED-FLOW CELL

For a reaction with an absorbance change  $\Delta A^*$

$$\Delta A^* = \log_{10}(V_o^A/V_f^A) - \log_{10}(V_o^A/V_i^A) \quad (2.9.4.1)$$

where  $V_i$  and  $V_f$  are the initial and final voltages respectively.

Therefore

$$\Delta A^* = \log_{10}(V_i^A/V_f^A) \quad (2.9.4.2)$$

Depending on whether the reaction is accompanied by a decrease or increase in absorbance during the reaction

$$V_i^A = V_f^A \pm \Delta V^A$$

Therefore

$$\Delta A^* = \log_{10}(1 \pm \Delta V^A/V_f^A) = \frac{1}{2.303} \ln(1 \pm \Delta V^A/V_f^A) \quad (2.9.4.3)$$

For a small change in  $A^*$  ( $<0.05$ ) only the first term of the expansion of  $\log_{10}(1+\Delta V/V_f)$  need be considered,

$$\therefore \Delta V^A = \pm 2.303 \cdot \Delta A^* \cdot V_f^A \quad (2.9.4.4)$$

Therefore, for changes in voltage to be equated with changes in absorbance  $\Delta V^A/V_f^A$  must be  $<0.05$ , and this should always be checked.

Using equations (2.9.3.4) and (2.9.4.4) we can relate the change in voltage observed in the stopped-flow experiment to a change in absorbance measured in the spectrophotometer

$$\Delta V^A = 2.303 \Delta A \cdot l^* \cdot V_f^A \quad (2.9.4.5)$$

This equation should be used to ensure that the total change in the absorbance is being observed, i.e. a fast transient is not taking place

outside the time range of the stopped-flow.

The noise level ( $N$ ) for the detection system over the wavelength range 350-700nm is always below 1mV for signals upto 20V (with a smoothing time constant of 1msec.). If accurate kinetic data are to be obtained, the signal change to noise ratio ( $\Delta V^A/N$ ) must be  $\sim 5$ . Hence, the smallest change which may be measured is  $\sim 5$ mV. If  $V_f$  is 2.15V the 5mV change represents an absorbance change of 0.005, then an amplitude of 100mV corresponds to an absorbance change of 0.1 in a 1cm optical cell.

#### 2.9.5 The Relationship between Emission Photomultiplier Voltage and Concentration Changes

The quantitative correlation between the stopped-flow absorbance amplitude and concentration is discussed in section 2.9.4. However, the quantitative correlation between the stopped-flow fluorescence amplitude and concentration is much more complex. The problems involved in the correlation of fluorescence amplitudes and concentration are the same as those encountered in the construction of a spectro fluorimeter which enables the measurement of true emission spectra. Most spectro fluorimeters are of single beam type and have no compensation for the wavelength dependent efficiency of the excitation light source, monochromators and photomultiplier. If a correct excitation or emission spectrum is to be recorded these instrumental parameters must be adjusted so that the overall efficiency of the instrument is independent of wavelength.

The correction of the excitation light output is fairly simple to achieve<sup>(24)</sup>. The light beam is split before it reaches the sample cell; one part of the beam passes through the sample and one part strikes a thermopile (which, of course, must have a wavelength independent response

to light intensity). The uncorrected excitation signal is divided by the thermopile signal, thereby correcting for the change in excitation light intensity and with wavelength.

The correction of the emission spectrum is more complex<sup>(24)</sup>. A tapped potentiometer generates a pre-determined correction programme (voltage vs wavelength), which is multiplied by the output of the photomultiplier. The correction programme is determined from a point by point plot of the ratio of the intensity of reflection from a magnesium oxide block placed in the cell compartment to the thermopile output.

From this brief discussion it can be seen that in order to attempt a correlation between fluorescence amplitudes observed in the stopped-flow instrument with those observed in the spectro fluorimeter both instruments must be adapted to record corrected spectra. If the path length and bandpass of the spectro fluorimeter and stopped-flow instrument are the same the amplitude observed in the stopped-flow experiment would be related to the change observed in the spectro fluorimeter by an appropriate scale factor.

However, the path length in the spectro fluorimeter is 5mm and in the stopped-flow instrument it is 2mm. The difference in the path length means that the "inner-filter effect" will complicate any attempt to correlate the observed fluorescence changes in the spectro fluorimeter and stopped-flow instruments. The inner-filter effect operates in two ways (1) absorption of the exciting light means that the light intensity decreases as it traverses the cell, consequently all the molecules in the light beam do not receive equal illumination; (2) re-absorption of the emitted light will also result in a reduced fluorescence signal. This latter effect is only important if the absorption and fluorescence spectra overlap to any great extent.

The inner-filter effect becomes increasingly important if the

absorbance rises above 0.05. A solution which has an absorbance of 0.25 in a 5mm cell has an absorbance of only 0.1 in the stopped-flow cell. It is clearly seen that the fluorescence changes in the 5mm and 2mm cells are not simply related, i.e. the fluorescence signal or change in a 5mm cell is not 2.5 times that in the 2mm cell.

If the absorbance is to be kept below 0.05, the concentration of the dyes used in this study would have to be  $<2 \times 10^{-6}$  M. Dye concentrations of this magnitude not only lead to practical problems of detecting fluorescence changes with adequate signal-to-noise ratios, but also the adsorption of dyes at these low concentrations onto the syringes, observation cells etc. may adversely effect the observed kinetic behaviour.

In general, the fluorescence amplitudes encountered in the course of this work are large. The expected amplitude  $\Delta F$  may then be obtained by measuring the fluorescence signal of the initial and final solutions directly in the stopped-flow instrument. The initial signal  $F_i$  is determined by mixing dye at concentration  $C_A^0$ , with water in the stopped-flow instrument. The final signal at  $t=\infty$ ,  $F_f$ , is determined by mixing the same concentration of dye with the surfactant solution in the stopped-flow instrument. In both cases the final concentration of dye (the fluorescent species is  $C_A^0/2$ . The expected amplitude is given by

$$\Delta F = F_f - F_i$$

The influence of background scattered light on the observed fluorescence signals is small providing the excitation and emission wavelengths are separated by at least 10nm. The present experimental configuration has a bandpass of 6.6nm, for excitation, and emission monochromators. Hence, for acridine orange the range of excitation and emission wavelengths is 489-495nm and 523-529nm respectively. The separation of excitation and emission wavelengths is at least 18nm and the background signal, which arises from light scattered around the observation cell and by dust

particles in the solution, will be small. The level of the background signal may be determined with water in the observation cell. When the excitation and emission wavelengths are 492nm and 526nm respectively, and with the emission photomultiplier operating at maximum sensitivity (9 dynodes 1000V), the background signal is 20mV. The fluorescence signal obtained, under identical operating conditions, from a solution of  $1 \times 10^{-5}$  M acridine orange is 1.0V. The background light intensity is therefore only 2% of the total light intensity and can be effectively neglected.

The general importance of measuring the amplitude observed in the stopped-flow experiments can not be overemphasised. If the observed kinetic amplitude is less than the amplitude observed in the static total amplitude measurements, a mechanism involving at least two steps which cause changes in the observed property must be invoked. (Any fast process occurring in times less than the dead-time are not observed, and can only be inferred from a precise amplitude analysis). The variation of experimental conditions may cause changes in the relative amplitudes of the two or more processes and thus further information regarding the mechanism can be obtained.

#### 2.9.6 Determination of the "Dead-time" of the Stopped-Flow Instrument

The "dead-time" of the instrument is the time taken for the liquid to flow from the mixer entrance to the point of observation. It therefore represents a lower limit to the rate of the reactions which may be studied.

The dead-time for the instrument was determined by measuring the observed amplitude ( $\Delta V_1$ ), of a trace obtained from a study of a reaction with a relaxation time of  $\sim 20$  msec. The reaction chosen was between aquo Cobalt<sup>II</sup> and PADA, since the rate constant is accurately known<sup>(25)</sup>, was chosen. The expected amplitude ( $\Delta V_2$ ) can be calculated from a knowledge

of the absorption change for the reaction and equation (2.9.4.5). Then  $\Delta V_1$  and  $\Delta V_2$  are related by equation (2.9.6.1), where  $k$  is the rate constant for the reaction and  $\Delta t$  is the dead-time of the instrument.

$$(\Delta V_1/\Delta V_2) = \exp(-k\Delta t) \quad (2.9.6.1)$$

At 298K,  $k$  is  $36 \text{ sec.}^{-1}$ . From static measurements the expected amplitude  $\Delta V_2$  is 90mV. The mean of five determinations of the observed amplitude  $\Delta V_1$  is  $84 \pm 2 \text{ mV}$ . Using equation (2.9.6.1) the dead-time is calculated to be  $1.4 \pm 0.3 \text{ msec.}$  when the driving pressure is  $\sim 7 \times 10^4 \text{ Pa}$ . From the path length of the observation chamber and the distance from the mixer to the point of observation (20mm) we may calculate both the linear and volume flow velocities. These are  $14.3 \pm 2 \text{ msec.}^{-1}$  and  $45.5 \text{ cm}^3 \text{ sec.}^{-1}$  respectively.

Cavitation is not found to be a problem and this is usually the case when the linear flow velocity is less than  $20 \text{ msec}^{-1(26)}$ . From the determined flow velocity and the path length the Reynolds number is calculated to be 7,500, which is considerably greater than the value required for the onset of turbulent flow (1,200). It is necessary to obtain turbulent flow conditions to ensure that the solution is homogeneous across the observation point. Turbulent flow also assists the process of mixing.

### 2.9.7 Determination of Mixing Efficiency

The mixing efficiency was evaluated in the following way<sup>(27)</sup>. A solution of  $1 \times 10^{-2} \text{ M}$  sodium hydroxide was mixed with a solution of  $2 \times 10^{-2} \text{ M}$  acetic acid to which had been added  $\sim 1 \times 10^{-5} \text{ M}$  bromo Cresol green ( $\text{pK}_a = 4.90$ ) as indicator. On mixing neutralisation occurs and the pH of the system is changed. This causes the bromo Cresol green to change

colour and the reaction is followed at 410nm. Since the neutralisation is diffusion-controlled<sup>(28)</sup> and the indicator reaction coupled to it is also diffusion-controlled<sup>(29)</sup>, the reaction will be complete within the dead-time of the stopped-flow instrument. The oscilloscope traces obtained were completely horizontal, identical with those obtained by mixing water with water. This indicates that complete mixing had been achieved within the dead-time of the instrument.

Typical traces obtained with this instrument are shown in figure 2.9.7.1 a-c.

## 2.10 Derivation of Relaxation Expressions<sup>(12-14)</sup>

### 2.10.1 Single-Step Association-Dissociation Equilibrium

Consider the simple equilibrium represented by equation (2.10.1.1) where only species C absorbs light at a particular wavelength.



$$K = \frac{k_{12}}{k_{21}} \quad (2.10.1.2)$$

Activity coefficients have been neglected in the above equation.

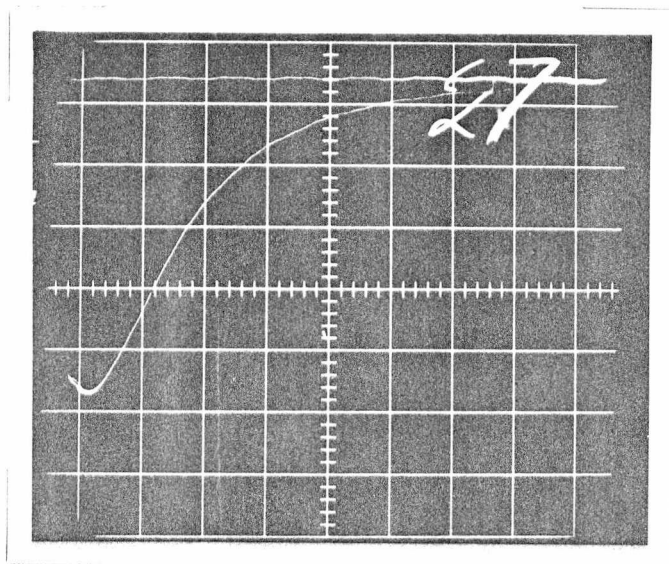
For small displacements from equilibrium the concentrations of the reactants, at time t, may be expressed as:

$$[A] = [\bar{A}] + \Delta[A]$$

$$[B] = [\bar{B}] + \Delta[B]$$

$$[C] = [\bar{C}] + \Delta[C]$$

where  $[\bar{A}]$ ,  $[\bar{B}]$  and  $[\bar{C}]$  are the equilibrium concentrations of A, B and C at the final temperature  $T+\Delta T$ , and  $\Delta[A]$ ,  $\Delta[B]$  and  $\Delta[C]$  are the small time dependent concentration changes.



(a)  $\text{AO}^+/\text{SDS}$  A

$$[\text{AO}^+] = 1 \times 10^{-5} \text{M}$$

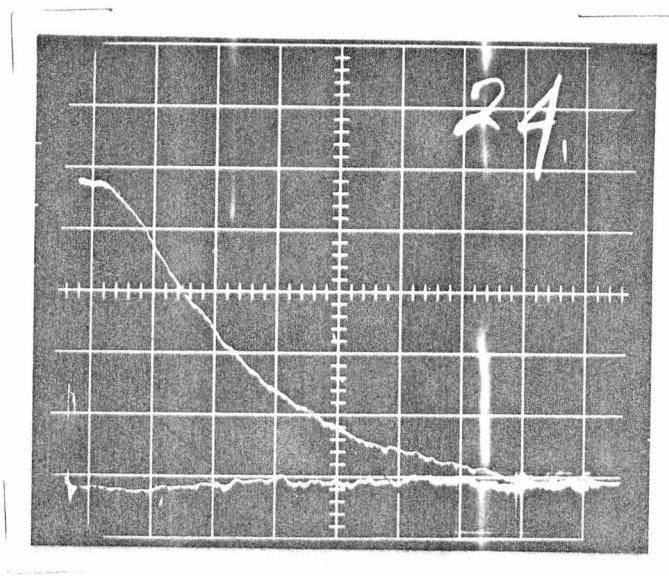
$$[\text{SDS}] = 1.5 \times 10^{-2} \text{M}$$

$$\lambda = 498 \text{nm}, V^0 = 2.2 \text{V}$$

$\Delta A = 1\%$

20ms/20mV

Temp. 298.2K



(b)  $\text{AO}^+/\text{SDS}$  F

$$[\text{AO}^+] = 1 \times 10^{-5} \text{M}$$

$$[\text{SDS}] = 1.5 \times 10^{-2} \text{M}$$

$$\lambda_{\text{ex}} = 492 \text{nm},$$

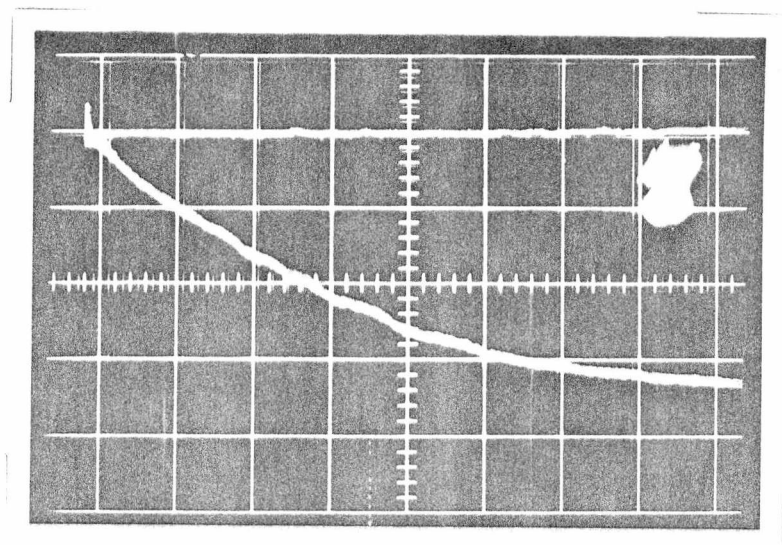
$$\lambda_{\text{em}} = 526 \text{nm},$$

$$V^0 = 2.0 \text{V}.$$

$\Delta F = 5\%$

20ms/100mV

Temp. 298.2K



(c)  $\text{AO}^+/\text{SDS}$   $I^S$

$$[\text{AO}^+] = 1 \times 10^{-5} \text{M}$$

$$[\text{SDS}] = 5 \times 10^{-4} \text{M}$$

$$\lambda_{\text{scat}} = 492/492 \text{nm}$$

$$\Delta I^S = 0.5\% \quad V^0 = 4.0 \text{V}.$$

5sec/20mV

Temp. 298.2K

FIGURE 2.9.7.1

TYPICAL STOPPED-FLOW TRANSIENTS

The rate equation is given by:

$$-\frac{d[A]}{dt} = -\frac{d[B]}{dt} = \frac{d[C]}{dt} = k_{12}[A][B] - k_{21}[C] \quad (2.10.1.3)$$

From the stoichiometry of the system

$$\Delta[A] = \Delta[B] = -\Delta[C] \equiv x \quad (2.10.1.4)$$

Substituting equations (2.10.1.2) and (2.10.1.4) into equation (2.10.1.3) and neglecting terms in  $x^2$  we obtain:

$$\frac{dx}{dt} = -\{k_{12}[\bar{A}] + [\bar{B}] + k_{21}\}x \quad (2.10.1.5)$$

As shown before  $A = A_0 e^{-t/\tau}$ , the absorbance  $A$  is a measure of the displacement from equilibrium i.e  $x$  therefore  $x = x_0 e^{-kt}$  when the constant term  $k \equiv \tau^{-1}$ . Therefore, from equation (2.10.1.5)

$$\tau^{-1} = k_{12}([\bar{A}] + [\bar{B}]) + k_{21} \quad (2.10.1.6)$$

If the concentration of either A or B is much larger than the concentration of the other then the concentration of say A is essentially time independent and we obtain the expression:

$$\tau^{-1} = k_{12}[A] + k_{21} \quad (2.10.1.7)$$

The values of  $k_{12}$  and  $k_{21}$  can be obtained from the slope and intercept of the linear plot of  $\tau^{-1}$  as  $[A]$ .

### 2.10.2 Consecutive Multi-Step Equilibrium

Let us now consider the more complex system shown by equation

(2.10.2.1)



$$K_{12} = \frac{k_{12}}{k_{21}} \quad (2.10.2.2)$$

$$K_{23} = \frac{k_{23}}{k_{32}} \quad (2.10.2.3)$$

The system has only two independent rate expressions. Any two of the three may be chosen to be independent. The system therefore, has only two relaxation times

$$\frac{d[A]}{dt} = -k_{12}[A][B] + k_{21}[C] \quad (2.10.2.4)$$

$$\frac{d[C]}{dt} = k_{12}[A][B] - k_{21}[C] - k_{23}[C] + k_{32}[D] \quad (2.10.2.5)$$

$$\frac{d[D]}{dt} = k_{23}[C] - k_{32}[D] \quad (2.10.2.6)$$

Because of their shortness (2.10.2.4) and (2.10.2.6) will be used.

From the stoichiometry

$$\Delta A = \Delta B \quad (2.10.2.7)$$

$$-\Delta C = \Delta A + \Delta D \quad (2.10.2.8)$$

Substituting equations (2.10.2.7) and (2.10.2.8) into (2.10.2.4) and (2.10.2.6) and neglecting square terms we obtain

$$\frac{d\Delta[A]}{dt} = -(k_{12}[\overline{A+B}] + k_{21}\Delta[A] - k_{21}\Delta[D]) \quad (2.10.2.9)$$

$$= k_{23}\Delta[C] - k_{32}\Delta[D] \quad (2.10.2.10)$$

$$\frac{d\Delta[D]}{dt} = -k_{23}\Delta[A] - (k_{23}+k_{32})\Delta[D] \quad (2.10.2.11)$$

These equations have the general form

$$\frac{d}{dt}(\Delta[X]_i) = \sum_{j=1}^n a_{ij}(\Delta[X]_j) \quad i, j = 1 \dots n \quad (2.10.2.12)$$

where  $a_{ij}$  are functions of the various rate constants and equilibrium concentrations  $[X]_j$ .

The relaxation times are then obtained by solving the determinant,  $\det(a_{ij} - \tau^{-1}\delta_{ij})=0$  ( $\delta_{ij}$  is the Kroenecker delta).

If one of the steps is much more rapid than the other then it may be considered to be in equilibrium during the relaxation of the other step. If the first step is much more rapid than the second then  $\tau_1^{-1}$  will be given by equation (2.10.1.6)

$$\tau_1^{-1} = k_{12}([A] + [B]) + k_{21}$$

The slower relaxation time may be obtained by a similar procedure. We must, however, define  $\Delta C$  in terms of  $\Delta D$ .

Since the first step is always at equilibrium with respect to the second step

$$k_{12}[A][B] = k_{21}[C] \quad (2.10.2.13)$$

which leads to

$$k_{12}([A] \Delta[B] + [B] \Delta[A]) = k_{21} \Delta[C] \quad (2.10.2.14)$$

substituting from equation (2.10.2.8) and rearranging

$$\Delta[C] = \frac{-k_{12}([A] + [B])}{k_{12}([A] + [B]) + k_{21}} \cdot \Delta[D] \quad (2.10.2.15)$$

substituting into equation (2.10.2.10)

$$\frac{d\Delta[D]}{dt} = \frac{-k_{12}k_{23}([\bar{A}] + [\bar{B}]) \Delta[D]}{k_{12}([\bar{A}] + [\bar{B}]) + k_{21}} - k_{32}\Delta[D] \quad (2.10.2.16)$$

Hence

$$\tau_2^{-1} = \frac{k_{12}k_{23}([\bar{A}] + [\bar{B}])}{k_{12}([\bar{A}] + [\bar{B}]) + k_{21}} + k_{32} \quad (2.10.2.17)$$

We may also derive these expressions using the two linearised differential equations from equations <sup>(30)</sup> (2.10.2.9) and (2.10.2.11)

$$-\frac{d}{dt} \Delta[A] = a_{11}\Delta[A] + a_{12}\Delta[D] \quad (2.10.2.18)$$

$$-\frac{d\Delta[D]}{dt} = a_{21}\Delta[A] + a_{22}\Delta[D] \quad (2.10.2.19)$$

where  $a_{11} = k_{12}([\bar{A}] + [\bar{B}]) + k_{21}$

$$a_{12} = k_{21}$$

$$a_{21} = k_{23}$$

$$a_{22} = k_{23} + k_{32}$$

The expression for the two relaxation times  $\tau_1, \tau_2$  is then

$$\tau_1^{-1} = \frac{a_{11} + a_{22}}{2} (1 + (1-b)^{\frac{1}{2}}) \quad (2.10.2.20)$$

$$\tau_2^{-1} = \frac{a_{11} + a_{22}}{2} (1 - (1-b)^{\frac{1}{2}}) \quad (2.10.2.21)$$

where  $b = \frac{4(a_{11}a_{22} - a_{12}a_{21})}{(a_{11} + a_{22})^2}$

for  $1 \gg b$  and expanding  $(1-b)^{\frac{1}{2}}$  and omitting square and higher terms

$$(1-b)^{\frac{1}{2}} = 1 - b/2$$

then

$$\tau_1^{-1} = a_{11} + a_{22} \quad (2.10.2.22)$$

$$\tau_2^{-1} = a_{11}a_{22} - a_{12}a_{21} \quad (2.10.2.23)$$

If two relaxation processes are observed then

$$a_{11} \gg a_{22} \quad (2.10.2.24)$$

or

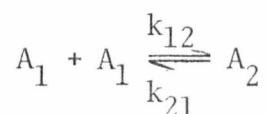
$$a_{22} \gg a_{11} \quad (2.10.2.25)$$

If condition (2.10.2.24) holds then the relaxation times are given by the same equations as before i.e. (2.10.1.6) and (2.10.2.17).

### 2.10.3 Relaxation Amplitudes

A relaxation experiment yields two different types of information: the exponential time constants and the amplitude of the relaxation. So far we have only discussed the time constants. We can obtain further information from the relaxation amplitudes, which are a function of the thermodynamic properties of the reaction under investigation. A knowledge of the relaxation amplitudes will allow determination of various thermodynamic parameters and help in the elucidation of the mechanism.

Consider a simple one step dimerisation reaction<sup>(19)</sup>



For spectrophotometric detection where the initial light intensity  $I$  is given by the signal received by the photomultiplier

$$\Delta I/I = 2.3 \Delta A$$

where A is the absorbance of the solution

$$A = \epsilon C_A^0 l$$

where  $\epsilon$  is the extinction coefficient of the solution at the wavelength of the experiment and  $C_A^0$  is the total concentration of the reactants.

The amplitude of the relaxation process  $\Delta \bar{A}$  for a small temperature perturbation  $\delta T$  is given by

$$\Delta \bar{A} = \phi_{12} (\partial \ln L / \partial T) C_A^0 l \delta T \quad (2.10.3.1)$$

where  $\phi_{12}$  is the amplitude factor.

If we define  $L = K_{12} C_A^0$  and  $s = K_{12} C_A$  where  $C_A$  is the concentration of monomer and  $K_{12}$  is the equilibrium constant.

The amplitude factor  $\phi_{12}$  is given by

$$\phi_{12} = L (\partial \epsilon / \partial s) (\partial s / \partial L) \quad (2.10.3.2)$$

Now 
$$\partial \ln K_{12} = (\Delta H_{12}^0 / RT^2) \delta T \quad (2.10.3.3)$$

The amplitude is therefore

$$\Delta \bar{A} = \phi_{12} C_A^0 l (\Delta H^0 / RT^2) \delta T \quad (2.10.3.4)$$

Now 
$$\epsilon = \epsilon_{A_2} + (\epsilon_{A_1} - \epsilon_{A_2}) / (1+2s) \quad (2.10.3.5)$$

and 
$$L = s(1+2s) \quad (2.10.3.6)$$

The amplitude factor is now

$$\phi_{12} = \{ -2s / [(1+2s)(1+4s)] \} \epsilon_{A_1}^{-\epsilon_{A_2}} \quad (2.10.3.7)$$

If the response of the photomultiplier is linear then  $\Delta V/V = \Delta I/I$  where  $\Delta V$  is the signal change.

We may now plot  $\Delta \bar{A}/C_A^0$  versus  $\phi_{12}$ ; if we know  $K_{12}$  and  $(\epsilon_{A_1}^{-\epsilon_{A_2}})$  we may obtain  $\Delta H_{12}^0$  from the slope.

There are alternative methods<sup>(12,31-33)</sup> of obtaining expressions relating observed signal changes to the thermodynamic parameters of the system.

Thusius et al<sup>(33)</sup> have demonstrated a straightforward method of obtaining expressions for the amplitudes. For the reaction



$$\Delta \bar{A} = (\Delta H^0/RT^2) \cdot [1/\bar{A} + 1/\bar{B} + 1/\bar{AB}]^{-1} \cdot (\epsilon_{AB}^{-\epsilon_A^{-\epsilon_B}}) \quad (2.10.3.8)$$

This approach has been used to calculate  $\Delta H$  for the binding of proflavine to trypsin and the binding of proflavine to DNA<sup>(33)</sup>.

It is well known that one can not "prove" a mechanism, it is only possible to show that all the experimental evidence is consistent with the proposed mechanism. It is, therefore, important to show that the same mechanism can be satisfactorily fitted to equilibrium, relaxation times and amplitudes.

### 2.11 The Stopped-Flow Method

The stopped-flow method is a logical extension of classical kinetic procedures. The solutions are mixed rapidly and the resultant solution is then brought to a sudden halt. The changes in concentration are then

transient at discrete moments in time. During recording, each sample of the signal is converted into a digital number and stored in the memory. In the case of the DL905 there are 1024 words of memory, and amplitude resolution is to one part in 256 (8 bits).

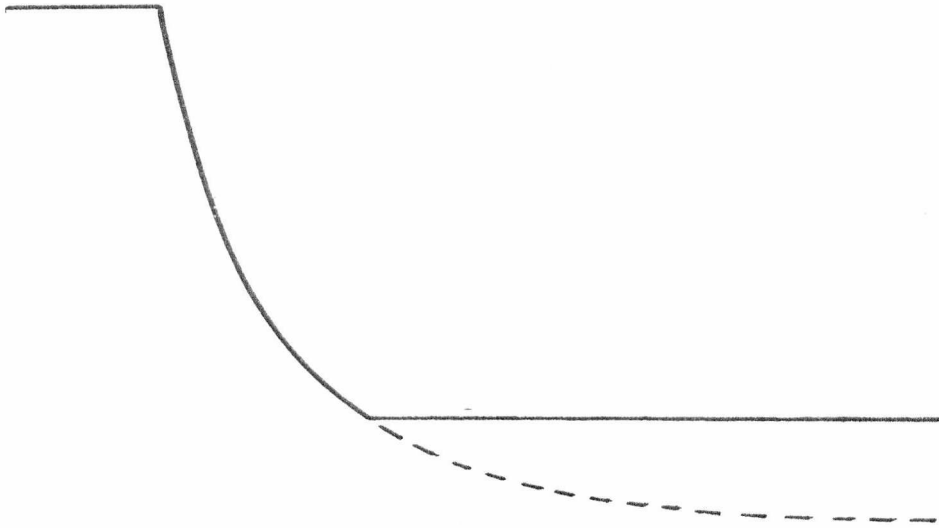
The first 1000 points of the record stored in the memory are reconstructed via a digital-to-analogue converter as a repeating sequence of 1000 values, so that the reconstructed transient may be viewed continuously on a non-storage oscilloscope (Tektronix 545B).

The amplitude of the transient may be up to 50 volts, but the essential point to remember is that the recorder amplifier voltage must be set as closely as possible to the total amplitude. This ensures that close to the maximum amplitude of  $1/256$  is achieved. If the transient amplitude is larger than the recorder setting, the trace is "clipped" and if it is smaller the trace contains "steps". (See figures 2.12.2.1 a & b).

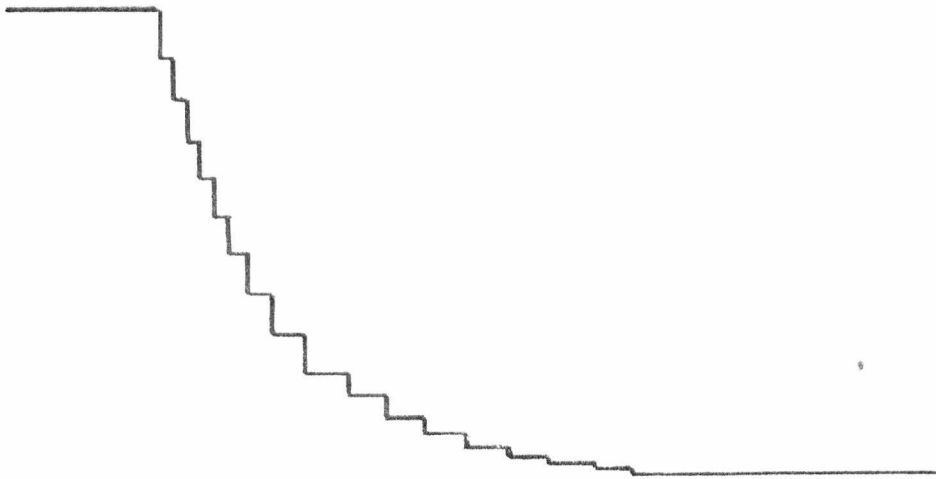
The quartz crystal time-base (accuracy 0.05%) for the recorder can be varied from  $200\mu\text{S}$  to 10 sec. for 1000 points. This means that the fastest sampling time per point is  $200\text{nS}$ . Therefore, a transient consisting of approximately 20 points may be accurately evaluated giving a fastest measurable time of  $4\mu\text{S}$ .

The transient recorder has pre-trigger and delay modes, which may be set to pre-trigger by any amount up to 999 points or delay the sweep by up to 9.99 times the sweep time. The pre-trigger mode may be used to observe pre-trigger flow characteristics in the stopped-flow apparatus. The delay mode may be used to eliminate fast transients in either temperature-jump or stopped-flow experiments which will allow easy observation of slow processes. The DL905 also has a facility for sweeping a certain number of points at one rate and the rest at another, slower rate. This may prove useful to the easy separation of a very fast and





a. "CLIPPED" TRACE - RELAXATION AMPLITUDE LARGER THAN TRANSIENT RECORDER SETTING



b. "STEPPED" TRACE - RELAXATION AMPLITUDE MUCH SMALLER THAN TRANSIENT RECORDER SETTING

FIGURE 2.12.2.1

EXAMPLES OF INCORRECT TRANSIENT RECORDER SETTINGS

very slow transients. Therefore, it can be seen that the transient recorder is far more versatile than a conventional storage oscilloscope.

The Data Dynamics 1132 paper tape punch interface is the 905/ASC, the data code used being ASC 11. Each data word is punched as a group of three characters preceded by a "line-feed" code. Every three rows of binary correspond to one point on the transient, ranging from 0.255. The paper tape is then fed through the University Computer.

This reads the tape, converts the information back into signal size in millivolts, compiles the program and calculates the rate constants, errors, etc. according to the Algol program used and the results required. The programs are described in Appendix II.

## REFERENCES

- (1) B.H. Robinson, A. Löffler and G. Schwarz, *J. Chem. Soc. Faraday I*, 1973, 69, 56.
- (2) A. Albert, The Acridines (2nd ed. Arnold, London, 1966) p.346.
- (3) A. Albert, The Acridines (2nd ed. Arnold, London, 1966) p.320.
- (4) D.T.Y. Chen and K.J. Laidler, *Canad. J. Chem.*, 1959, 37, 599.
- (5) P. Mukerjee and A.K. Ghosh, *J. Amer. Chem. Soc.*, 1970, 92, 6403.
- (6) A. Bernhard, B.F. Lee and Z.H. Tashjian, *J. Mol. Biol.*, 1966, 18, 405.
- (7) V. Vitagliano and L. Costantino, *J. Phys. Chem.*, 1970, 74, 197.
- (8) M. Hilda and T. Saruki, *Bull. Chem. Soc. Jap.*, 1970, 43, 2291.
- (9) J. Clifford and B.A. Pethica, *Trans. Faraday Soc.*, 1964, 60, 1483.
- (10) F.W. Gray, J.F. Gerecht and I.J. Krems, *J. Chem. Soc.*, 1955, 20, 511.
- (11) V.A. Motsavage and H.B. Kostenbauder, *J. Colloid Interface Sci.*, 1963, 18, 603.
- (12) M. Eigen, Techniques of Chemistry, Vol. VI, G.G. Hammes ed., (3rd ed. Wiley-Interscience, New York, 1974) Chap. III.
- (13) E.F. Caldin, Fast Reactions in Solution, (Blackwell, Oxford, 1964).
- (14) D.N. Hague, Fast Reactions, (Wiley) 1971.
- (15) Messanlagen Studiengesellschaft mbH Göttingen, W. Germany.
- (16) G.G. Hammes, Techniques of Chemistry, Vol. VI, G.G. Hammes ed., (3rd ed. Wiley Interscience, New York, 1974) p.159.
- (17) R. Rigler, C-R. Rabl and T.M. Jovin, *Rev. Sci. Instr.*, 1974, 45, 580.
- (18) H.J. Li and D.M. Crothers, *J. Mol. Biol.*, 1969, 39, 461.
- (19) B.H. Robinson, A. Seelig-Löffler and G. Schwarz, *J. Chem. Soc. Faraday I*, 1975, 71, 815.
- (20) G. Czerlinski and G. Schreck, *J. Biol. Chem.*, 1964, 239, 913.

- (21) J. Janin, R van Rapenbush, P. Truffa-Bachi and G.N. Cohen, *Eur. J. Biochem.*, 1969, 8, 128.
- (22) M.A. Cobb, Ph.D Thesis, University of Kent, 1972.
- (23) K.J.A. Hargreaves, M.Sc. Thesis, University of Kent, 1974.
- (24) H.K. Howerton, Fluorescence, G.G. Guilbert, ed. (Arnold, London, 1967) p.233.
- (25) M.A. Cobb and D.N. Hague, *Trans. Faraday Soc.*, 1971, 67, 3069.
- (26) B. Chance, Techniques of Chemistry, Vol. VI, G.G. Hammes ed. (3rd ed. Wiley Interscience, New York, 1974) p.26.
- (27) R.L. Berger, Rapid Mixing and Sampling Techniques in Biochemistry ed. B. Chance, R.H. Eisenhardt, Q.H. Gibson and K.K. Longberg-Holm, (Academic Press, New York, 1964).
- (28) M. Eigen, *Angew. Chem. Intl. Edn.*, 1964, 3, 1.
- (29) J.J. Auborn, P. Warrick and E.M. Eyring, *J. Phys. Chem.*, 1971, 75, 2488.
- (30) G.H. Czerlinski, Chemical Relaxation, (M. DeBber, New York, 1966).
- (31) G.G. Hammes and P.R. Schimmel, The Enzymes, Part 2 ed. P.D. Boyer, (Academic Press, New York, 1970).
- (32) D. Thusius, *J. Amer. Chem. Soc.*, 1972, 94, 356.
- (33) D. Thusius, G. Foucalt and F. Guillain, Dynamic Aspects of Conformation Changes in Biological Macromolecules, ed. C. Sadron (D. Reidel, 1973).
- (34) A.A. Frost and R.G. Pearson, Kinetics and Mechanism (2nd ed. Wiley, London, 1961).
- (35) J.E. Crooks, P.A. Tregoaan and M.S. Zetter, *J. Phys. E.*, 1970, 3, 73.

CHAPTER 3

A COOPERATIVE MODEL FOR MICELLE FORMATION

## CHAPTER 3

### A COOPERATIVE MODEL FOR MICELLE FORMATION

#### 3.1 Introduction

The self-association of hydrophobic molecules in aqueous solutions is not confined to detergent molecules; self-association is exhibited by drugs, dyes, proteins and surfactants of physiological importance such as bile salts. The modes of self-association may be very different for solutes with different molecular structures and geometry. In this chapter some general self-association models are examined, and their applicability to the self-association of surfactants to form micelles of narrow and wide size distributions is indicated. It will be shown that most self-association models do not predict a "Critical Micelle Concentration". A necessary condition for the formation of micelles of reasonable aggregation number ( $z = 20-100$ ) over a small but finite range of surfactant concentration is that the self-association model should introduce cooperativity in the early stages.

In the development of any theory of micelle formation, it is important to consider possible structures for micelles, and aggregated species leading to micelles, and the relative stabilities of these aggregates if a clear understanding of the self-association process is to be gained. It is well known that the aggregation of planar dye units, e.g. acridine orange, leads to formation of oligomeric stacks in a non-cooperative manner<sup>(1)</sup>. Non-cooperative self-association means that  $K_{r-1}, r \leq K_{12}$  for



In this case, the concentration of the (r+1)mer  $C_{r+1}$ , will always be less than (or equal to, as the total concentration  $C_A^0 \rightarrow \infty$ )  $C_r$ . Hence, no critical formation of any particular n-mer is possible. These systems may, therefore, be considered as self-associating without micelle formation. It is, however, possible to invoke a model involving modest positive cooperativity. The existence of relatively stable pre-micelle aggregates at surfactant concentrations close to the CMC is predicted. Pre-micelle aggregation has been postulated for a number of  $C_{10}$ - $C_{14}$  surfactants<sup>(2-4)</sup>, but in general observations close to the CMC are difficult to interpret relying mainly on deviations from the Onsager slope of conductivity plots<sup>(5)</sup>.

The approach discussed in this chapter is based on modifications of the multi-equilibrium scheme reported previously for the stacking of small charged molecules such as acridine dyes.

For many years micelles were considered to be perfectly monodisperse, i.e. the weight-average molecular weight,  $N_w$ , is equal to the number-average molecular weight,  $N_n$ . More recently, it has been recognised that micelles will in general be polydisperse<sup>(6)</sup>. Experimental evidence regarding the degree of polydispersity is difficult to obtain. Theoretical calculations show that narrow size distributions may be common<sup>(6)</sup> (width at half-height  $\approx 10$ ), and this implies that the mean aggregation number above the CMC does not vary significantly with the total concentration of surfactant for  $C_A^0 < 5 \text{ CMC}$ .

In any realistic approach to micelle formation in aqueous media the experimental generalisations described above will have to be incorporated into the model, and explained on the basis of (free) energetic considerations.

Finally, it must be stressed that before meaningful conclusions can be drawn from kinetic measurements, it is essential to have a sound

theoretical thermodynamic base for the interpretation of the data. The cooperative step-wise self-association model is favoured over alternative approaches since it is more easily applicable to the analysis of kinetic measurements obtained by perturbation relaxation measurements. Furthermore, it allows an explanation of micelle formation at the molecular level, by means of the well-established concept of cooperativity.

### 3.2 Step-Wise Self-Association Models

This section will consider the various self-association models which have been applied to micelle formation. Consideration will be given to whether or not the model leads to a CMC, the type of size-distribution and the structure of possible aggregates.

The complete description of a self-associating system requires a knowledge of all the equilibrium constants,  $K_{r-1,r}$ . Even when the number of oligomers is small, this is very difficult because the experimental uncertainties in one  $K_{r-1,r}$  value will affect those of all the others.

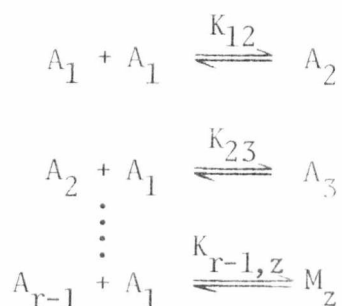
Experimental approaches available for studying self-associating systems are usually unsuitable for a detailed analysis. Those based on spectroscopy of any kind require the determination of a characteristic parameter e.g. extinction coefficient for every oligomer in the system. This makes the determination of  $K_{r-1,r}$  values very difficult. The equilibrium methods rely upon the estimate of the free monomer concentration as a function of the total equivalent concentration. In general, these methods do not afford sufficient precision to allow the determination of more than one or two association constants accurately.

It is, therefore, necessary to consider models of self-association in which the step-wise association constants are allowed to vary in some predetermined manner.

### 3.2.1 Non-Cooperative Step-Wise Self-Association

This scheme has been extensively employed for the analysis of the stacking of charged planar dye molecules<sup>(1)</sup> and the self-association of purine and pyrimidine bases of nucleosides<sup>(7)</sup>.

The model employs only one parameter, a step-wise association constant, which is assumed to be independent of the size of the oligomer



where  $K_{12} = K_{23} \dots K_{r-1,z} = K$ .

It is useful to define a dimensionless parameter  $s$

$$s = K C_1$$

The total concentration ( $C_A^O$ ) is given by

$$C_A^O = C_1 + 2C_2 + 3C_3 \dots + zC_z \quad (3.2.1.1)$$

where  $C_A^O$  is the total concentration of A,  $C_1$ ,  $C_2$  etc. and the concentration of  $A_1$ ,  $A_2$ , etc.

From the Law of Mass Action:-

$$C_1 = C_1 \quad (3.2.1.2)$$

$$C_2 = K C_1 C_1 \quad (3.2.1.3)$$

$$= C_1 s \quad (3.2.1.4)$$

$$C_3 = K C_1 C_2 = C_1 s^2 \quad (3.2.1.5)$$

⋮

$$C_z = K_1 C_1 C_{r-1} = C_1 z^{-1} \quad (3.2.1.6)$$

from which the total equivalent concentration ( $C_A^0$ ) is obtained by the application of the Law of Mass Conservation:

$$C_A^0 = \sum_{r=1}^{\infty} r C_r \quad (3.2.1.7)$$

$$= C_1 + 2C_2 + 3C_3 + \dots + zC_z \quad (3.2.1.8)$$

$$= C_1 (1 + 2s + 3s^2 + \dots + z s^{z-1}) \quad (3.2.1.9)$$

The sum of an infinite series of the type  $1 + 2x + 3x^2 + \dots$

is  $(1-x)^{-2}$

therefore,

$$C_A^0 = C_1 / (1-s)^2 \quad (3.2.1.10)$$

So that 
$$(C_1 / C_A^0)^{1/2} = 1 - K C_1 \quad (3.2.1.11)$$

Equation (3.2.1.11) will enable the determination of  $K$  if  $C_1$  is known as a function of the total concentration  $C_A^0$ .

The characteristic features of this association model are that the number and weight average molecular-weights are slowly varying functions of the total concentration, the aggregates are very polydisperse and the average degree of association is usually quite low 2-5.

### 3.2.2 Step-Wise Association Model with Slowly Varying Equilibrium Constants

In this model the variation of the equilibrium constant is pre-

determined by an explicit function. The variation of  $K_{r-1,r}$  with  $r$  may indicate either small positive ( $K_{r-1,r}$  increases with  $r$ ) or negative ( $K_{r-1,r}$  decreases with  $r$ ) cooperativity.

For example, using a function which allows for a repulsive coulombic potential between nearest neighbours the model is developed below.

$$\text{The overall free energy change is } \Delta G_{r,r+1}^O = \Delta G_{st}^O + \Delta G_{el,r}^O \quad (3.2.2.1)$$

where  $\Delta G_{st}^O$  represents the contribution from short range "hydrophobic interactions" independent of  $r$  and  $\Delta G_{el,r}^O$  the repulsive potential.  $\Delta G_{el,r}^O$  is given by equation (3.2.2.2)

$$\Delta G_{el,r}^O = (N_A e_o^2 / \sigma a) \sum_1^r (1/r) \quad (3.2.2.2)$$

where  $N_A$  is Avagadro's constant,  $e_o$  the electronic charge,  $a$  is the average separation of surfactant head groups, and  $\sigma$  is a screening factor which is equal to the effective dielectric constant experienced by the aggregate. As  $\sigma$  is increased the repulsive effect between molecules is decreased.  $\sigma$  can vary between 1 and  $\infty$ .

The summation term represents the repulsive potential of the added surfactant molecules with the first, second ...  $r^{\text{th}}$  nearest neighbour in the aggregate.

$$\text{In general } K_{r,r+1} = \exp(-\Delta G_{r,r+1}^O / RT). \quad (3.2.2.3)$$

Separating  $\Delta G_{r,r+1}^O$  into its hydrophobic and coulombic terms we obtain

$$K_{r,r+1} = \exp(-\Delta G_{st}^O / RT) \exp(-q \sum (1/r)) \quad (3.2.2.4)$$

$$\text{where } q = N_A e_o^2 / \sigma a RT$$

For simplicity we define

$$\exp(-\Delta G_{st}^O / RT) = K_o \quad (3.2.2.5)$$

Then

$$K_{12} = K_0/\exp(q) \quad (3.2.2.6)$$

$$K_{23} = K_{12}/\exp(q(\frac{1}{2})) \quad (3.2.2.7)$$

$$K_{34} = K_{12}/\exp(q(\frac{1}{2} + \frac{1}{3})) \quad (3.2.2.8)$$

$$K_{r,r+1} = K_{12}/\exp(q \sum_2^r (1/r)) \quad (3.2.2.9)$$

Now  $\lim(\sum_1^r 1/r - \ln r) = c = 0.57721$  (Euler's constant)

For  $r \rightarrow \infty$ ,  $\exp \sum_2^r 1/r = r/b$

where  $r/b = \exp(-(1-c)) = 1.53$

For smaller values of  $r$ ,  $b$  is no longer constant but varies from 1.33 at  $r = 2$  to 1.53 at  $r = \infty$ . A satisfactory approximation is made by assuming  $b$  to be a constant equal to 1.4. Then the theory gives

$$K_{r,r+1} \approx K_{12}(b/r)^q \leq K_{12} \quad (n = 2 \rightarrow \infty) \quad (3.2.2.10)$$

For strong electrostatic repulsion i.e.  $\sigma \rightarrow 1$  or  $q \gg 1$ ,

$$K_{12} \gg K_{r,r+1} \quad (r = 2 \rightarrow \infty). \quad (3.2.2.11)$$

This case applies to charged dye self-association when only  $K_{12}$  is considered significant.

For weak electrostatic repulsion i.e.  $\sigma \rightarrow \infty$  or  $q \ll 1$ ,

$$K_{12} = K_{r,r+1} \quad (r = 2 \rightarrow \infty) \quad (3.2.2.12)$$

i.e. all the equilibrium constants are equal.

For the case of medium electrostatic repulsion i.e.  $\sigma = N_A e_0^2/a RT$

or  $q = 1$

$$K_{r,r+1} = K_{12}(b/r) \quad (r = 2 + \infty) \quad (3.2.2.13)$$

In this case the equilibrium constants  $K_{r,r+1}$  slowly decrease as  $r$  is increased. This case will now be considered in detail.

As before we define

$$K_{12} C_1 = S \quad (3.2.2.14)$$

then by the Law of Mass Action

$$C_1 = C_1 \quad (3.2.2.15)$$

$$C_2 = K_{12} C_1 C_1 = C_1 s \quad (3.2.2.16)$$

$$C_3 = b/r K_{12} C_1 \cdot C_2 = ((bs)^2 \cdot C_1/b)/2 \quad (3.2.2.17)$$

⋮

$$C_r = b/r K_{12} C_1 \cdot C_{r-1} = ((bs)^{r-1} \cdot C_1/b)/(r-1)! \quad (3.2.2.18)$$

The total equivalent concentration is then given by

$$C_A^O = C_1/b \sum (r+1)(bs)^r/r! \quad (3.2.2.19)$$

For the example shown above i.e.  $K_{r-1,r}$  decreasing as  $r$  increases, the system will exhibit negative cooperativity. The formation of larger aggregates in preference to smaller ones is therefore less favourable. The case of slight positive cooperativity i.e.  $K_{r-1,r}$  increasing with  $r$ , leads to a very polydisperse system in which the distribution of oligomeric species is dependent on the total concentration. Therefore neither of the models can predict a CMC and the general properties of the proposed model are inconsistent with micelle

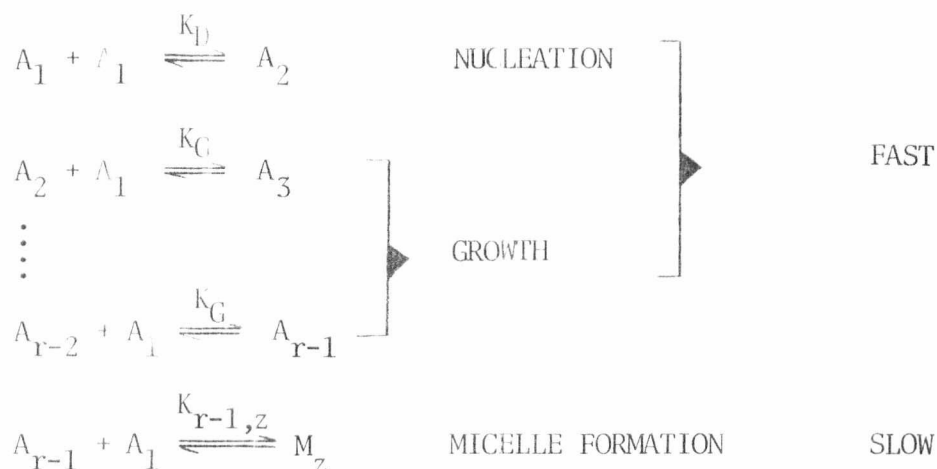
formation.

### 3.2.3 The Infinite Cooperativity Model of Krescheck et al<sup>(8)</sup>

The most common thermodynamic approach to micelle formation, due to Krescheck et al, assumes a homogeneous system and is based on a step-wise aggregation scheme similar to those already discussed.

The model assumes the co-existence of micelles  $M_z$  in dynamic equilibrium with surfactant monomers above the CMC. All other species are assumed to be present at negligible concentrations. Until recently, most of the kinetic measurements obtained on micellar systems have been interpreted on the basis of the Krescheck model. However, very recently a number of new approaches have been developed notably by Muller<sup>(9)</sup>, Nakagawa<sup>(10)</sup>, Hoffmann et al<sup>(11)</sup> and Aniansson and Wall<sup>(12)</sup>.

Now we have on the Krescheck scheme



The equilibria  $A_r + A_1 \rightleftharpoons A_{r+1}$  ( $r = 1 \rightarrow 100$ ) are all assumed to be set up rapidly, the rate-limiting step in the micelle-breakdown process being the removal of the first monomer from the micelle, controlled by rate constant  $k_{r,r-1}$ .

The other assumptions of the Krescheck model are:

- (1) For  $C_A^0 > \text{CMC}$

$$C_r, C_1 \gg C_2 \dots\dots C_{r-1}$$

$$\text{and } C_1 \approx \text{CMC}$$

(2) For  $C_A^0 < \text{CMC}$

$$C_1 \approx C_A^0$$

It is therefore necessary that:

$$K_D \ll K_{r-2,r-1} (r = 3 \rightarrow r-1) \ll K_{r-1,z} \quad (3.2.2.1)$$

It can be seen that the overall model is comprised of steps representing, nucleation, growth and micelle formation. If the underlying assumptions regarding the intermediate concentrations are to hold, it is necessary to regard the simple Krescheck model as representative of a very highly cooperative self-association, i.e.

$K_G = K_{23}$  etc  $\gg K_D$ . If  $q$  is defined as  $K_G/K_D$ , then  $q$  (cooperativity parameter)  $\rightarrow \infty$ .

$$\text{Now if we define } K_G C_1 = s \quad (3.2.2.2)$$

$$\text{then } K_D = s/q \quad (3.2.2.3)$$

From the Law of Mass Action

$$C_1 = C_1 \quad (3.2.2.4)$$

$$C_2 = \frac{K_G}{q} C_1 \cdot C_1 = \frac{C_1}{q} s \quad (3.2.2.5)$$

$$C_3 = \frac{C_1}{q} s^2 \quad (3.2.2.6)$$

$$C_{r-1} = \frac{C_1}{q} s^{r-2} \quad (3.2.2.7)$$

Let  $K_{r-1,z} = pK_G$

$$\text{then } C_z = p/q C_1 s^{r-1} \quad (3.2.2.8)$$

$$C_A^0 = C_1 + \frac{C_1 s}{q} + \frac{C_1 s^2}{q} \dots + \frac{p}{q} C_1 s^{r-1} - \frac{C_1}{q} \sum_r^{\infty} r s^{r-1} \quad (3.2.3.9)$$

The term  $\frac{C_1}{q} \sum_r^{\infty} r s^{r-1}$  accounts for all species above aggregation number  $z$  and therefore effectively limits the micelle to aggregation number  $z$ .

$$C_A^0 = C_1 + \frac{C_1}{q}((1-s)^2 - 1) + \frac{p}{q} C_1 s^{r-1} - \frac{C_1}{q} \sum_r^{\infty} r s^{r-1} \quad (3.2.3.10)$$

$$C_A^0 = C_1 \left\{ \frac{1}{q}(1-s)^2 + \frac{(q-1)}{q} \right\} + \frac{p}{q} C_1 s^{r-1} - \frac{C_1}{q} \left\{ \sum_r^{\infty} \frac{r(1-s)+s}{(1-s)^2} \right\} \quad (3.2.3.11)$$

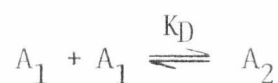
Although the model is simple and may allow an easy interpretation of the kinetic measurements it is obviously unrealistic. It cannot allow for polydispersity.

The models discussed so far (i.e. non-cooperative and infinitely cooperative) represent the two limiting cases of a more general cooperative model for step-wise self-association discussed in the next section.

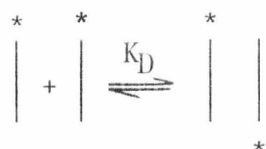
#### 3.2.4 General Cooperative Model for Micelle Formation

The approach developed here is more complex than those described so far. It is increasingly apparent that the early models, although convenient are oversimplified. As more information, particularly accurate kinetic data, becomes available, it is clear that micelle dissociation is not adequately described by a single step.

The first step in any self-association process must be the dimerisation of monomer units, characterised by an equilibrium constant,  $K_D$



There is evidence, from NMR measurements, that surfactant monomers can be more or less adequately represented as rigid rods<sup>(13)</sup>, at least up to a chain-length of 16 - no appreciable bending or coiling of the individual surfactant chains takes place. The dimerisation may then be represented diagrammatically (where the head group (\*) can be charged or uncharged) as:



It is to be expected that there may be some preference for head to tail dimerisation. This dimerisation, however, is associated with the nucleation step. On building up the aggregates beyond the dimer state there are three possibilities. (Ignoring head group effects).

(1) The growth of a linear (one-dimensional) chain:



Assuming only nearest-neighbour interactions (i.e. neglecting any long-range coulombic effects due to charged surfactants), it is clear that the free-energy potential between adjacent surfactant molecules which is responsible for stabilising the aggregate (mainly hydrophobic and dispersive forces) is expected to be independent of aggregate length ( $r$ )

$$\text{i.e. } K_D = K_{r-1,r} \quad (r = 3 \rightarrow \infty)$$

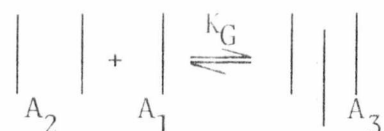
$K_D$  and  $K_{r-1,r}$  are expected to increase with increasing hydrocarbon chain-length.

The formation of such linear r-mers cannot be expected to exhibit CMC phenomena for the reasons already stated. It is, therefore, necessary to introduce aggregate structures which will allow a cooperative interaction between surfactant chains as the aggregation proceeds beyond the dimer stage. There are two possible ways of introducing a cooperative interaction into the growth process.

- (i) the growth of a two-dimensional lamellar sheet
- (ii) the growth of a "loose micelle".

(2) The growth of lamellar aggregates:

The first step in this process is



The hydrocarbon-water interface eliminated in this growth step is likely to be up to a factor of two greater than in a linear growth step. If we define

$$\begin{aligned} \Delta G_{st,D}^0 &= -RT \ln K_D \quad (\text{For nucleation}) & (3.2.4.1) \\ &\approx \Delta G_{st,r-1,r}^0 \end{aligned}$$

then we expect for lamellar growth

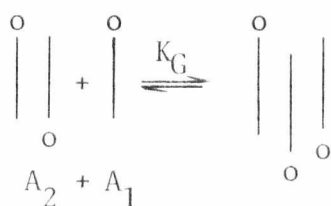
$$\Delta G_{st,D}^0 \leq \Delta G_{st,G}^0 = -RT \ln K_G \leq 2\Delta G_{st,D}^0 \quad (3.2.4.2)$$

We may therefore define a cooperativity parameter ( $q$ ) such that  $K_G = q K_D$ , and from equation (3.2.4.2) we expect  $q$  to vary roughly between 1 and  $K_D$  in a real situation. Furthermore, we expect  $K_G$  to be independent

of  $r$  to a first approximation for the build-up of lamellar aggregates.

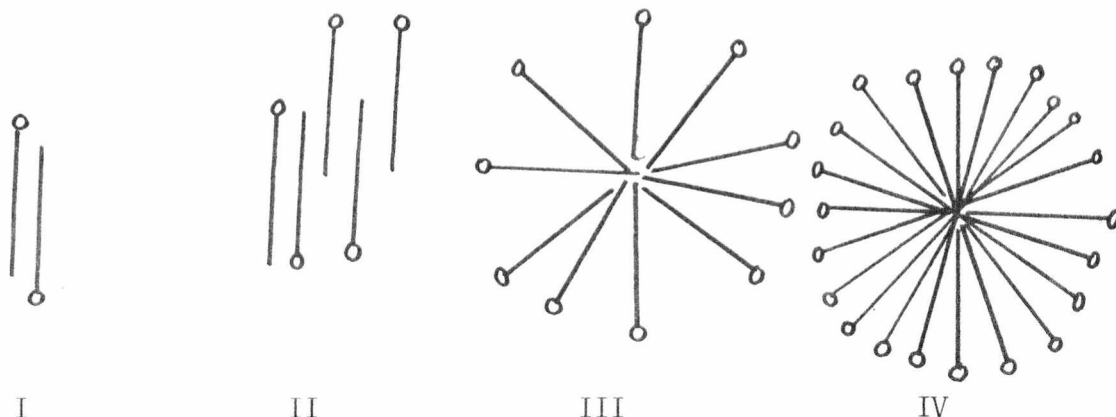
(3) The growth of "loose micelles"

The build-up of this type of structure is much more difficult to visualise, and it is difficult to see how small aggregates of this type could be stabilised to the extent required such that  $K_G > K_D$ . However, the process maybe represented diagrammatically as:



The lamellar aggregates may become more like a "loose" micelle as the aggregation number increases and the "loose" micelle then "fills up" to become a true micelle. The lamellar structure offers strong stabilisation at low  $r$ , and the "loose" micelle allows greater overall stabilisation as the head group interaction potential changes due to counter-ion adsorption.

So we may have a range of structures thus:



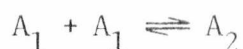
Where the true micelle (4) is formed over a small concentration range this may take the form of a cooperative phase transition (similar to the  $\alpha$ -helix to random-coil transition and liquid-crystal mesophase transitions). Transitions between lamellar and spherical structures have been postulated previously in connection with bio-membrane action<sup>(14)</sup>.

The model therefore describes a cooperative build-up of lamellar aggregates, with the possibility of a cooperative phase transition to aspherical micelle at the CMC. The phase transition may be viewed as a required device to limit the size of the aggregates and produce a range of  $z$  values.

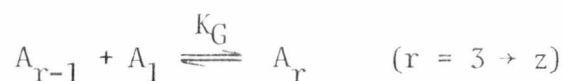
It is not clear over what range of concentrations below the CMC these aggregates ("loose micelles") are likely to build-up. It may be that they would occur at concentrations only just below the measured CMC and so would be difficult to detect and distinguish from true micelles by the usual physical methods.

### 3.2.5 Mathematical Treatment of the Cooperative Model

The nucleation step is:



Further growth could be obtained by the build-up of linear aggregates  $A_1'$ , but for systems exhibiting modest positive cooperativity ( $q > 1$ ), the formation two-dimensional aggregates  $A_r$ , is preferred, since  $K_q > K$  for  $q > 1$ . (In the simple treatment proposed here, linear aggregates beyond the dimer stage are ignored). Therefore, we have



To a first approximation  $K_G \neq f(r)$ .

The final step is the cooperative "phase-transition" between lamellar

aggregates and spherical micelles



For simplicity, we assume only a particular value of  $r$  can produce the "phase-transition". More detailed calculations could easily allow for this transition over a range of values from  $r-x$  to  $r+x$  ( $x < r$ ) with

$$0 = Y-x < Yr-x+c < Y > Yr+x-c > Yr+x = 0 \quad (c = 0 \rightarrow x).$$

This would allow any shape of size distribution to be obtained.

As previously described the dimensionless parameter  $s (= K_G C_1)$  is introduced to enable the concentration of the various aggregates to be expressed in a simple mathematical form.

By means of the Law of Mass Action (neglecting activity coefficients)

$$C_1 = C_1 \quad (3.2.5.1)$$

$$C_2 = K_{G/q} C_1 C_1 = (s/q) C_1 \quad (3.2.5.2)$$

$$C_3 = (s^2/q) C_1 \quad (3.2.5.3)$$

⋮

$$C_r = (s^{r-1}/q) C_1 \quad (3.2.5.4)$$

$$C_z = (Y s^z/q) C_1 \quad (3.2.5.5)$$

From the Law of Mass Conservation:-

$$C_A^0 = \sum_1^z r C_r + z C_z \quad (3.2.5.6)$$

$$= (C_1/q) \{ 2s + 3s^2 \dots r-1 s^{r-2} + r s^{r-1} \} + C_1 \quad (3.2.5.7)$$

$$+ (C_1 Y z s^z)/q \quad (3.2.5.8)$$

$$\text{Since } \sum_2^{\infty} rs^{r-1} = (1-s)^{-2} - 1 \quad (3.2.5.9)$$

$$\text{and } \sum_2^{\infty} (r+1)s^r = s^z(1-s)^{-2}\{z(1-s)+1\} \quad (3.2.5.10)$$

$$\text{then } \sum_2^z rs^{r-1} = (1-s)^{-2} - 1 - s^{z-1} \left\{ z(1-s)^{-1} + s(1-s)^{-2} \right\} . \quad (3.2.5.11)$$

Since  $C_1 = s/K_G$

$$\begin{aligned} C_A^0 = (s/K_G) \left\{ q^{-1}(1-s)^{-2} + (q-1)/q \right\} - (s/K_G) \left\{ s^{z-1} q^{-1} \left\{ z(1-s)^{-1} + s(1-s)^{-2} \right\} \right\} \\ + (s/K_G) \left\{ z \cdot 1/s^{z-1} q^{-1} \right\} \end{aligned} \quad (3.2.5.12)$$

The concentration of monomer  $-C_1-$  for any value of  $s = s/K_G$ . The concentration of spherical micelle expressed in terms of monomers  $-zC_z-$  for any value of  $s = (s/K_G) \left\{ z \cdot 1/s^{z-1} q^{-1} \right\}$ .

It is possible to define the CMC qualitatively as the total concentration at which

$$C_1 = zC_z \quad \text{i.e. when } s = (q/zY)^{z-1} . \quad (3.2.5.13)$$

It is also possible to calculate the concentration of intermediate aggregates. Such aggregates are likely to predominate at concentrations just below the CMC. If the probability of the formation of spherical micelles is low (i.e.  $Y < K_G C_1$ ) the aggregation number will increase beyond  $z$ . However, only a small range of spherical  $z$ -mers is stable. Therefore whether lamellar or spherical aggregates predominate depends to a large extent on the ratio  $Y/s$ .

Equation (3.2.5.12) can be readily simplified if a less complex model is adopted. For example, if only one type of aggregate is formed, as in

the case of lamellar aggregates,  $Y = 0$  and:

$$C_A^0 = \left\{ s/K_G q \right\} \left\{ (1-s)^{-2} + q-1 \right\} \quad (3.2.5.14)$$

If  $q = 1$ , i.e. the growth is non-cooperative

$$C_A^0 = \left\{ s/K_G \right\} \left\{ (1-s)^{-2} \right\} \quad (3.2.5.15)$$

If only a monomer-dimer equilibrium is present, i.e.  $q = 0$  we have:

$$C_A^0 = s(1+2s)/K_D \quad (\text{where } s = K_D C_1) \quad (3.2.5.16)$$

For the situation where cooperativity is especially strong

$$q \rightarrow \infty \quad \text{and} \quad Y \rightarrow \infty$$

Then

$$C_A^0 = \left\{ s/K_G \right\} \left\{ 1 + zYs^{z-1} q^{-1} \right\} \quad (3.2.5.17)$$

$$= s/K_G \quad (\text{for } C_A^0 < \text{CMC}) \quad (3.2.5.18)$$

i.e.  $C_1 = C_A^0$ , until spherical micelles are formed, when  $s = 1.0$

This highly cooperative combination is shown in figure 3.2.5.1.

At total concentrations below A, only monomer is present in solution (A is equal to  $K_G^{-1}$ ). Above A, the monomer concentration is buffered, ( $dC_1/dC_A^0 = 0$ ) and the only species being formed are micelles  $M_z$ . The concentration at B =  $2/K_G^{-1}$  and  $C_1 = zC_z$ , which gives a more quantitative measure of the CMC. However, this situation represents a limiting case for which we must assume  $q > 10^3$ . Many surfactants exhibit CMC's around  $10^{-3}$  M (see figure 1.2.1, Chapter 1). This implies  $K_G \sim 10^3 \text{M}^{-1}$  and then  $K_D$

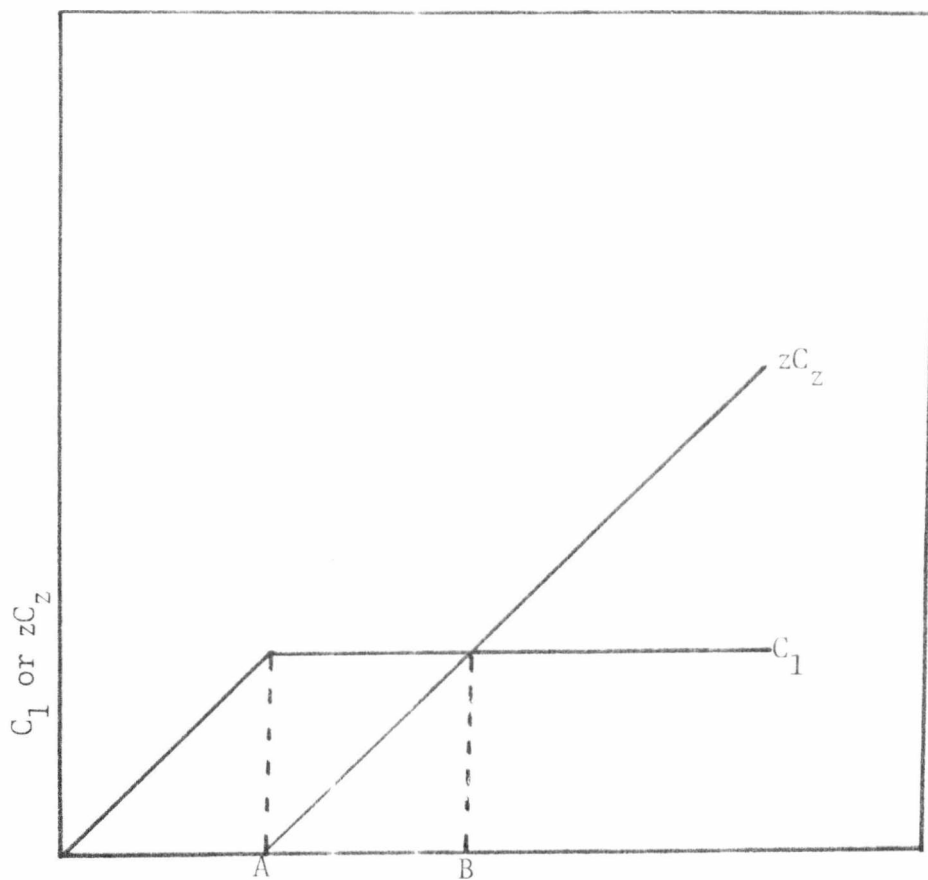


FIGURE 3.2.5.1

DEPENDENCE OF  $C_1$  AND  $zC_z$  ON  $C_A^0$  FOR THE CASE OF INFINITE  
COOPERATIVITY  $q = \infty$ ,  $Y = \infty$

must be  $< 1M^{-1}$ . Since we have argued that it is unlikely for  $q$  to be  $> 2K_D$ , the limiting situation is not to be expected for surfactants with CMC's greater than  $10^{-3}M$ .

More realistic models must assume very different values for  $q$  and  $K_D$ . In figure 3.2.5.2 the effect of finite cooperativity  $q$  on the concentration of monomer close to the CMC is shown. It can be seen that deviations from limiting behaviour occur at progressively lower values of  $s$  as  $K_G C_A^0$  is increased. The plot was computed by means of equation (3.2.5.12).

Mukerjee<sup>(15)</sup> has suggested that likely values of  $K_D$  are in the region  $10^{-2}M^{-1}$  for  $C_{10}-C_{14}$  surfactants. Since  $q$  is related to  $K_D$ , values of

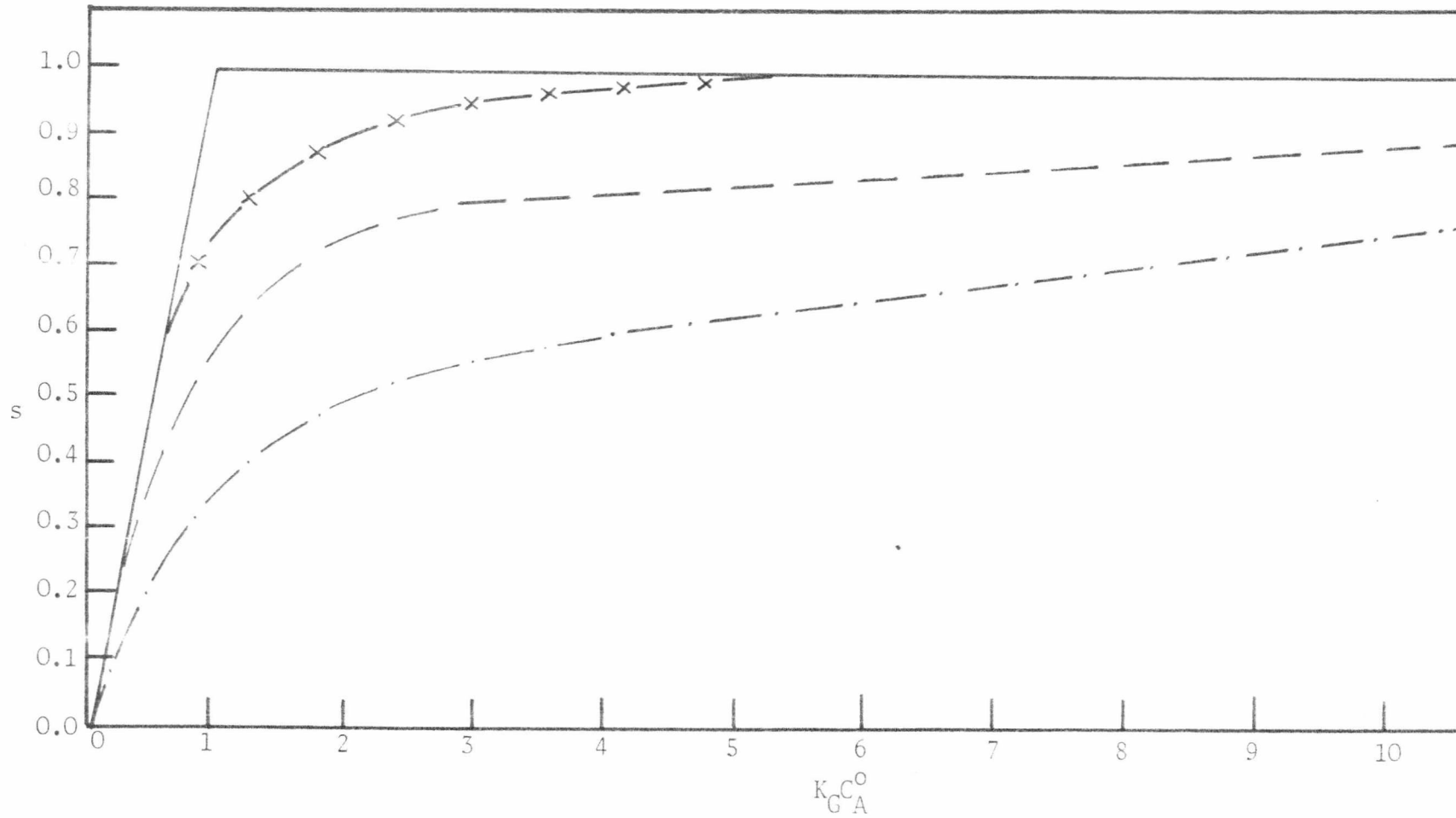


FIGURE 3.2.5.2

DEPENDENCE OF  $s$  ON  $K_G C_A^0$  FOR MICELLAR SYSTEMS EXHIBITING FINITE COOPERATIVITY. —  $q = 10^4$ , -x-x-  $q = 10^2$ ,  
 - - -  $q = 10$ , - · - · -  $q = 1$

$10^2-10^4\text{M}^{-1}$ , and CMC's in the  $10^{-2}-10^{-4}\text{M}$  region, as found experimentally.

For surfactants in which the spherical micelle predominates, large values of  $Y$  are indicated. The effect of changing the adjustable parameters -  $K$ ,  $q$ ,  $z$ ,  $Y$  - is shown in figures 3.2.5.3 - 10 for the complete model. The figures show:-

- (i) For the likely situation of  $10 < q < 100$  and  $z = 10^2$ , there is a progressive build-up of pre-micelle aggregates in a concentration range within a factor of 2 or so below the CMC. The CMC is clearly difficult to define in this situation; it is probably most usefully described as when  $C_1 = zC_z$ , and so this definition is adopted for the general cooperative scheme.
- (ii) The CMC is then not very sensitive to large changes in  $Y$ . (Figures 3.2.5.3 and 4).
- (iii) The presence of pre-micelle aggregates is sensitive to the value of  $q$ , but no such aggregates are formed below the CMC for  $q > 10^3$ . (Figures 3.2.5.5-8).
- (iv) The CMC increases proportionately as  $z$  increases and the likelihood of pre-micelle aggregates increases as  $z$  increases.
- (v) If a threshold concentration of micelle is required by the process used for detecting the CMC, then practically it may be useful to use an alternative definition of the CMC as when  $zC_z$  reaches a certain absolute concentration e.g.  $10^{-5}\text{M}$ . With the CMC defined in this way, the plots shown in figures



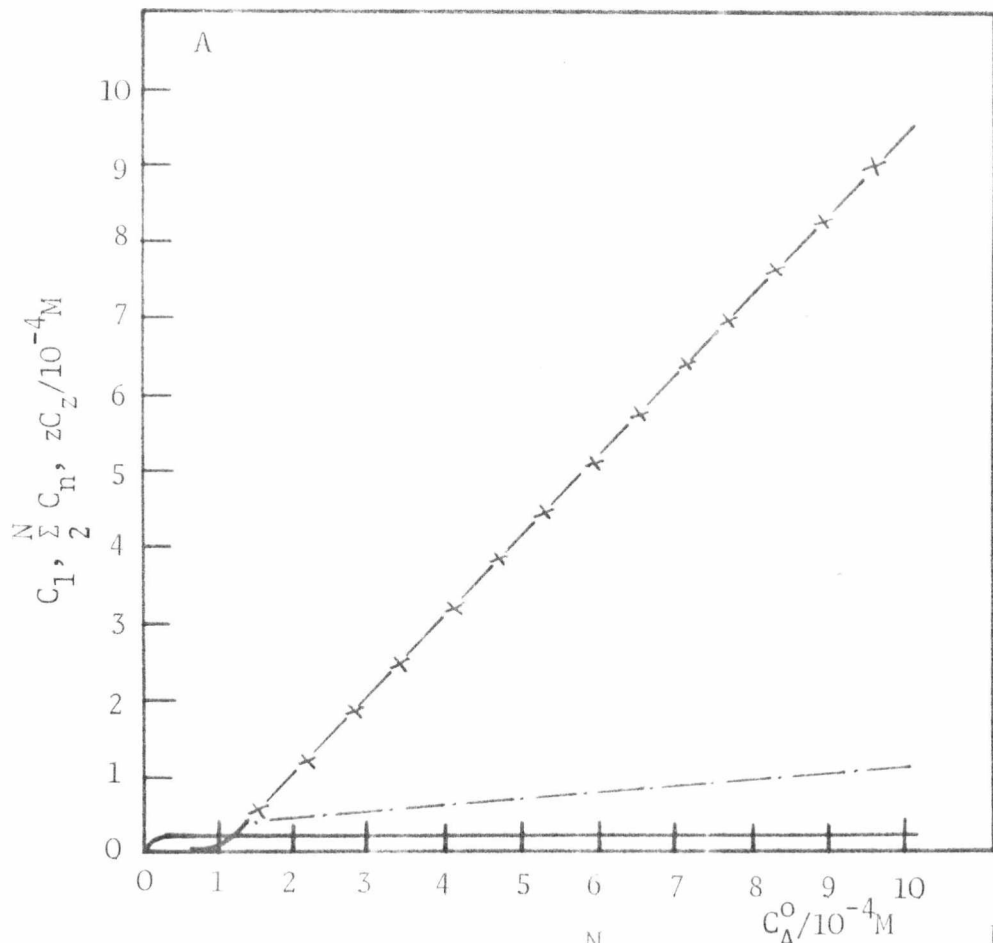


FIGURE 3.2.5.5 DEPENDENCE OF  $C_1$ ,  $\sum \frac{N}{2} C_n$  &  $zC_z$  ON  $C_A^0$   $z = 60$   
 $K_D = 30M^{-1}$   
 $Y = 10^3, q = 500$

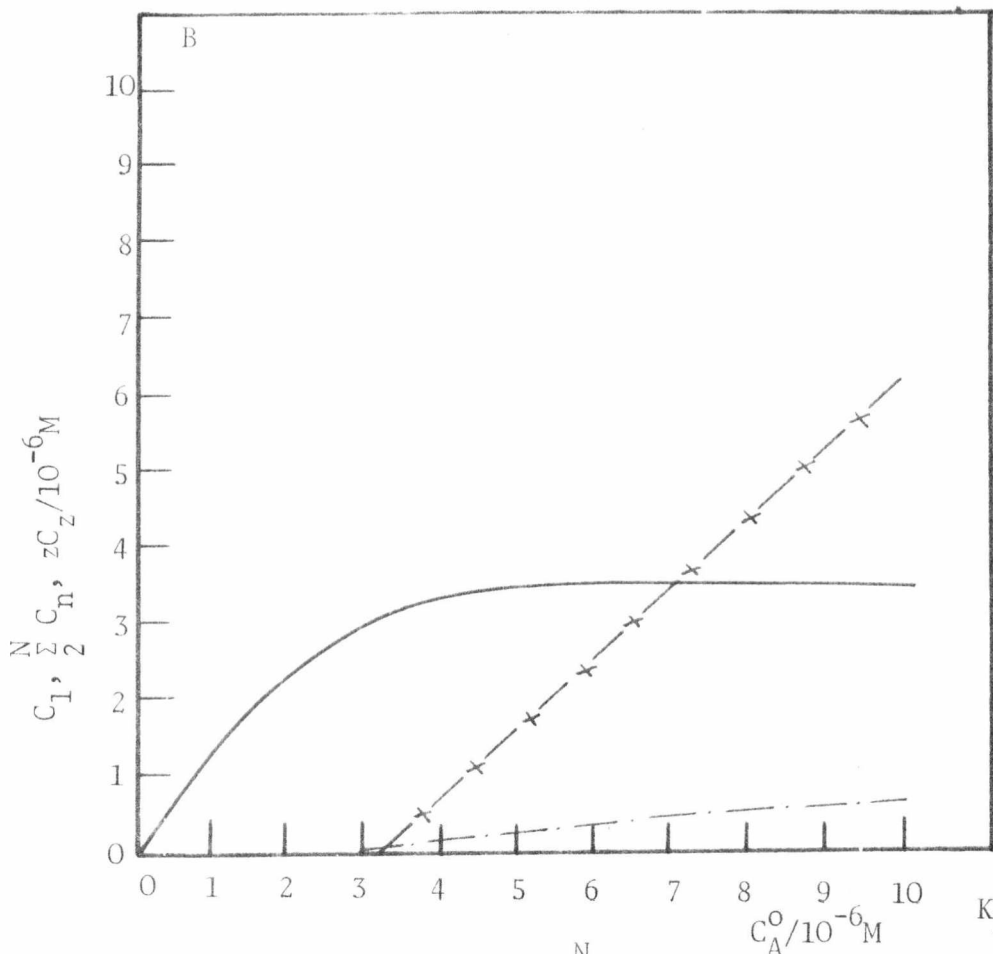


FIGURE 3.2.5.6 DEPENDENCE OF  $C_1$ ,  $\sum \frac{N}{2} C_n$  AND  $zC_z$  ON  $C_A^0$   $z = 60$   
 $K_D = 30M^{-1}$   
 $q = 10^4$

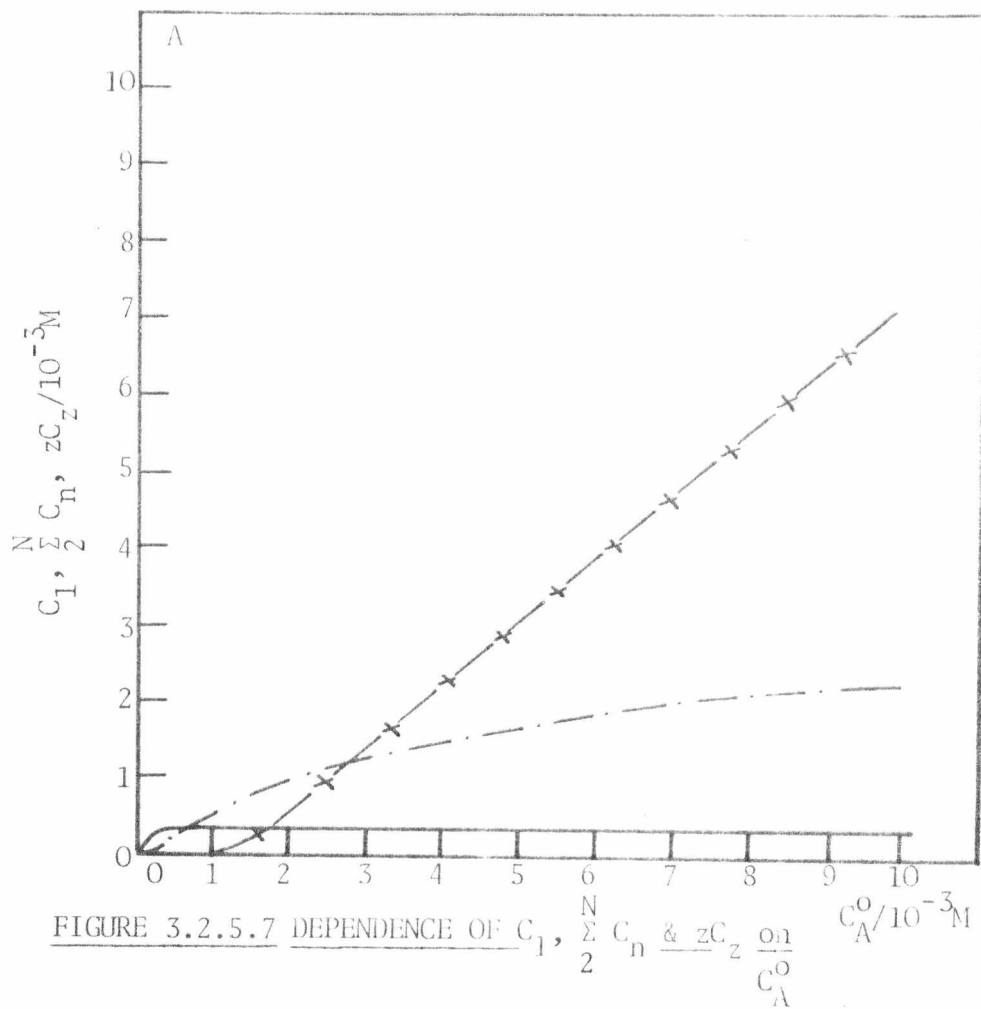


FIGURE 3.2.5.7 DEPENDENCE OF  $C_1, \sum_{n=1}^N C_n$  &  $zC_z$  ON  $C_A^0$

$z = 60$   
 $K_D = q = 50$

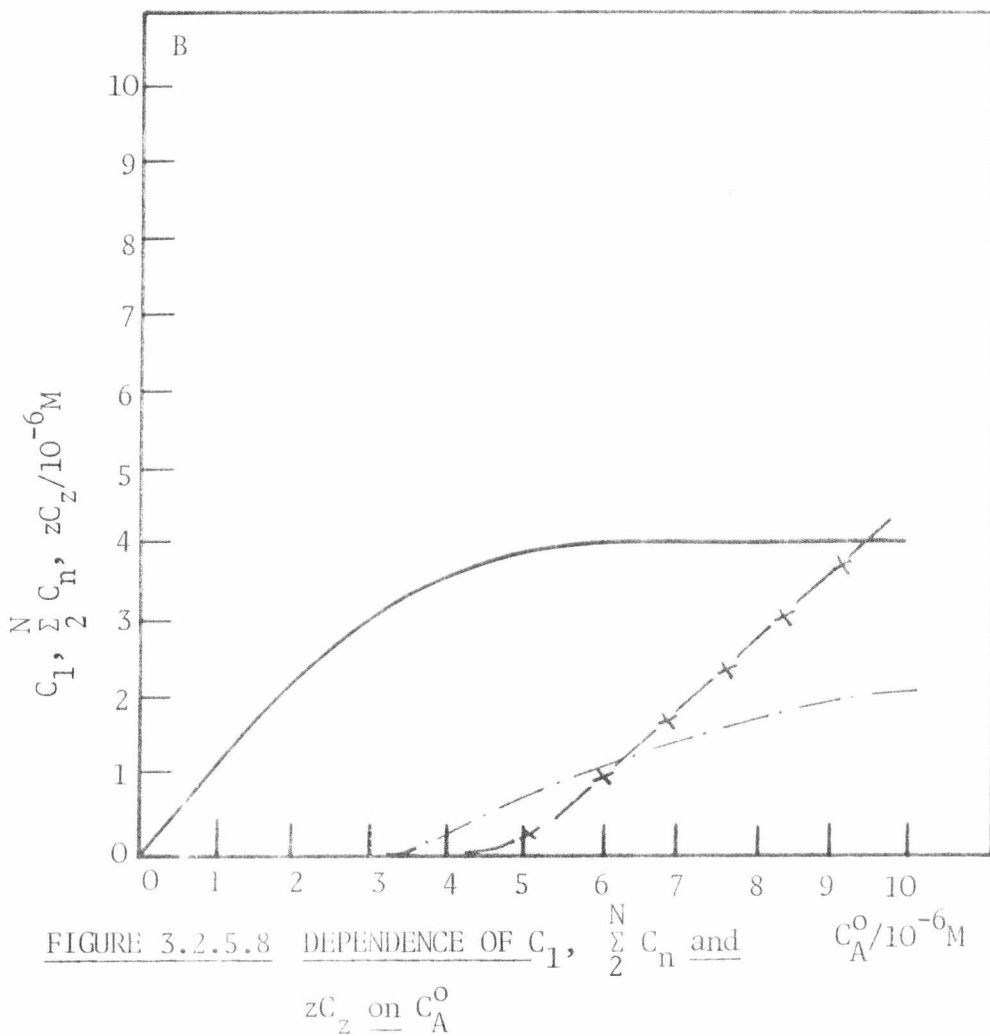


FIGURE 3.2.5.8 DEPENDENCE OF  $C_1, \sum_{n=1}^N C_n$  AND  $zC_z$  ON  $C_A^0$

$z = 60$   
 $K_D = q = 500$

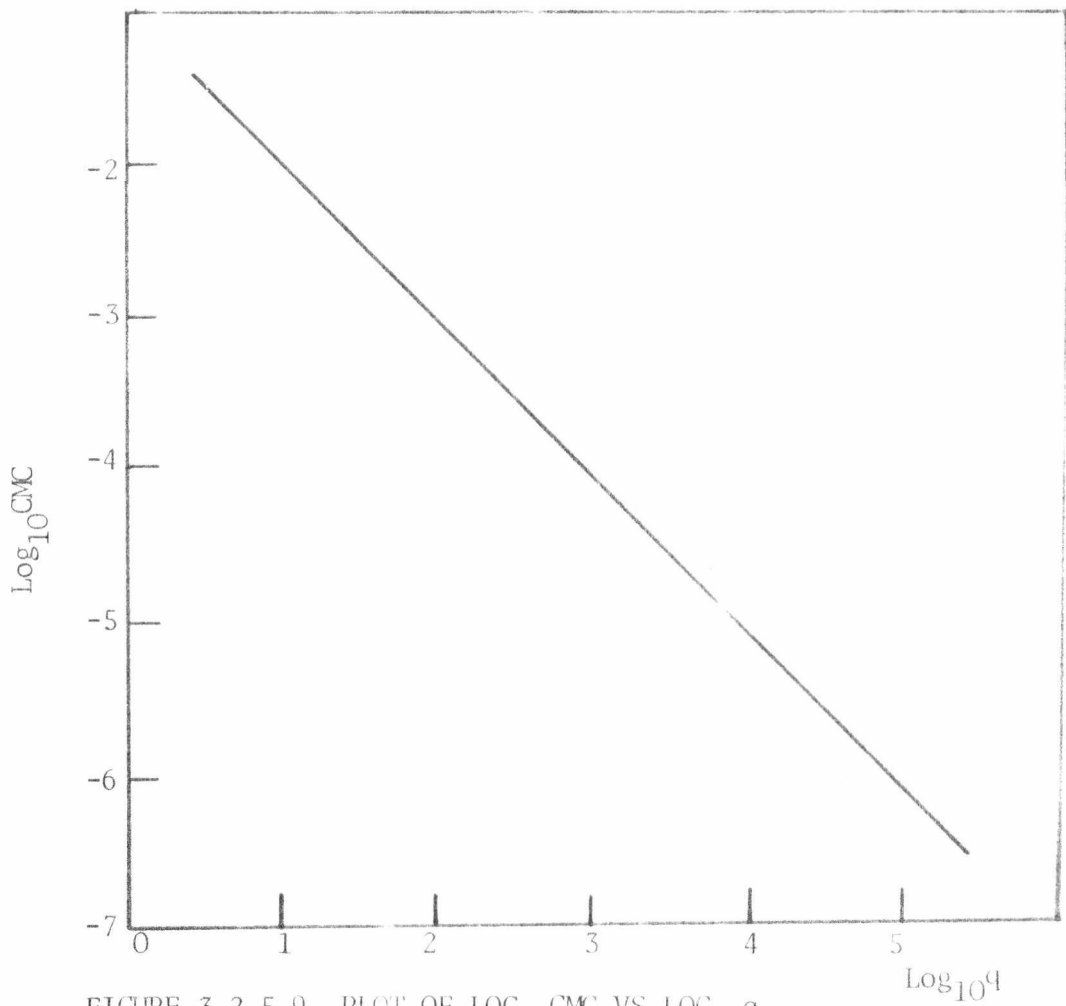


FIGURE 3.2.5.9 PLOT OF  $\text{LOG}_{10} \text{CMC}$  VS  $\text{LOG}_{10} q$   
 $z = 60, K_D = 30M^{-1}, Y = 10^3$

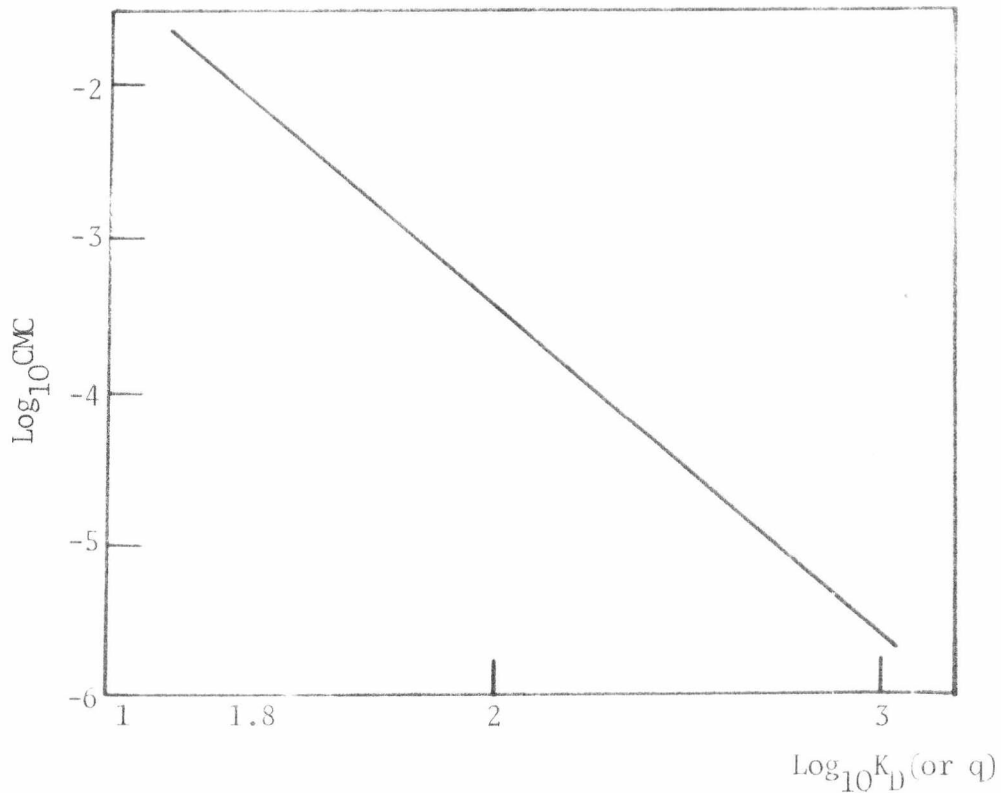


FIGURE 3.2.5.10 PLOT OF  $\text{LOG}_{10} \text{CMC}$  VS  $K_D \text{ (or } q)$   
 $z = 60, Y = 10^3$

3.2.5.9 & 10 are obtained for the dependence of the CMC on  $q$  and  $K_{D,q}$  (when both are varied synchronously).

- (vi) Values of  $K_D = 25$ ,  $q = 25$ ,  $z = 60$  and  $Y = 10^4$  give a good representation of the behaviour of sodium dodecyl sulphate in aqueous solution. (Figure 3.2.5.11).

The model allows several further predictions which are capable of experimental verification:

- (i) It is to be expected that as the hydrocarbon chain-length of the surfactant increases,  $K_D$  and  $q$  would increase. Therefore, as the hydrocarbon chain-length decreases, the growth of pre-micellar aggregates would seem to be more likely, although this is compensated to some extent by the lower value of  $z$ .
- (ii) The value of  $Y$  would be sensitive to the hydrocarbon chain-length and to  $M$ , the sharpness of the transition would increase as  $z$  increased. Such a process would also be sensitive to the presence of small amounts of "impurities": in contrast to the nucleation and growth processes.
- (iii) The effect of ionic strength on the micelle formation process is expected to operate primarily through an increase in  $K_D$  and  $K_G$ . In the aggregation process for charged surfactants, the counterion can operate through a charge-screening mechanism. From studies on charged dyes, an ionic strength of 0.1M should lead to a doubling of  $K_D$  and  $K_G$ , and a

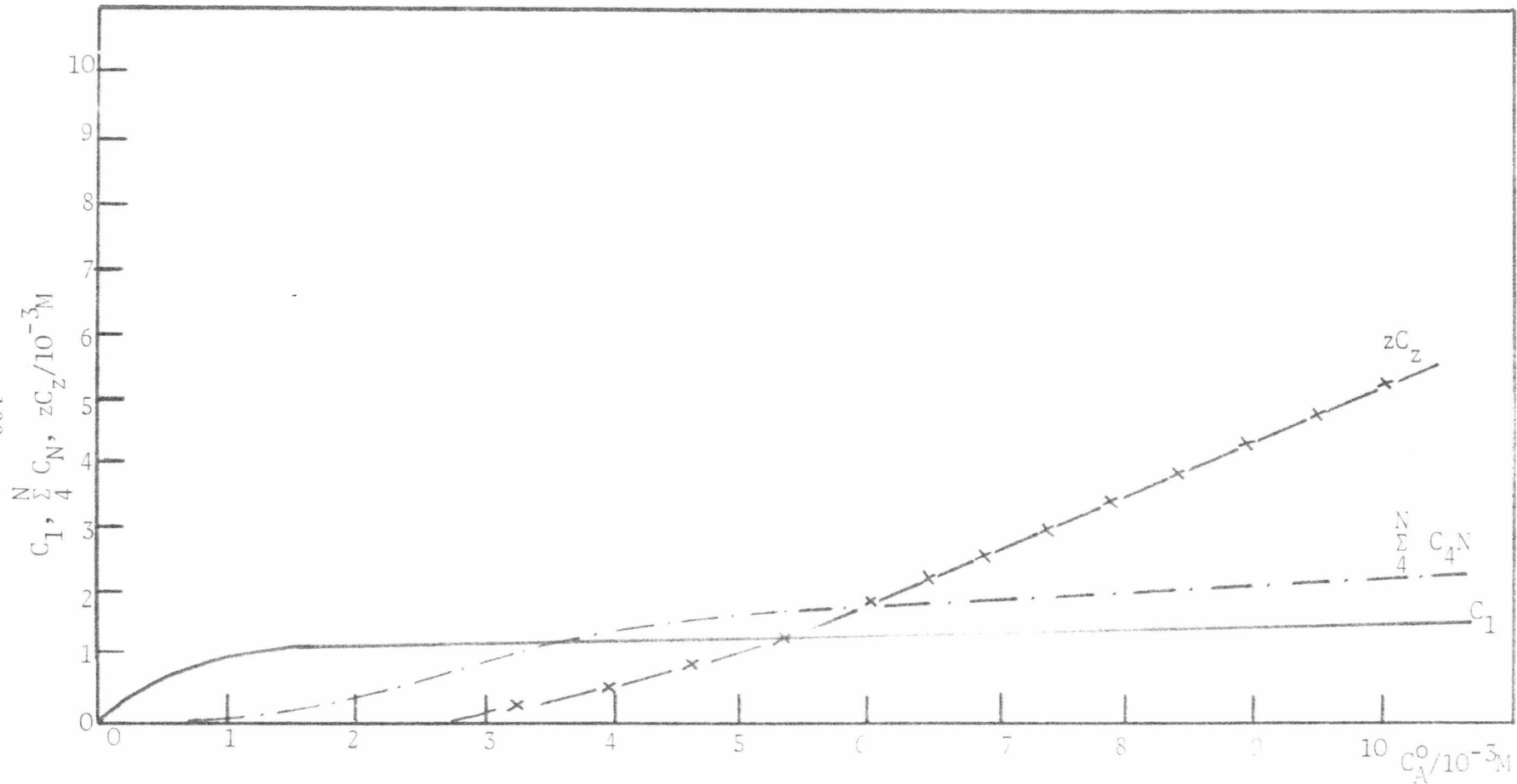


FIGURE 5.2.5.11

REPRESENTATION OF DEPENDENCE OF  $C_1$ ,  $\sum_{n=4}^N C_n$  and  $zC_z$  FOR SODIUM DODECYL SULPHATE  $z = 60$ ,  $K_D = q = 25$ ,  
 $Y = 10^4$

corresponding decrease of the CMC.

For micellar systems in water, the ultrasonic technique detects a relaxation process in the microsecond time range<sup>(16-17)</sup>. An analogous relaxation (generally time unresolvable) has also been observed using the temperature-jump<sup>(18-20)</sup> and pressure-jump methods<sup>(21)</sup>. On the model proposed, this relaxation may be associated with the exchange of monomeric surfactant to and from a micelle or the exchange of a monomer end-unit to and from a lamellar aggregate. The slow relaxation detected by temperature-jump<sup>(18-20,22)</sup> and pressure-jump<sup>(23)</sup> may be due to the cooperative phase-transition (which is known to be slow in the case of the liquid crystalline-crystalline phase transition of dimyristoyl L- $\alpha$ -Lecithin bilayers)<sup>(24)</sup> and/or the complete dissolution of the micelle.

The most recent and comprehensive kinetic and thermodynamic model of micelle formation has been given by Aniansson et al<sup>(25)</sup>. The model put forward by Aniansson et al is essentially similar to the one developed here. The micelle is considered polydisperse and is formed via a small nucleus (6-10 monomers). The build-up from the nucleus stage is rapid and must be considered to be a cooperative process.

## REFERENCES

- (1) B.H. Robinson, A. Löffler and G. Schwarz, *J. Chem. Soc. Faraday I*, 1973, 69, 56.
- (2) F. Franks and H.T. Smith, *J. Phys. Chem.*, 1964, 68, 3581.
- (3) P. Mukerjee, K.J. Mysels and C.I. Dulin, *J. Amer. Chem. Soc.*, 1958, 62, 1390.
- (4) D. Eagland and F. Franks, *Trans. Faraday Soc.*,
- (5) P. Mukerjee, K.J. Mysels and C.I. Dulin, *J. Amer. Chem. Soc.*, 1958, 62, 1400.
- (6) P. Mukerjee, *J. Phys. Chem.*, 1972, 76, 565.
- (7) P.O.P. Ts'o, Molecular Association in Biology, ed. B. Pullman, (Academic Press, New York, 1968), p.39
- (8) G.C. Krescheck, E. Hamori, G. Davenport and H.A. Scheraga, *J. Amer. Chem. Soc.*, 1966, 88, 246.
- (9) N. Muller, *J. Phys. Chem.*, 1972, 76, 3017.
- (10) T. Nakagawa, *Colloid Polymer Sci.*, 1974, 252, 56.
- (11) R. Folger, H. Hoffmann and W. Ulbricht, *Ber. Bunsenges Phys. Chem.*, 1974, 78, 986.
- (12) E.A.G. Aniansson and S.N. Wall, *J. Phys. Chem.*, 1974, 78, 1024.
- (13) N. Muller, Reaction Kinetics in Micelles, ed. E. Cordes (Plenum, New York, 1973).
- (14) J.A. Lucy, *J. Theoret. Biol.*, 1965, 7, 360.
- (15) P. Mukerjee, *J. Phys. Chem.*, 1965, 69, 2821.
- (16) E. Graber, J. Lang and R. Zana, *Kolloid-Z-Z Polym.*, 1970, 238, 470.
- (17) P.J. Sams, E. Wyn-Jones and J. Rassing, *Chem. Phys. Lett.*, 1972, 12, 233.
- (18) K. Takeda and T. Yasunaga, *J. Colloid Interface Sci.*, 1973, 45, 406.
- (19) B.C. Bennion, L.K.J. Tong, L.P. Holmes and E.M. Eyring, *J. Phys. Chem.*, 73, 3288.

- (20) J. Lang and E.M. Eyring, *J. Polymer Sci.*, 1972, A-210, 89.
- (21) J. Lang, C. Tondre, R. Zana, R. Bauer, H. Hoffmann and W. Ulbricht, *J. Phys. Chem.*, 1975, 79, 276.
- (22) K. Takeda and T. Yasunaga, *J. Colloid. Interface Sci.*, 1972, 40, 127.
- (23) T. Yasunaga, H. Oguri and M. Miura, *J. Colloid. Interface Sci.*, 1967, 23, 352.
- (24) T.Y. Tsong, *Proc. Nat. Acad. Sci.*, 1974, 71, 2684.
- (25) E.A.G. Aniansson, S.N. Wall, M. Almgren, H. Hoffmann, I. Kielmann, W. Ulbricht, R. Zana, J. Lang and C. Tondre, *J. Phys. Chem.*, 1976, 80, 905.

CHAPTER 4

DETERMINATION OF CRITICAL MICELLE CONCENTRATIONS BY

THE DYE-PROBE TECHNIQUE

## CHAPTER 4

### DETERMINATION OF CRITICAL MICELLE CONCENTRATIONS BY THE DYE-PROBE TECHNIQUE

#### 4.1 Introduction

There are a great many methods which may be used to determine the CMC of surfactant solutions, some of which have already been mentioned in Chapter 1. Since the object of the present work has been to study the interaction of "hydrophobic" dyes with surfactants both above and below the CMC, the CMC's were determined by the "dye-probe" method<sup>(1)</sup>.

The dye-probe method relies on the dye exhibiting (i) a change in extinction coefficient ( $\epsilon$ ) and/or (ii) a shift in the main absorption peak for spectrophotometric detection, and/or (iii) a change in quantum yield for fluorescence detection, as the concentration of surfactant is increased beyond the CMC.

Although this is the most convenient and widely applied method for the determination of CMC's for all classes of surfactants<sup>(2)</sup>, it has been criticised in the past because it tends to produce values of the CMC for a given surfactant which are up to 15% lower than the values obtained by surface-tension or conductivity methods<sup>(3)</sup>. This decreased CMC has been attributed to the formation of dye-induced micelles, in which the dye-surfactant ratio may be as low as 1:10<sup>(4)</sup>. The dye which has been generally used for CMC determinations is the rod-shaped pinacyanol chloride. Mukerjee et al have discussed the effects of this dye on the CMC of sodium dodecyl sulphate in some detail<sup>(4)</sup>. Their conclusions are (i) the CMC is dependent on the concentration of the dye (ii) curiously the CMC approaches the surface-tension value as the dye concentration is increased (iii) the "dye-rich" micelles become "normal" micelles as the micellar concentration is increased and (iv) on increasing the ionic

strength the CMC values obtained by ~~the~~ dye approach those from surface-tension and conductivity. There is some independent evidence from fluorescence energy-transfer experiments<sup>(5)</sup>, for the formation of dye-rich micelles at concentrations very close to the CMC.

In the present study it is found that for planar acridine and related dyes: (i) the CMC's are not dependent on dye concentration in the range  $4 \times 10^{-7} \text{M} - 3 \times 10^{-5} \text{M}$ , (ii) the CMC's are independent of dye structure and (iii) the CMC's are approximately 10% lower than surface-tension and conductance literature values<sup>(3)</sup>.

#### 4.2 Spectrophotometric Determination of CMC's

The characteristic observations described below apply to all the dyes used in this study. The specific case of acridine orange ( $\text{AO}^+$ ) interacting with sodium dodecyl sulphate (SDS) will be discussed in detail since it exemplifies the approach.

From the acridine orange-sodium dodecyl sulphate visible absorption spectrum in figure 4.2.1a, two distinct types of interaction are apparent. For a fixed total concentration of dye ( $\sim 10^{-5} \text{M}$ ), and concentrations of SDS below the CMC the spectrum of  $\text{AO}^+$  exhibits both a hypsochromic shift (492 to 468 nm) and hypochromism at the monomer peak wavelength 492 nm, the extinction coefficient at 492 nm decreasing from 55,000 to  $20,000 \text{M}^{-1} \text{cm}^{-1}$  as the concentration of SDS is increased below the CMC. Both these effects have been observed previously from the process of planar sandwich-type stacking of the dye alone<sup>(6)</sup>, ("end-on" aggregation will lead to a blue-shift of the absorption peak)<sup>(7)</sup>.

No isosbestic point is observed showing that there are at least three absorbing species in solution. These are most likely to be monomer, dimer and some form of stacked dye. This type of behaviour seems to indicate the formation of a mutually-induced aggregate species involving

both the positively-charged dye and the surfactant anion.

The spectra of the dye-surfactant solutions below the CMC are time dependent to some extent, the intensity of absorption decreasing with time<sup>(8)</sup>, due to the slow build-up of colloidal size particles in the solution. The increase in turbidity takes place over a period of many minutes, generally the decrease in absorbance is not more than 20% over a period of thirty minutes. Turbidity first becomes apparent at SDS concentrations of approximately  $10^{-4}$ M and continues up to approximately  $2 \times 10^{-3}$ M. Above  $2 \times 10^{-3}$ M the turbidity decreases and the rate of formation of the larger aggregates becomes very slow.

To reduce the effect of turbidity on the absorption spectra, the surfactant and dye solutions are separately pre-thermostatted. The stock dye solution was then added to the diluted surfactant solution in a graduated flask and after shaking  $3\text{cm}^3$  were rapidly transferred to the cuvette. The time required for thermostating in the spectrophotometer was thereby reduced to less than two minutes and so the effect of turbidity on the recorded spectra is negligible.

In order to confirm that the observed slow effect was due to aggregation of the dye below the CMC due to a mutually-induced process involving both dye and surfactant ion, and was not simply a specific ion-pair interaction with the sulphate headgroup or an ionic strength effect, the possibility of an interaction of  $\text{AO}^+$  with sodium methyl sulphate (SMeS) was investigated. It was found that for concentration of SMeS up to 0.2M, only small changes in the  $\text{AO}^+$  spectrum were observed. The magnitude of these changes can be attributed solely to the increase in the extent of dimerisation of the dye with increasing ionic strength (I) of the solution. The dimerisation constant ( $K_D$ ) of the dye has been previously found to be  $1 \times 10^4 \text{M}^{-1}$ ,  $I = 0$  and  $1.6 \times 10^4 \text{M}^{-1}$ ,  $I = 0.1$ <sup>(6)</sup>.

The strength of the induced aggregation interaction, estimated from

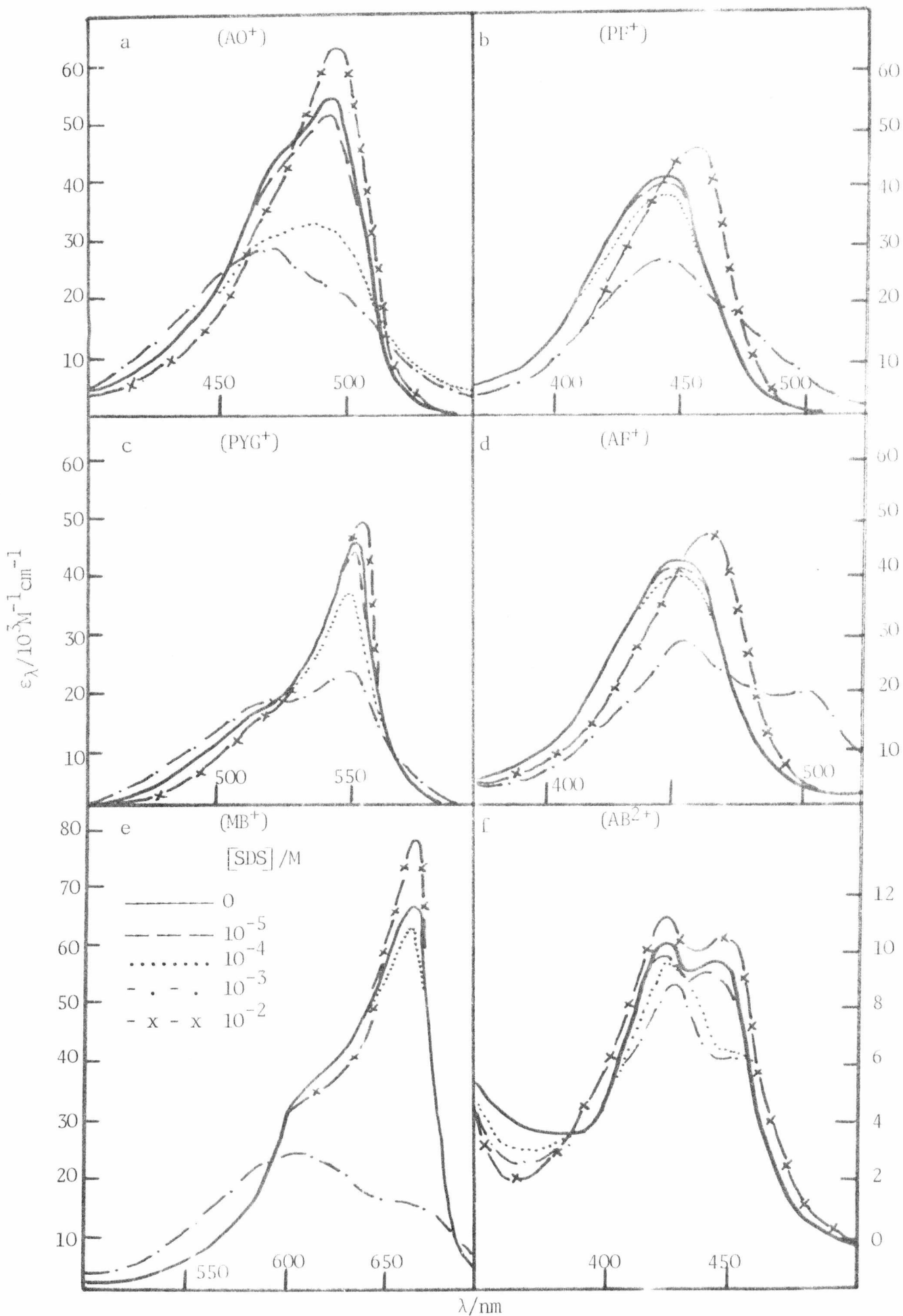


FIGURE 4.2.1 ABSORPTION SPECTRA FOR THE INTERACTION BETWEEN DYES AND SODIUM DODECYL SULPHATE AT 298.2K

the concentration of surfactant corresponding to the mid-point of the "S" shaped-binding curves ( $K_{SD}$ ) (for example figures 4.2.2,3) increases as the alkyl-chain length of the surfactant increases. The larger the value of  $K_D$  of the dye concerned the stronger the interaction, see table 4.2.1.

The solutions become cloudy in the region of surfactant-to-dye ratios 10-100. The extent of the cloudiness is dependent upon  $K_D$ , the chain-length of the surfactant, concentration of the dye.

Also the rate of growth of aggregates also increases with  $K_D$  and the surfactant chain-length (see Chapter 5 for kinetic details). The driving force for the interaction must be the hydrophobicity of the dye and surfactant alkyl-chains. Since the dye and surfactant are electrostatically held together the mutual aggregation process is unhindered by repulsive coulombic interactions. The term mutually-induced is applied to the aggregation process, since the process is dependent on the natural tendency for both species to aggregate in solution. This is greatly enhanced when the charge repulsion is reduced.

In the region of the CMC there is an increase in the extinction coefficient at the new  $\lambda_{max}$  of 498nm, which corresponds to a slight red shift of the absorption maximum of the monomer  $AO^+$  in free solution. The bathochromic shift indicates that the dye becomes incorporated (absorbed) into some part of the micelle. The dye-surfactant solutions above the CMC are stable and the absorption spectrum is unchanged over a period of twenty-four hours. These spectral changes resemble those observed for the binding of  $AO^+$  to DNA<sup>(9)</sup>. The pre-CMC interaction is similar to the outside stacking of the dye i.e. a weak electrostatic binding site, and the spectrum of  $AO^+$  above the CMC is similar to that of the intercalated dye, although the red-shift is not so pronounced.

An isosbestic point is observed at 525nm for concentrations of surfactant ( $C_{10}$ - $C_{16}$ ) above the CMC which indicates that the dye is in

TABLE 4.2.1

## STRENGTH OF DYE-SURFACTANT INTERACTION BELOW THE CMC

DYE	$10^{-2}K_D/M^*$	SURFACTANT		$10^{-3}K_{SD}/M$
		n	HEAD GROUP	
AO <sup>+</sup>	100	10	SO <sub>4</sub> <sup>-</sup>	2.2
		12	SO <sub>4</sub> <sup>-</sup>	13
		12	SO <sub>3</sub> <sup>-</sup>	2.6
		12	 -SO <sub>3</sub> <sup>-</sup>	21
		14	SO <sub>4</sub> <sup>-</sup>	70
		16	SO <sub>4</sub> <sup>-</sup>	400
PF <sup>+</sup>	5	10	SO <sub>4</sub> <sup>-</sup>	0.7
		12	SO <sub>4</sub> <sup>-</sup>	4
MB <sup>+</sup>	70	12	SO <sub>4</sub> <sup>-</sup>	1.6
PYG <sup>+</sup>	30	12	SO <sub>4</sub> <sup>-</sup>	0.6
AF <sup>+</sup> †	~1	12	SO <sub>4</sub> <sup>-</sup>	60
AB <sup>2+</sup> †	~5	12	SO <sub>4</sub> <sup>-</sup>	4

\* see Chapter 2 for references.

† Estimated during the course of this work.

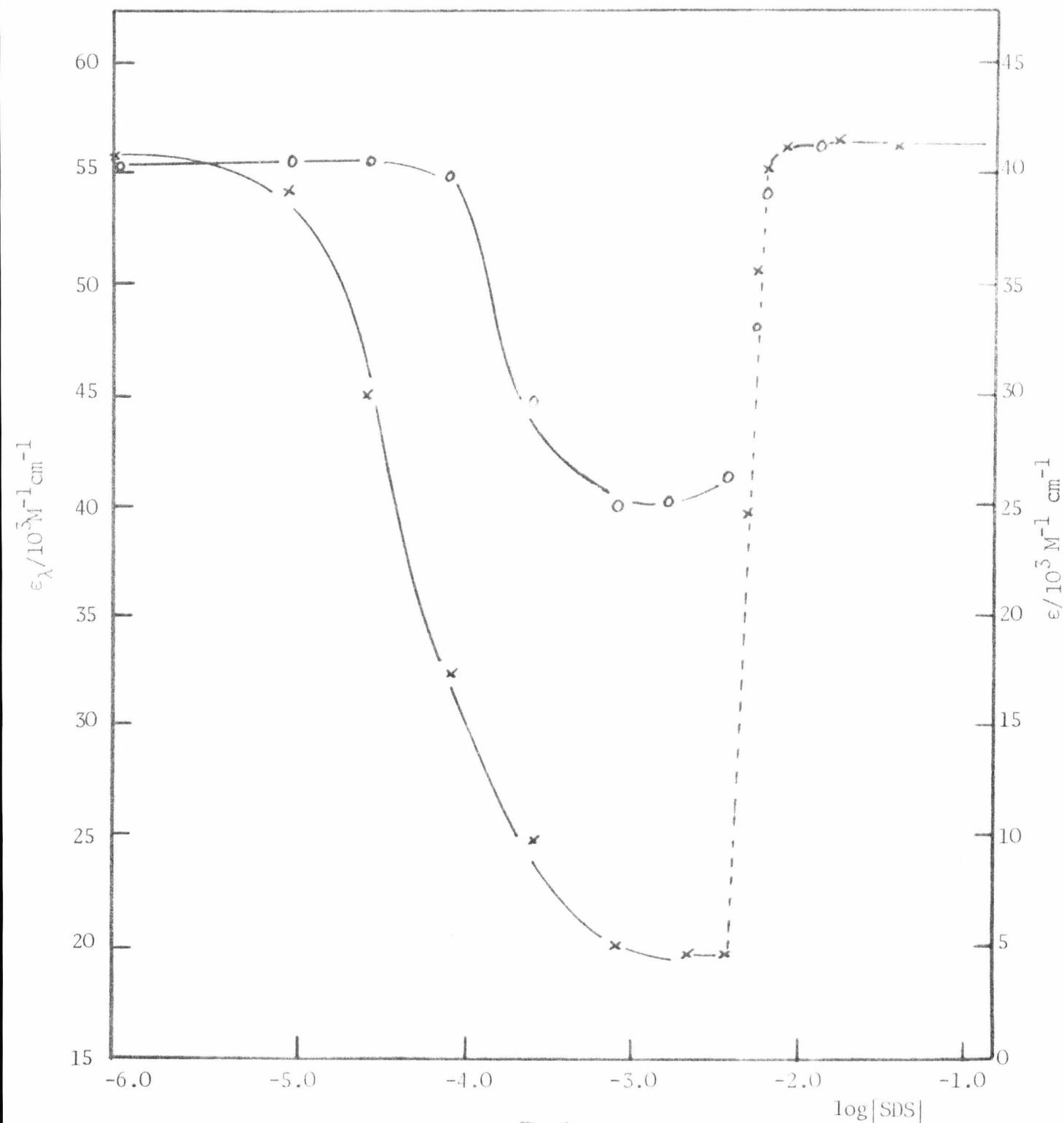


FIGURE 4.2.2 PLOT OF  $\epsilon_{\lambda \text{nm}} \text{ M} \log_{10} [\text{SDS}]$  FOR DETERMINATION OF THE CMC

-x- AO<sup>+</sup><sub>492nm</sub>, -o- PF<sup>+</sup><sub>444nm</sub>

[Dye]  $1 \times 10^{-5} \text{ M}$ , Temp 298.2K

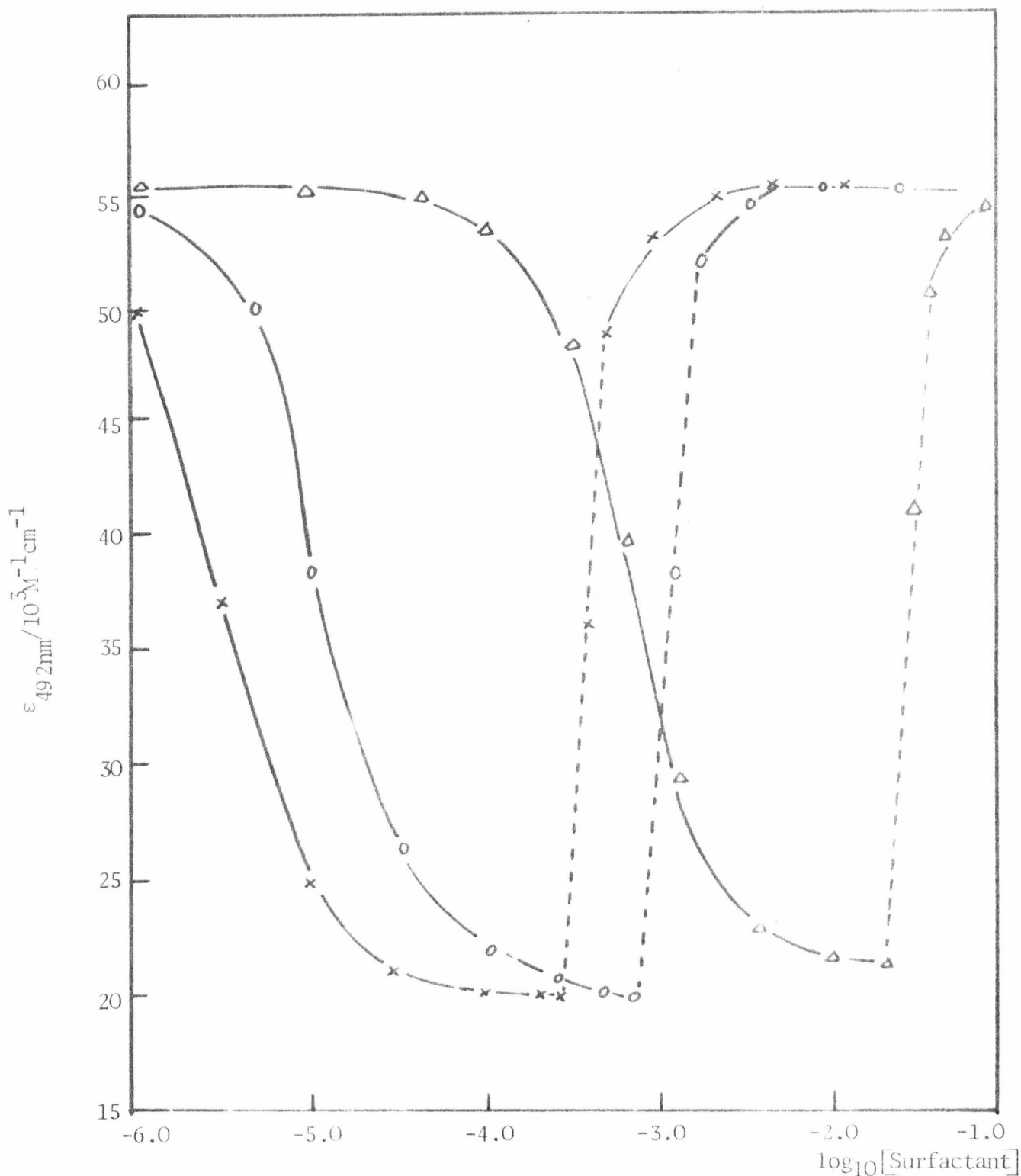


FIGURE 4.2.3 PLOT OF  $\epsilon_{492\text{nm}}(\text{AO}^+)$  VS  $\text{LOG}_{10} [\text{SURFACTANT}]$  FOR DETERMINATION OF THE CMC -x- C<sub>16</sub>, -o- C<sub>14</sub>, -Δ- C<sub>10</sub>

$[\text{AO}^+] = 1 \times 10^{-5} \text{M}$ , Temp 298.2K

equilibrium between the pre-micellar mutually-induced and absorbed states, shown schematically in figure 4.2.4.

The CMC of sodium dodecyl sulphate has also been determined using the unprotonated form of acridine orange. The pka of acridine orange is 10.45<sup>(10)</sup>. The determination of the CMC was carried out at pH 11 and 13. The spectrum of the unprotonated form of the dye is very different from that of the protonated dye. The unprotonated form has an extinction coefficient of  $1.8 \times 10^4 \text{ M}^{-1} \text{ cm}^{-1}$  at the maximum of 440nm.

At the lower pH, the dye spectrum above the CMC was identical with that of the dye in neutral solution, which suggests that the dye is protonated at the surface of the micelle. It is known that a pH gradient exists in the region of the micelle surface<sup>(11)</sup>. This pH gradient is a result of the high surface potential of the micelle ( $\psi^0$ ) -120mV for SDS. Hartley<sup>(12)</sup> has shown that the pH at the surface of the micelle  $\text{pH}_s$ , is related to the pH in bulk solution  $\text{pH}_b$ , by the equation

$$\text{pH}_s = \text{pH}_b - \psi^0/59.16 \quad (4.2.1)$$

Hence, for the SDS micelle, if the pH in the bulk solution is 11, the pH in the region of the micelle surface  $\approx 9$ . The dye will therefore be  $\approx 99\%$  protonated as it diffuses into a region close to the micelle surface.

To ensure that the unprotonated form of the dye is absorbed by the micelle, the bulk solution pH was adjusted to 13 with NaOH, so that the surface pH is then approximately 11. Unlike the system where the  $\text{pH}_s$  is  $\approx 9$ , the spectrum of the dye when absorbed by the micelle  $\text{pH}_s \approx 11$ , is very different from that of the protonated form. This suggests that the dye is absorbed in the unprotonated form. The extinction coefficient is  $2.0 \times 10^4 \text{ M}^{-1} \text{ cm}^{-1}$  at the  $\lambda_{\text{max}} = 446\text{nm}$ .

In fact, if the surface pH = 11, there should be approximately 20%

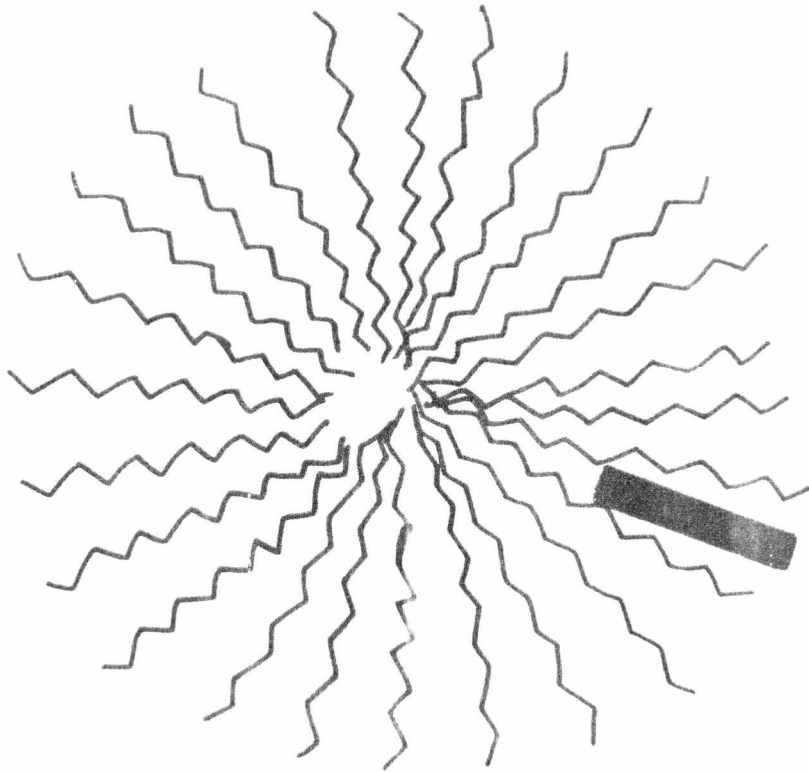


FIGURE 4.2.4

SCHEMATIC DIAGRAM OF A DYE ABSORBED INTO THE PALISADE LAYER  
OF A MICELLE

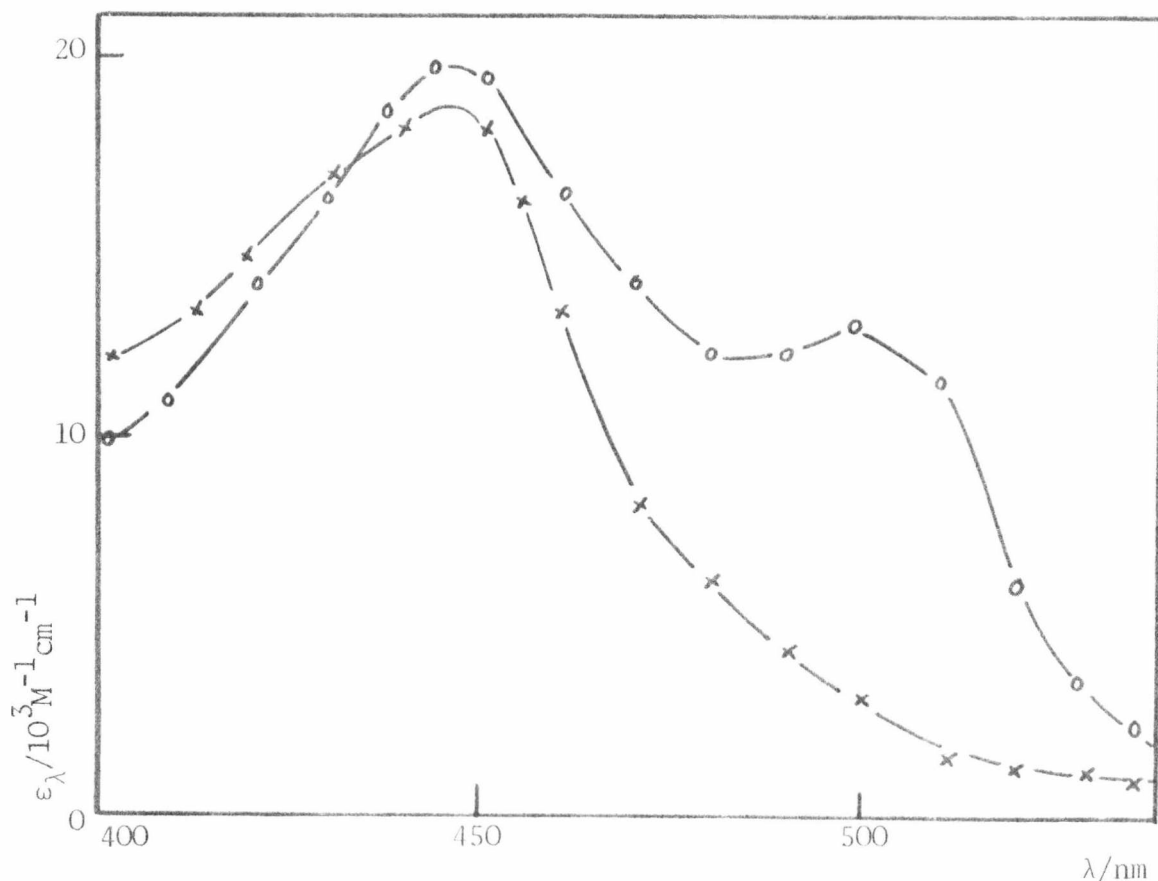


FIGURE 4.2.5

ABSORPTION SPECTRA FOR UNPROTONATED AO (pH = 13) WITH SDS - (x) -  
 SDS =  $10^{-4}M$ , - (o) - SDS =  $10^{-2}M$  (AO)  $1 \times 10^{-5}M$ , TEMP 298.2K

protonated dye. The spectrum of the dye in this system has a secondary peak at 498nm which corresponds to protonated dye. The absorbance of this peak is consistent with approximately 20% of the dye being absorbed by the micelle in the protonated form (figure 4.2.5). Thus, this method of direct dye absorption gives a sensitive measure of the surface pH of micelles.

The CMC has also been determined for the similar surfactants sodium dodecyl sulphonate (SDSn) and sodium dodecyl benzene sulphonate (SDBSn) (figure 4.2.6) by means of acridine dyes. The CMC of SDSn is very similar to that of SDS (table 4.3.1), while the CMC of SDBSn is lower by a factor of approximately four. The CMC of SDBSn is therefore equivalent to that

of sodium tetradecyl sulphate (STetS) (a  $C_{14}$  surfactant). The benzene group appears to contribute the same hydrophobic free energy as two  $-CH_2-$  groups. The limiting extinction coefficient of the dye absorbed in SDBSn micelles is the same as that for SDS micelles which indicates that the benzene group does not have a measurable effect on the dye spectra.

Most of the dyes used have a tendency to self-associate (oligomerise) in free solution<sup>(6,13-17)</sup>, i.e. they do not obey Beer's Law as the concentration is increased. However, when absorbed by the micelles the dyes do obey Beer's Law to much higher concentrations than in free solution, figure 4.2.7 and table 4.2.2. Deviations from Beer's Law occur for the absorbed dye only when the micelle to dye ratio (M/D) is less than one. This observation indicates that only one dye is absorbed by each micelle, unless the M/D ratio falls below one, when more than one dye is absorbed the absorption spectrum is expected to change. The observation is confirmed by energy-transfer studies between Thionine and methylene blue in SDS micelles<sup>(18)</sup>.

In order to establish the environment of the dye when absorbed by micelles, the spectrum of  $AO^+$  in various solvents was measured. It was found that neither extinction coefficient nor  $\lambda_{max}$  correlate well with solvent polarity, figure 4.2.8. This is, however, not unusual and the spectrum may depend on such complex parameters as the work of cavity formation in the micelle and the loss of aqueous solvation<sup>(19)</sup>.

It is difficult to assess which solvent apparently provides the best model for the dye environment when absorbed by the micelle. A consideration of  $\lambda_{max}$  and extinction coefficient suggests that dodecanol is perhaps a reasonable model. A summary of the  $\lambda_{max}$  and extinction coefficient for the dyes in various environments is given in table 4.2.3.

The main features of the spectral changes for the other dye-surfactant systems, shown in figure 4.2.1b-f, are fundamentally similar to

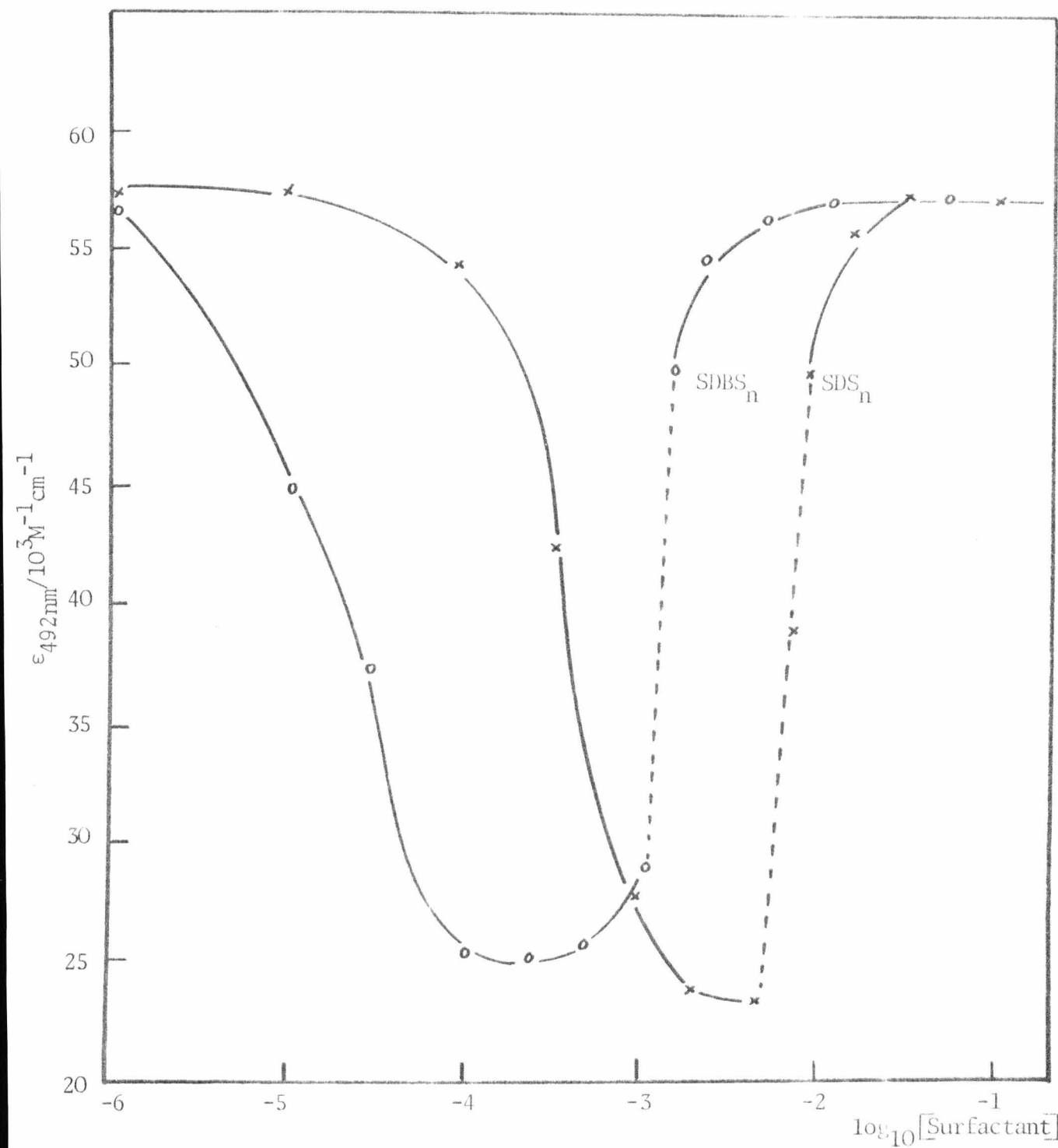


FIGURE 4.2.6 PLOT OF  $\epsilon_{492\text{nm}}(\text{AO}^+)$  VS  $\text{LOG}_{10}[\text{SURFACTANT}]$  FOR DETERMINATION OF THE CMC

-o- SDBS<sub>n</sub>, -x- SDS<sub>n</sub>

$[\text{AO}^+] 1 \times 10^{-5} \text{M}$ , Temp 298.2K

TABLE 4.2.2

VARIATION OF EXTINCTION COEFFICIENT (492nm) OF ACRIDINE ORANGE AS A  
 FUNCTION OF MICELLE/DYE RATIO

$10^2 \text{SDS/M}$	$10^5 M_z/\text{M}$	$10^5 \text{AO}^+/\text{M}$	M/D	$A_{492\text{nm}}$	$\epsilon_{492\text{nm}}/10^5 \text{M}^{-1} \text{cm}^{-1}$
1.50	13.3	0.85	16.1	0.55	66.6
1.497	13.2	1.65	8.0	1.14	66.6
1.492	13.2	4.125	3.2	2.65	66.7
1.485	13.1	12.375	1.06	8.0	66.8
1.00	5.0	13.2	0.38	7.6	57.8

$$M_z = C_A^0 - \text{CMC}/z$$

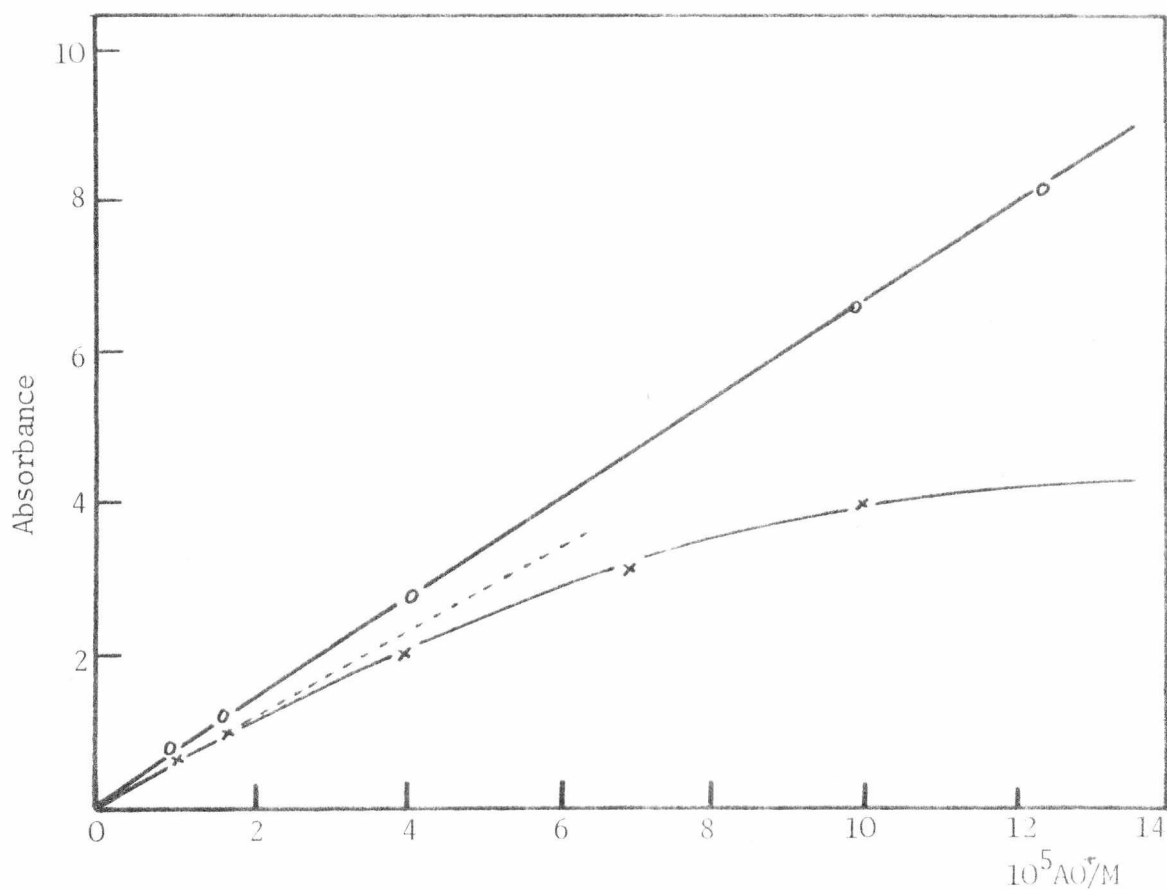


FIGURE 4.2.7

PLOT OF ABSORBANCE  $49_{\text{Zmm}}$  VS  $[\text{AO}^+]$

-(x)-  $\text{AO}^+$  only    -o-  $\text{AO}^+$  absorbed by SDS micelles  $\sim 1.3 \times 10^{-4} \text{M}$

Temp 298.2K

those described above for  $\text{AO}^+$ -SDS, i.e. below the CMC the dyes exhibit a tendency to stack which is dependent on the tendency of the dye to self-associate in free solution. Above the CMC the dyes are absorbed by the micelle which is associated with an increase in the extinction coefficient. The graphs of extinction coefficient against  $\log_{10}[\text{surfactant}]$  are shown in figures 4.2.9-12.

The small changes in absorption spectrum observed for atebriene may reflect its difficulty in entering the micelle. The double positive charge may hold the dye very close to the micelle/water interface and it will consequently not experience a significant change in the polarity of its environment.

TABLE 4.2.3

VALUES OF  $\lambda_{\max}$  AND EXTINCTION COEFFICIENT FOR DYES IN VARIOUS ENVIRONMENTS

DYE	AQUEOUS		MICELLE (SDS > 10 <sup>-2</sup> M)		MAXIMUM STACKING	
	$\lambda_{\max}$ / (nm)	$\epsilon\lambda_{\max_1} / 10^3 \text{M}^{-1} \text{cm}^{-1}$	$\lambda_{\max_2}$	$\epsilon\lambda_{\max_2} / 10^3 \text{M}^{-1} \text{cm}^{-1}$	$\lambda_{\max_3}$	$\epsilon\lambda_{\max_3} / 10^3 \text{M}^{-1} \text{cm}^{-1}$
AO <sup>+</sup>	492	55.9	498	63.0	465	30
AO	440	18.0	445	20.0	-	
AF <sup>+</sup>	446	41.0	452	47.1	440	33
AB <sup>2+</sup>	420	9.0	428	11	-	-
MB <sup>+</sup>	665	825	660	90	590	30
PF <sup>+</sup>	444	42.1	448	46.0	438	27
PYG <sup>+</sup>	546	45.9	549	50.0	512	20
MG <sup>+</sup>	610	87	625	91	575	50
Rh6G <sup>+</sup>	525	85	532	87	510	47

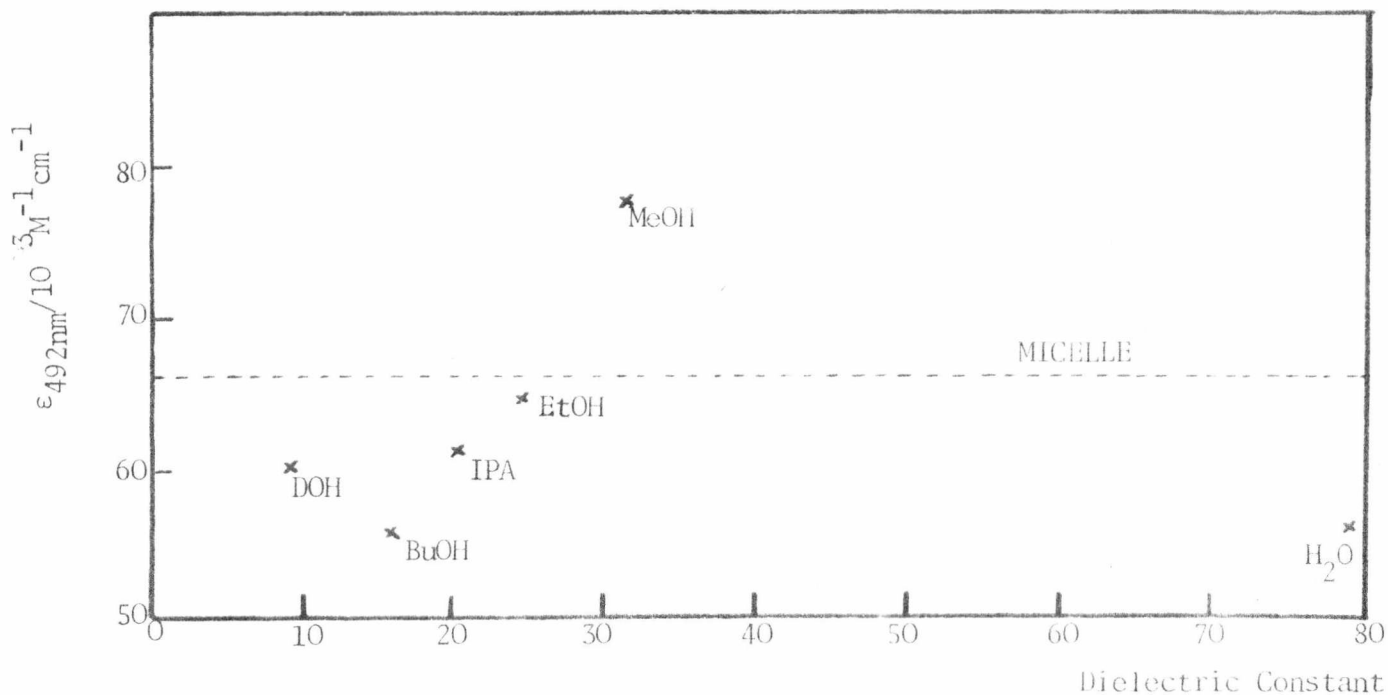


FIGURE 4.2.8

SOLVENT DEPENDENCE OF EXTINCTION COEFFICIENT OF AO

DOH = Dodecanol, IPA = Isopropyl alcohol

$[AO] = 1 \times 10^{-5} M$ , Temp 298.2K

4.3 Fluorimetric Determination of CMC's

The  $AO^+$  monomer has an emission peak at 526nm (excitation wavelength 492nm). This emission is quenched as the concentration of dye is increased due to the planar stacking of the dye ions. Concentrations of SDS below the CMC cause a quenching of fluorescence which remains quenched on further addition of surfactant until the CMC is reached when a dramatic increase in fluorescence intensity at 526nm occurs to a value  $\approx 3$  times greater than that for free dye ( $10^{-5} M$ ). This indicates that the dye is restored to the monomer form and is resident in a partly hydrophobic environment. The fluorescence intensity reaches a limiting value for concentrations of surfactant in excess of twice the CMC. Figure 4.3.1. These changes parallel those observed for the absorption spectrum, and are general for all dyes and surfactants investigated in the course of this work.

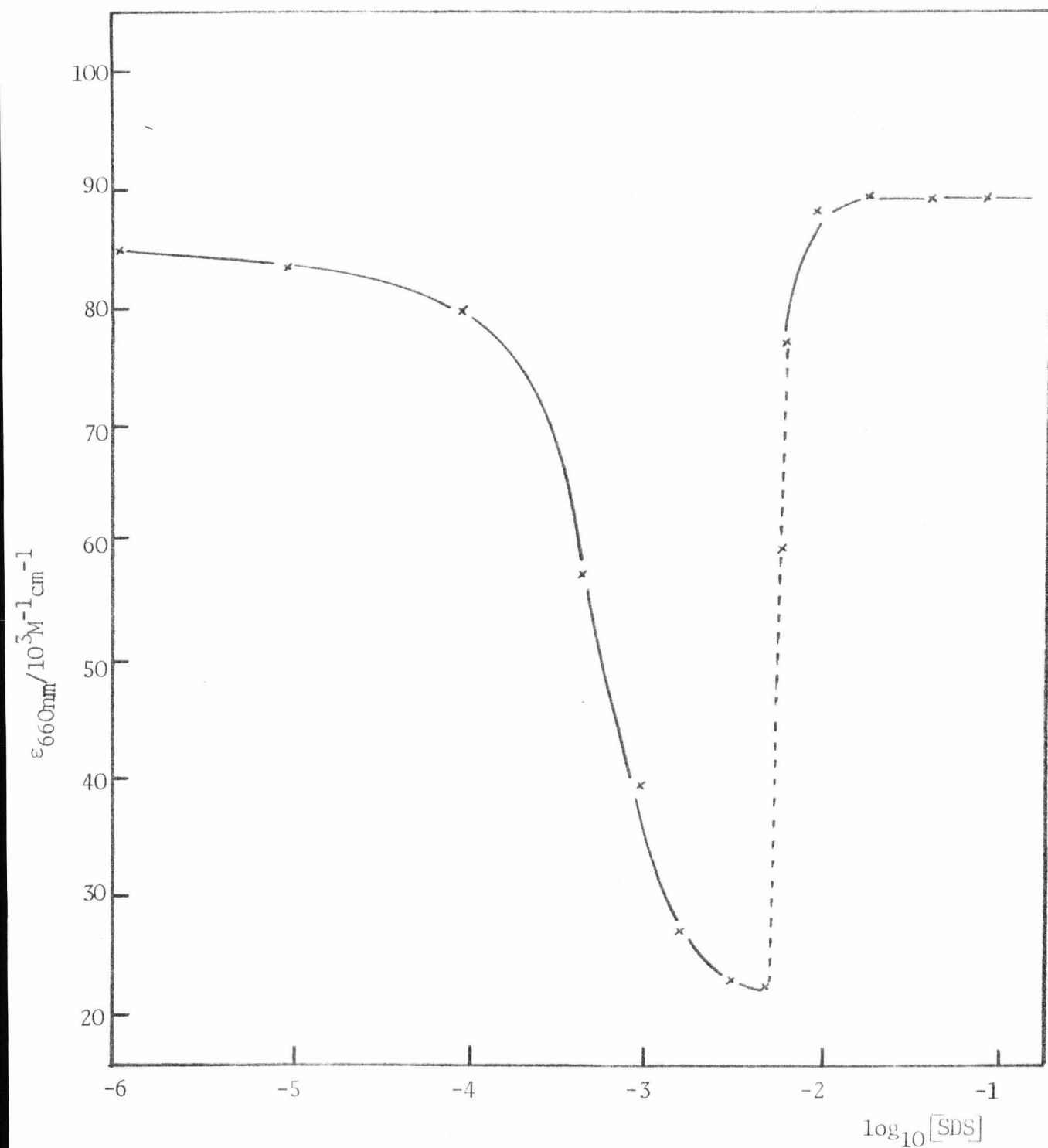


FIGURE 4.2.9 PLOT  $\epsilon_{660\text{nm}} [\text{MB}^+]$  VS  $\text{LOG}_{10} [\text{SDS}]$  FOR DETERMINATION OF THE CMC

$[\text{MB}^+] = 1 \times 10^{-5} \text{ M}$  Temp 298.2K

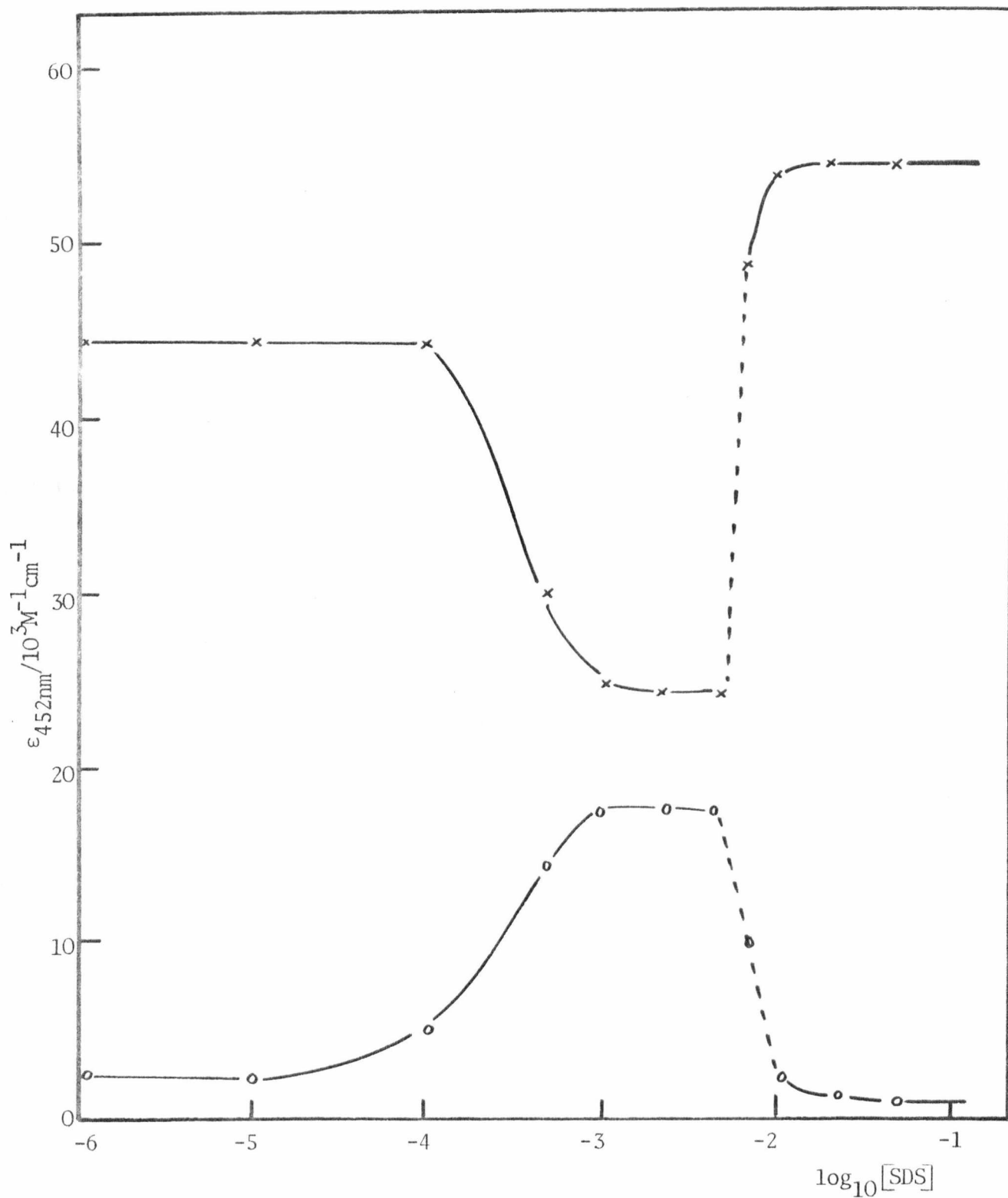


FIGURE 4.2.10 PLOT OF  $\epsilon_{452\text{nm}}(\text{AF}^+)$  -x-,  $\epsilon_{492\text{nm}}$  -o-, VS  $\text{LOG}_{10}[\text{SDS}]$  FOR  
DETERMINATION OF THE CMC

$[\text{AF}^+] 1 \times 10^{-5} \text{M}$ , Temp 298.2K

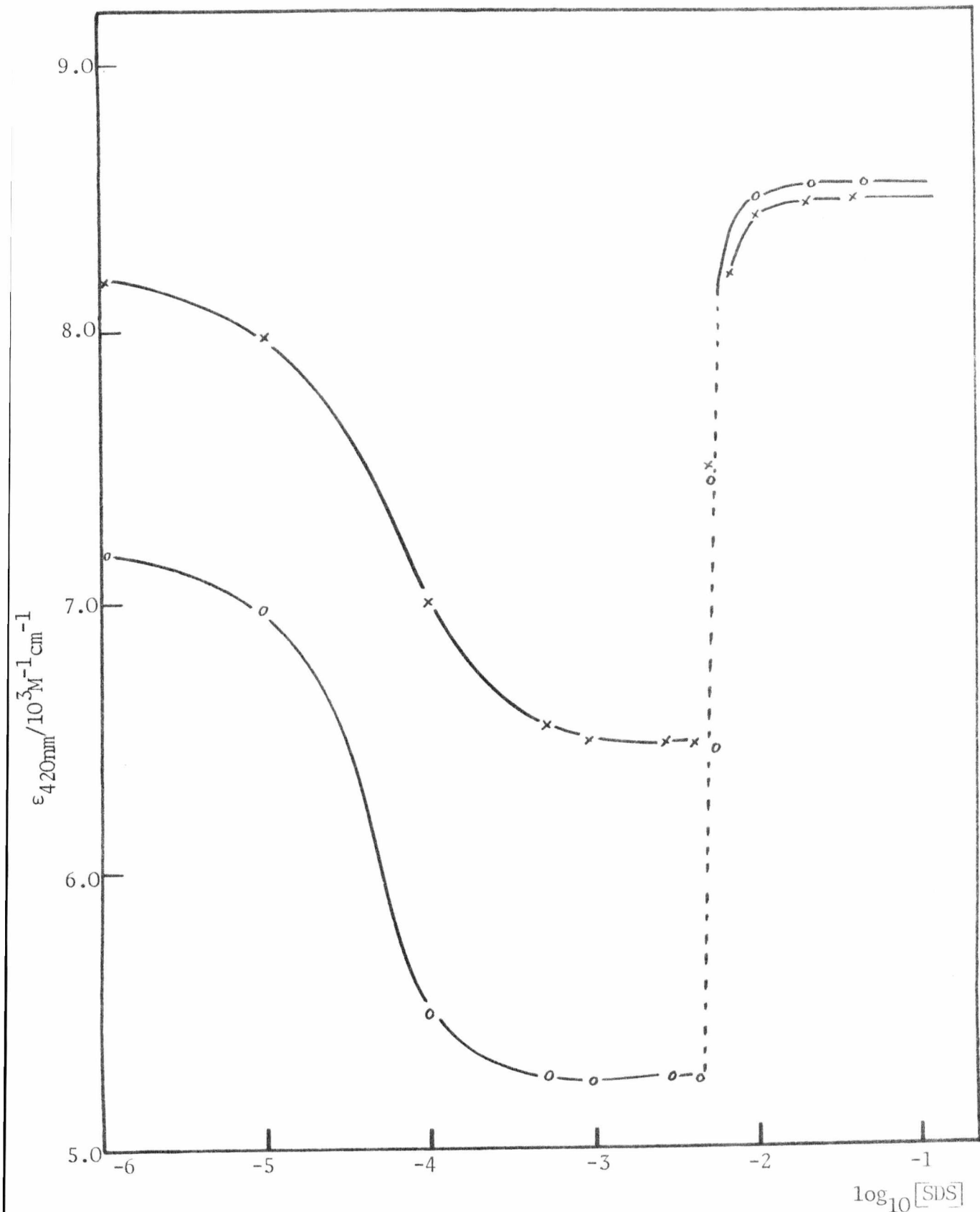


FIGURE 4.2.11 PLOT OF  $\epsilon_{420\text{nm}}$  -x-, -o-  $450\text{nm}(\text{AB}^{2+})$  VS  $\text{LOG}_{10}[\text{SDS}]$  FOR DETERMINATION OF THE CMC

$[\text{AB}^{2+}] 1.2 \times 10^{-5} \text{M}$ , Temp 298.2K

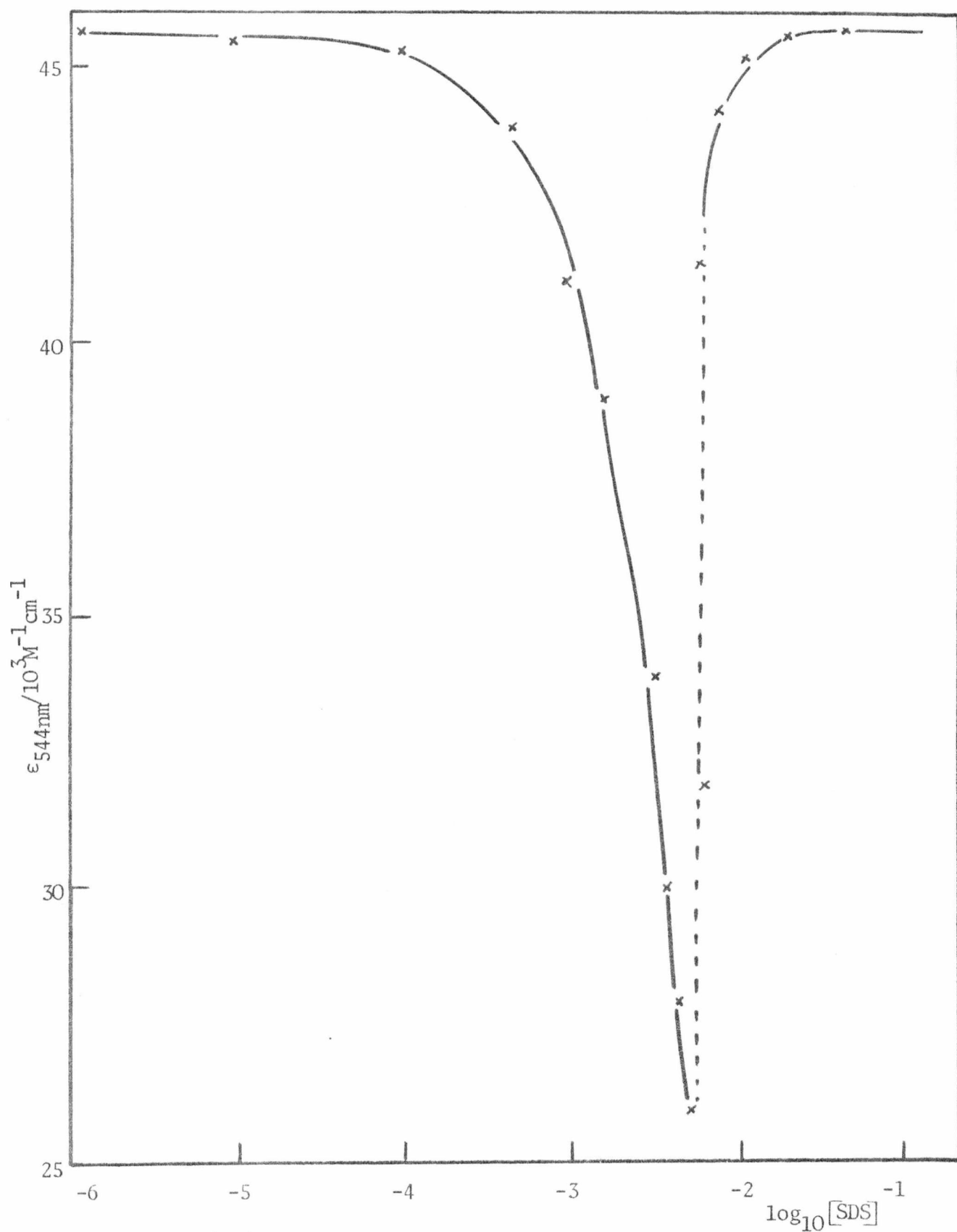


FIGURE 4.2.12 PLOT OF  $\epsilon_{544\text{nm}}(\text{PYG}^+)$  VS  $\text{LOG}_{10}[\text{SDS}]$  FOR DETERMINATION OF THE CMC

$[\text{PYG}^+] 1 \times 10^{-5} \text{ M}$ , Temp 298.2K

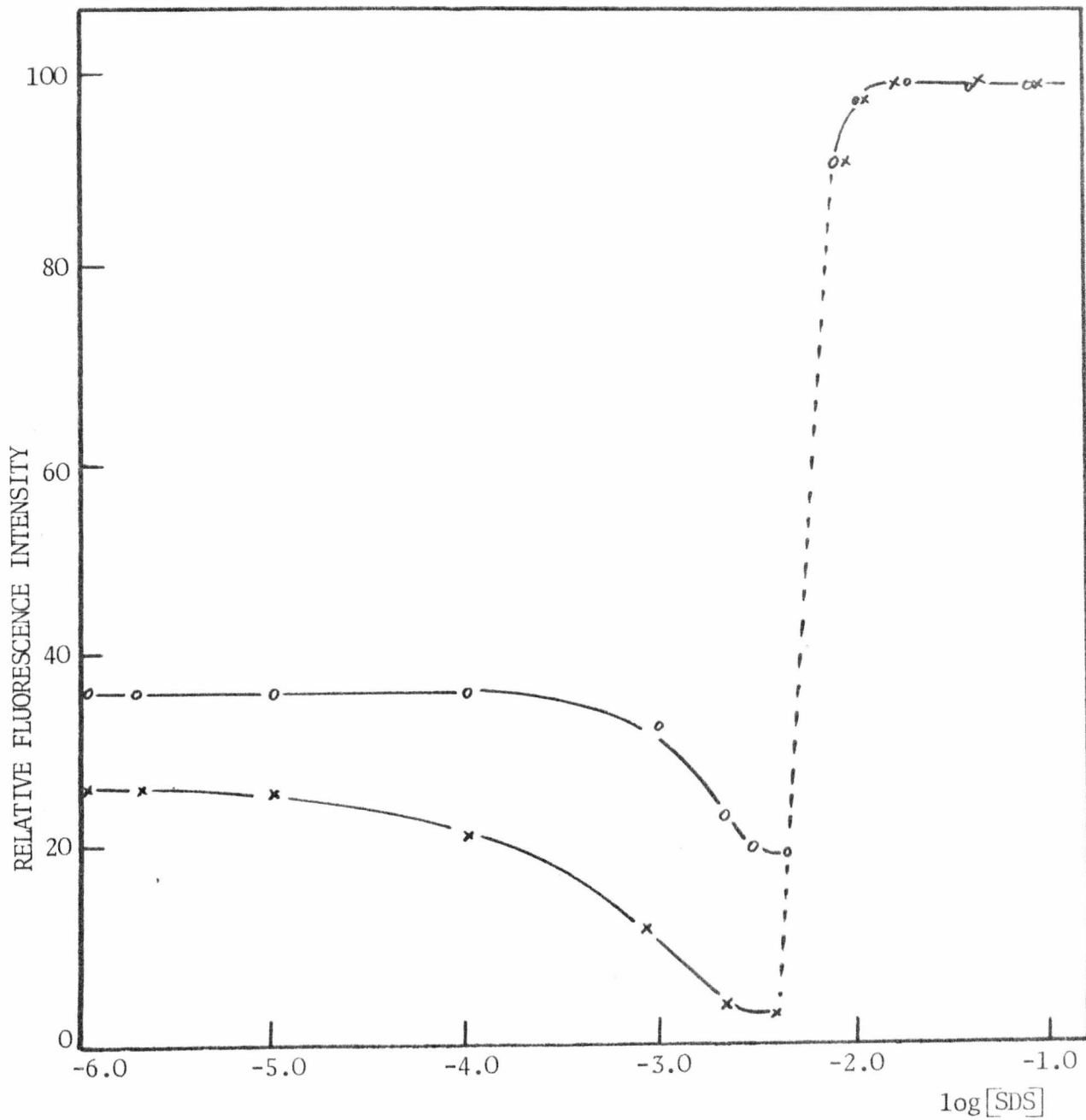


FIGURE 4.3.1 PLOT OF FLUORESCENCE INTENSITY VS  $\text{LOG}_{10}[\text{SDS}]$  FOR DETERMINATION OF THE CMC

-x-  $\text{AO}^+$ , -o-  $\text{PF}^+$

$[\text{Dye}] 5 \times 10^{-6} \text{M}$ , Temp 298.2K

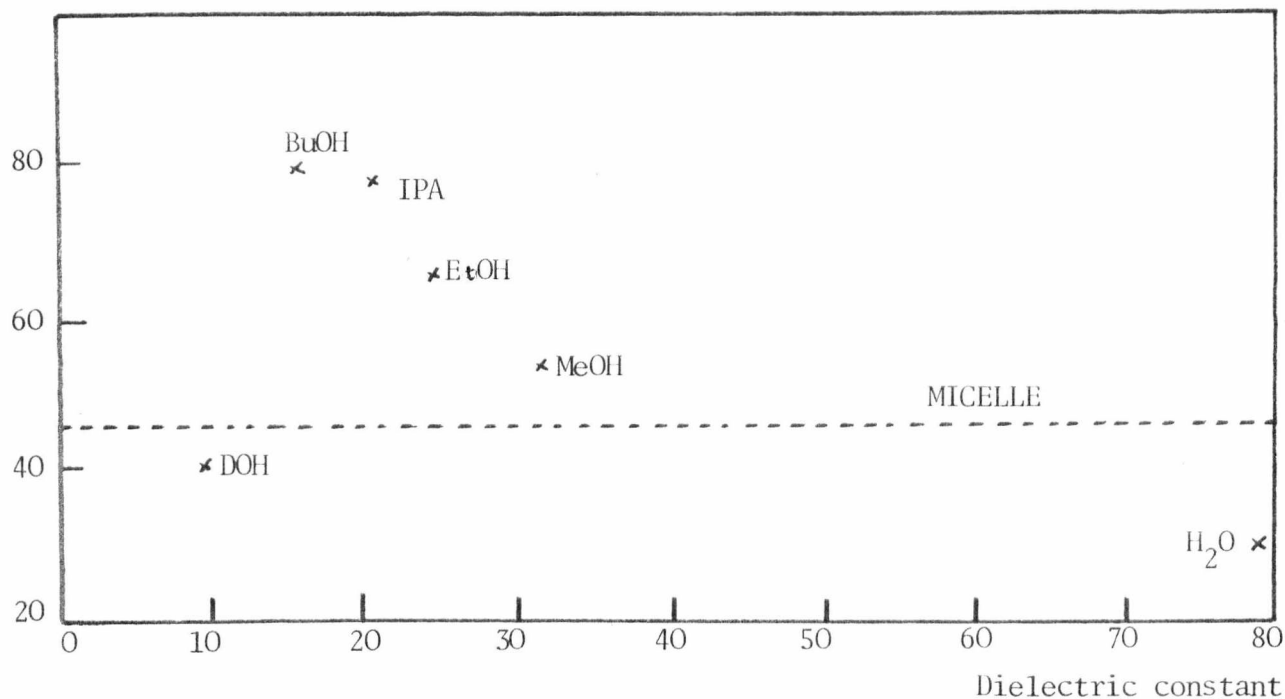


FIGURE 4.3.2

SOLVENT DEPENDENCE OF FLUORESCENCE INTENSITY OF AO<sup>+</sup>

$$[AO^+] = 1 \times 10^{-5} M, \text{ Temp } 298.2 K$$

The fluorescence changes, like the absorption changes, are similar to those observed for the binding of AO<sup>+</sup> to DNA<sup>(20)</sup>.

The fluorescence intensity of the dye was investigated in the same reference solvents as were used for the absorption spectra. Again, no correlation between fluorescence intensity and solvent polarity was observed, figure 4.3.2. Dodecanol again provides perhaps the best model for the dye environment.

The CMC for both absorption and fluorescence measurements is taken as the mid-point of the transition between the pre-CMC value and the limiting value.

The CMC values determined in the course of this work are shown in table 4.3.1.

TABLE 4.3.1

CMC DETERMINATION BY THE DYE-PROBE METHOD. SODIUM DODECYL SULPHATE

[Dye] /M	[NaCl] /M	10 <sup>3</sup> CMC/M				Method
		Temp/K				
		293	298	308	318	
3x10 <sup>-5</sup> AO <sup>+</sup>	0.10	1.35	1.25			A,F
1x10 <sup>-5</sup>	0.00	7.2	7.0	7.0		A,F
	0.01	5.2	5.0	5.1		A,F
	0.05	2.0	1.95			A,F
	0.10	1.35	1.30	1.40	1.50	A,F
4x10 <sup>-6</sup>	0.20		0.96			A,F
	0.05		2.05			F
	0.10		1.37			F
	0.05 MgCl <sub>2</sub>		1.05			F
8x10 <sup>-7</sup>	0.10 MgCl <sub>2</sub>		0.83			F
	0.00		7.1			F
1x10 <sup>-5</sup>	5% MeOH		7.05			A
	10% MeOH		7.10			A
1x10 <sup>-5</sup> PF <sup>+</sup>	0.00		7.1	7.0	7.0	A,F
	0.05		1.95	1.97	1.99	A,F
	0.10		1.30	1.29	1.37	A,F
	0.20		0.95			A
4x10 <sup>-6</sup>	0.00		7.0			F
3x10 <sup>-6</sup>	0.00		7.0			F
4x10 <sup>-6</sup>	0.05 MgCl <sub>2</sub>		1.05			F
	0.00		7.0			F
8x10 <sup>-7</sup>	0.10		7.05			F
1x10 <sup>-5</sup> AF <sup>+</sup>	0.00		7.08			
1x10 <sup>-5</sup> AB <sup>2+</sup>	0.00		7.0			A,F
1x10 <sup>-5</sup> MB <sup>+</sup>	0.00		7.0			A
1x10 <sup>-5</sup> PYG <sup>+</sup>	0.00		7.0			A,F
1x10 <sup>-5</sup> Rh6G <sup>+</sup>	0.00		4.0			A
			7.5			F
1x10 <sup>-5</sup> MG <sup>+</sup>	0.00		~3			A
C <sub>n</sub> H <sub>2n+1</sub> SO <sub>4</sub> <sup>-</sup> Na <sup>+</sup>		10 <sup>3</sup> CMC/M*	Temp./K	Method		
n						
16		0.51	316	A		
14		2.05	303	A,F		
10		30.5	298	A,F		

cont/..

TABLE 4.3.1 (CONT.)

[Dye] /M	[NaCl] /M	10 <sup>3</sup> CMC/M				Method
		TEMP/K				
		293	298	308	318	
1x10 <sup>-5</sup> AO <sup>+</sup> SDS <sub>n</sub> }	0.00		9.4			A,F
1x10 <sup>-5</sup> AO <sup>+</sup> SDBS <sub>n</sub> }	0.00		1.6			A,F

#### 4.4 Determination of the CMC of Anionic Surfactants by Non-Acridine Dyes

To determine whether the behaviour of the planar acridine type dyes with anionic surfactants is general and applicable to other classes of dye, the interaction between SDS and the dyes Malachite green and Rhodamine 6G was investigated.

Results obtained with both dyes show that the determination of the CMC of anionic surfactants cannot be unambiguously obtained with all types of cationic dye probe.

The dye Malachite green exhibits hypochromism below the CMC as the concentration of surfactant is increased. When the surfactant concentration has reached a value approximately a factor of four below the true CMC of the surfactant, the extinction coefficient begins to increase slowly. The extinction coefficient reaches a limiting value at a surfactant concentration approximately equal to the true CMC (figure 4.4.1). Clearly the dye is causing a major perturbation of the equilibria of the micelle-formation process. This may take the form of inducing micelle-formation around the dye which has a non-planar propellar shape.

Unlike Malachite green, Rhodamine 6G is geometrically closely related to the planar acridine type dyes. Rhodamine 6G exhibits hypochromism below the CMC of the surfactant. The transition between pre-micellar and micellar bound dye is sharp, similar to that observed with the acridine type dyes (figure 4.4.2). However, the transition observed spectrophotometrically is different and lower (by a factor of approximately two) than that observed fluorimetrically. The concentration of surfactant at which the spectrophotometric transition occurs is approximately half the true CMC of the surfactant. A possible explanation is that the dye Rhodamine 6G induces micelle formation (due to the geometric configuration of the dye itself and the relative orientation of dye and surfactant molecules in the pre-micellar region), and these micelles contain more than one dye.

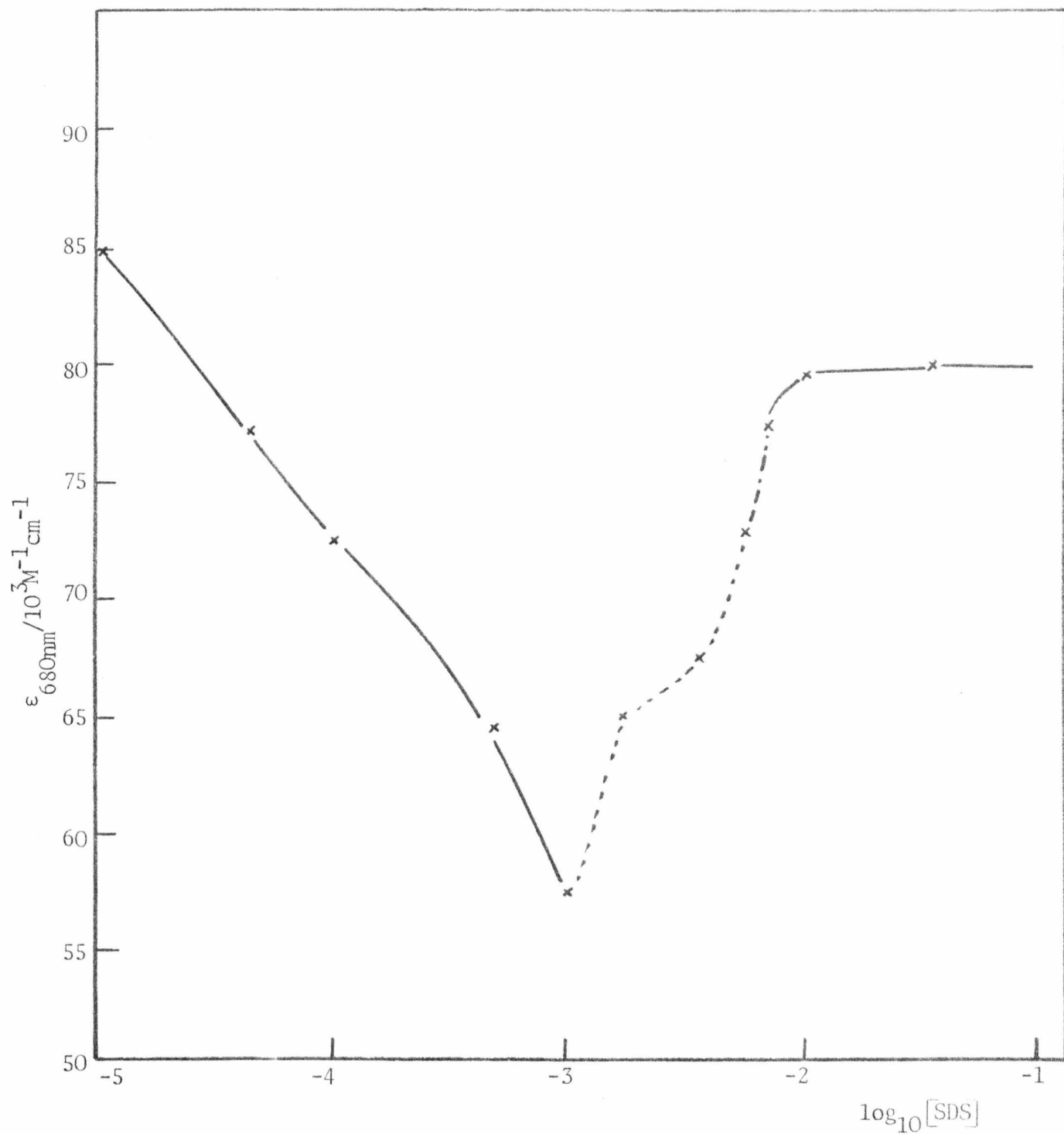


FIGURE 4.4.1 PLOT OF  $\epsilon_{680\text{nm}}(\text{Mg}^{2+})$  VS  $\text{LOG}_{10}[\text{SDS}]$  FOR DETERMINATION OF THE CMC

$[\text{Mg}^{2+}] 1 \times 10^{-5} \text{M}$ , Temp 298.2K

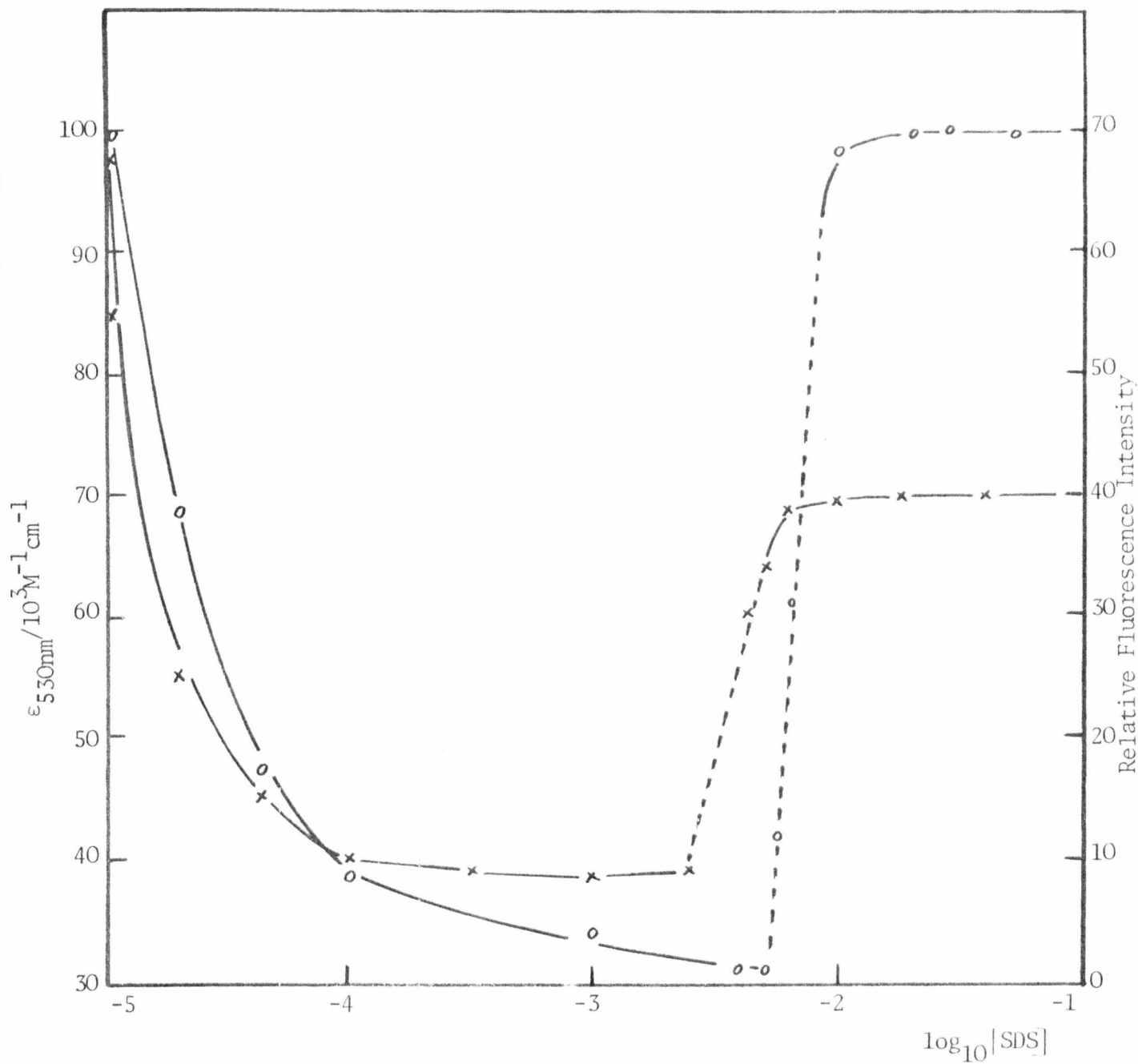


FIGURE 4.4.2 PLOT OF  $\epsilon_{530\text{nm}}$ -x- and FLUORESCENCE INTENSITY -o- ( $\text{Rh6G}^+$ ) $_{580\text{nm}}$  VS  $\text{LOG}_{10}[\text{SDS}]$  FOR DETERMINATION OF THE CMC

$[\text{Rh6G}^+] 1 \times 10^{-5} \text{ M}$ , Temp 298.2K

The extinction coefficient would still increase because of the lower polarity of the dye environment, while the fluorescence would remain quenched until there were only one dye per micelle. This would result in different apparent CMC values.

Since both Malachite green and Rhodamine 6G give rise to anomalous CMC values further investigation was discontinued. The use of such dyes as probes for the determination of CMC values must be viewed with considerable caution.

#### 4.5 General Conclusions

The data presented from absorbance and fluorescence measurements suggests that the dye is neither in a wholly hydrocarbon nor wholly aqueous environment. If we consider the strong coulombic attraction between the dye and the micelle surface, coupled with the tendency of the dye to self-associate in free solution i.e. to remove itself from an aqueous environment, the most plausible location for the dye is within the outer palisade layer of the micelle (figure 4.2.4).

The use of dye-probes as a method for the determination of CMC values may be summarised as follows:-

(i) planar acridine-type dye spectra (absorbance and fluorescence) are very sensitive to the CMC of anionic surfactants.

(ii) for acridine-type dyes the CMC values measured by absorbance and fluorescence are identical and independent of dye charge, structure and concentration.

(iii) below the CMC the strength of the interaction between dye and surfactant increases with surfactant chain-length and the tendency of the dye to self-associate in free solution.

(iv) non-planar dyes appear to disrupt the micelle-forming process which leads to anomalous CMC values.

It must be stated that the CMC determined by the dye-probe method has no theoretical basis, but is simply an indication of the concentration at which micelles begin to form in solution in the presence of the dye.

## REFERENCES

- (1) M.L. Corrin, H.B. Klevens and W.D. Harkins, *J. Chem. Phys.*, 1946, 14, 216.
- (2) K. Shinoda, T. Nakagawa, B. Tamamushi and T. Isemura, *Colloidal Surfactants*, (Academic, New York, 1963) p.10
- (3) P. Mukerjee and K.J. Mysels, *Critical Micelle Concentrations of Aqueous Surfactant Systems*, NSRDS-NBS 36, 1970.
- (4) P. Mukerjee and K.J. Mysels, *J. Amer. Chem. Soc.*, 1955, 77, 2937.
- (5) J. Hevesi, E. Bálint and E. Lehoczki, *Acta Phys. Polonica*, 1970, A38, 829.
- (6) B.H. Robinson, A. Löffler and G. Schwarz, *J. Chem. Soc. Faraday I*, 1973, 69, 56.
- (7) E. Coates, *J. Soc. Dye. and Colourists*, 1969, 85, 355.
- (8) G. Schwarz and A. Seelig-Löffler. To be published.
- (9) R.W. Armstrong, T. Kuruzsev and U.P. Strauss, *J. Amer. Chem. Soc.*, 1970, 92, 3174.
- (10) A. Albert, *The Acridines* (2nd ed. Arnold, London, 1966) p.170
- (11) P. Mukerjee, *J. Phys. Chem.*, 1964, 68, 3567.
- (12) G.S. Hartley and J.W. Row, *Trans. Faraday Soc.*, 1940, 36, 101.
- (13) G.R. Haugen and W.H. Melhuish, *Trans. Faraday Soc.*, 1964, 60, 381.
- (14) L.P. Gianneschi and T. Kuruzev, *J. Chem. Soc., Faraday II*, 1974, 70, 1334.
- (15) S. Massari, P. Dell'Antone, R. Colona and C.F. Azzone, *Eur. J. Biochem.*, 1974, 13, 1038.
- (16) P. Mukerjee and A.K. Ghosh, *J. Amer. Chem. Soc.*, 1970, 92, 6419.
- (17) A. Albert, *The Acridines* (2nd ed. Arnold, London, 1966) p.346
- (18) G.S. Singhal, E. Rabinowitch, J. Hevesi and V. Srinivasan, *Photochem. Photobiol.*, 1970, 11, 531.

- (19) R.L. Reeves, M.S. Maggio and L.F. Costa, *J. Amer. Chem. Soc.*, 1974, 96, 5917.
- (20) S. Yamabe, *Arch. Biochem. Biophys.*, 1969, 130, 148.

C H A P T E R 5

KINETIC INVESTIGATION OF THE INTERACTION BETWEEN ACRIDINE DYES  
AND ANIONIC SURFACTANTS BELOW THE CRITICAL MICELLE CONCENTRATION

## CHAPTER 5

### KINETIC INVESTIGATION OF THE INTERACTION BETWEEN ACRIDINE DYES AND ANIONIC SURFACTANTS BELOW THE CRITICAL MICELLE CONCENTRATION

#### 5.1 Introduction

The previous chapter dealt with the equilibrium properties of the interaction between acridine dyes and anionic surfactants below the CMC. The kinetic aspects of this interaction will now be considered.

Two distinct kinetic processes have been observed by the stopped-flow method;

- (i) a fast process (I) in the msec time range which results in a decrease in absorbance and fluorescence intensity,
- (ii) a slow process (II) in the  $1-10^2$  sec range is also observed by light-scattering.

These experimental observations are discussed in terms of the mutually-induced mechanism introduced in Chapter 4.

The initial aggregation process I will be complex, the addition of dye and surfactant to a growing aggregate may take place in any order. The addition of a dye unit to a growing aggregate may be diffusion-controlled (with a rate similar to the dimerisation of the dye in free solution). The absorbance and fluorescence spectra indicate that good overlap is achieved between the orbitals of the dyes (i.e. separation  $\approx 0.4$  nm) <sup>(1)</sup>.

A simple sequential scheme (A) is shown below



The addition of D or S to the DS unit will depend on the relative concentrations of dye and surfactant and the values of  $K_2$  and  $K_3$ .

There are other pathways which must be considered and a full multi-pathway mechanism is given later.

The observed rate of the aggregation ( $k(\text{obs})_I$ ), process I is dependent on  $K_D$  for the dye, the observed rate decreases with decreasing  $K_D$ . Also, the observed rate is found to increase substantially with increasing surfactant chain-length. The kinetic observations therefore "mirror" the equilibrium measurements. It is found that the effect of head-group is small.

The slow aging process (II) which follows the build-up of dye-surfactant aggregates is considered to be similar to the dye-induced macromolecule aggregation recently described by Schwarz et al<sup>(2)</sup>. They propose that the initial cooperative dye binding to macromolecular chains (e.g. acridine orange - poly  $\alpha$ -L glutamate) is followed by aggregation of two or more chains. Although the partial neutralisation of charge on the macromolecule by the dye favours aggregation it is not the sole driving force. An increase in ionic strength, which should favour the aggregation of like charged species, does so only if a certain amount of dye is bound. This observation implies that the dye plays a more important role than simple charge neutralisation. Schwarz et al conclude that the dye molecules are bound to more than one chain.

The macromolecular chain is, of course, a time independent structure while the dye-surfactant aggregates are not. Nevertheless, it is proposed that the slow aging process (II) occurs in a similar manner to that described above.

## 5.2 Experimental Procedure

### 5.2.1 Stopped-flow Kinetics

The kinetic measurements were performed by mixing dye with surfactant. The mixing ratio was 1:1. The dye concentration range was  $1-4 \times 10^{-5}$  M. The kinetic transients were observed by absorbance, fluorescence and light-scattering modes. The wavelengths of observation were:-

PF <sup>+</sup>	AO <sup>+</sup>	
444 nm	492 nm	absorbance,
444/510 nm	492 nm/526 nm	fluorescence,
-	492 nm/492 nm	light-scattering.

All the measurements were carried out in the absence of added ionic strength, unbuffered (pH ~7) and at 298.2K.

The observed rate constants from all the kinetic measurements are the mean of at least five transients. Errors are standard deviations.

### 5.2.2 Manual Mix Kinetics

The kinetic measurements of process II for acridine orange were performed on an Aminco-Bowman Ratio-Recording Spectrofluorimeter, operated in the non-ratio mode, 492 nm/492 nm.

The manual mixing of the dye and surfactant solutions was achieved as follows. Dye and surfactant solutions (pre-thermostatted at 298.2K) were drawn into two separate  $1\text{cm}^3$  syringes. The syringes were then attached

via polyethylene tubing to a polyethylene 'Y' adaptor. The solutions were then forced through the adaptor into the fluorescence cuvette in the thermostatted cell holder. The mixing was complete within 1 second. The change in light-scattering ( $I^S$ ) was recorded on a continuously running X-Y recorder (Servoscribe RE511). Rate constants were obtained from the slope of a plot of  $\log_{10} I^S$  against time.

### 5.2.3 Temperature-Jump Kinetics

The solutions for use in the temperature-jump experiments were pre-thermostatted, mixed and transferred to the temperature-jump cell as rapidly as possible. Solutions contained 0.01-0.1M NaCl. The initial temperature of the solutions was 295K and they were subjected to a temperature-jump of 3K. Due to the aging of the solutions, only qualitative results could be obtained. The temperature-jumps were performed approximately two minutes after the initial mixing of the solutions.

The wavelength of observation was 492nm.

## 5.3 Results: Stopped-Flow

### 5.3.1 Effect of Dye Concentration and Structure

The transient absorbance and fluorescence amplitudes of process I is found to be consistent with the equilibrium amplitude. The transients are good exponentials in all cases. The transient absorbance amplitude changes sign at 470nm for acridine orange and 420nm for proflavine which is consistent with equilibrium spectral data (see figures 4.2.1a,b).

The decrease in the fluorescence intensity to zero indicates that at least the dimer dye aggregate is formed. Further aggregation cannot (in this case) affect the fluorescence intensity<sup>(3)</sup>. However, the initial decrease in absorbance associated with process I gives the same observed rate constant as that obtained by fluorescence measurements. This suggests

that the process involves only dimer formation or that dimer formation is the rate-determining step.

Plots of observed rate constants  $k(\text{obs})_I$  against dye concentration (for a given surfactant concentration) are non-linear, figure 5.3.1.1.

### 5.3.2 Effect of Surfactant Concentration and Chain-Length

The observed rate of interaction between dyes and sodium n-alkyl sulphates is found to increase with increasing surfactant concentration and chain-length.

For a given dye the plot of  $k(\text{obs})_I$  against surfactant concentration is linear at high surfactant concentration, but the plot exhibits curvature at low surfactant concentrations. (Figures 5.3.2.1,2,3,4,5). The data in the low surfactant concentration region ( $<10^{-4}\text{M}$ ) where curvature is exhibited is experimentally difficult to obtain. The transient fluorescence amplitudes are very small and the rates very slow. Data in this region is therefore subject to large errors.

It is not possible to plot  $k(\text{obs})_I$  against [surfactant-dye] and obtain any meaningful results.

The effect of surfactant chain-length on  $k(\text{obs})_I$  is shown in figures 5.3.2.1 - 5. In figure 5.3.2.6 the slope of the plot of  $k(\text{obs})_I$  against surfactant concentration for a given dye-surfactant system is plotted against dye concentration. It must be noted that the slope of this plot is dependent on the dye and surfactant, but the intercept is dependent only on the surfactant chain-length. The ratio of the intercepts SDS/SDeS = 5.5 (which is similar to the ratio of the CMC's). This may reflect the difference in the aggregation tendency of the two surfactants.

The effect of changing the surfactant head-group can be seen in figures 5.3.2.1, 5. The pre-CMC interaction observed spectroscopically of  $\text{AO}^*/\text{SDSn}$  is not as strong as that for  $\text{AO}^*/\text{SDS}$  (Chapter 4  $K_{S1}$  values). The kinetic

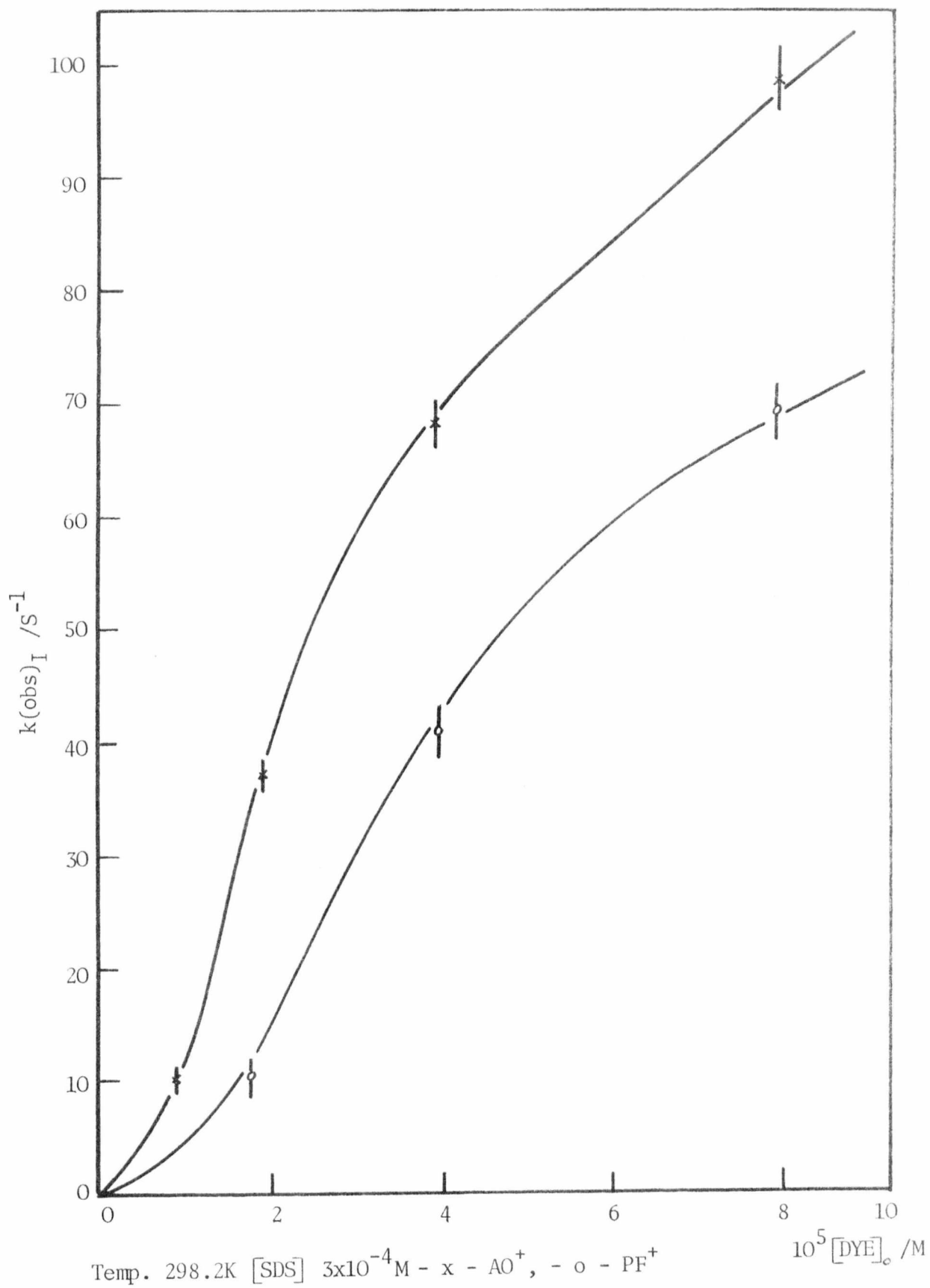


FIGURE 5.3.1.1

PLOT OF  $k(\text{obs})_I$  VS  $[\text{DYE}]_o$

data supports this view. Similarly, the interaction of AO<sup>+</sup>/SDBSn is stronger than for AO<sup>+</sup>/SDS, this is due mainly to the effect of the benzene group which, as seen from the CMC determinations, is equivalent to 2CH<sub>2</sub> groups. For a surfactant concentration of 10<sup>-3</sup>M the k(obs)<sub>I</sub> for different surfactants are shown in table 5.3.2.1.

TABLE 5.3.2.1

COMPARISON OF RATES OF PRE-CMC DYE INTERACTION

	k(obs) <sub>I</sub> /s <sup>-1</sup>	10 <sup>3</sup> CMC/M	10 <sup>3</sup> K <sub>SD</sub> <sup>AO+</sup> /M
SDBSn	1400*	1.6	21
SDSn	80	9.4	2.6
SDS	150	7.0	13
SDeS	40	30.5	2.2

Temp. 298.2K

\* Extrapolated value.

K<sub>SD</sub><sup>AO+</sup> is a measure of the equilibrium constant for the DS interaction (see Chapter 4).

From these results it can be seen that the difference between SO<sub>4</sub><sup>-</sup> and SO<sub>3</sub><sup>-</sup> is small (approximately a factor of 2), but between SO<sub>3</sub><sup>-</sup> and  it is much larger (approximately a factor of 20). This factor of 20 is much larger than that for SDeS to SDS (approximately 4) which implies that

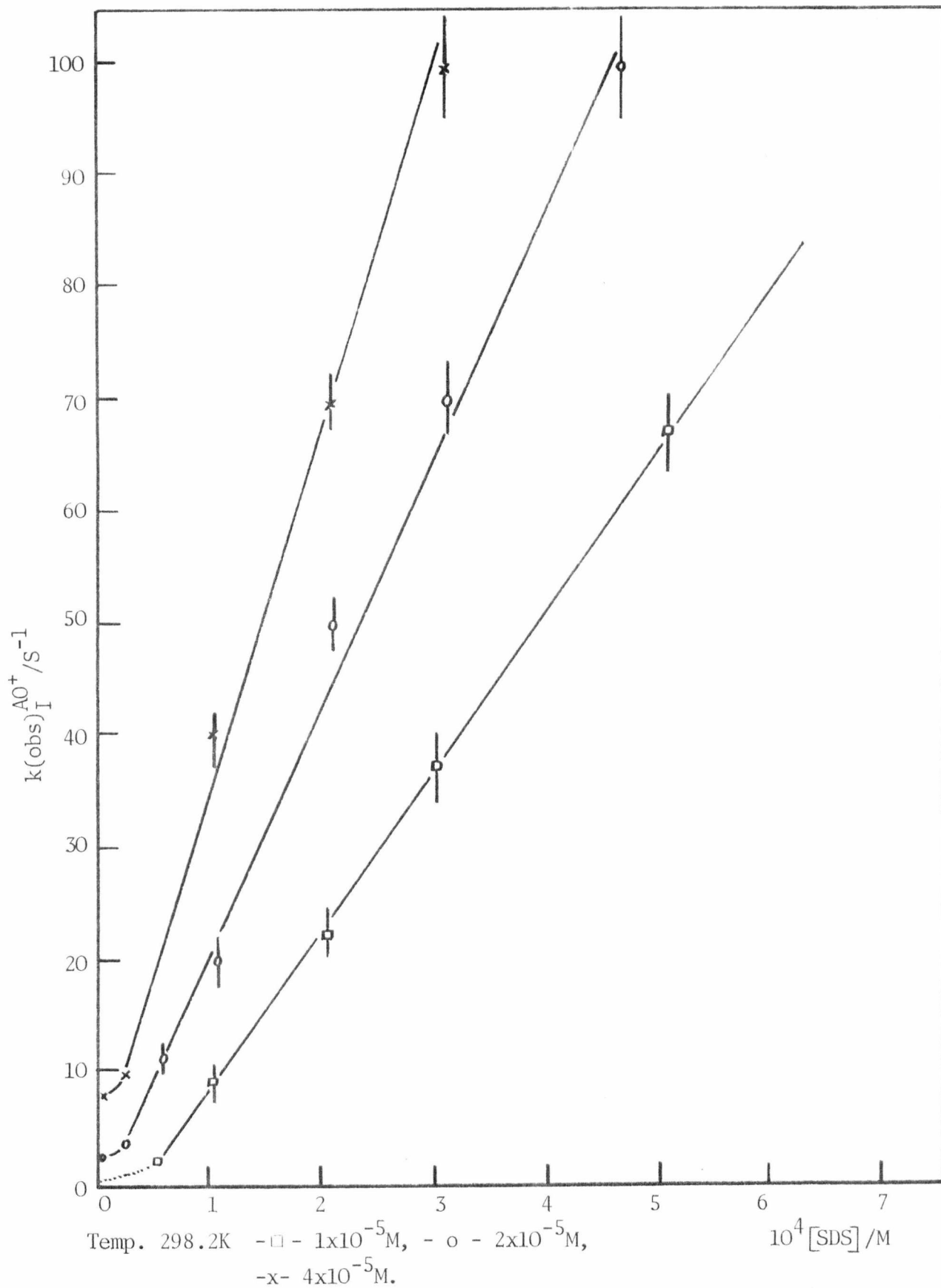


FIGURE 5.3.2.1

PLOT OF  $k_I^{\text{AO}^+}$  VS  $[\text{SDS}]$  FOR THE PRE-CMC INTERACTION

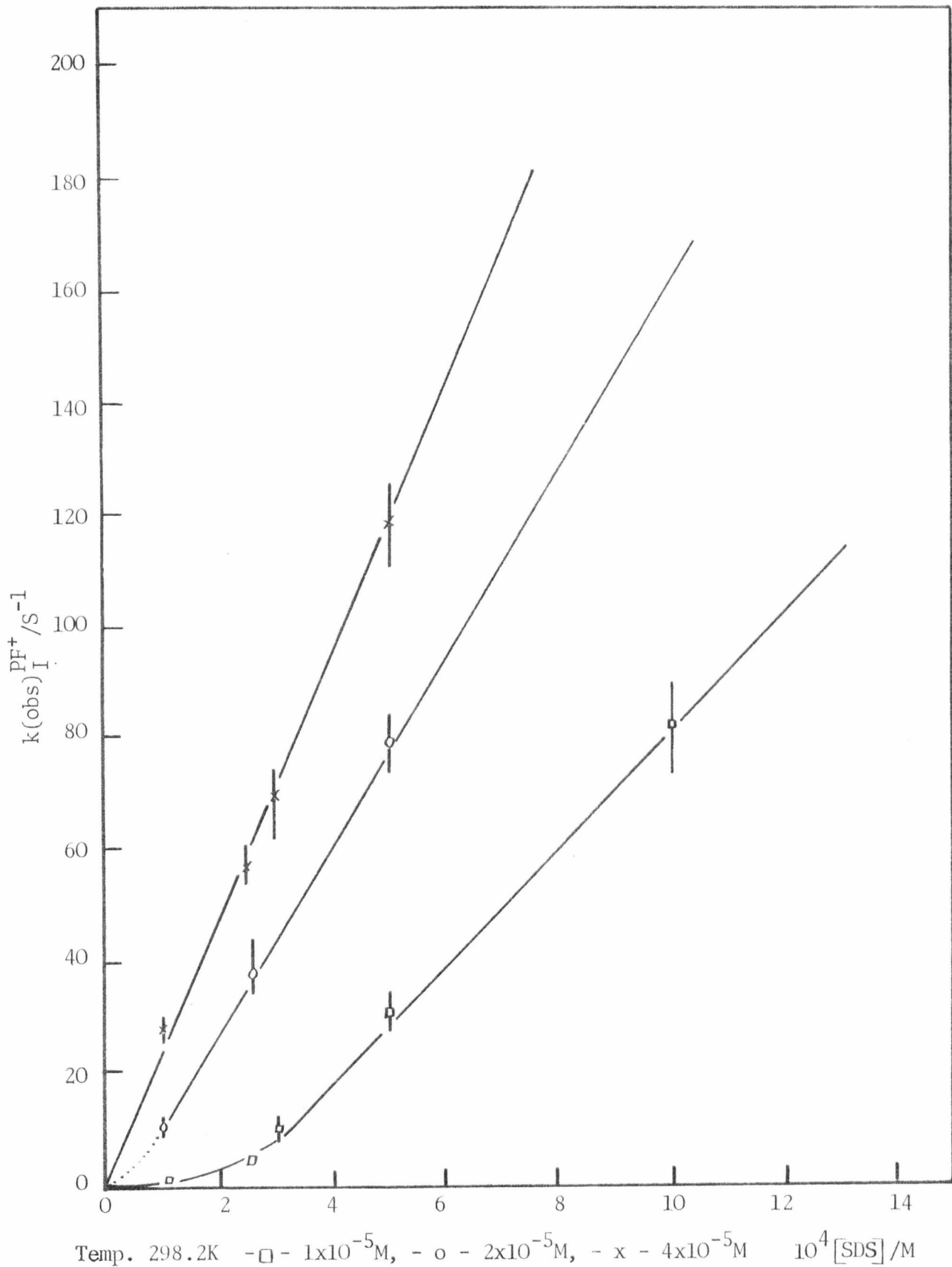


FIGURE 5.3.2.2

PLOT OF  $k(\text{obs})_I^{\text{PF}^+}$  VS  $[\text{SDS}]$  FOR THE PRE-CMC INTERACTION

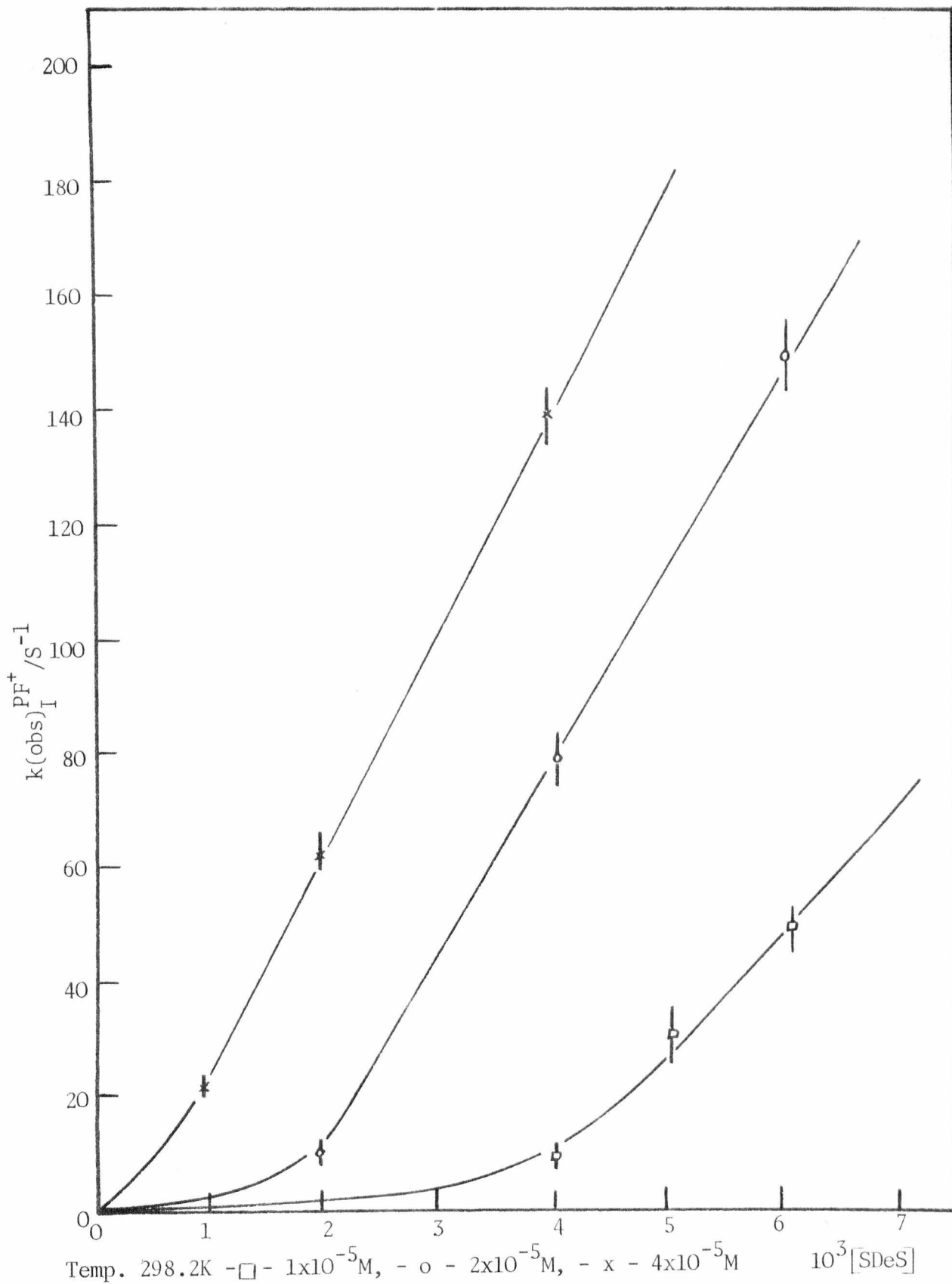


FIGURE 5.3.2.3

PLOT OF  $k(\text{obs})_I^{\text{PF}^+}$  VS  $[\text{SDeS}]$  FOR THE PRE-CMC INTERACTION

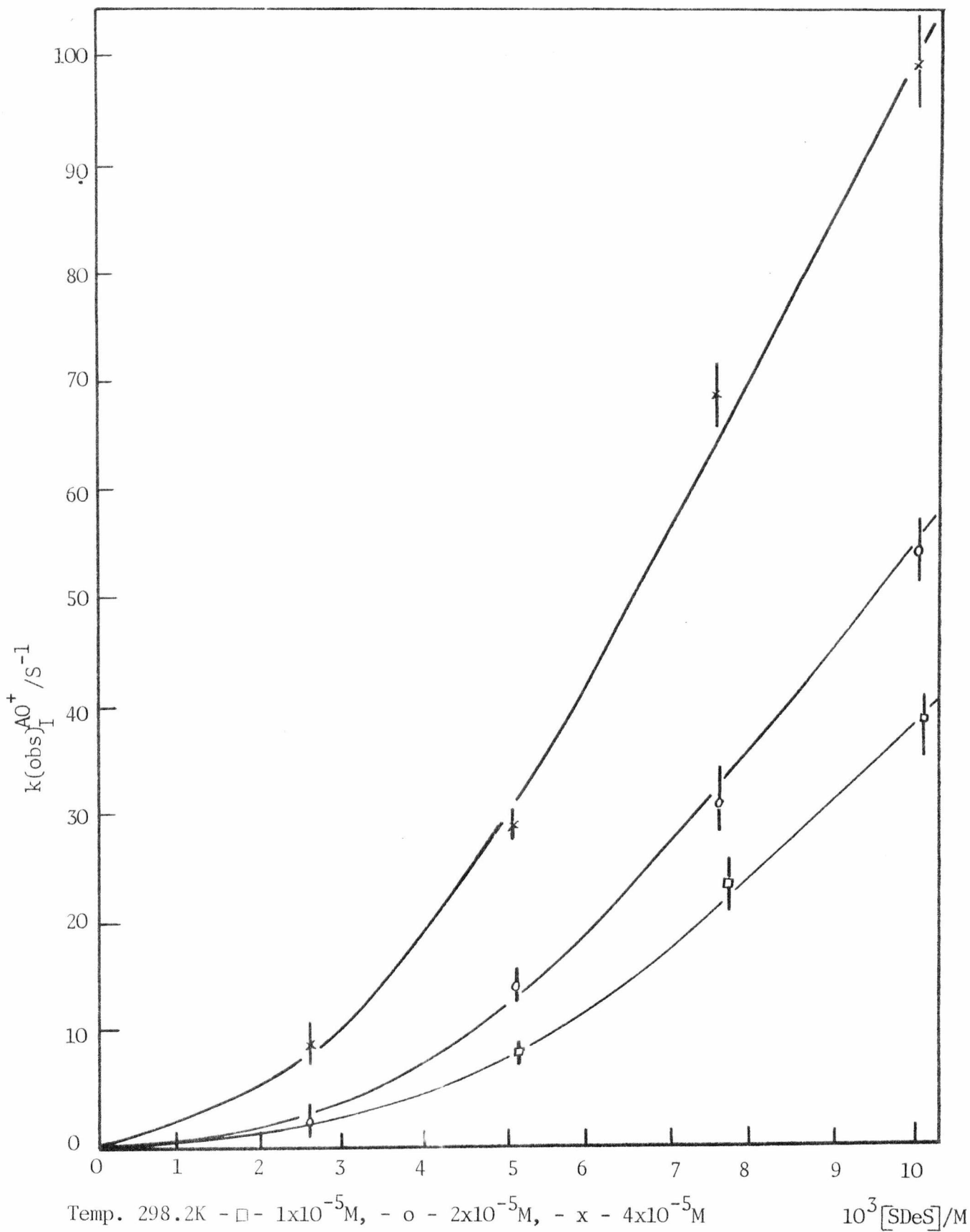


FIGURE 5.3.2.4

PLOT OF  $k(\text{obs})_{\text{I}}^{\text{AO}^+}$  VS  $[\text{SDeS}]$  FOR THE PRE-CMC INTERACTION

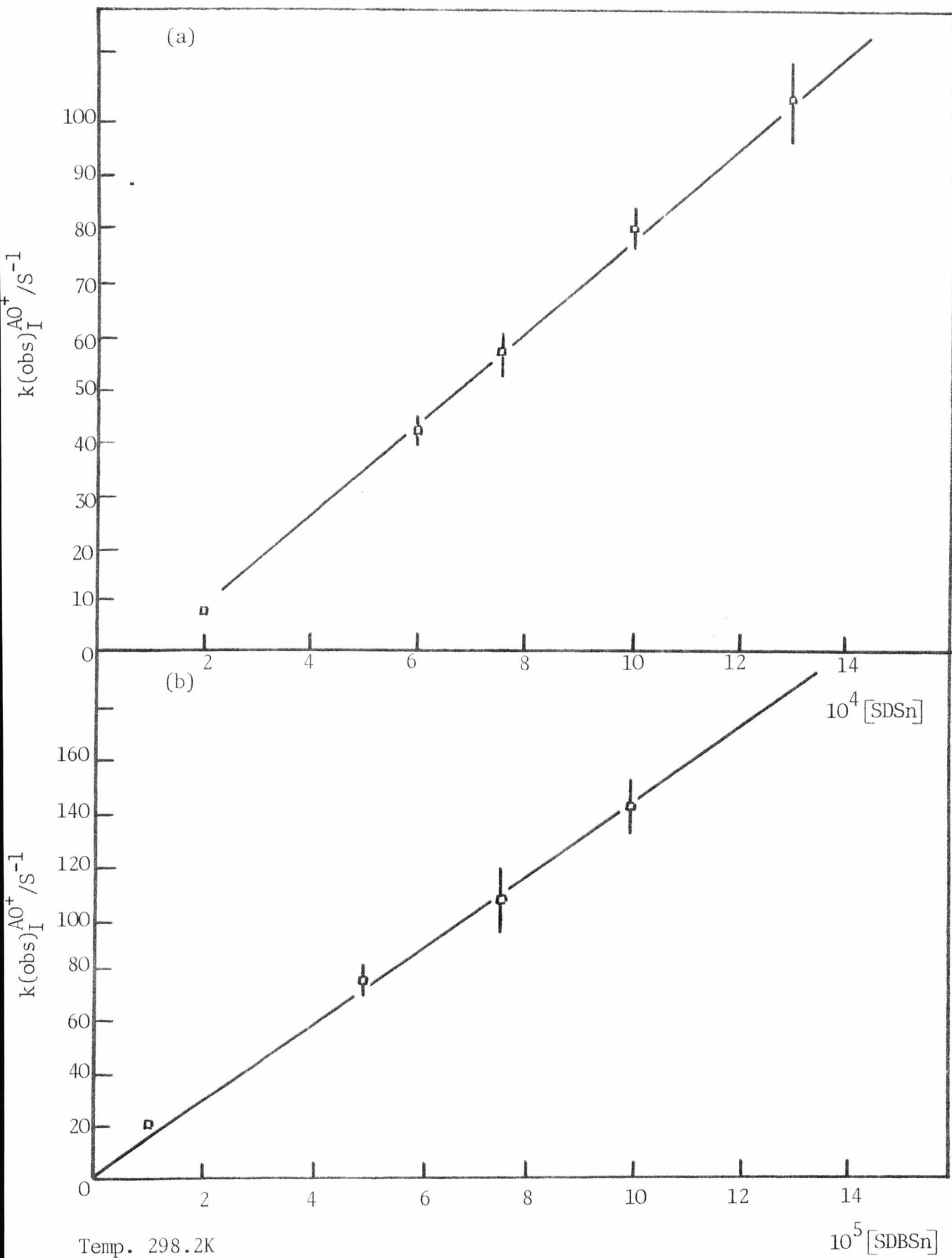


FIGURE 5.3.2.5

(a) PLOT OF  $k_I^{AO+}$  VS  $[SDSn]$  & (b)  $k_I^{AO+}$  VS  $[SDBSn]$

FOR THE PRE-CMC INTERACTION

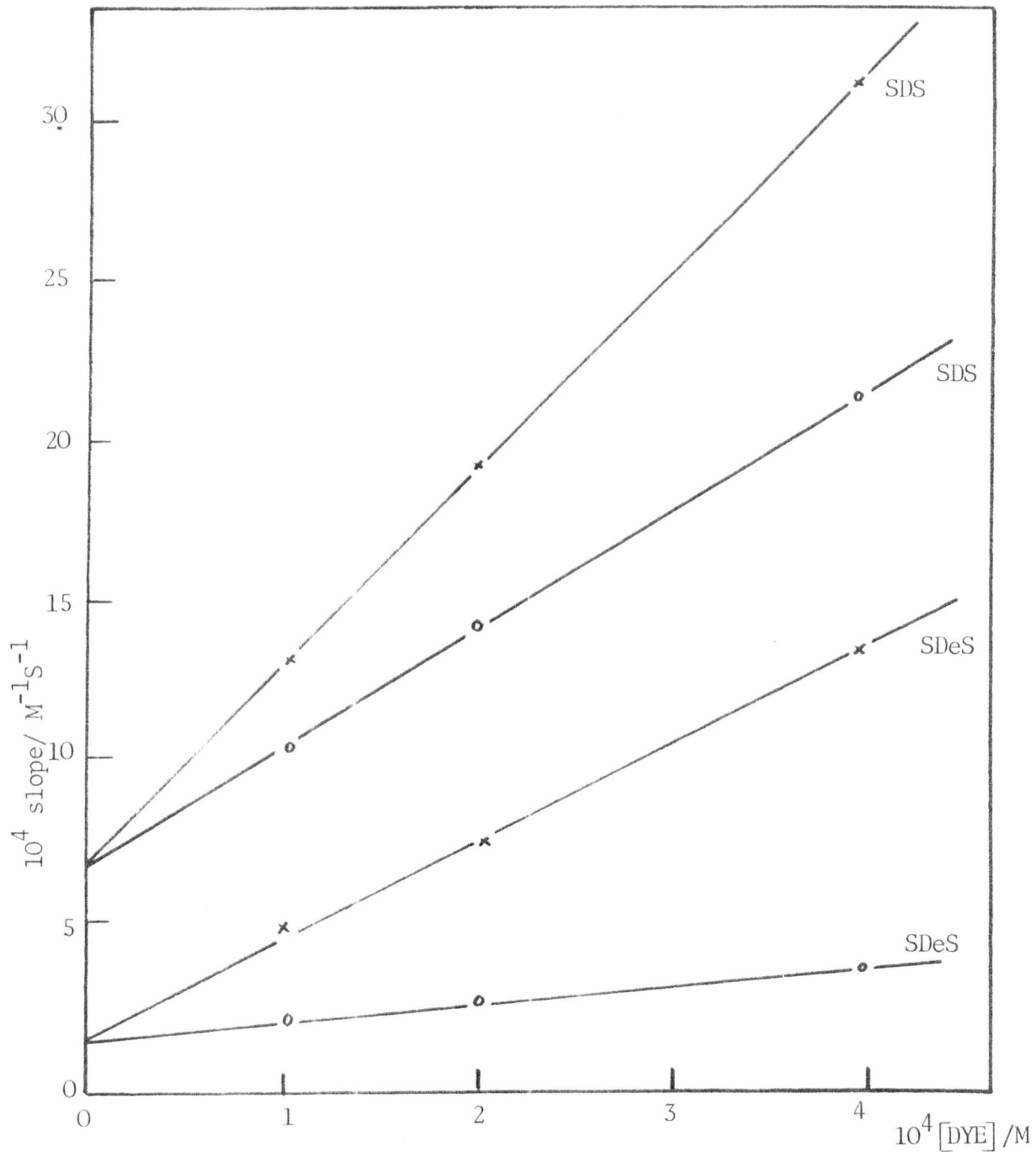


FIGURE 5.3.2.6

PLOT OF SLOPES VS  $[DYE]$

the effect of the benzene group is not a simple hydrophobic one equal to 2CH<sub>2</sub> groups. A specific interaction with acridine ring cannot be ruled out.

The only qualitative trend which emerges is that the observed rate is greater the lower the CMC of the surfactant.

The very slow aging process II has only been investigated for the AO<sup>+</sup>/SDS system. It was found that the rate of production of large aggregates decreased with increasing surfactant concentration. At all concentrations the rate of large aggregate production was found to be much slower than the initial rate of the fluorescence decrease, table 5.3.2.2.

TABLE 5.3.2.2

COMPARISON OF RATES OF FLUORESCENCE DECREASE (I)

AND LIGHT-SCATTERING INCREASE (II)

[SDS]/M	FLUORESCENCE $k(\text{obs})_{\text{I}}/\text{s}^{-1}$	SCATTER $k(\text{obs})_{\text{II}}/\text{s}^{-1}$
$1 \times 10^{-5}$	6.6	$5.3 \times 10^{-2}$
$1 \times 10^{-4}$	10.6	$2.2 \times 10^{-3}$
$1 \times 10^{-3}$	130	$4.1 \times 10^{-4}$

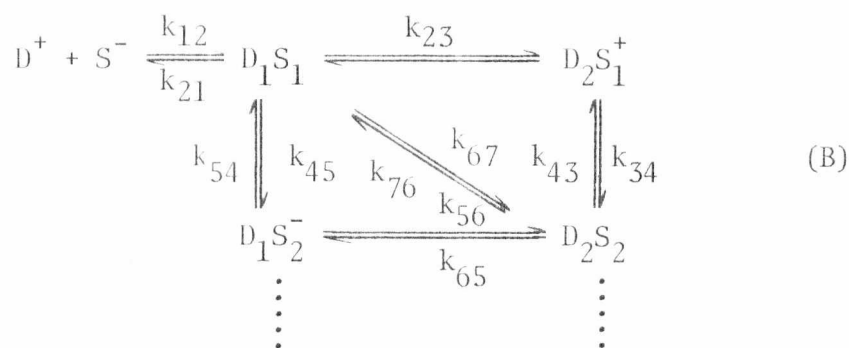
Temp. 298.2K [AO<sup>+</sup>] =  $1 \times 10^{-5}$ M

## 5.4 Mechanism

### 5.4.1 The Fast Process I

The observed rate of the fast process measured by fluorescence and absorbance is the same. Fluorescence detection can only follow the aggregation of the dye up to the dye dimer stage. It is assumed that the absorbance observed rate also corresponds to the formation of a dye dimer unit.

The full reaction scheme (B) is given below.

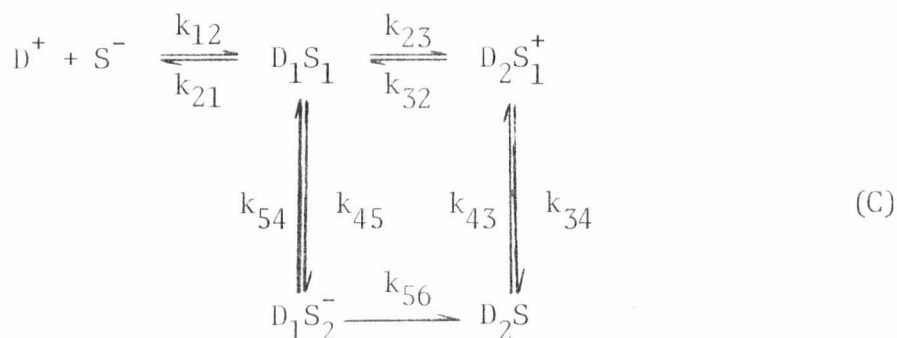


The addition of dye to a  $D_xS_y$  species is expected to be more favourable than dye dimerisation in free solution because of the more favourable coulombic interaction. Hence,

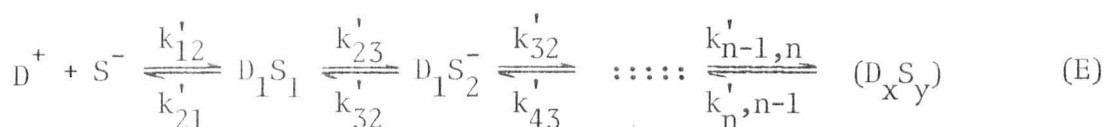
$$K_{23} (= D_2S_1^+ / D^+ D_1S_1) > 10^4 M^{-1} \quad (4)$$

If the addition of dye is diffusion-controlled, the reverse rate constants  $k_{32}$  and  $k_{65} \ll 10^5 s^{-1}$ ,  $10^5 s^{-1}$  being the value obtained for the dye acridine orange in free solution<sup>(4)</sup>. For the dye surfactant dimer ( $D_2S_2$ ), the charge repulsion between dye molecules will be negligible. Therefore,  $k_{65}$  will be very small.

The aggregation of dye surfactant monomers directly to give  $D_2S_2$  is considered unlikely. Scheme (B) then reduces to (C):-



Scheme (C) remains complex and a rigorous solution will not be attempted. We may, however, split scheme (C) into two pathways (D) and (E).



The first step is common to both schemes and is likely to be diffusion-controlled. Since the tendency to aggregate in free solution is much greater for the dye than for the surfactant ( $K_D^{AO^+}/K_D^{SDS} \sim 10^2$ ) scheme (D) will be the most important one. Scheme (E) will become important at high surfactant concentrations i.e.  $[S]/[D] \approx 10^2$ . This means that  $K_{23} \gg K'_{23}$ , so that the stability of  $D_2S_1^+ \gg D_1S_2^-$ .

From the dye spectrum (i.e. hypochromism and the hypsochromic shift) it is clear that added dye stacks in a "sandwich-type" manner with the dye in a  $D_xS_y$  aggregate.

The dye-surfactant structure may be represented by:



where the D D spacing will be  $\sim 0.4\text{nm}$ .<sup>(1)</sup>

The spectral evidence suggests that not all the dye is present in the stacked form. The limiting spectrum below the CMC is not consistent with a fully stacked system<sup>(1)</sup>. The dye must therefore exist in monomer, dimer and stacked environments. This situation is represented by:



A very detailed spectral analysis may reveal the relative amounts of dye bound as monomer, dimer and stack<sup>(5)</sup>. The slow aging of the solutions does, however, present considerable experimental difficulties.

In general, the kinetic measurements were performed in the region where  $[S]/[D] < 10^2$  and scheme (D) will be considered in more detail.

Application of the relaxation method to system (D) leads to two decoupled relaxation times<sup>(6)</sup>:

$$\tau_I^{-1} = k_{12}([D] + [S]) + k_{21} \quad (5.4.1.1)$$

$$\tau_{II}^{-1} = \frac{k_{23}[D](\overline{DS} + [D] + 2[S] + 2K_{21})}{[D] + [S] + K_{21}} + k_{32} \quad (5.4.1.2)$$

$$= \frac{k_{23}[D]([\overline{DS}] + [D] + 2[S] + 2/K_{12})K_{12}}{1 + K_{12}([D] + [S])} + k_{32} \quad (5.4.1.3)$$

Terms in  $[D]^2$ ,  $[\overline{DS}][D]$  and  $[D][S]$  may be neglected when compared with  $[S]$ . Equation (5.4.1.3) then reduces to

$$\tau_{II}^{-1} = \frac{k_{23} 2[D]}{1 + K_{12}([D] + [S])} + k_{32} \quad (5.4.1.4)$$

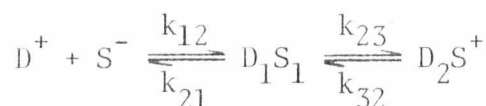
Now the ion-pair formation constant for uni-univalent ions  $K_{12} \approx 10M^{-1}$ <sup>(7)</sup>

then  $k_{12}([\bar{D}] + [\bar{S}]) \approx 10^{-2}$

Hence  $\tau_{II}^{-1} = k_{23} 2[\bar{D}] + k_{32}$  (5.4.1.5)

Equation (5.4.1.5) does not predict a dependence on surfactant concentration. Therefore, either the mechanism or the relaxation method are not applicable in this case. For the relaxation method to be applicable to the stopped-flow method the stopped-flow must be used in the "concentration-jump" mode. This would involve an experiment in which the concentration of the reagents are changed by 5-10% i.e. a small perturbation of the equilibrium. For the mixing reaction employed here this is clearly not the case.

A different analysis must therefore be attempted. The steady-state method will be used<sup>(8)</sup>:



The rate of appearance of  $[D_2S]$  is given by

$$\frac{d[D_2S]}{dt} = k_{23}[D] \cdot [DS] - k_{32}[D_2S] \quad (5.4.1.6)$$

Now, if  $[DS]$  is in steady-state

$$\frac{d[DS]}{dt} = k_{12}[D][S] + k_{32}[D_2S] - k_{21}[DS] - k_{23}[DS][D] = 0 \quad (5.4.1.7)$$

$$\therefore [DS] = \frac{k_1[D][S] + k_{32}[D_2S]}{(k_{21} + k_{23}[D])} \quad (5.4.1.8)$$

A further simplification may be made if the formation of  $D_2S$  is considered to be irreversible i.e.  $k_{32}[D_2S] = 0$ .

Then

$$\text{rate} = \frac{d[D_2S]}{dt} = k_{23}[D][DS] \quad (5.4.1.9)$$

$$= \frac{k_{23}k_{12}[D]^2[S]}{k_{21} + k_{23}[D]} \quad (5.4.1.10)$$

Now, as before,  $K_{12} \sim 10M^{-1}$  and it is most likely that  $k_{12}$  will be diffusion controlled (similar to the dye dimerisation rate constant).  $k_{12} \sim 10^{10}$  which will make  $k_{21} \sim 10^9$ .

Rearrangement of equation (5.4.1.10) gives

$$\text{rate} = \frac{d[D_2S]}{dt} = \frac{k_{23}K_{12}[D]^2[S]}{1 + k_{23}/k_{21}[D]} \quad (5.4.1.11)$$

$k_{23}$  will be similar to the dye-dimerisation rate constant  $\sim 10^{10}$  and  $k_{21} \sim 10^9$ . Therefore,  $k_{23}/k_{21}[D] \ll 1$  and,

$$\text{rate} = \frac{-d[D]}{dt} = (k_{23}K_{12}[D][S])[D] \quad (5.4.1.12)$$

$$\therefore k(\text{obs}) = k_{23}K_{12}[D][S] \quad (5.4.1.13)$$

Hence a plot of  $k(\text{obs})$  vs  $[S]$  should be linear with a slope of  $k_{23}K_{12}[D]$ . Of course, this relationship is not strictly correct since  $[D]$  is not constant except under conditions where complex formation is small. However, the plots of  $k(\text{obs})$  vs  $[S]$  are good straight lines. For very low  $[S]$  the plots curve to go through the origin. The linear portions of the plots have been used to calculate values of  $k_{23}$ .

Assuming  $K_{12} = 10M^{-1}$ ,  $[D] = [D^0]$  Values of  $k_{23}$  are shown in table 5.4.1.1.

A preliminary initial-rates analysis of some of the data has been carried out by Dr. A. James<sup>(9)</sup> leads to rate constants of the same order of magnitude i.e. close to diffusion controlled.

The initial rate of the reaction is given by

$$\text{Initial rate} = k_{23}[\text{DS}][\text{D}^0] = \text{initial slope } [\text{D}^0] \quad (5.4.1.14)$$

$$= k_{23}K_{12}[\text{D}^0]^2 \cdot [\text{S}^0] \quad (5.4.1.15)$$

where  $[\text{D}^0]$  and  $[\text{S}^0]$  are the total concentrations of dye and surfactant.

The signal change is  $\Delta A/A$  (or  $\Delta F/F$ ) therefore the initial slope is  $\Delta A/A \cdot 1/\Delta T$  where  $\Delta T$  is the time interval.

$$\text{Initial rate} = \Delta A/A \cdot 1/\Delta T [\text{D}^0] = k_{23}K_{12}[\text{D}^0]^2 [\text{S}^0] \quad (5.4.1.16)$$

$$\therefore k_{23}K_{12} = \Delta A/A \cdot 1/\Delta T \cdot 1/[\text{D}^0][\text{S}^0] \quad (5.4.1.17)$$

This analysis is more rigorous since it depends on the initial slope which is calculated for the first few percent of the reaction and the change in  $[\text{D}]$  will not affect the results.

The rates obtained are close to, but significantly different from the diffusion-controlled limit calculated by the Debye-Smolochowski<sup>(10)</sup> equation

$$k_{\text{diff}} = 4\pi N_A D_{AB} \left\{ \frac{\theta}{e^{\theta}-1} \right\} 10^{-3} \text{ M}^{-1}\text{S}^{-1}$$

$$\text{and } \theta = Z_A Z_B e_o^2 / \epsilon k T a$$

where  $N$  = Avogadro's number,  $D_{AB}$  = translational diffusion coefficient of the ions,  $Z_A, Z_B$  = charge on the ions,  $e_o$  = electronic charge,  $\epsilon$  = dielectric constant and  $a$  = distance of closest approach of the ions in the encounter complex.

TABLE 5.4.1.1

CALCULATED VALUES OF  $k_{23}$

$K_{12} = 10M^{-1}$	SDS			
	AO <sup>+</sup>		PF <sup>+</sup>	
$10^5  D^+ /M$	$10^4 \text{slope}/M^{-1}S^{-1}$	$10^9 k_{23}/M^{-1}S^{-1}$	$10^4 \text{slope}/M^{-1}S^{-1}$	$10^9 k_{23}/M^{-1}S^{-1}$
1	14	1.4	11	1.1
2	20	1.0	14	0.7
4	32	0.8	24	0.6
		SDeS		
1	5	0.5	2	2.0
2	8	0.4	3	1.5
4	16	0.4	4	2.0
		SDSn		
1	10	1.0		
		SDBSn		
1	14	1.4		

For a dielectric constant of 80,  $a = 0.95\text{nm}$  (equivalent to two water molecules between the ions) and  $D_{AB} = 1 \times 10^{-5} \text{ cm}^2 \text{ s}^{-1}$ , we find that  $k_{\text{diff}} \approx 2.4 \times 10^9 \text{ M}^{-1} \text{ s}^{-1}$ .

The rate constants obtained are almost the same as those for the free dye dimerisation process and the dimerisation of N(10) alkyl derivatives of acridine orange<sup>(11)</sup>.

The rate constants are approximately independent of dye concentration, this is in contrast to the free dye results<sup>(11)</sup>. This must be due to the influence of the surfactant but whether this is primarily an electrostatic effect or not is unclear.

Surfactant chain-length does not seem to have a significant effect on the rate constants and this is to be expected for rates so close to the diffusion-controlled limit.

#### 5.4.2 The Slow Aging Process and Dissolution Kinetics

At this stage it is not possible to give a quantitative mechanism, the slow process II has only been investigated in a preliminary way and few experimental observations have been made so far.

The slow aggregation process which involves the build-up of large dye-surfactant species may follow a similar mechanism to that described by Schwarz et al<sup>(2)</sup> for the aggregation of dye-polyelectrolyte complexes at high ionic strength and  $[D]/[\text{Polyelectrolyte anion}] \approx 1$ .

This process is one in which polyelectrolytes already bound with dye associates with other polyelectrolyte chains. The presence of dye aids the process by neutralisation of the polyelectrolyte charged groups.

It was found that the rate of build-up of scatter (i.e. build-up of aggregate) decreased with increasing surfactant concentration, i.e. rate of aggregate build-up is greater at low S/D.

The dissolution kinetic measurements consist of mixing a solution of dye/micelle with water such that the final concentration is below the CMC. It is found that:-

- (i) the absorbance and fluorescence change is equal to the calculated value,
- (ii) the rate is the same measured by absorbance or fluorescence,
- (iii) the rate for  $\text{AO}^+$  is slower than for  $\text{PF}^+$ ,
- (iv) very complex transients are observed.

The traces consist of at least two relaxations, sample traces are shown in figure 5.4.2.1. It is not possible to analyse the traces quantitatively but the trend in the time to reach completion will be outlined.

The time to reach completion increases with increasing surfactant

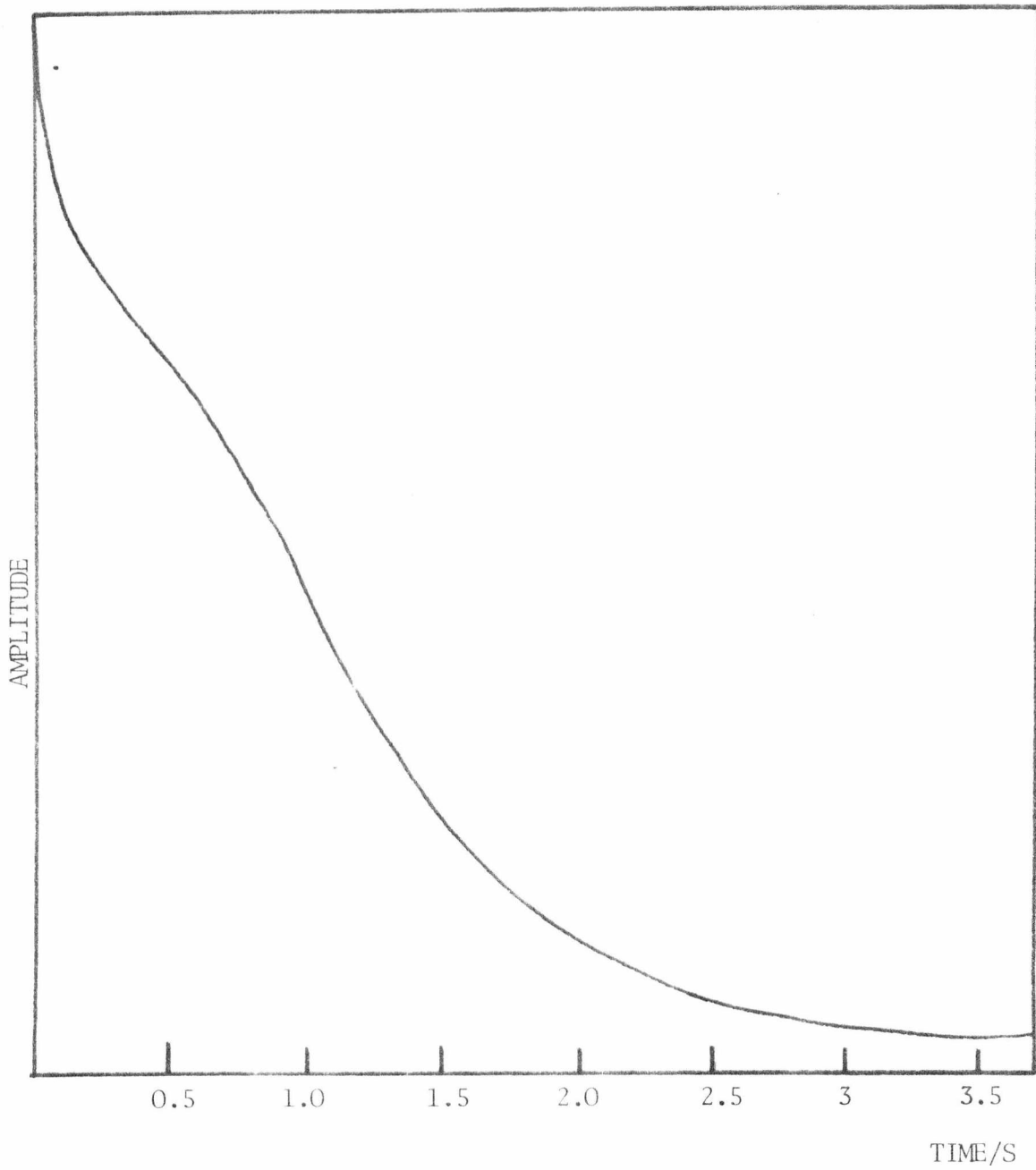


FIGURE 5.4.2.1

SAMPLE TRACE FOR DISSOLUTION EXPERIMENT

concentration. Table 5.4.1.

This is in direct contrast to the results from temperature-jump studies on pre-CMC solutions.

TABLE 5.4.1

TIME TO COMPLETION ( $T_{\infty}$ ) FOR DISSOLUTION KINETICS

Temp. 298.2K, [DYE]  $1 \times 10^{-5}$ M

$10^3 [\text{SDS}]_F / \text{M}$	AO <sup>+</sup>	$T_{\infty}/S$	PF <sup>+</sup>
3.0	1.8		0.5
3.5	3.5		0.8
4.0	8.5		1.4
5.0	16		2.4

The amplitude of the fast process (<20msec) is too small to make only quantitative measurements of the rate. It should, however, represent the initial release of dye from the micelle. The slow process may represent the build-up of large aggregates which involve dye and surfactant.

## 5.5 Temperature-Jump Investigation of the Pre-CMC Dye-Surfactant Solutions

### 5.5.1 Results

The pre-CMC dye-surfactant exhibit slow aging which results in the production of turbid solutions which contain large aggregates. The aging process prevents a quantitative analysis of the temperature-jump kinetics of the system. A qualitative description of the relaxation times and

amplitudes will be given.

Systems which exhibit this type aging process may usefully be studied by means of the stopped-flow temperature-jump technique<sup>(11)</sup>. This technique would enable temperature-jumps to be performed within 2msec of mixing the solutions before the large aggregates to form. Temperature-jumps may also be performed at different times after mixing has taken place. This would enable a systematic study of the effect of the build-up of large aggregates.

Both systems studied ( $\text{AO}^+/\text{SDS}$  and  $\text{PF}^+/\text{SDS}$ ) exhibit a maximum of three relaxations (I, II and III) each separated by at least two orders of magnitude. The general features of these are as follows:

- (i) occurs in the  $\mu\text{s}$  time region, with an increase in absorbance (at  $\lambda_{\text{max}}$  of the dye, I);
- (ii) occurs in the ms time range, the amplitude of which is independent of wavelength and exhibits a decrease in absorbance (turbidity) (II);
- (iii) occurs in the s time range, with an increase in absorbance at  $\lambda_{\text{max}}$  of the dye (III).

The time constant for the fast relaxation (I) is approximately constant (at constant dye concentration) and is  $\sim 15\mu\text{sec}$  for acridine and proflavine. The absorbance amplitude of the relaxation process for both dyes is found to decrease as the surfactant concentration increases. The amplitude of the fast process for acridine orange is in the same direction (but smaller) than for the dye in free solution<sup>(4)</sup>. Proflavine in free solution at the concentrations used in this experiment has a relaxation time too fast to detect by the temperature-jump method<sup>(12,13)</sup>.

The intermediate (II) wavelength independent relaxation is always

in the narrow range 0.5-2msec. The relaxation amplitude decreases with increasing surfactant concentration. The surfactant concentration at which this relaxation becomes detectable depends on the dye and the added ionic strength. For both dyes the relaxation becomes detectable at a lower surfactant concentration as the added ionic strength is increased.

TABLE 5.5.1.1

LOWEST SDS CONCENTRATION FOR THE DETECTION OF RELAXATION (II)

Temp. 298.2K

IONIC STRENGTH(NaCl)	AO <sup>+</sup>	PF <sup>+</sup>
	10 <sup>4</sup> [SDS] /M	
0.01	-	-
0.05	5.0	2.1
0.10	1.9	1.2

The slowest relaxation time (III) is extremely difficult to measure accurately. The relaxation times are so slow that convective cooling of the solution after the temperature-jump interferes with the chemical relaxation of the system. However, qualitative trends may be observed.

The relaxation time decreases as the surfactant concentration approaches the CMC. The relaxation times are faster for acridine orange than proflavine.

TABLE 5.5.1.2

SLOW (III) RELAXATION TIMES FOR PRE-CMC TEMPERATURE-JUMPSYSTEMS AO<sup>+</sup>/SDS AND PF<sup>+</sup>/SDS

Temp. 298.2K      I = 0.01 NaCl

$10^4 [\text{SDS}] / \text{M}$	$\tau / \text{s}$ AO <sup>+</sup> /SDS	$\tau / \text{s}$ PF <sup>+</sup> /SDS
1.0	1.6*	-
2.0	0.8*	-
5.0	0.5	1.4*
7.5	0.3	0.8*
10.0	0.1	0.55

$$[\text{Dye}] = 1.5 \times 10^{-5} \text{M}$$

\* Extrapolated values

These relaxation times are largely independent of added ionic strength up to 0.1. The amplitude decreases rapidly with increasing surfactant concentration, it is also wavelength dependent.

5.5.2 Discussion

An unambiguous assignment of the relaxation times to molecular processes cannot be made from the experimental observations reported here. Some possibilities will be considered.

The amplitude change and the rate of the fast process I is consistent

with the production of monomer dye. Hence, the relaxation may arise from either (i) the monomer-dimer dye equilibrium similar to that in free solution or, (ii) an equilibrium between dye on the aggregate and free dye.

For Proflavine, at the concentrations used only, ~1% is present in the dimer form. This is sufficient to produce a detectable relaxation under the conditions used. (It would also be much more rapid than the one measured<sup>(12,13)</sup>). This may indicate that the process is most likely (ii), although it is not possible to distinguish between the many types of dye-aggregate equilibrium which may occur.

The intermediate relaxation (II) results in a change in turbidity and it is not very concentration dependent. The change in turbidity must mean that the size of the aggregates is temperature dependent. This has been observed previously by Schwarz et al<sup>(2)</sup>.

The slow relaxation (III) time is most likely to be associated with the loss of tightly bound dye from the aggregate.

Further measurements are necessary before firm conclusions can be drawn about any of the three relaxation processes. Investigation of the size of the aggregate by light-scattering techniques and the temperature dependence of the size together with more extensive light-scattering temperature-jump measurements would be most useful.

## REFERENCES

- (1) G. Schwarz and S. Klose, *Eur. J. Biochem.*, 1972, 29, 249.
- (2) G. Schwarz and A. Seelig-Löffler, To be published.
- (3) C.A. Parker, Photoluminescence of Solutions, (Elsevier, New York 1968) p.344.
- (4) B.H. Robinson, A. Seelig-Löffler and G. Schwarz, *J. Chem. Soc. Faraday*, 1, 1975, 71, 815.
- (5) G.S. Schwarz, *Eur. J. Biochem.*, 1970, 12, 442.
- (6) G. Czerlinski, Chemical Relaxation, (Marcel Dekker Inc., New York, 1966).
- (7) C.W. Davies, Ion Association, (Butterworths, London, 1962).
- (8) K.J. Laidler, Chemical Kinetics, 2nd ed. (McGraw-Hill, New York, 1965).
- (9) A.D. James, personal communication.
- (10) P. Debye, *Trans. Electrochem. Soc.*, 1942, 82, 265.
- (11) A.D. James and B.H. Robinson, *Adv. Molecular Relax. Processes*, 1976, 8, 287.
- (12) G. Czerlinski, in Rapid Mixing and Sampling Techniques in Biochemistry, ed. B. Chance, R.H. Eisenhardt, Q.H. Gibson and K.K. Lonberg-Holm (Academic Press, New York, 1964).
- (13) D.H. Turner, G.W. Flynn, S.K. Lundberg, L.D. Faller and N. Sutin, *Nature*, 1972, 239, 215.
- (14) M.M. Farrow, N. Purdie, A.L. Cummings, W. Hermann Jr. and E.M. Eyring, Chemical and Biological Applications of Relaxation Spectrometry, ed. E. Wyn-Jones (Nato Advanced Study Institute Series, D. Reidel, Dordrecht, Holland, 1975).

C H A P T E R 6

THE INTERACTION OF CATIONIC DYES WITH

ANIONIC MICELLES

## CHAPTER 6

### THE INTERACTION OF CATIONIC DYES WITH ANIONIC MICELLES

#### 6.1 Introduction

The interaction of small molecules with surfactant systems (emulsions, micelles, etc.) has been extensively investigated<sup>(1-4)</sup>. The major proportion of these studies involve the interaction of water-insoluble solutes (benzene, polycyclic hydrocarbons etc.) with micelles in aqueous solution. A number of different interactions have been observed.

(1) Hydrotopy<sup>(5)</sup>, this is the increase in the solubility of substances in water due to the presence of large amounts of additives. For example, the solubility of benzoic acid is increased from 2.9 to 8.7g per 1000g of solvent when 2M sodium benzene sulphonate solution is used as solvent in place of water<sup>(6)</sup>. The phenomena essentially involves changes in solvent structure; Mckee<sup>(7)</sup> considers the process to be a salting-in effect.

(2) Solubilisation has been defined by McBain as "the spontaneous passage of solute molecules of a species insoluble in water into an aqueous solution of a surfactant in which a thermodynamically stable solution is formed"<sup>(8)</sup>. Solubilisation may involve either the diffusion of the added solute molecules from the bulk phase (insoluble solids, oil droplets etc.) into the micelle or the formation of micelle containing solute by a process of surfactant monomer enclosing small amounts of solute. Beyond a certain concentration of added solute the micelle becomes saturated with the solute and emulsification is observed.

It should be noted that the processes of hydrotopy and solubilisation

should not be necessarily considered as separate phenomena. There is a continuous gradation in the behaviour of sodium salts of fatty acids as solubilisers<sup>(9)</sup>. For a homologous series the solubilising properties of the lower members ( $C_1$ - $C_4$ , which do not form micelles) become evident at high concentration 30-50% by weight; for the higher members ( $C_5$ - $C_{11}$ ) this concentration is much lower.

(3) Blending<sup>(10)</sup> is a broad term for processes which can be distinguished from solubilisation by the study of phase diagrams<sup>(11)</sup>. The phenomena involves the mutual solubility of two normally immiscible liquids by the addition of a surfactant. For example, dodecylamine hydrochloride added to chloroform in small amounts<sup>(12)</sup> will enable the chloroform to dissolve large quantities of water - upto 45 moles/mole of surfactant.

Hydrotrophy requires a high concentration of reagent (of the order of 1M) and probably operates through a molecular association mechanism, and may be considered to be a solvent effect similar to that which has been observed in solvent effects with polycyclic hydrocarbons<sup>(13)</sup>.

Solubilisation on the other hand is found to occur at much lower concentrations and is first observed above the CMC of surfactants.

In this chapter the kinetic investigation of the interaction between water-soluble positively-charged polycyclic aromatic dyes and negatively-charged micelles in aqueous solution is discussed.

The equilibrium absorption and fluorescence measurements discussed in Chapter 4 lead to the conclusion that the dyes are incorporated into the outer palisade layer of the micelle. The positive charge on the dye keeps it close to the surface and the hydrophobic nature of the dye promotes its entry into the outer hydrocarbon region of the micelle. Since the dye molecule is charged and water soluble we have introduced the term "absorption" to distinguish the process from the solubilisation of water

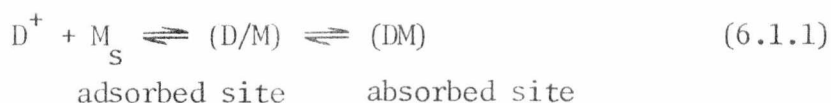
insoluble species.

The process of adsorption/absorption of molecules onto/into micelles has been widely studied by a variety of static techniques including light-scattering<sup>(14)</sup>, solubility<sup>(15)</sup> and spectrophotometry<sup>(16,17)</sup>. In a few cases the dynamics of the absorbed molecules has been studied, predominately by ESR<sup>(18-20)</sup> and NMR<sup>(21,22)</sup> techniques. Some stopped-flow kinetic studies on the adsorption/absorption of the dye pinacyanol chloride have recently been made<sup>(23)</sup>. The kinetics of the solubilisation of an aqueous suspension of *Achaleplasma laidlawii* membrane fragments have also been reported<sup>(24)</sup>.

In this study three types of experiment have been performed:

(1) The dye is mixed with pre-formed micelles in a stopped-flow instrument. A limiting rate is reached for the absorption process independent of dye and micelle concentration. For a given micelle the absorption process is very sensitive to the shape and charge of the dye, subtle changes result in large kinetic effects. Dyes with the same geometry and charge are absorbed at very similar rates. The rate of absorption is found to decrease as the hydrocarbon chain-length of the surfactant is increased; the effect of surfactant head-group is, however, small. The absorption rate is affected by the addition of excess ions (increasing ionic strength) co-solvents and potential impurities.

The mechanism proposed for the absorption of the dye into the micelle is a two-step process which involves a rapid (diffusion-controlled) adsorption of the dye onto the charged micelle surface. This is followed by a slow intercalation or absorption of the dye into a more strongly bound site in the hydrocarbon region of the micelle



The mechanism is related to proposed schemes for the binding of similar dyes to DNA<sup>(25,26)</sup> and the fluorescent probe 8-anilino-1-naphthalene sulphonate (ANS) to lecithin bilayers<sup>(27)</sup>. In the case of DNA, two binding sites for the dye have been postulated; a weak external electrostatic site and a stronger hydrophobic site which involves the intercalation of the dye between the base pairs. A significant difference between DNA and micellar systems is that the structure of DNA is time-independent, but the micelle has a dynamic structure. The lifetime of micelles is of the order of milliseconds<sup>(28)</sup>.

For the binding of ANS to lecithin bilayers two relatively slow processes are observed by the stopped-flow technique in the millisecond and second time ranges. Both processes are independent of ANS concentration, which suggests a unimolecular process. The fast process is analogous to that observed for micellar systems and is thought to represent the reorientation and entry of the dye into the outer region of the bilayer following rapid electrostatic binding. The slow process is thought to represent the transport of the dye across the bilayer.

(2) Ionic-strength jump experiments have been performed on these systems. This procedure involves the formation of micelles on mixing in the stopped-flow instrument. The consequent interaction is almost independent of dye and the rate increases linearly with micelle concentration. The proposed mechanism is more complex than the straightforward absorption mechanism.

(3) Temperature-jump perturbation relaxation experiments have been performed on a number of solutions containing acridine dye and micelle in equilibrium. Complex transients result which indicate at least two relaxation processes which have opposing amplitudes at low ionic strength.

It was observed that the slower of the two processes was largely

independent of type of dye at low ionic strength but was dependent to a small extent on dye type and concentration in 0.1M sodium chloride solutions.

## 6.2 Experimental Conditions

### 6.2.1 Direct Interaction of Dye and Micelle above the CMC

Using the stopped-flow apparatus described in Chapter 2, dye solution is mixed in a 1:1 ratio with surfactant solution such that the final concentration of surfactant is above the CMC. For SDS at zero added ionic strength the initial concentration is greater than  $1.5 \times 10^{-2} \text{M}$ .

The same final conditions may be obtained by diluting a solution of surfactant (concentration  $> 2 \text{ CMC}$ ) which contains dye with water. Provided the concentrations are controlled so that the resultant change in absorbance or fluorescence is large (absorbance change  $> 0.01$ , see figs. 4.2.2, 3, 6, 3.1 ) good transients may be obtained. Because the absorbance and fluorescence intensity reach a limiting value with increasing surfactant concentration the range of surfactant concentration in which this experiment may be successfully performed is severely restricted with 1:1 mixing. For the SDS/AO<sup>+</sup> system the range of SDS concentration is  $1.5 \times 10^{-2} - 2 \times 10^{-2} \text{M}$ .

The addition of cosolvent or ionic strength may be made to either solution without affecting the kinetic results.

The solutions were unbuffered, but the pH of the solutions was generally close to 7<sup>(29)</sup>. In the case of experiments carried out at final pH's of 11 and 13 the pH was obtained using sodium hydroxide and no buffer.

To investigate the interaction of dye-surfactant aggregate with micelle the following procedure was adopted. Dye and surfactant solutions were separately pre-thermostatted, mixed and transferred rapidly to the stopped-flow reservoir syringes. The kinetic measurements were performed

two minutes after the initial mixing of dye and surfactant. It was necessary to perform the stopped-flow experiment a set time after pre-mixing dye and surfactant. The aging of the solution which leads to the build-up of large aggregates (Chapter 5) changes the rate of absorption. In general, the solutions were thermostatted to  $\pm 0.05\text{K}$  and the temperature measured with a Comark electronic thermometer as described in Chapter 2.

### 6.2.2 Ionic-Strength Jump Experiments

In these experiments dye solution containing sodium chloride is mixed with surfactant solution at a concentration less than the CMC in pure water. The conditions are controlled such that after mixing the surfactant concentration is greater than the CMC for the final ionic strength employed. For example, for a final ionic strength of  $0.1\text{M}$ , then the range of SDS concentration which will produce micelles is  $2.8 - 6.5 \times 10^{-3}\text{M}$ . The usable range of surfactant concentration is again small with 1:1 mixing.

### 6.2.3 Temperature-Jump Experiments

The solutions were made up, without buffer, in  $0.1\text{M}$  sodium chloride. The solutions were protected from photodecomposition by closing the shutter between jumps. Each solution was "jumped" no more than five times.

The rate constants were determined from photographic records of the oscilloscope trace which were analysed by the method of Crooks et al<sup>(30)</sup>. The data-capture system (Chapter 2) was also employed. The rate constants obtained were the average of at least four individual traces. Errors are standard deviations.

The wavelength of observation was  $\lambda_{\text{max}_2}$  (i.e. in the micelle) for absorbance and  $\lambda_{\text{max}_{\text{ex}}} / \lambda_{\text{max}_{\text{em}}}$  for fluorescence (see table 4.2.3).

## 6.3 The Interaction of Dye with Sodium-n-alkyl Sulphate Micelles

### 6.3.1 The Effect of Variation in Dye Structure

The rate of absorption of dyes into sodium-n-alkyl sulphate micelles is strongly dependent on the structure of the dye. Results are shown in table 6.3.1.1 and figures 6.3.1.1-4. It should be noted that at high micelle concentration ( $>1.5$  CMC), the rate of absorption is independent of both micelle and dye concentration (dye concentration  $2.5 \times 10^{-6}$  -  $5 \times 10^{-5}$  M). A characteristic rate constant ( $k_{obs}$ ) is measured for a particular dye-micelle system. For concentrations of surfactant close to the CMC, the observed rate constant for absorption is apparently slower. This type of behaviour is common to all cationic dye-anionic micelle systems investigated here, although it is not common to all dye-micelle systems<sup>(31,32)</sup>. The interaction of anionic dyes with some cationic micelles does not lead to a limiting rate at high surfactant concentration.

The stopped-flow transient amplitudes observed by absorbance and fluorescence monitoring are between 90 to 95% of the values calculated from equilibrium measurements (figure 6.3.1.5) for the transition between free and absorbed dye. The small deviations may be attributed to the monomer dye absorbed on the micelle surface having slightly different spectra from monomer dye in free solution. (This may be due to the different dielectric constant at the micelle surface owing to the high local ionic strength)<sup>(33)</sup>.

A significant result is that dyes which have the same geometric shape are absorbed at very similar rates. (Table 6.3.1.1). The rates observed are very much slower than the rate of exchange of surfactant molecules with micelles<sup>(28)</sup>. Also the exchange rates observed for uncharged molecules such as benzene<sup>(22)</sup>, p-xylene<sup>(19)</sup> & cyclohexane<sup>(22)</sup> are much greater than the rates observed here. These observations indicate that the absorption mechanism is completely different from the mechanism of

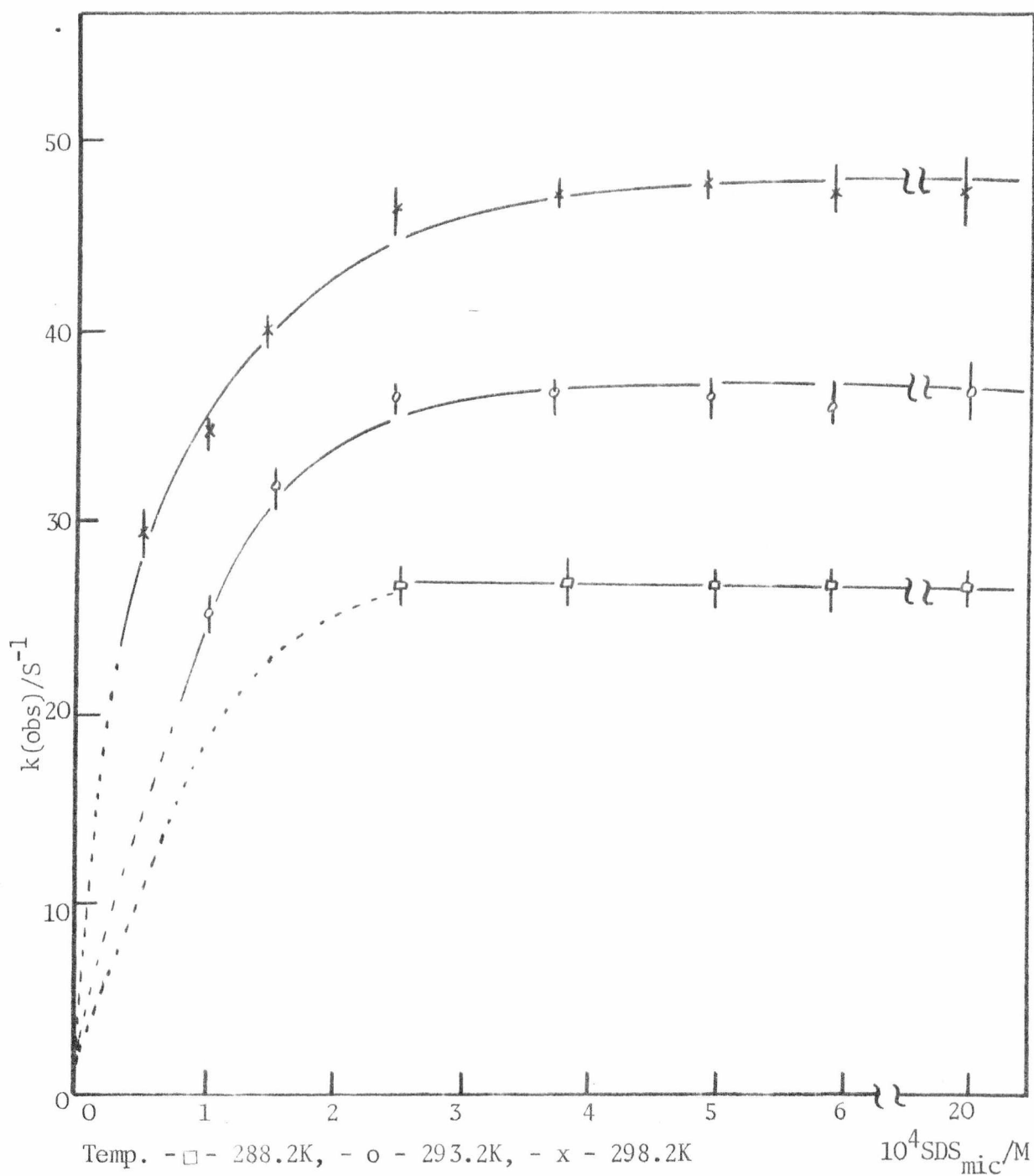


FIGURE 6.3.1.1

PLOT OF  $k(\text{obs})/\text{S}^{-1}$  VS MICELLE CONCENTRATION FOR ACRIDINE ORANGE/SDS

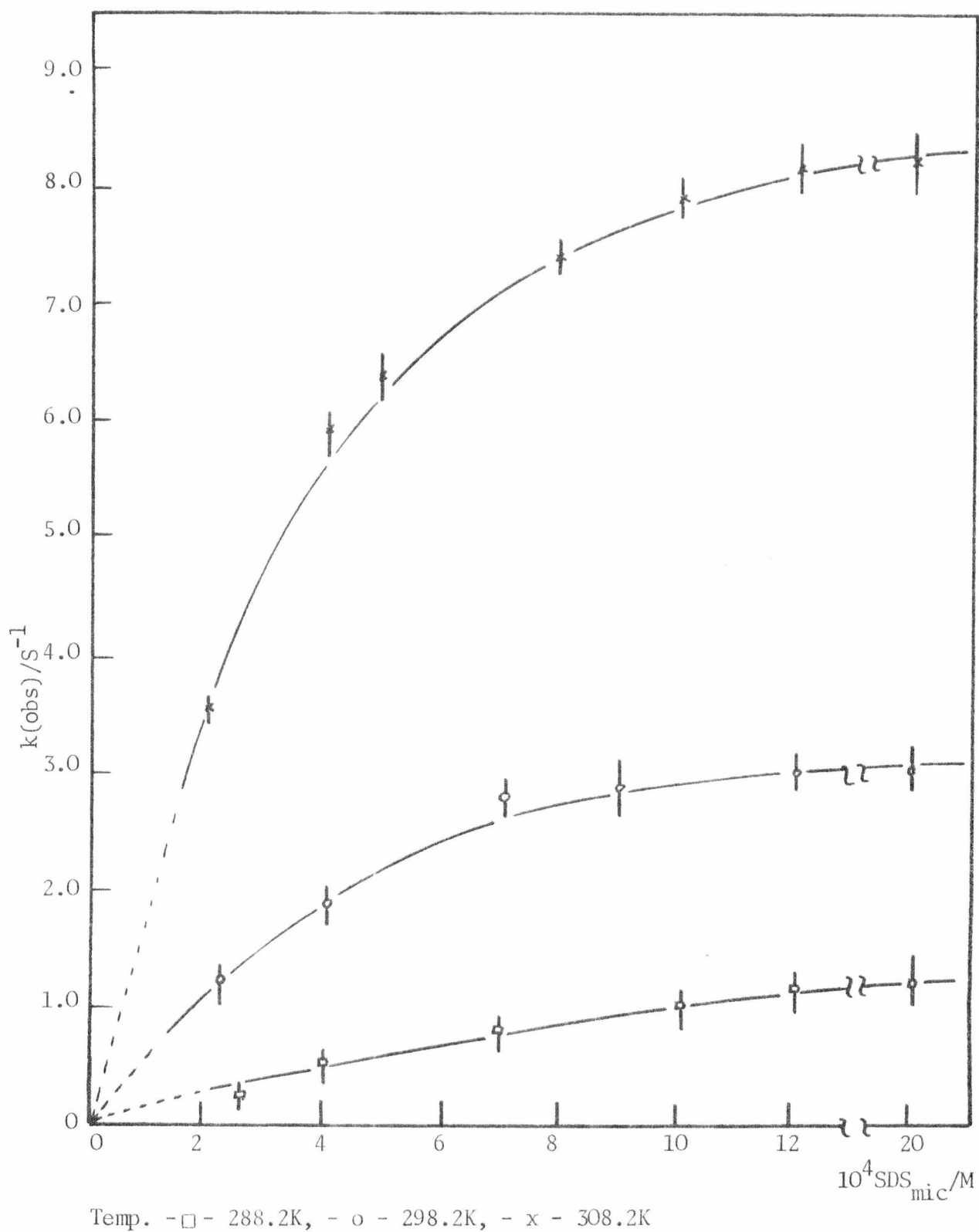
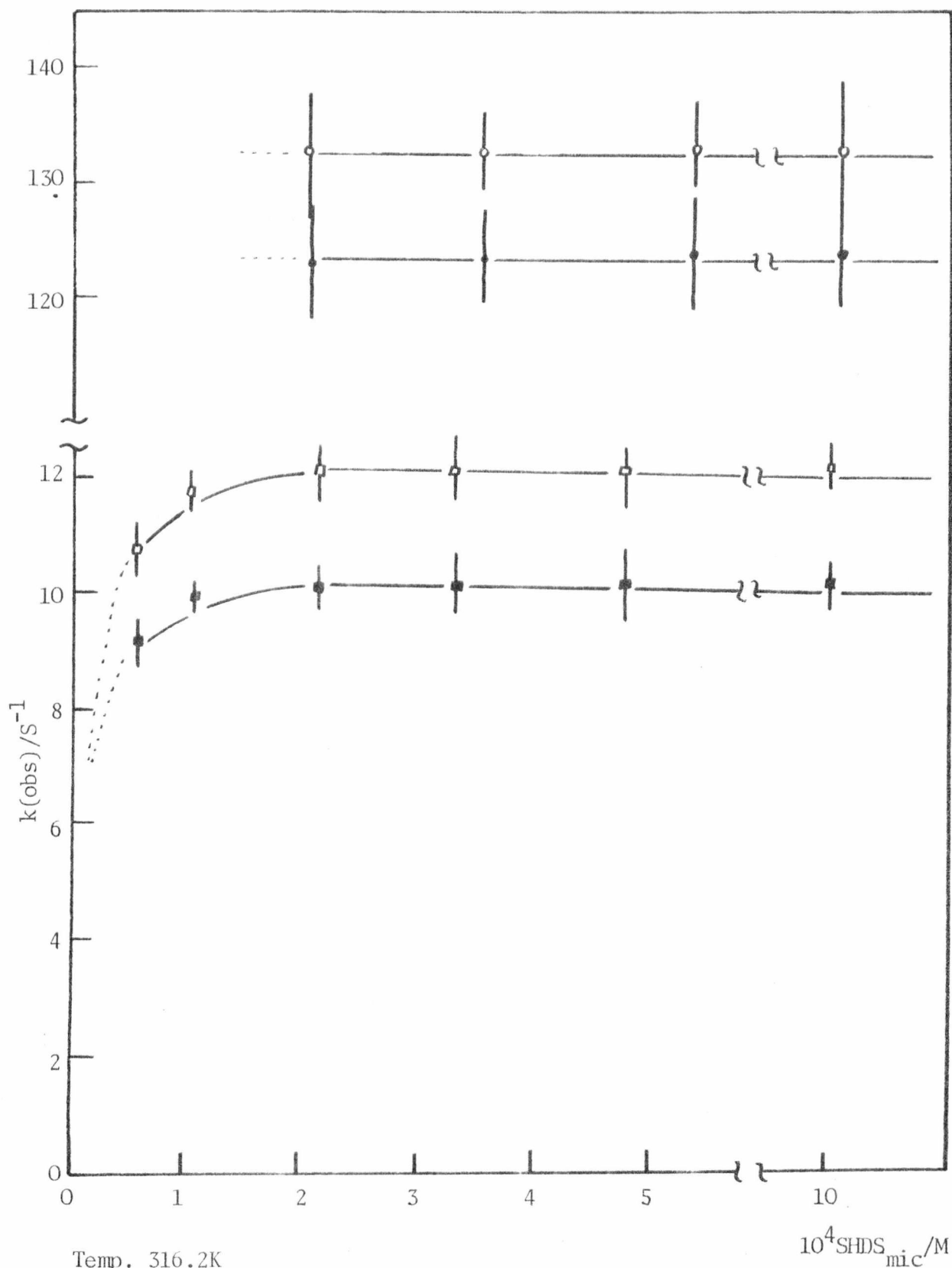


FIGURE 6.3.1.2

PLOT OF  $k(\text{obs})/\text{S}^{-1}$  VS MICELLE CONCENTRATION FOR ATEBRINE/SDS



Temp. 316.2K

Acridine Orange -  $\square$  - absorbance, -  $\blacksquare$  - fluorescence.

Proflavine -  $\circ$  -, Acriflavine -  $\bullet$  -

FIGURE 6.3.1.3

PLOT OF  $k(\text{obs})/S^{-1}$  VS MICELLE CONCENTRATION/SHDS

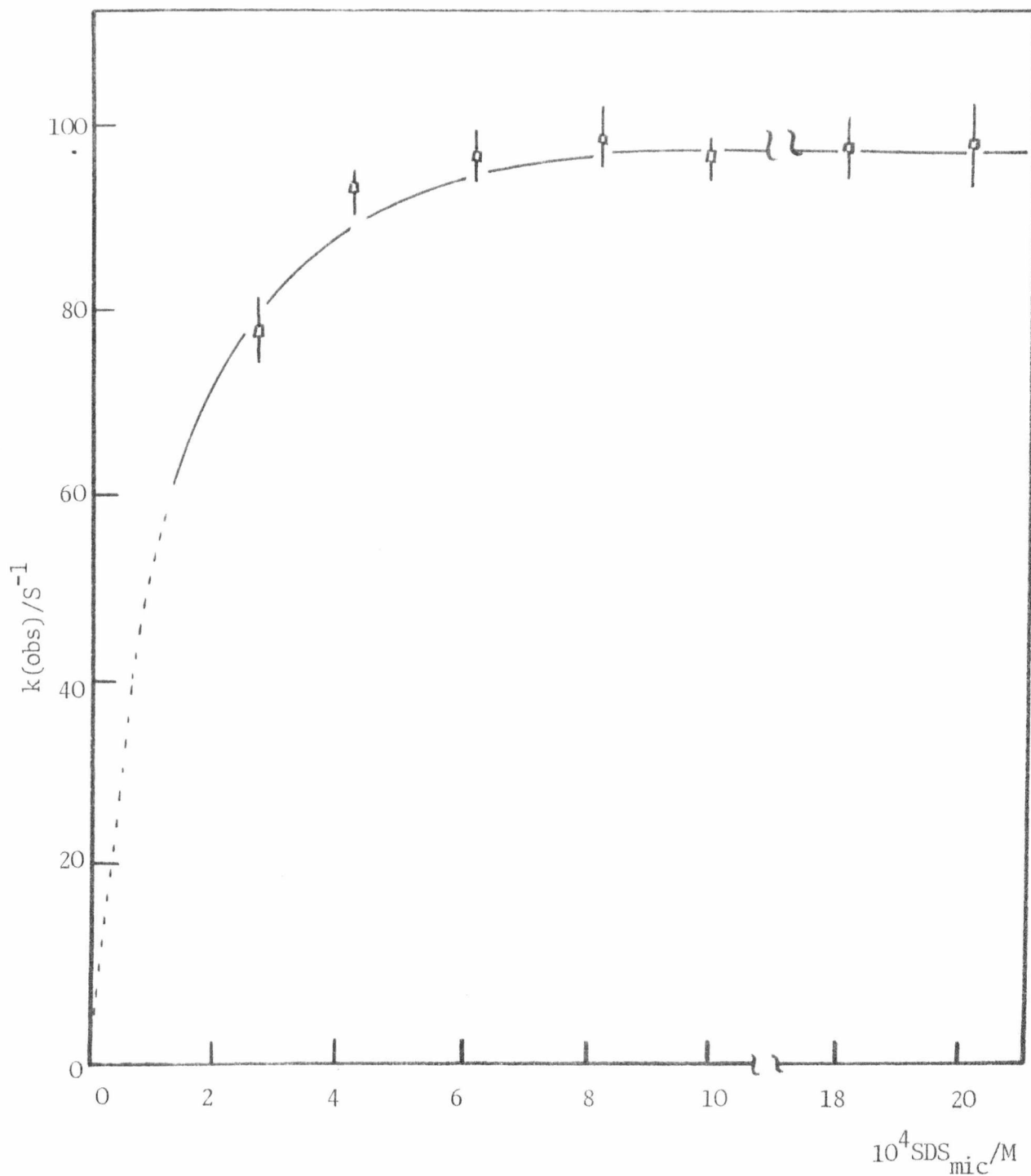


FIGURE 6.3.1.4

PLOT OF  $k(\text{obs})/\text{S}^{-1}$  VS MICELLE CONCENTRATION FOR

ACRIFLAVINE/SDS

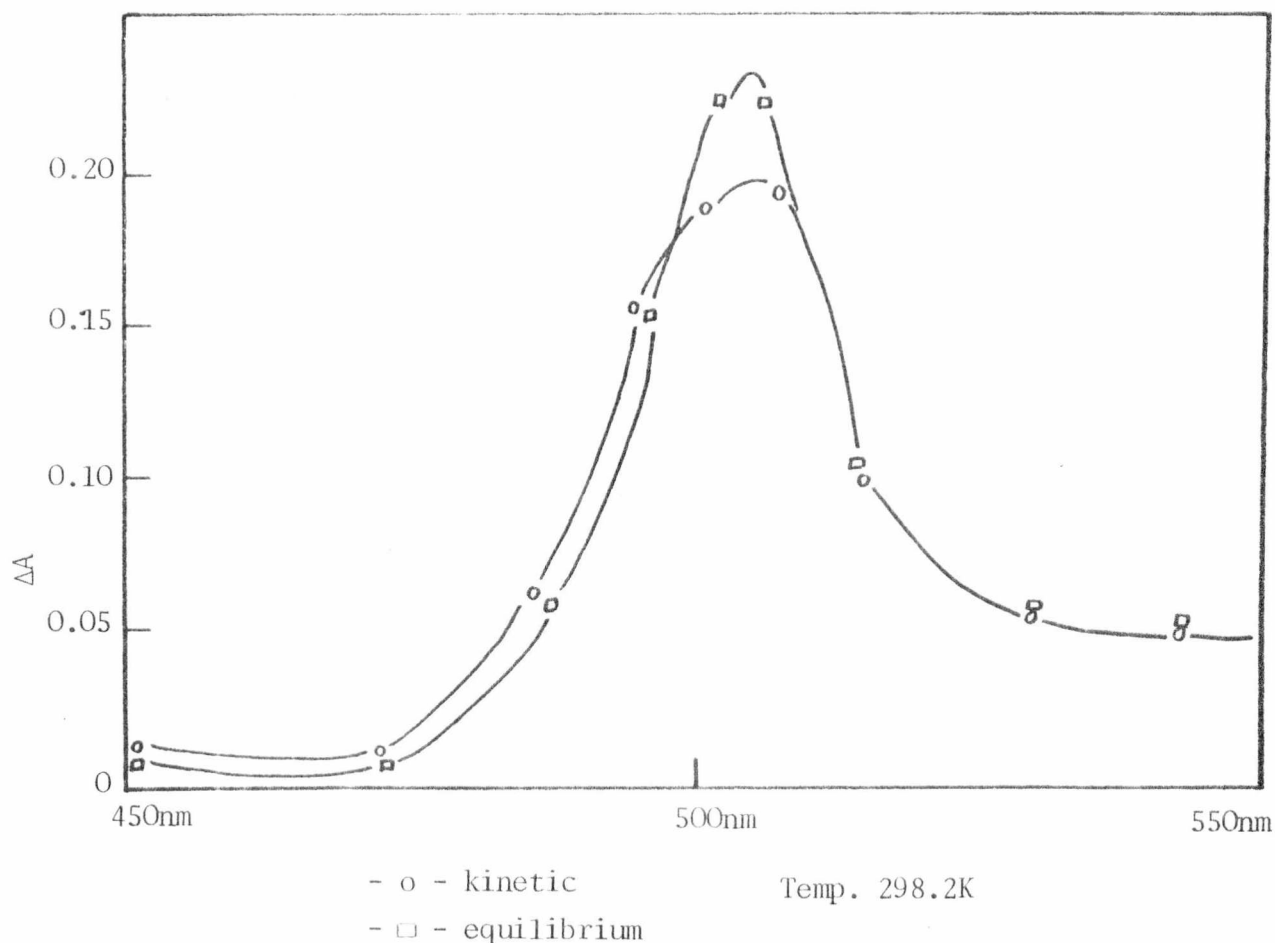


FIGURE 6.3.1.5

KINETIC AND EQUILIBRIUM DIFFERENCE SPECTRUM FOR THE AO/SDS INTERACTION

surfactant exchange.

The results for the absorption of the dye-surfactant aggregates are difficult to obtain due to the slow build-up in the pre-mixed dye-surfactant solution of large aggregates. However, the results should be considered in order to obtain an overall picture of the absorption process.

The results are shown in table 6.3.1.2. As before, a limiting rate is observed which at 298.2K is approximately 0.6 of that for the dye alone. The rate is independent of dye and surfactant concentration (dye concentration  $4 \times 10^{-7} - 10^{-5}$ , surfactant  $5 \times 10^{-4} - 2.5 \times 10^{-3}$ ) when the surfactant concentration is such that maximum aggregation is indicated from the spectra (Chapter 4, figure 4.2.2 ). The rate of absorption of the aggregate decreases as the age of the solution increases, and the size of the

TABLE 6.3.1.1 : DEPENDENCE OF RATE OF ABSORPTION ON DYE STRUCTURE FOR SDS

DYE	T/K	$k(\text{obs})_{23}/\text{s}^{-1}$	$\Delta G^\ddagger/\text{kJmol}^{-1}$	$\Delta H^\ddagger/\text{kJmol}^{-1}$	$\Delta S^\ddagger/\text{Jmol}^{-1}\text{K}^{-1}$	$K_D/\text{dm}^3 \text{mol}^{-1}$
AO <sup>+</sup>	298.2	47.6 ± 3.4	35.7 ± 4.4	63.2 ± 7.7	-92.2 ± 10.1	1x10 <sup>4(34)</sup>
AO <sup>+</sup> /1.25M MeOH	298.2	100.7 ± 10.2	60.5 ± 5.9	61.8 ± 7.1	-4.4 ± 2.7	
MB <sup>+</sup>	298.2	47.7 ± 3.1	35.9 ± 4.7	63.2 ± 7.5	-92.0 ± 10.7	2.3x10 <sup>3(35)</sup>
PYG <sup>+</sup>	298.2	47.2 ± 3.5	36.4 ± 4.9	63.3 ± 7.1	-89.9 ± 10.9	8.3x10 <sup>2(36)</sup>
AB <sup>2+</sup>	298.2	1.40 ± 0.2	68.1 ± 8.1	71.9 ± 9.0	-12.1 ± 2.3	~1x10 <sup>2(37)</sup>
AB <sup>2+</sup> /0.1 NaCl	298.2	25.9 ± 4.6	55.4 ± 7.6	65.9 ± 7.1	-33 ± 6.7	
PF <sup>+</sup>	298.2	>500				5x10 <sup>2(38)</sup>
AF <sup>+</sup>	298.2	>500				5x10 <sup>2(39)</sup>
AF <sup>+</sup>	283.2	100 ± 10				
Rh6G <sup>+</sup>		17.5 ± 3.6				
MG <sup>+</sup>		25.9 ± 4.1				
CV <sup>+</sup>		>500				

TABLE 6.3.1.2

DEPENDENCE OF RATE OF ABSORPTION OF DYE-SURFACTANT AGGREGATE

Temp. 298.2K

SYSTEM	$k(\text{obs})_{23}/\text{s}^{-1}$	$\Delta G^\ddagger/\text{kJmol}^{-1}$	$\Delta H^\ddagger/\text{kJmol}^{-1}$	$\Delta S^\ddagger/\text{Jmol}^{-1}\text{K}^{-1}$
AO <sup>+</sup> /SDS	~35	~74.4	~64	~+33
AB <sup>2+</sup> /SDS	~0.8 ± 0.2	~58	~70	~+40

$\Delta G^\ddagger$  and  $\Delta S^\ddagger$  calculated for 298K.

aggregates is increased, see Chapter 5.

An important result is that for very low dye concentration ( $<10^{-6}$ ) when no large aggregates are present, but the fluorescence spectra indicate that the dye is at least in the dimeric state, the rate of absorption is still slower than for free  $AO^{\ddagger}$ .

The results suggest that the mechanism involves a break-up of the aggregate before absorption of the dye may take place.

### 6.3.2 The Effect of pH

It has already been pointed out (Chapter 4, 4.2.3) that the double-layer of the micelle affects the pH at the surface.  $pK_s$  is the pK of the dye measured in the presence of surfactant

$$\begin{aligned} pH_s &= pH_b - \psi/60 \\ pK_s &= pK_b - \psi/60 \end{aligned} \tag{6.3.2.1}$$

where subscript b refers to bulk solution.

Therefore, an incoming dye will experience a pH gradient as it approaches the micelle surface.

The  $pK_a$ 's of the dyes in the absence and presence of micelles have been measured<sup>(32)</sup> and the results for acridine orange and atebrine are shown in table 6.3.2.1. The data suggest a surface potential of SDS micelles of -120 mV, which is in good agreement with the values reported by Hartley et al<sup>(40)</sup> and Mukerjee et al<sup>(41)</sup>.

The effect of increasing the surface pH causes deprotonation of the dyes at the micelle surface and an increase in the rate of absorption. Table 6.3.2.1.

A plot of  $k(\text{obs})$  against pH is shown in figure 6.3.2.1. The stopped-flow transients observed for the process are good single exponentials. This is because the protonated and deprotonated dyes are in rapid equi-

TABLE 6.3.2.1

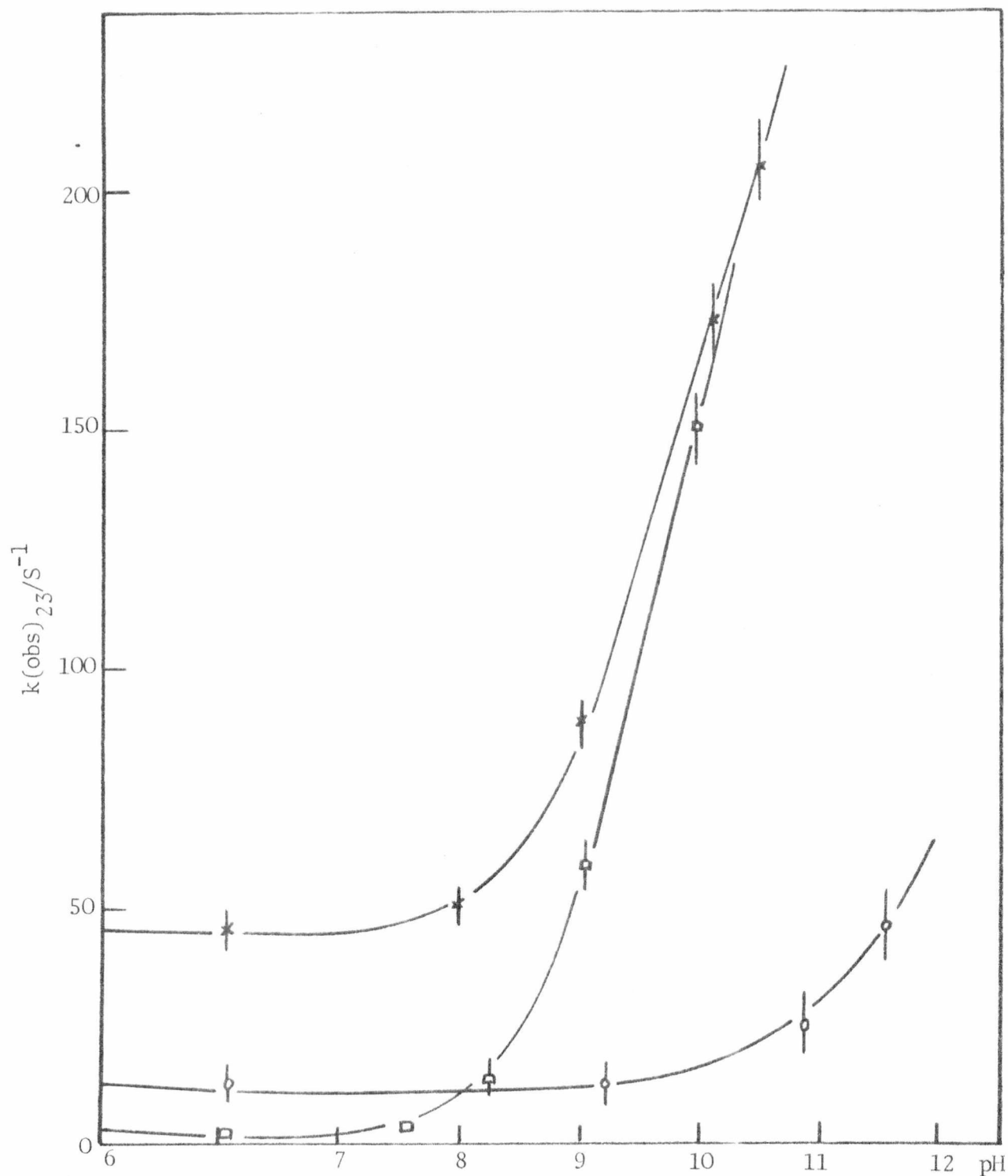
RATE OF ABSORPTION OF DEPROTONATED DYES INTO SDS MICELLES

T = 298.2K

DYE	$pK_a$ /WATER	$pK_a$ /MICELLE	$k(\text{obs}) (\text{DYE}^+)/S^{-1}$	$k(\text{obs})^* (\text{DYE})/S^{-1}$
AO	10.45 <sup>(42)</sup>	12.4 <sup>(32)</sup>	47.6 <sup>(31)</sup>	430 <sup>(32)</sup>
AB	7.95 <sup>(43)</sup>	10.6 <sup>(32)</sup>	1.40 <sup>(31)</sup>	210 <sup>(32)</sup>
NB <sup>†</sup>	9.9 <sup>(44)</sup>	12.2 <sup>(32)</sup>	7.6 <sup>(32)</sup>	51 <sup>(32)</sup>

\* Extrapolated values

† Nile Blue



Temp. 298.2K, [SDS]  $1.2 \times 10^{-2} \text{M}$

-□- AB<sup>2+</sup>/AB<sup>+</sup>, -○- NB<sup>+</sup>/NB, -x- AO<sup>+</sup>/AO

FIGURE 6.3.2.1

PLOT OF  $k(\text{obs})_{23}/\text{S}^{-1}$  VS pH

librium at the micelle surface.

The lower the charge on the dye, the more rapidly it is absorbed, which suggests that the charge on the dye is an important factor in the rate-determining step. The effect is much more pronounced for the dye  $AB^{2+}$  when it becomes  $AB^+$  than for  $AO^+ \rightarrow AO$ .

It has been pointed out by James et al.<sup>(32)</sup> that the increase in the rate constant occurs at a  $pK$  closer to the  $pK_s$  at the micelle surface than the  $pK_b$  in the bulk. This observation is strong evidence that the rate-determining step involves two forms of the dye. The rate is, therefore, dependent on the concentration of  $AO$  and  $AO^+$  in the surface region of the micelle and not in bulk solution.

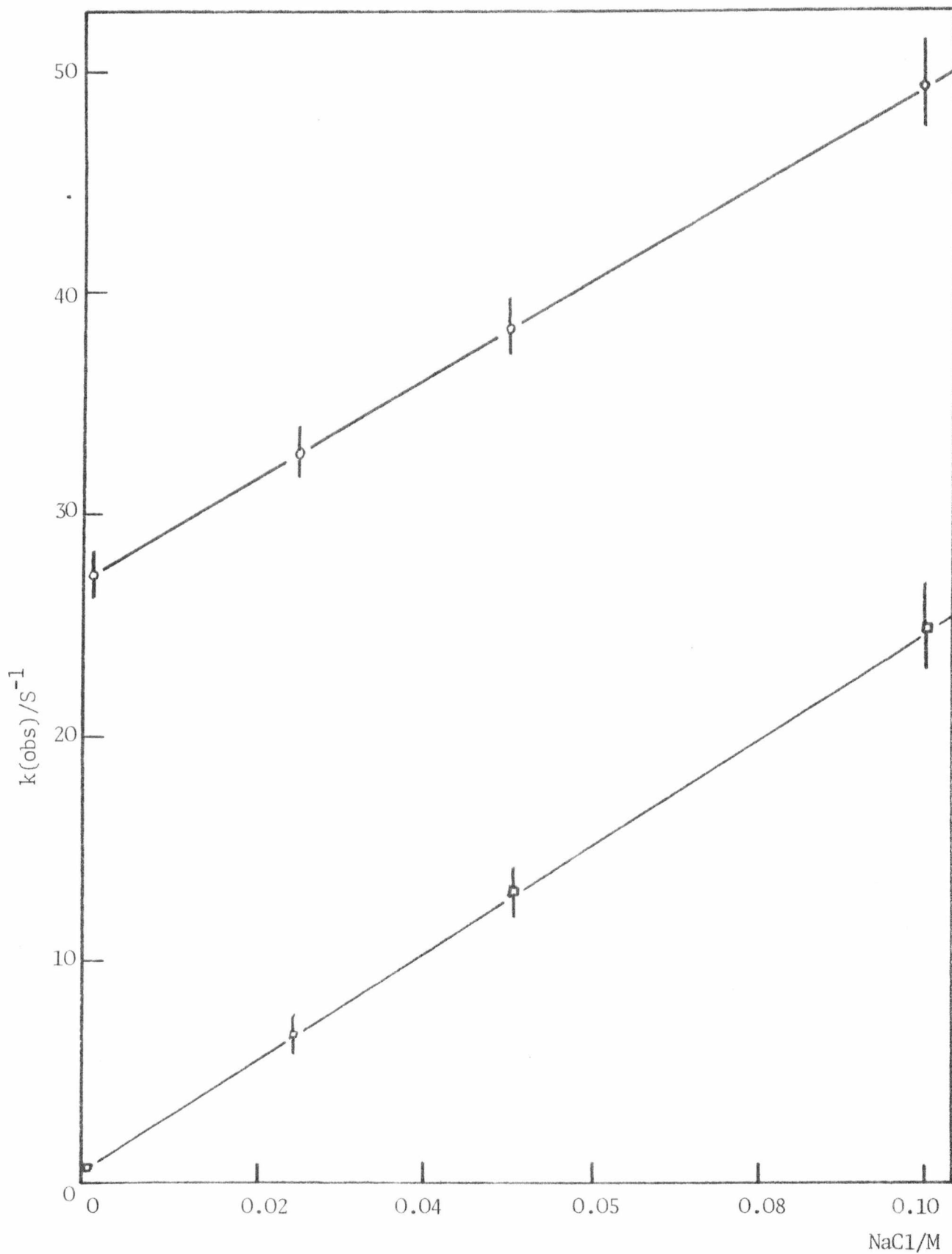
### 6.3.3 The Influence of Ionic Strength

The addition of ionic strength to micellar systems will lower the surface potential. This will lead to a lower CMC<sup>(46)</sup> and larger aggregation number<sup>(46)</sup>. This in turn will make the micelle slightly more compact at the surface<sup>(47)</sup>.

The rate of absorption is increased by the addition of ionic strength (figure 6.3.3.1). For the depositive dye  $AB^{2+}$  the rate is increased far more by the addition of NaCl than for unipositive dyes<sup>(32)</sup>. This observation supports the conclusion that the decrease in micelle surface potential is more important than the changes in micelle structure induced by the salt.

Similar increases in the rate of intercalation of  $AO^+$  into DNA have been reported<sup>(25)</sup>. This increase in the rate of absorption as ionic strength is added provides evidence that the separation of charges is an important factor. This may arise in two ways:-

- (i) the separation (compression) of the head-groups to allow room



Temp. 298.2K

FIGURE 6.3.3.1

PLOT OF  $k(\text{obs})$  VS ADDED NaCl FOR THE ABSORPTION OF  $\circ$   $\text{AO}^+$  AND  $\square$   $\text{AB}^{2+}$  BY

SDS MICELLES

for the dye to enter the micelle, will involve an increase in the local charge density. The mutual repulsion of head groups will be reduced by the presence of added salt;

(ii) the separation of the dye and head group charges as the dye passes into the micelle interior will be aided by added salt.

It has been shown\* that the addition of tetra-methyl and tetra-ethyl ammonium salts produce a proportionally larger increase in  $k(\text{obs})$ . These salts also cause a larger decrease in the CMC<sup>(48)</sup>, which implies that they bind more strongly to the micelle.

The greater kinetic effect of the tetra-alkyl ammonium salts may be due to a combination of a larger reduction in surface potential and disruption of the micelle surface. The tetra-ethyl ammonium cation is more effective than the tetra-methyl ammonium cation.

The observation of a limiting rate of absorption in systems with added salt suggests that for the surfactant concentration range studied (e.g. up to 0.1M SDS) the degree of counterion binding is largely constant.

The amplitude of the fluorescence and absorption changes for the reaction decreases linearly (up to 0.1M NaCl) with the increase in added ionic strength. The static measurements show that the fluorescence and absorbance of the final solutions (i.e. absorbed dye) are unaffected by added salt. The decrease in amplitude therefore implies an enhancement of fluorescence intensity and absorbance of the dye adsorbed at the micelle surface. These observations suggest a lower dielectric constant at the micelle surface which may be due to the enhanced counterion binding<sup>(33,49)</sup>.

#### 6.3.4 Addition of Cosolvent and Potential Impurities

The addition of methanol as cosolvent (up to 2.5M) does not significantly affect the CMC of SDS<sup>(50,51)</sup> (Chapter 4, table

---

\* (W. Knoche personal communication)

There is no evidence in the literature that the addition of methanol causes changes in micelle size or aggregation number. It is, however, thought that methanol and other short-chain alcohols interact with the micelles and remain close to the surface<sup>(51)</sup>.

The results in table 6.3.4.1 show that the addition of methanol causes a large increase in the rate of absorption of  $AO^+$ . The log of the rate constant of absorption of  $AO^+$  increases linearly with added methanol up to 2.5M (figure 6.3.4.1). The effect of methanol may be two-fold. Methanol is known to increase the rate of osmotic swelling of liposomes<sup>(52)</sup>. The suggested mechanism is that the methanol causes a disordering and "opening" of the surface structure of the liposome. A similar effect may operate in this case, which will enable the dye to pass more easily into the micelle.

Alkyl sulphate micellar systems are prone to a number of impurities. These would most likely be the parent alcohol (present possibly as unreacted starting material<sup>(53)</sup> and as the result of hydrolysis<sup>(54)</sup>) and alkyl sulphate homologues. For these reasons the influence of dodecanal and sodium tetradecylsulphate on the rate of absorption of  $AO^+$  into SDS micelles were investigated. It is seen that quite substantial amounts of these species do not have a large effect on the observed rate (table 6.3.4.1 and figure 6.3.4.2). Both cause a small decrease in rate.

The addition of dodecanal would be expected to decrease the surface charge density which on its own would lead to an increase in rate, but the reduced charge density will also lead to a "tightening" of the surface structure. Addition of up to 15 dodecanal molecules per micelle results in a decrease in rate of 15%. It appears that the "tightening" effect is dominant in this case.

The addition of STS up to 10 per micelle has a less pronounced effect than the addition of dodecanal. STS is unlikely to reduce the surface

TABLE 6.3.4.1

EFFECT OF ADDITIVES ON THE RATE OF ABSORPTION OF  
ACRIDINE ORANGE INTO SDS MICELLES

Temp. 298.2K, [SDS]  $1.5 \times 10^{-2} \text{M}$

ADDITIVE	$k(\text{obs})/\text{sec}^{-1}$
-	$47.6 \pm 3.1$
1.25M $\text{CH}_3\text{OH}$	$100 \pm 7.0$
2.50M	$160 \pm 20$
0.05 $\text{C}_{12}\text{H}_{25}\text{OH}^*$	$41.6 \pm 3.0$
0.125	$37.6 \pm 3.0$
0.03 $\text{C}_{14}\text{H}_{29}\text{SO}_4^- \text{Na}^*$	$42.6 \pm 3.1$
0.082	$41.6 \pm 3.1$

\* Mole fraction of micelle concentration

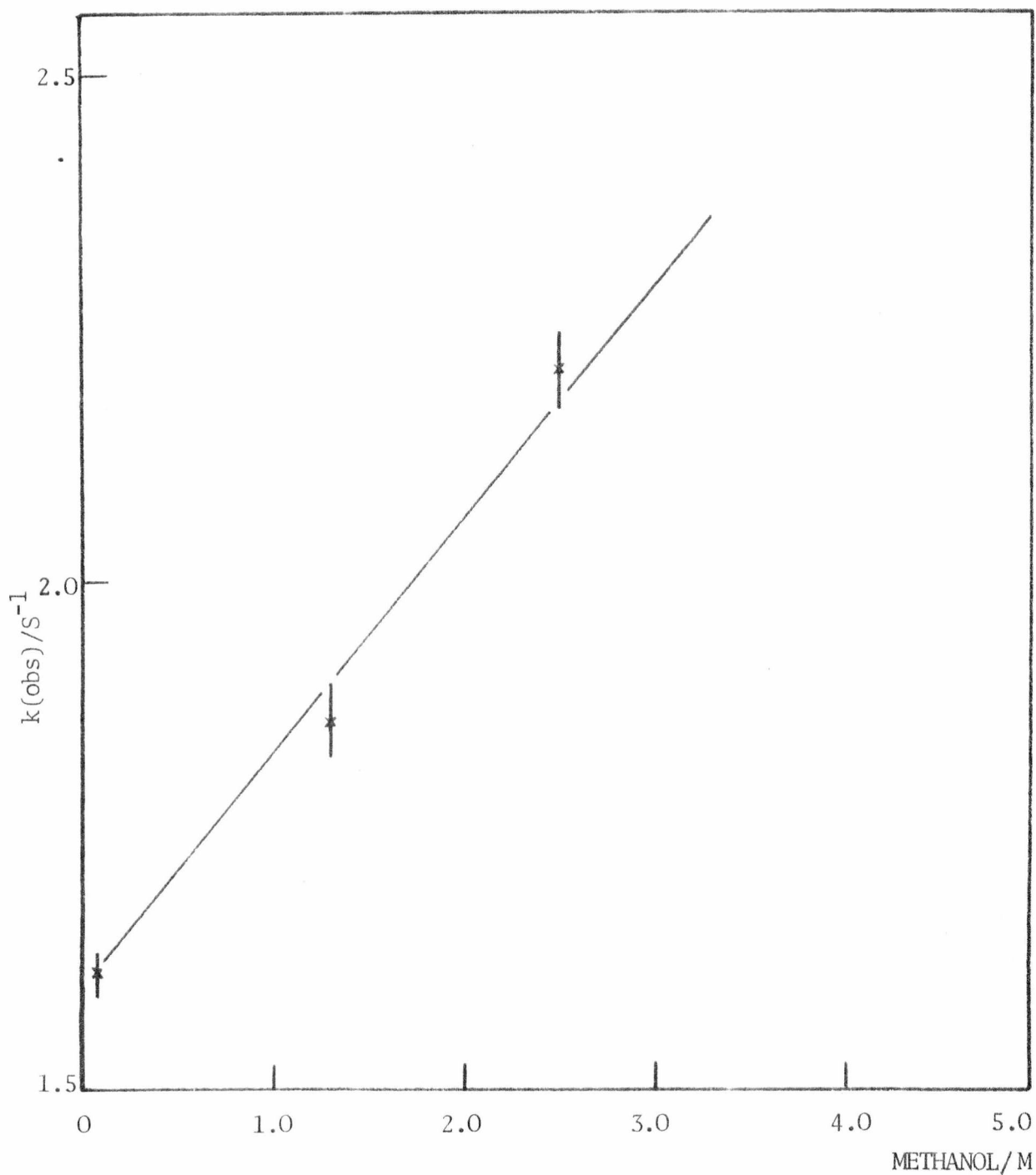


FIGURE 6.3.4.1

PLOT OF LOG  $k(\text{obs})/\text{S}^{-1}$  VS CONCENTRATION OF COSOLVENT METHANOL

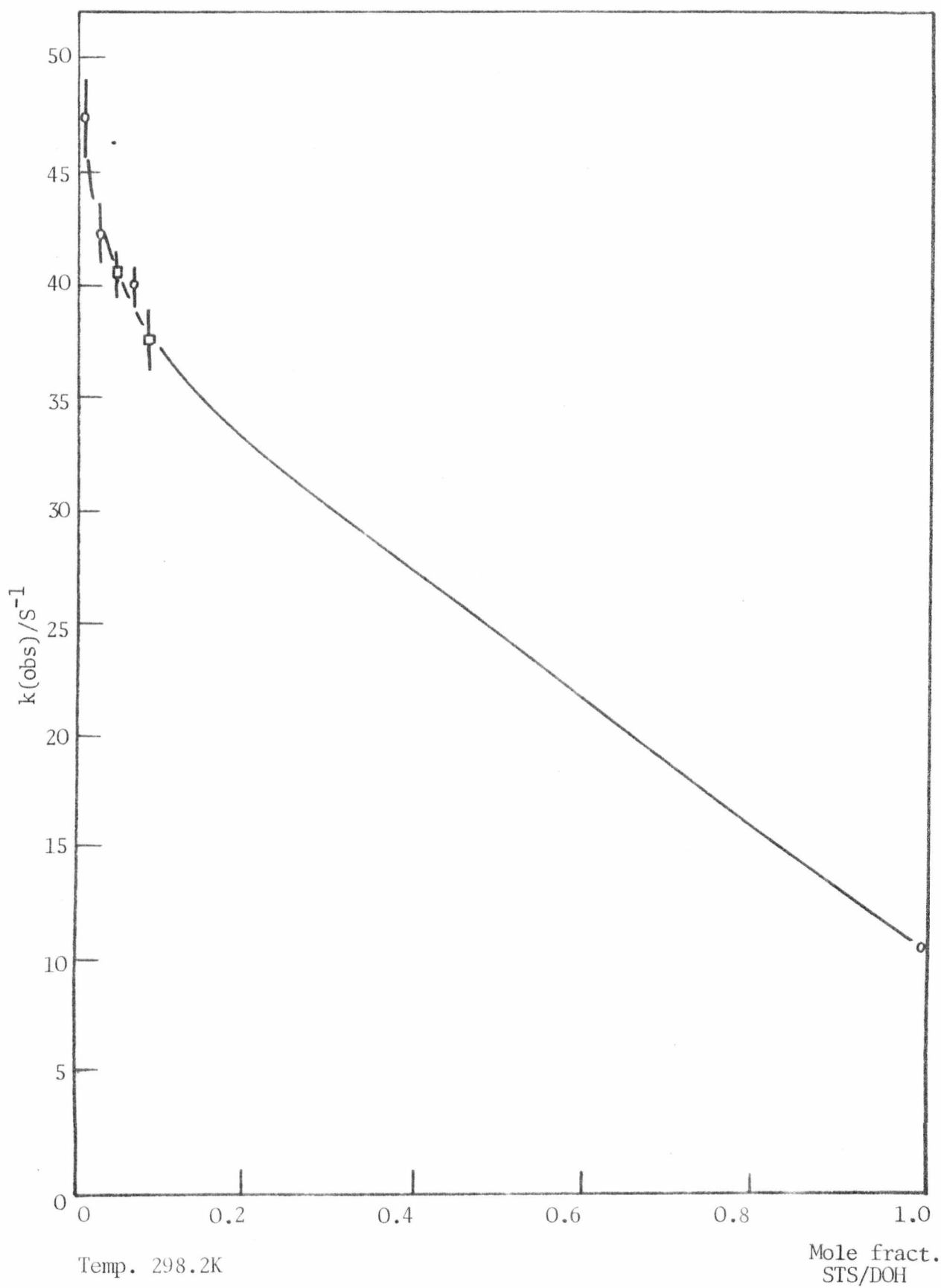


FIGURE 6.3.4.2

PLOT OF  $k(\text{obs})/\text{S}^{-1}$  VS MOLE FRACTION OF ADDITIVE

charge density of the parent SDS micelle. The extra free energy of addition of STS molecules may result in a tighter micelle structure which would account for the small decrease in observed rate.

#### 6.3.5 Variation in Surfactant Chain-Length and Head-Groups

The results in table 6.3.5.1 and figures 6.3.5.1-4 and 6.3.1.4 show that the rate of absorption of acridine dyes is strongly dependent on the hydrocarbon chain-length of the surfactant. The rate decreases with increasing chain-length. It has already been pointed out that as the chain-length of the surfactant increases, the CMC is lowered, the micelle has a larger aggregation number, is more compact at the surface and the charge-density increases<sup>(48)</sup>. (Chapter 1, table 1.3.5.1).

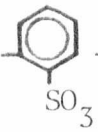
The decrease in surface area per head-group and the increase in the charge density as the surfactant chain-length increases would both be expected to decrease the rate of absorption.

It is found that there is an increasing discrepancy between the rate constants found by absorbance and fluorescence methods as the chain-length of the surfactant increases (table 6.3.5.1). It is possible that the change in the absorbance and fluorescence spectra are differently affected by the environment and the fluorescence change occurs further into the micelle than the absorbance change.

The variation in the rate of absorption of  $A0^+$  into micelles with sulphonate or benzene sulphonate head-groups are little different from the sulphate. (Table 6.3.5.1). This indicates that in these micelles the packing and surface charge density are much the same as for the sulphate micelle. The result for the benzene sulphate (equivalent to CMC to STS) suggests that the effect of the benzene group is small.

TABLE 6.3.5.1

EFFECT OF SURFACTANT CHAIN LENGTH ON THE RATE OF ABSORPTION  
 INTO SODIUM N-ALKYL SULPHATE MICELLES

DYE	n	T/K	$k(\text{obs})_A/S^{-1}$	$k(\text{obs})_F/S^{-1}$
AO <sup>+</sup>	10	298.2	180±10	185±15
	12	298.2	47.6±3	48.3±3.4
	14	298.2	11.9±1.5	9.5±1.0
	16	316.2	13.1±1.2	9.4±1.1
PF <sup>+</sup>	12	298.2	-	>500
	16	316.2	-	133±15
AF <sup>+</sup>	16	316.2	-	125±15
AO <sup>+</sup>	C <sub>12</sub> H <sub>25</sub> SO <sub>3</sub> <sup>-</sup> Na	298.2	53±5	45±3
	C <sub>12</sub> H <sub>25</sub>  -Na <sup>+</sup>	298.2	88±7	
AB <sup>2+</sup>	12	298.2	3.1±0.03	33±0.2
	14	298.2	33.3±2.5	34.1±3.6

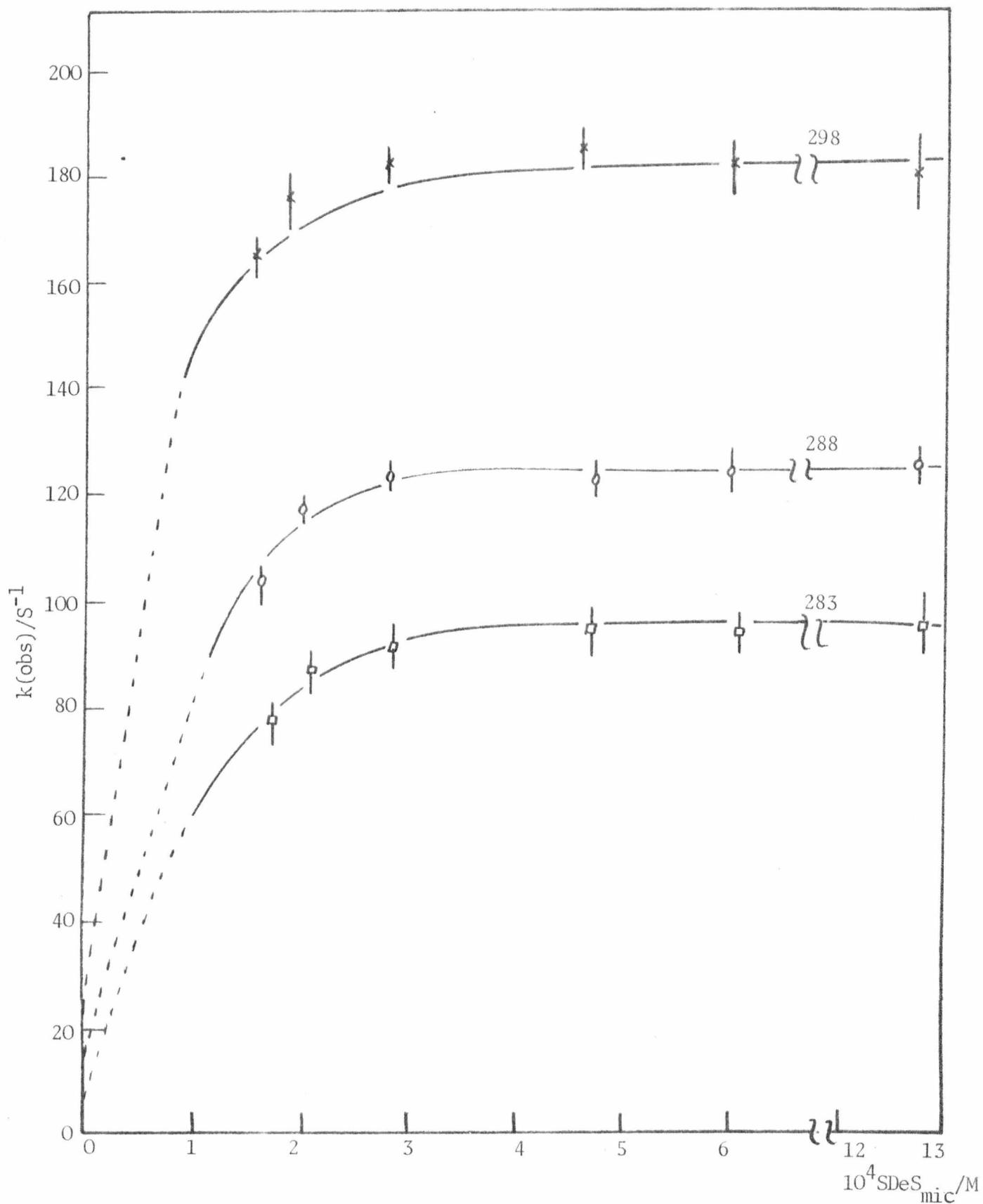
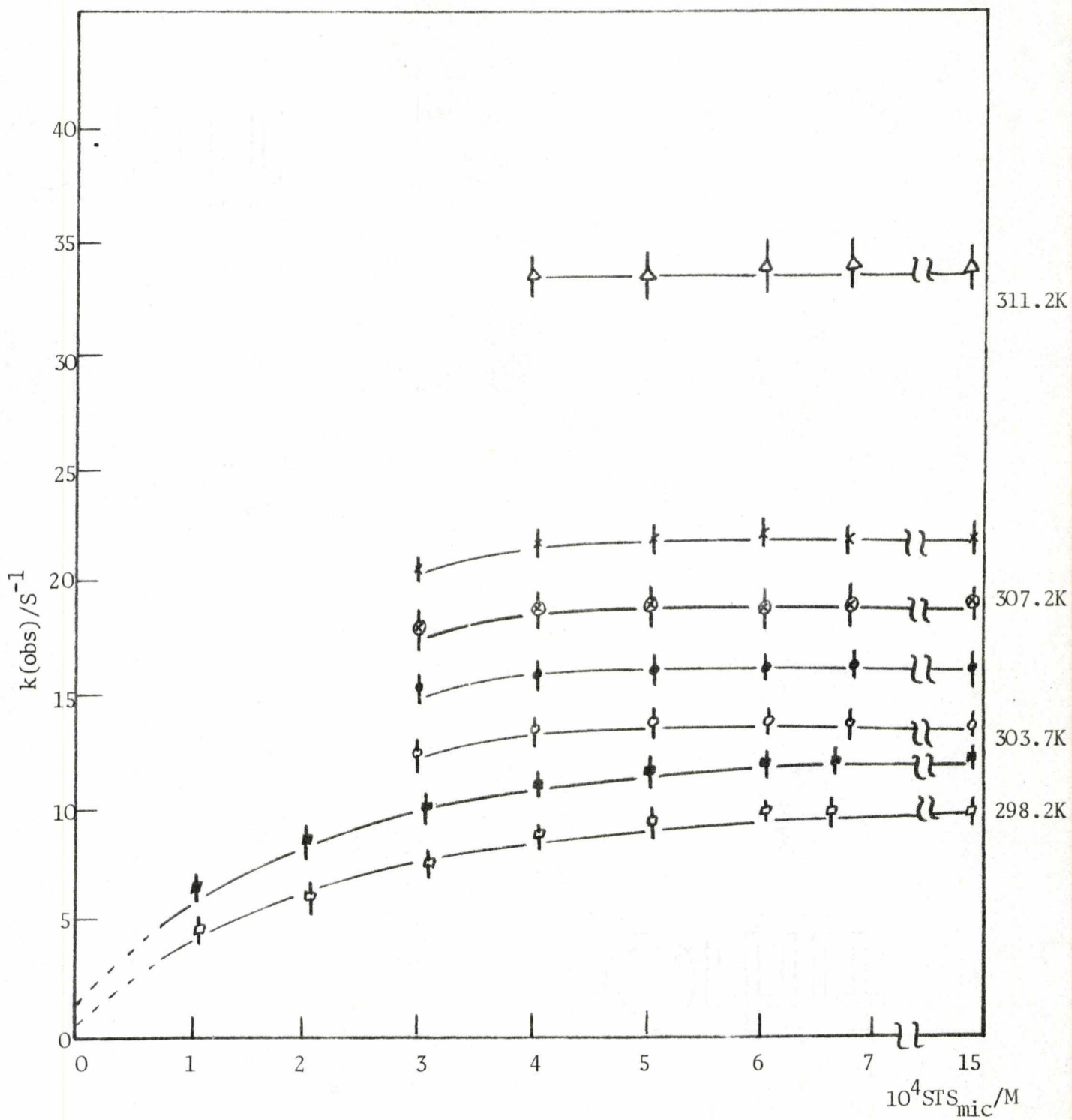


FIGURE 6.3.5.1

PLOT OF  $k(\text{obs})/\text{S}^{-1}$  VS MICELLE CONCENTRATION FOR ACRIDINE ORANGE/SDeS



Open points A  
Filled points F

FIGURE 6.3.5.2

PLOT OF  $k(\text{obs})/\text{S}^{-1}$  VS MICELLE CONCENTRATION FOR ACRIDINE ORANGE/STS

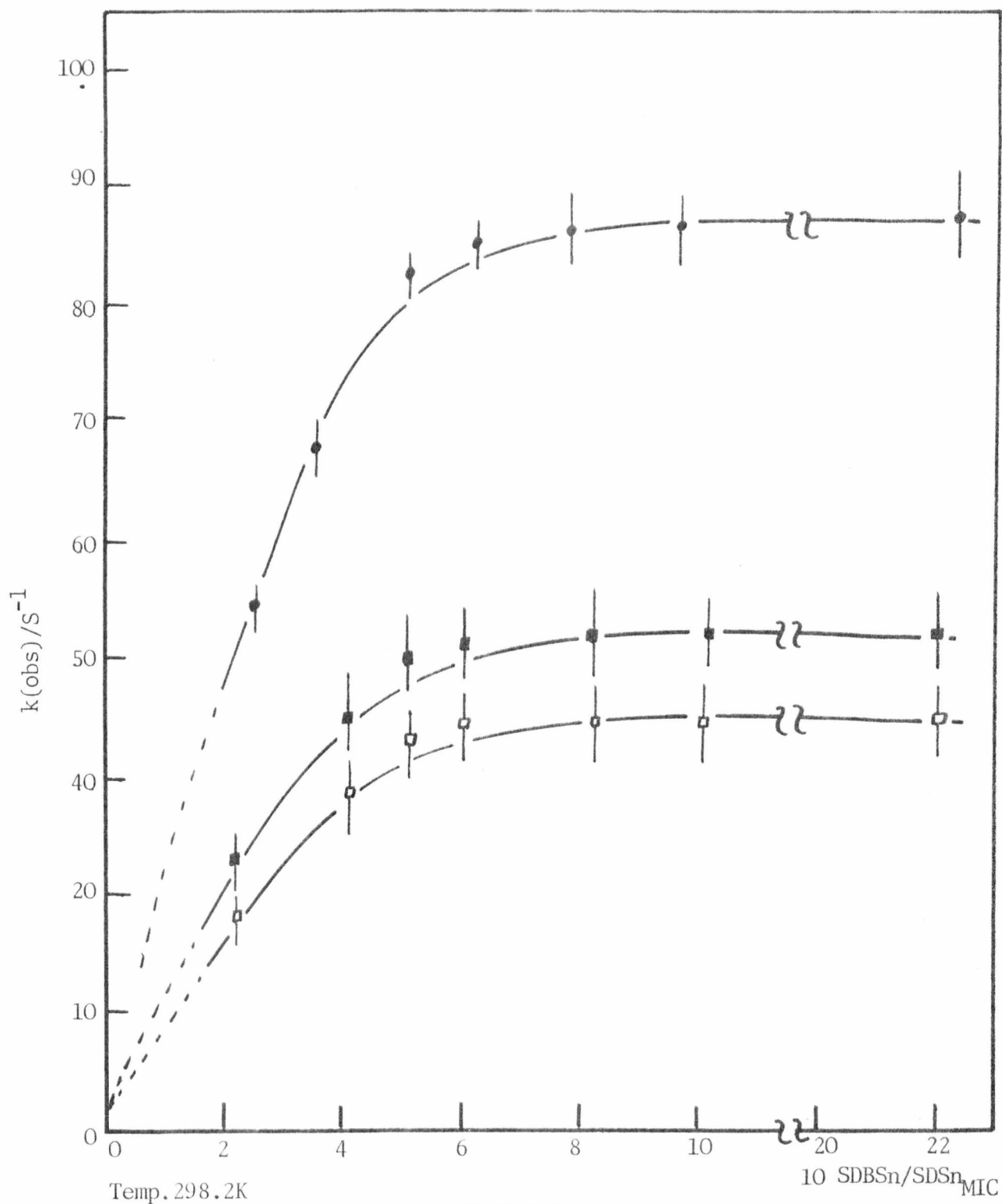


FIGURE 6.3.5.3

PLOT OF  $k(\text{obs})/\text{S}^{-1}$  VS MICELLE CONCENTRATION FOR ACRIDINE ORANGE/SDBSn/SDSn

-■- SDBSn, -○- SDSn

Open points A  
Filled points F

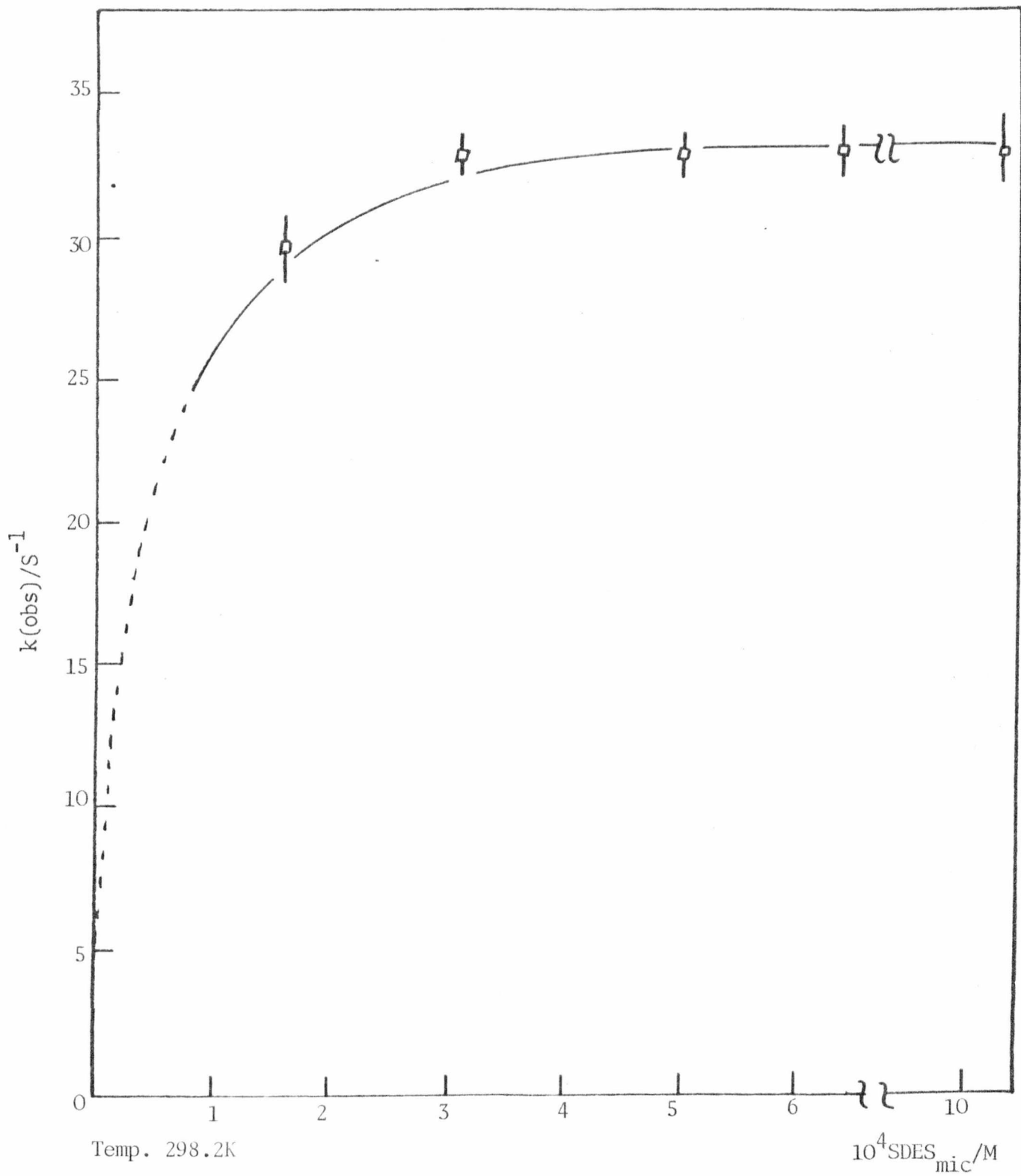


FIGURE 6.3.5.4

PLOT OF  $k(\text{obs})/\text{S}^{-1}$  VS MICELLE CONCENTRATION FOR ATEBRINE/SDeS

### 6.3.6 Discussion of the Activation Parameters

The activation parameters for a number of the absorption processes are given in tables 6.3.1.1,2 and 6.3.5.1. For the sake of convenience they are reproduced in table 6.3.6.1. The Arrhenius plots from which these values are derived are shown in figures 6.3.6.1-4.

For the dye absorption process the activation enthalpy arises from three sources:

- (i) the separation (compression) of surface head-groups to enable the dye to enter the micelle;
- (ii) the separation of dye and surfactant head-group (electrostatically bound);
- (iii) the production of a cavity in the micelle to hold the dye (i.e. the breaking of favourable hydrophobic interactions between hydrocarbon chains).

The first two are electrostatic in origin ( $\Delta H_{el}^\ddagger$ ) and the last hydrophobic ( $\Delta H_{hyd}^\ddagger$ ). The overall enthalpy is given by

$$\Delta H^\ddagger = \Delta H_{el}^\ddagger + \Delta H_{hyd}^\ddagger \quad (6.3.6.1)$$

The increase in the activation energy with increasing surfactant chain-length is consistent with an increase in:

- (i) the surface charge density of the micelle, which increases the electrostatic contribution to  $\Delta H^\ddagger$  by increasing the charge attraction between dye and micelle surface;
- (ii) the tightness of the surface structure due to the increased hydrophobic free energy of the longer chains will cause an increase in  $\Delta H_{hyd}^\ddagger$ .

The addition of salts leads to a reduction in  $\Delta H^\ddagger$ . The effect will

TABLE 6.3.6.1

## ACTIVATION PARAMETERS FOR DYE ABSORPTION PROCESSES

DYE	SURFACTANT	$\Delta G^\ddagger/\text{kJmol}^{-1}$	$\Delta H^\ddagger/\text{kJmol}^{-1}$	$\Delta S^\ddagger/\text{Jmol}^{-1}\text{K}^{-1}$
AO <sup>+</sup>	SDeS	60.5 ± 6.1	22.7 ± 4.4	-120 ± 15.6
	SDS	63.2 ± 7.7	35.7 ± 4.4	-92.2 ± 10.1
	SDS/1.25M Methanol	61.8 ± 7.1	60.5 ± 5.9	-4.4 ± 2.7
	STS	68.1 ± 6.9	50.2 ± 5.7	-60.5 ± 12.3
	SHDS	71.8 ± 7.6	60.8 ± 7.6	-31.6 ± 10.7
MB <sup>+</sup>	SDS	63.2 ± 7.5	35.9 ± 4.7	92.0 ± 10.7
PYG <sup>+</sup>	SDS	63.3 ± 7.1	36.4 ± 4.9	89.9 ± 10.9
PF <sup>+</sup>	SHDS	64.6 ± 9.3	61.2 ± 10.3	-11.1 ± 5.1
AB <sup>2+</sup>	SDS	71.9 ± 9.0	68.1 ± 8.1	-12.1 ± 2.3
	SDS/0.1 NaCl	65.9 ± 7.1	55.4 ± 7.6	-33.0 ± 6.7
AO <sup>+</sup> /SDS	SDS	~64	~74.4	~+33
AB <sup>2+</sup> /SDS	SDS	~70	~58	~+40

$\Delta G^\ddagger$  and  $\Delta S^\ddagger$  calculated for 298K.

TABLE 6.3.6.1

## ACTIVATION PARAMETERS FOR DYE ABSORPTION PROCESSES

DYE	SURFACTANT	$\Delta G^\ddagger/\text{kJmol}^{-1}$	$\Delta H^\ddagger/\text{kJmol}^{-1}$	$\Delta S^\ddagger/\text{Jmol}^{-1}\text{K}^{-1}$
AO <sup>+</sup>	SDeS	60.5 ± 6.1	22.7 ± 4.4	-120 ± 15.6
	SDS	63.2 ± 7.7	35.7 ± 4.4	-92.2 ± 10.1
	SDS/1.25M Methanol	61.8 ± 7.1	60.5 ± 5.9	-4.4 ± 2.7
	STS	68.1 ± 6.9	50.2 ± 5.7	-60.5 ± 12.3
	SHDS	71.8 ± 7.6	60.8 ± 7.6	-31.6 ± 10.7
MB <sup>+</sup>	SDS	63.2 ± 7.5	35.9 ± 4.7	92.0 ± 10.7
PYG <sup>+</sup>	SDS	63.3 ± 7.1	36.4 ± 4.9	89.9 ± 10.9
PF <sup>+</sup>	SHDS	64.6 ± 9.3	61.2 ± 10.3	-11.1 ± 5.1
AB <sup>2+</sup>	SDS	71.9 ± 9.0	68.1 ± 8.1	-12.1 ± 2.3
	SDS/0.1 NaCl	65.9 ± 7.1	55.4 ± 7.6	-33.0 ± 6.7
AO <sup>+</sup> /SDS	SDS	~64	~74.4	~+33
AB <sup>2+</sup> /SDS	SDS	~70	~58	~+40

$\Delta G^\ddagger$  and  $\Delta S^\ddagger$  calculated for 298K.

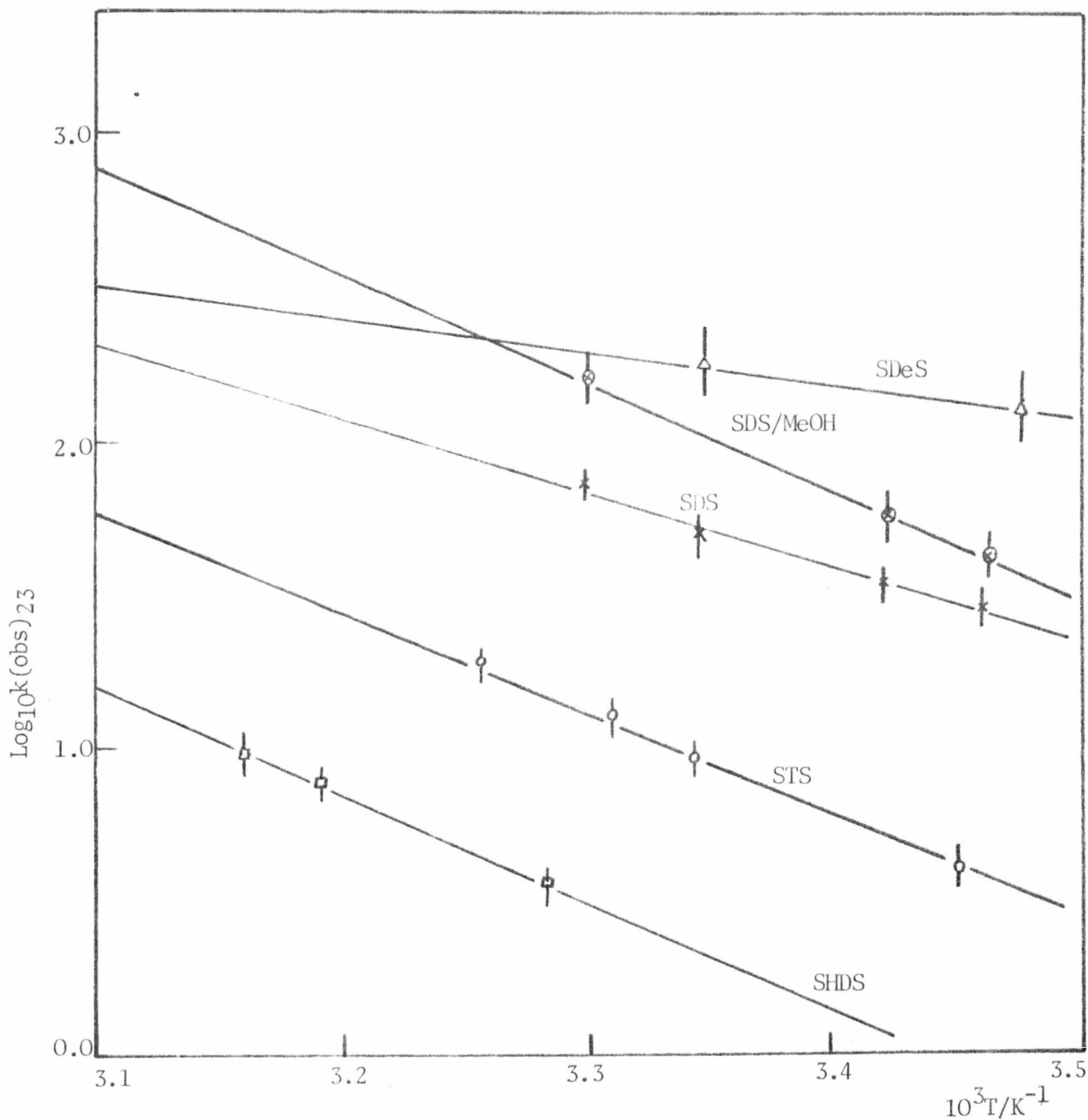


FIGURE 6.3.6.1

ARRHENIUS PLOTS FOR ABSORPTION OF ACRIDINE ORANGE BY MICELLES

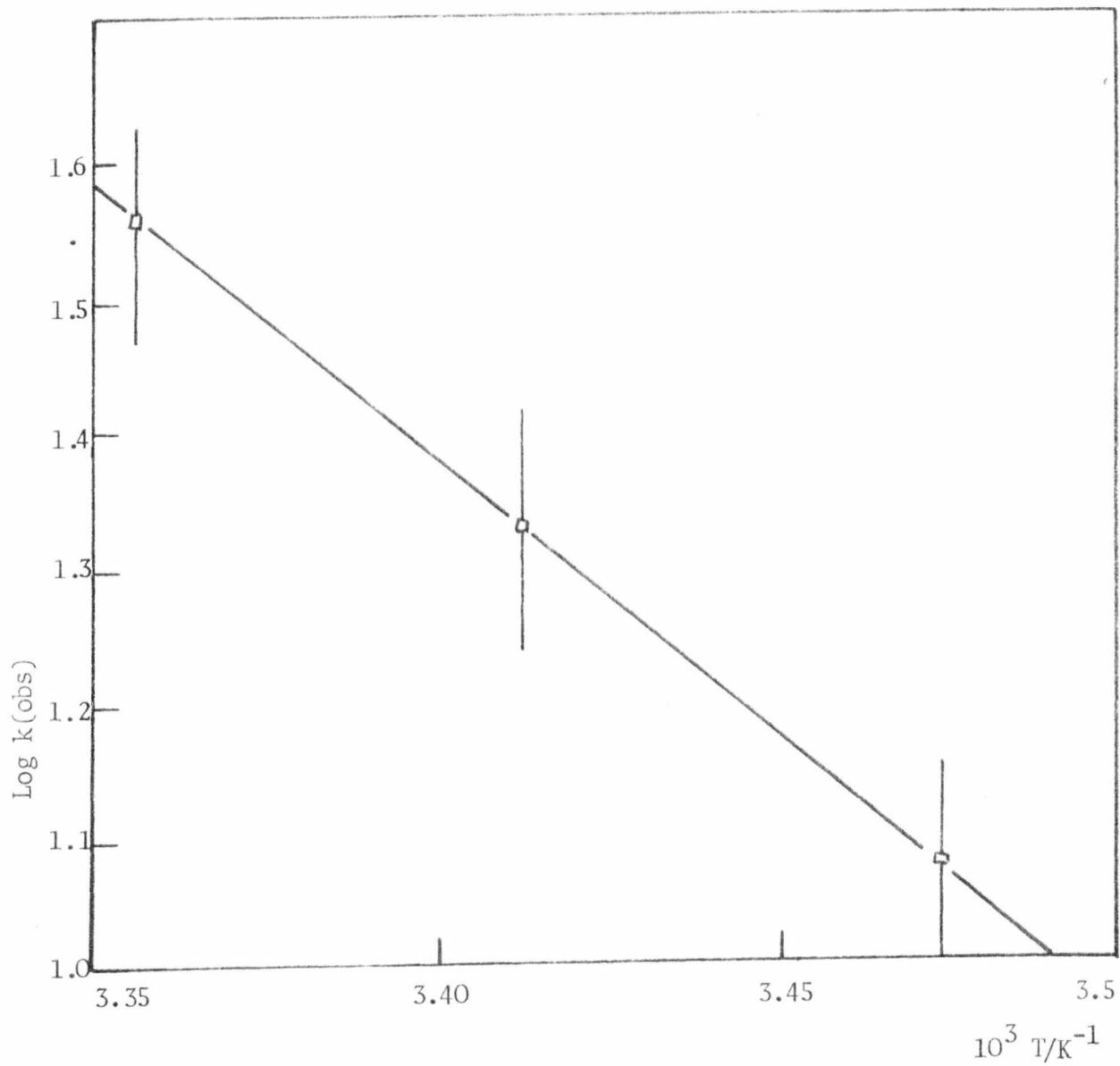


FIGURE 6.3.6.2

ARRHENIUS PLOT FOR ABSORPTION OF DYE SURFACTANT AGGREGATE  $\text{AO}^+/\text{SDS}$

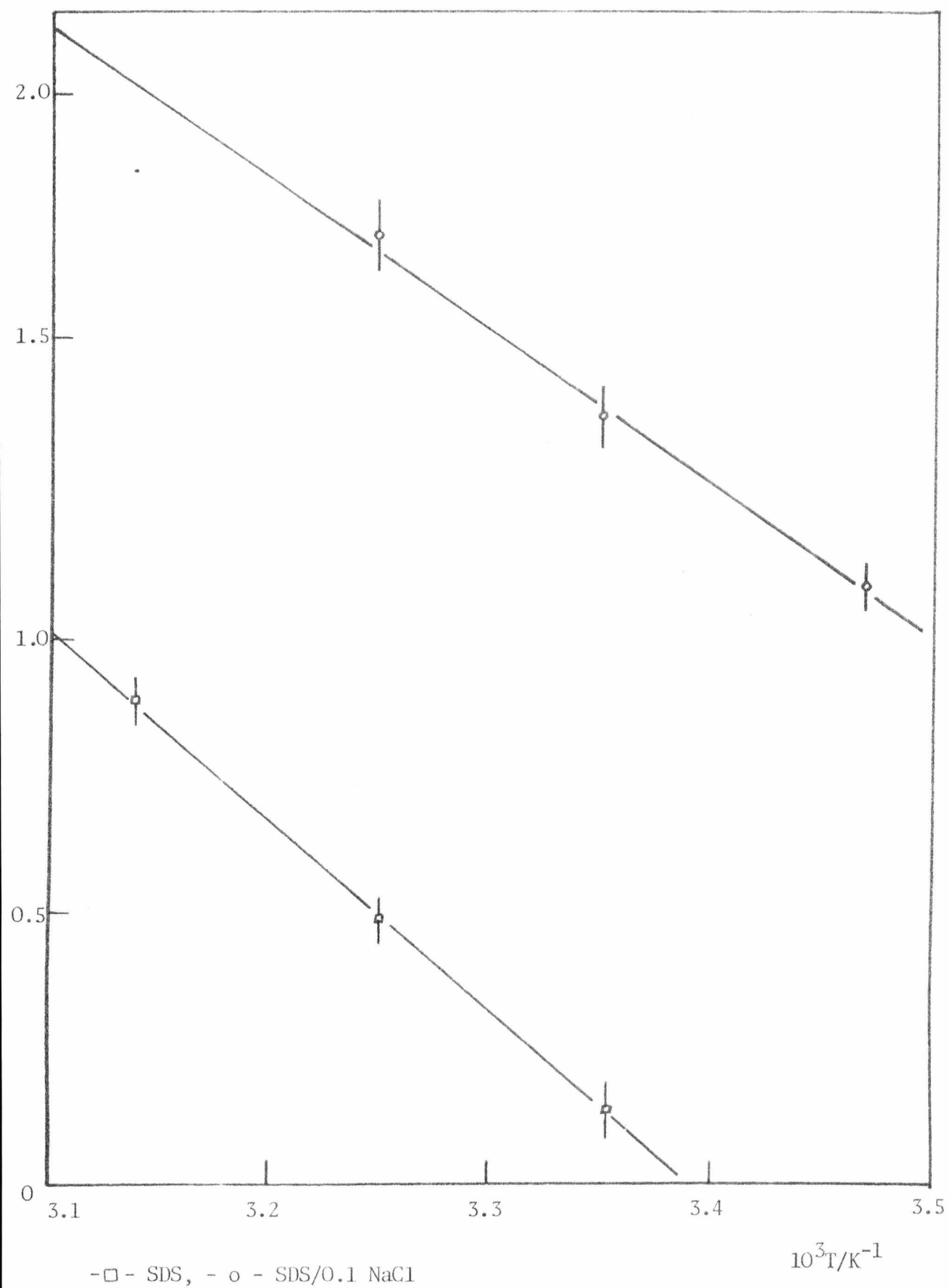


FIGURE 6.3.6.3

ARRHENIUS PLOTS FOR THE ABSORPTION OF  $xAB^{2+}$  BY SDS MICELLES

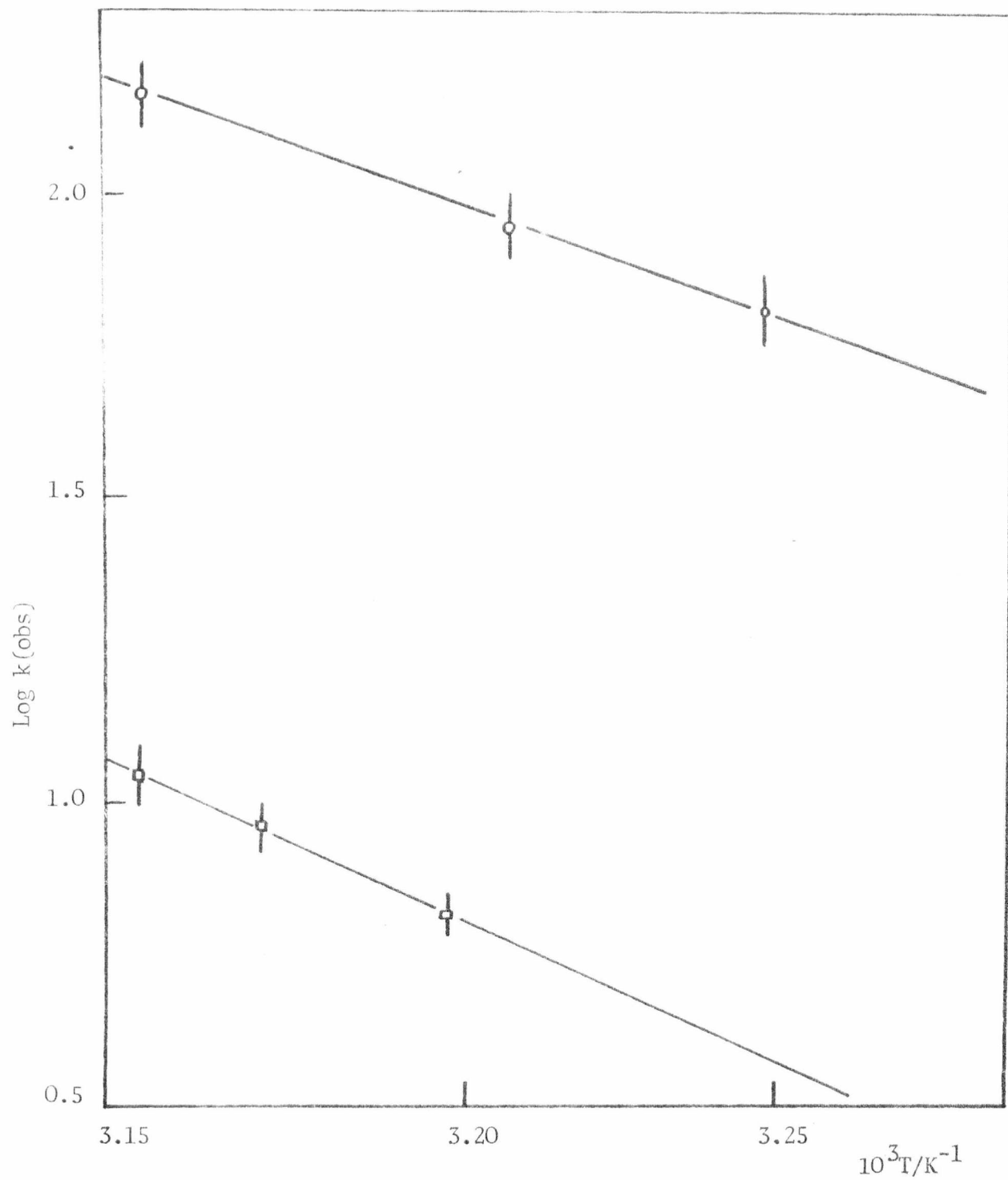


FIGURE 6.3.6.4

ARRHENIUS PLOT FOR ABSORPTION OF  $\text{Ac}^+$  - □ -,  $\text{PF}^+$  - ○ - BY SDS

operate primarily by a reduction in the charge attraction between dye and micelle surface. The increased salt concentration will also aid the separation (compression) of micelle head-groups necessary to form the cavity for the dye to enter.

For the dye acridine orange and a series of sodium-n-alkyl sulphates (without added salt) a plot of  $\Delta H^\ddagger$  against surfactant chain-length is linear. The slope is  $6.2 \text{kJmol}^{-1}$  per  $\text{CH}_2$  group (figure 6.3.6.5).

The difference in  $\Delta H^\ddagger$  between the dyes  $\text{AO}^+$  and  $\text{PF}^+$  for the absorption into SHDS micelles is small ( $\approx <10\%$ ). This indicates that the charge effects are approximately equivalent for unipositive dyes. The difference in the rates ( $\text{PF}^+$  factor of  $\sim 13$  faster than  $\text{AO}^+$ ) arises from a more favourable change in the entropy of activation for proflavine:

$$\Delta\Delta S_{\text{AO}^+/\text{PF}^+}^\ddagger = \Delta S_{\text{AO}^+}^\ddagger - \Delta S_{\text{PF}^+}^\ddagger = -21.5 \text{Jmol}^{-1} \text{K}^{-1} .$$

If the entropy of activation is governed primarily by desolvation and restriction of the dye motion, this figure should be constant for all the surfactants.

Provided the value of  $\Delta\Delta S_{\text{AO}^+/\text{PF}^+}^\ddagger$  is constant for various surfactant chain-lengths we may use equations (6.3.6.2,3) to calculate  $k(\text{obs})_{\text{PF}^+}^{\text{SDS}}$

$$\Delta G^\ddagger = \Delta H^\ddagger - T\Delta S^\ddagger \quad (6.3.6.2)$$

$$\Delta G^\ddagger = RT \ln(k(\text{obs})_{\text{PF}^+}^{\text{SDS}} h/kT) \quad (6.3.6.3)$$

where  $h$  = Planck's constant

$k$  = Boltzmann's constant

Using  $\Delta H_{\text{AO}^+/\text{SDS}}^\ddagger$  reduced by 10% as the value for  $\Delta H_{\text{PF}^+/\text{SDS}}^\ddagger$  we have

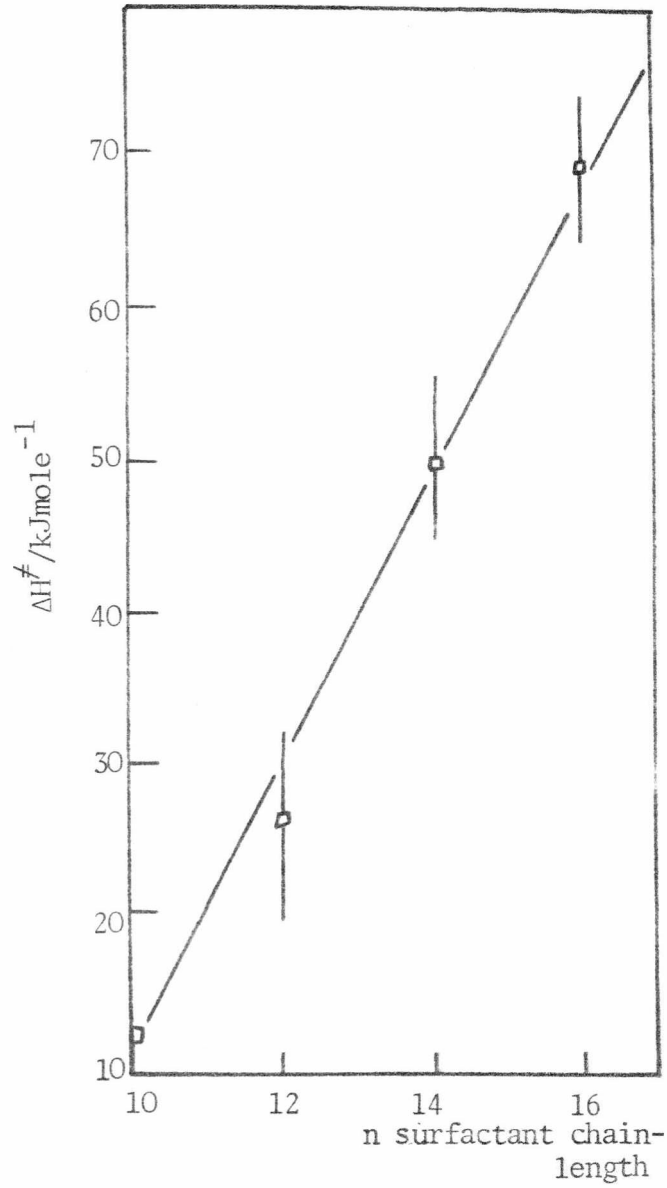


FIGURE 6.3.6.5 : PLOT OF  $\Delta H^\ddagger$  VS N FOR ABSORPTION OF  $\text{AO}^+$  BY MICELLES

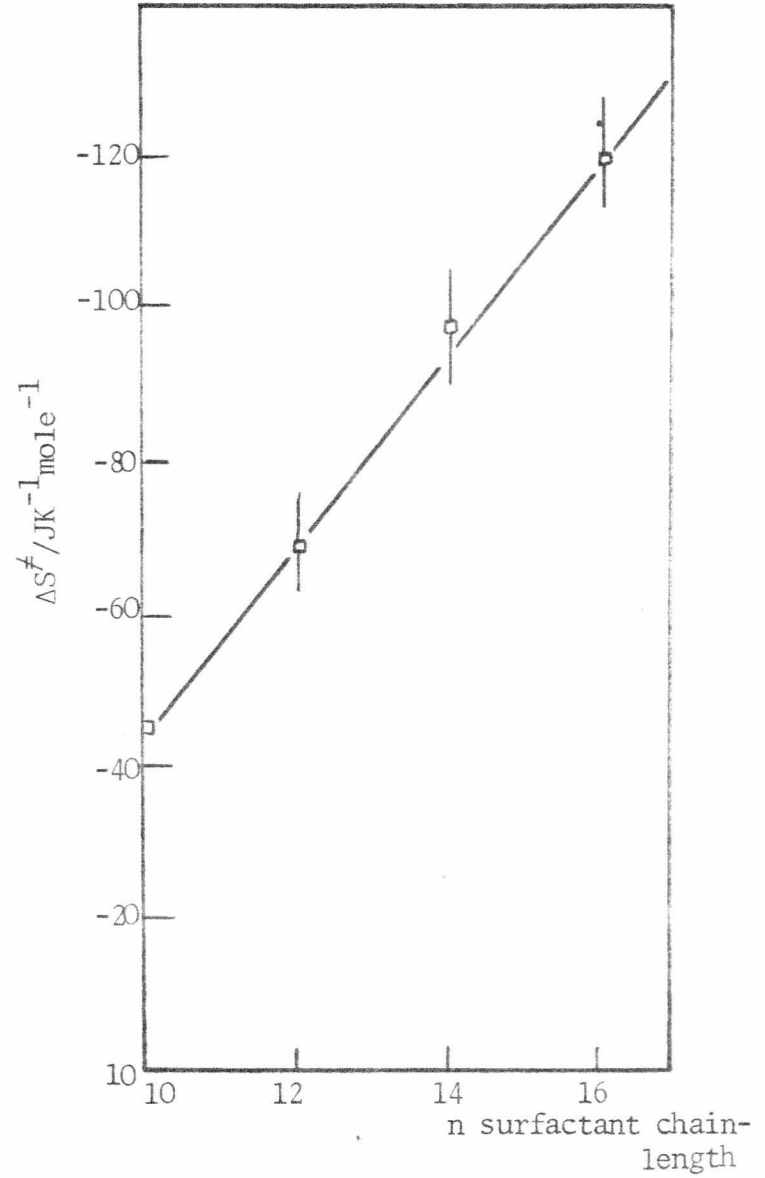


FIGURE 6.3.6.6 : PLOT OF  $\Delta S^\ddagger$  VS N FOR ABSORPTION OF  $\text{AO}^+$  BY MICELLES

$$\begin{aligned}\Delta G_{\text{PF}^+/\text{SDS}}^\ddagger &= 32.1 \pm 4 - (298(-70.7 \pm 8)) \\ &= 32.1 \pm 4 + 21 \pm 2 \\ &= 53.1 \pm 6\end{aligned}$$

At 298K

$$53.1 \pm 6 = 2.3 RT \log(k(\text{obs})_{\text{PF}^+}^{\text{SDS}} \cdot 1.6 \times 10^{-13})$$

$$k(\text{obs})_{\text{PF}^+}^{\text{SDS}} = 3.3 \times 10^3 \text{ sec}^{-1}$$

which is too fast to measure by the stopped-flow method.

This value of  $k(\text{obs})_{\text{PF}^+}^{\text{SDS}}$  is much greater than that calculated from the ratio of  $k(\text{obs})_{\text{PF}^+/\text{AO}^+}^{\text{SHDS}}$  which yields a value of  $\approx 700 \text{ sec}^{-1}$ . Thus the large difference between  $\text{AO}^+$  and  $\text{PF}^+$  is not a simple function of solvation. In order to reduce the  $k(\text{obs})_{\text{PF}^+}^{\text{SDS}}$  value calculated from  $\Delta S_{\text{AO}^+/\text{PF}^+}^\ddagger$  to that for the ratio of  $k(\text{obs})_{\text{PF}^+/\text{AO}^+}^{\text{SHDS}}$   $\Delta \Delta S_{\text{AO}^+/\text{PF}^+}^\ddagger$  would have to be decreased to  $-8 \text{ J mol}^{-1} \text{ K}^{-1}$ .

For acridine orange a plot of  $\Delta S^\ddagger$  versus surfactant chain-length is linear. The slope is  $-15 \text{ JK}^{-1} \text{ mol}^{-1}$  per  $\text{CH}_2$  (figure 6.3.6.6).

The origin of the large  $\Delta S^\ddagger$  values is difficult to ascertain. Undoubtedly in such a complex system a large number of factors may be operative.

The difference in  $\Delta S^\ddagger$  for  $\text{AO}^+$  and  $\text{PF}^+$  may be the result of the lower degree of solvation of the  $\text{PF}^+$  molecule compared with  $\text{AO}^+$ . This would result in a smaller number of water molecules being released into bulk solution as the dye enters the micelle. There may also be some specific steric requirements (due to the difference in size of the dyes) which will affect the loss of rotational and translational entropy of the dye and adjacent surfactant molecules in the micelle.

The increase in  $\Delta S_{AO^+}^\ddagger$  with chain-length is more difficult to explain. There could be a systematic variation in the amount of water released by the micelle as the dye binds. The shorter-chain micelles are certainly more open structures at the surface and may contain much more water than the longer-chain micelles. On entering the micelle some water must be released from the longer-chain micelles which cannot accommodate both dye and water. The shorter-chain micelles, however, may be capable of absorbing the dye and retaining the water because of their loose structure.

A further possible explanation of the difference in  $\Delta S^\ddagger$  with chain-length is that when the dye binds it may bring about considerable ordering of the local micelle structure and a consequent large decrease in the entropy. The degree of order induced by the dye is likely to decrease with chain-length since the longer chain micelles are already compact and will be much more difficult to order. The loose shorter-chain micelles are potentially more easily ordered by the presence of the dye.

It can be seen from table 6.3.1.1 that the activation enthalpy for the divalent dye  $AB^{2+}$  is approximately twice that for  $AO^+$ . This must reflect the greater charge attraction of the  $AB^{2+}$ . The entropy for  $AB^{2+}$  is  $-12 \text{ Jmol}^{-1} \text{ K}^{-1}$  this is a difference of  $+80 \text{ Jmol}^{-1} \text{ K}^{-1}$  from the value for  $AO^+$ . A possible origin of this large difference may be the loss of more solvation water from the chain of the  $AB^{2+}$  molecule.

The differences in enthalpy and entropy for  $AO^+$  and  $AO^+$  surfactant aggregate is shown in tables 6.3.1.1 and 2. The enthalpy is doubled in the case of the surfactant aggregate. This may reflect that breakdown of the aggregate is necessary before absorption can take place. The large difference in  $\Delta S^\ddagger$  ( $+120 \text{ Jmol}^{-1} \text{ K}^{-1}$ ) can be attributed to the loss of structured water from a dye surfactant monomer (which would form rapidly after its clearance from the parent aggregate). The changes are similar

for the  $AB^{2+}$  surfactant aggregate.

Hence,  $\Delta S_{AO}^\ddagger$  is made up of the following contributions

$$\Delta S^\ddagger = \Delta S_r^\ddagger + \Delta S_t^\ddagger + \Delta S_{HG}^\ddagger - \Delta S_{DH_2O}^\ddagger - \Delta S_{MH_2O}^\ddagger \quad (6.3.6.4)$$

where  $\Delta S^\ddagger$  ... is the observed entropy (-ve);  
 $\Delta S_r^\ddagger, \Delta S_t^\ddagger$  ... are the charges (-ve) in rotational and translational entropy of the dye respectively;  
 $\Delta S_{HG}^\ddagger$  ... is the charge (-ve) in the ordering of the head-groups on binding of a dye molecule;  
 $\Delta S_{DH_2O}^\ddagger, \Delta S_{MH_2O}^\ddagger$  ... are the release (+ve) of water from the dye and micelle on dye binding in the transition state.

### 6.3.7 Proposed Mechanism of Dye Absorption

The experimental evidence may be summarised as follows:

- (1) the rate of absorption of positively-charged planar acridine type dyes into negatively-charged micelles is a relatively slow process;
- (2) the rate is dependent on the geometry of the dye;
- (3) the rate is strongly dependent on the charge of the dye;
- (4) the rate is dependent on the charge density on the micelle surface;
- (5) the rate decreases as the surfactant chain-length increases;
- (6) the rate is only affected to a small extent by potential surfactant impurities;
- (7) addition of methanol increases the rate of absorption of the dye;
- (8) the rate of absorption reaches a limiting value and is independent of surfactant and dye concentration;
- (9) the mechanism must be consistent with the observed activation

parameters as discussed in section 6.3.6.

Any mechanism for the process of dye absorption by micelles must explain and be consistent with all the experimental results.

The interaction mechanism between dye and micelle cannot be represented by a simple electrostatic attraction between absorbed dye and the micelle surface. Such an interaction would show no pronounced dependence on surfactant chain-length or dye geometry. Also, the uncharged dye should react more slowly than the charged dye or not at all, which is in direct contradiction to the observed results. A simple electrostatic binding process would be expected to be very rapid ( $\mu\text{sec}$ ) and beyond the limits of the stopped-flow instrument.

An alternative mechanism is that the presence of the dye (following mixing with micellar solution) induces micelle formation around itself by progressive addition of surfactant. It has been suggested that the rate determining step could be the breakdown of the micelle to provide monomers for the build-up process.

This mechanism seems unlikely for several reasons:

(i) the surfactant would be expected to bind head-group first which would produce a high charge density and the structure would be energetically unfavourable;

(ii) allowing the alkyl chains to interact with the dye, the rate of micelle formation would be expected to parallel the stacking tendency of the dyes as measured by  $K_D$ , and this is not observed experimentally;

(iii) the rate of absorption is not expected to be dependent on the geometry of the dye;

(iv) an acridine orange molecule tagged with a  $C_{12}$  alkyl chain in the N(10) position is absorbed much more slowly than acridine orange

alone<sup>(45)</sup>. On the build-up mechanism it is expected that the tagged dye would react more rapidly than the dye alone;

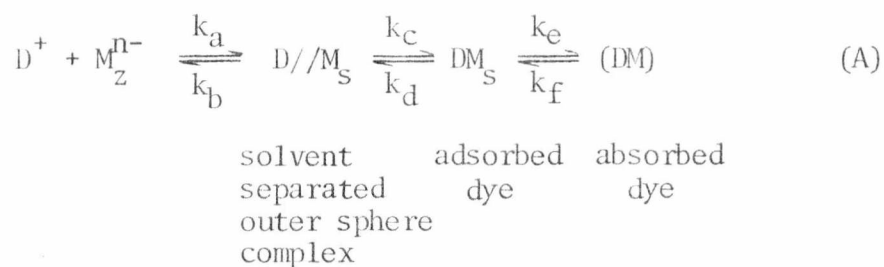
- (v) in general, when the process can occur (i.e. when the hydrophobic region of the dye is substantial enough to overcome the electrostatic repulsion) absorption of dyes with the same charge as the micelle is much more rapid than that of dyes with the opposite charge<sup>(45)</sup>;

(vi) the addition of ionic strength would be expected to decrease the rate of absorption if a build-up mechanism is operating. This again is in contradiction with the observed results.

It would appear that the absorbed dye is in a very stable environment when the dye is of opposite charge to the micelle. This is suggested by experiments in which absorbed dye is diluted with water in the stopped-flow apparatus. The dye is released very slowly in a complex process in the time range 1-10s.

Both the spectroscopic and kinetic evidence supports the hypothesis that the acridine type dyes are absorbed into a low polarity environment in the micelle, rather than simply electrostatically adsorbed at the micelle surface.

The following reaction scheme (A) is proposed as the dominant mechanism for the absorption at concentrations of surfactant much greater than the CMC i.e. >1.5 CMC.



where  $D^+$  is the dye

$M_z^{n-}$  is the micelle.

Since there is no restriction of a single-dye binding site on each micelle, we can define the concentration of binding sites on the micelle surface,  $M_S$ , as

$$M_S = \alpha(C_A^O - \text{CMC}) \quad (6.3.7.1)$$

where  $C_A^O$  = total concentration of surfactant  
 $\alpha$  = fraction of micelle surface charge not neutralised by counterion.

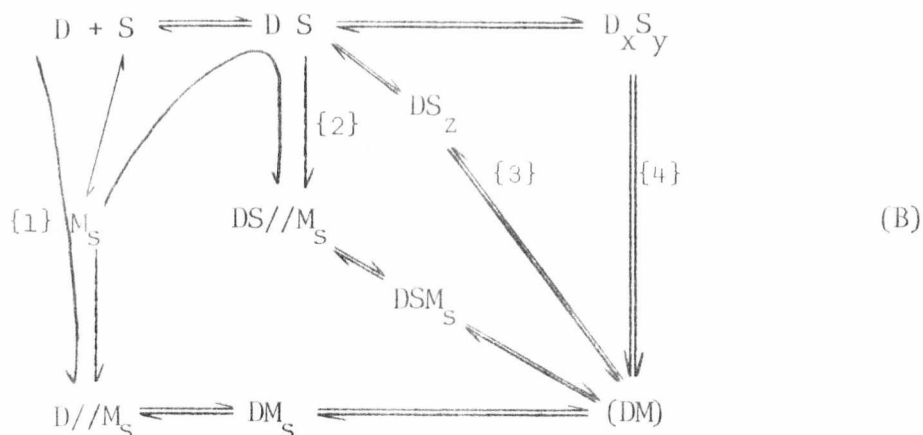
$$\begin{aligned} \text{Typically, } M_S &= 0.25(1 \times 10^{-2} - 0.7 \times 10^{-2}) \\ &= 0.25(0.3 \times 10^{-2}) \\ &= 7.5 \times 10^{-4} \end{aligned}$$

which is 75 times the concentration of the dye.

This pseudo first-order condition greatly simplifies the kinetic analysis and eliminates the possible complication of dye stacking on the micelle surface.

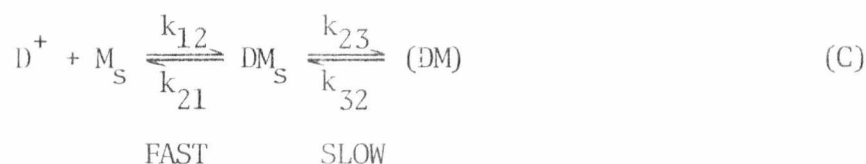
In scheme (A), the spectrally distinct species are D, (DM) and possibly  $DM_S$ . It is expected that the spectrum of  $DM_S$  will closely resemble D, except possibly, at high ionic strength.

The mechanism for low  $M_S/D$  values  $<10$  i.e. very close to the CMC, is likely to be much more complex and other interaction modes must be considered. These are proposed in scheme (B):



Route {1} is scheme (A), route {2} goes via a dye-surfactant species similar to that proposed by Yasunaga et al.<sup>(23)</sup>. The formation of the species  $D_2S_x$  ( $x=1 \dots n$ ) is rapid ( $<1\text{msec}$  at concentrations approaching the CMC) and the absorbance and fluorescence of any species containing  $D_2$  is very different (much smaller) than dye alone. This route may be eliminated because the observed amplitude is not consistent with interactions which involve  $D_2$  species. The dye-induced micelle mechanism is {3} and route {4} shows the absorption of a large dye-surfactant aggregate.

We will consider scheme (A). The formation of the adsorbed species,  $DM_s$ , is likely to be very rapid (close to diffusion-controlled). Hence, mechanism A may be simplified to give scheme (C):



The rate-determining step in the absorption will be the intra-molecular conversion of  $DM_s$  to  $(DM)$ . In general, for a small concentration-jump perturbation, two decoupled relaxation processes should be observed<sup>(55)</sup>.

For the fast adsorption step:-

$$\tau_I^{-1} = k(\text{obs})_I = k_{12}(\bar{D} + \bar{M}_S) + k_{21} \quad (6.3.7.2)$$

where  $\bar{D}$  and  $\bar{M}_S$  are the equilibrium concentrations of dye and micelle sites respectively.

If  $k_{12}$  is close to diffusion-controlled,  $\tau_I^{-1}$  is expected to be  $\sim 1\mu\text{sec.}$ , since  $K_{12} = k_{12}/k_{21} \approx 10^3 \text{M}^{-1}$  (31). The process will, therefore, be outside the time-range of the stopped-flow method, and will not be observed. Also, if  $D$  and  $DM_S$  are not spectrally distinct species then the fast adsorption process will have zero amplitude and will be unobservable by any spectrophotometric method.

The slow relaxation process is however detectable by the spectrophotometric stopped-flow method and is given by

$$\tau_{II}^{-1} = k(\text{obs})_{II} = \frac{K_{12}k_{23}[\bar{D} + \bar{M}_S] + k_{32}}{1 + K_{12}[\bar{D} + \bar{M}_S]} \quad (6.3.7.3)$$

For the general experimental conditions where  $[\bar{M}_S] \gg [\bar{D}]$  equation (6.3.7.3) becomes

$$\tau_{II}^{-1} = k(\text{obs})_{II} = \frac{K_{12}k_{23}[\bar{M}_S] + k_{32}}{1 + K_{12}[\bar{M}_S]} \quad (6.3.7.4)$$

also, if  $[\bar{M}_S] \geq 1/K_{12} \geq 10^{-3} \text{M}$  i.e. at high micelle concentration

$$\tau_{II}^{-1} = k_{23} + k_{32} \quad (6.3.7.5)$$

However, when  $K_{12}[\bar{M}_S] < 1$  i.e. close to the CMC equation (6.3.7.4) becomes

$$\tau_{II}^{-1} = K_{12}k_{23}[\bar{M}_S] + k_{32} \quad (6.3.7.6)$$

The experimentally observed variation in  $k(\text{obs})_{\text{II}}$  initially fulfill the requirements of equations (6.3.7.3) and (6.3.7.6), but at high concentration the concentration-independent equation (6.3.7.5) is obeyed. (Since only one rate constant is observed  $k(\text{obs})_{\text{II}}$  will be known as  $k(\text{obs})$ ).

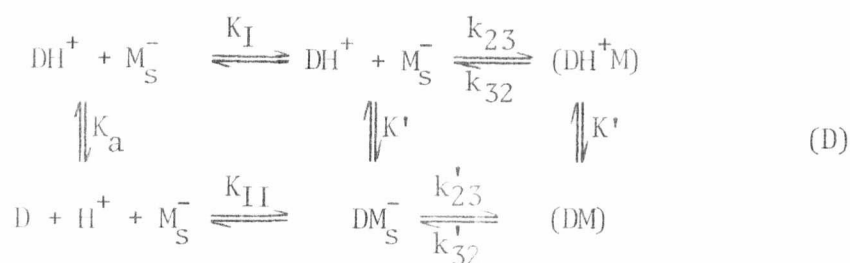
The very abrupt change in the absorbance and fluorescence spectra observed on going through the CMC suggests that  $k_{23} \gg k_{32}$ . Hence, the limiting values of  $k(\text{obs})$  in table 6.3.1.1 and 6.3.5.1 may be taken to be  $k_{23}$ . Additional evidence in support of this is that:-

(i)  $k(\text{obs})$  does not correlate with the dimerisation constant of the dye, and  $k_{32}$ , which measures the "residence time" of the dye in the micelle might be expected to correlate with  $K_{\text{D}}$ .

(ii) Dye-micelle dissolution kinetics (Chapter 5) suggest that  $k_{32}$  will be slow due to favourable coulombic interaction between dye and micelle.

(iii)  $k_{32}$  may be calculated from equation (6.3.7.6) when  $K_{\text{I}}|\bar{M}_{\text{S}}| \approx 0.1$ ,  $k_{32}$  is estimated to be  $1-5 \text{ sec}^{-1}$ .

The overall mechanism for the deprotonated/protonated dye is shown in scheme (D) <sup>(32)</sup>



Assuming the adsorption step is favourable in both cases i.e.  $K_{\text{I}}, K_{\text{II}} \gg 1\text{M}^{-1}$  and the back reactions  $k'_{32}, k_{32} \ll k_{23}, k'_{23}$ , we can write the rate equation

$$-\frac{d[\text{DH}^+ \text{M}_S] + [\text{DM}_S]}{dt} = k_{23}[\text{DH}^+ \text{M}_S] + k'_{23}[\text{DM}_S] \quad (6.3.7.7)$$

Now  $K' = \frac{[\text{DM}_S][\text{H}^+]}{[\text{DH}^+ \text{M}_S]}$  (6.3.7.8)

$$-\frac{d[\text{DH}^+ \text{M}_S] + K'[\text{DH}^+ \text{M}_S]/[\text{H}^+]}{-dt} = k_{23} + k_{23} \frac{K'}{[\text{H}^+]} [\text{DH}^+ \text{M}_S] \quad (6.3.7.9)$$

therefore,  $\frac{-d[\text{DH}^+ \text{M}_S]}{dt} = \frac{k_{23} + k_{23} \frac{K'}{[\text{H}^+]}}{1 + K'[\text{H}^+]}$   $[\text{DH}^+ \text{M}_S]$  (6.3.7.10)

and  $k(\text{obs}) = \frac{(k_{23} + k_{23} \frac{K'}{[\text{H}^+]})}{1 + K'[\text{H}^+]}$  (6.3.7.11)

It is clear that three pH regions can occur

pH  $\ll$  pK<sub>S</sub>,  $k(\text{obs}) = k_{23}$  i.e.  $K'/[\text{H}^+] \ll 1$  (6.3.7.12)

pH  $\gg$  pK<sub>S</sub>,  $k(\text{obs}) = k'_{23}$   $K'/[\text{H}^+] \gg 1$  (6.3.7.13)

pH = pK<sub>S</sub>,  $k(\text{obs}) = \frac{(k_{23} + k'_{23})}{2}$   $K'[\text{H}^+] = 1$  (6.3.7.14)

Assuming the pK<sub>a</sub> of the absorbed dye and adsorbed dye is the same  $k'_{23}$  may be calculated from equation (6.3.7.14). If 430 sec<sup>-1</sup> for AO, 210 sec<sup>-1</sup> for AB<sup>+</sup> and 51 sec<sup>-1</sup> for Nile Blue<sup>(32)</sup>.

### 6.3.8 Interaction of Non-Acridine Dyes with Micelles

The interaction of non-acridine dyes Rhodamine 6G and Malachite Green with SDS micelles was also investigated. From the spectroscopic evidence

TABLE 6.3.8.1

RATE OF ABSORPTION OF NON-ACRIDINE DYE BY SDS MICELLES

DYE	k(obs)/sec <sup>-1</sup>
Rh6G <sup>‡</sup>	17.5 ± 3.6
MG <sup>‡</sup>	25.9 ± 4.1
PCC <sup>(20)*</sup>	
CV*	>500

\*PCC is pinecyanol chloride

presented in Chapter 4 it appears that these dyes do not interact in precisely the same way as the planar dyes. The equilibrium measurements show that the CMC is substantially lowered in both cases.

It may be that the bulkiness of these dyes and an unfavourable geometry may inhibit interaction or absorption into the micelle. The dye may occupy a position at the exterior surface of the micelle. Since the apparent CMC is lowered so drastically, it may be that the dye in these cases is inducing micelle formation. The kinetic results are given in table 6.3.8.1.

It has also been found that the dye crystal violet, a propellor shaped triphenyl methane dye is absorbed very rapidly - too fast to be detected by the stopped-flow method<sup>(56)</sup>. The spectrum of the free crystal violet is very similar to that for the dye above the CMC, the extinction coefficient and  $\lambda_{\text{max}}$  are unchanged. The non-planarity of this dye may preclude complete entry into the micelle and only one arm may enter. This could be a very rapid process. It must also be pointed out that the interaction of the dye below and through the CMC is very complex<sup>(57)</sup>.

Yasunaga et al<sup>(23)</sup> have investigated the rate of absorption of the dye pinecyonal chloride a rod-shaped dye into SDS micelles. This system behaves in a qualitatively similar manner to the acridine type dye SDS systems. Yasunaga<sup>(23)</sup> argues in favour of a mechanism which goes via a dye-surfactant salt similar to route 2 in scheme (B).

## 6.4 Ionic Strength-Jump

### 6.4.1 Results

The ionic strength-jump experiment is radically different from the direct absorption experiments just described. An ionic strength-jump results in the formation of micelles from monomer surfactant molecules.

The stopped-flow transients obtained were all good exponentials. The observed rate constant for the absorption of the dye by the forming micelles

was found to increase linearly with increasing surfactant concentration, over the whole range which could be studied. (For 1:1 mixing the usable surfactant concentration range is limited by the CMC in aqueous and salt solutions). The observed rate is only slightly dependent on the type of dye. The ratio of slope of the plot  $k(\text{obs})$  vs surfactant concentration for  $\text{AO}^+/\text{PF}^+$  is  $\approx 2$  (figure 6.4.1.1).

Increasing the salt concentration causes a small change in the observed rates. An increase in the concentration of added NaCl from 0.1 to 0.2M results in a decrease in the slope of  $k(\text{obs})$  vs surfactant concentration of  $\approx 2$  (figure 6.4.1.2, table 6.4.1.1).

The limiting observed rate constant for the direct absorption process is slower than that which can be measured for the ionic strength-jump for the same added ionic strength. This observation together with the lack of a dramatic dye type dependence suggest that the mechanism is different from the direct absorption pathway. The mechanism is however expected to be complex since the surfactant concentration range is close to the CMC. From the data on the rate of dye-surfactant complex formation below the CMC, it is expected that a significant amount of  $\text{D}_x\text{S}_y$  complex may be formed during the dead-time of the stopped-flow apparatus.

The observed transient amplitude is approximately 50% of the calculated value for free dye to dye absorbed, and approximately 10% of the calculated value for dye-surfactant aggregate to dye absorbed. Whichever form of the dye is absorbed, this observation indicates either:

- (i) a fast process not observed by the stopped-flow method which is responsible for a change in dye spectrum, or,
- (ii) a change in dye spectrum caused by this observation indicates a fast process is occurring outside the time range of the stopped-flow method i.e.  $k(\text{obs}) > 10^3 \text{ s}^{-1}$ .

TABLE 6.4.1.1

k(obs) FOR IONIC STRENGTH EXPERIMENTS

Temp. 298.2K		k(obs)/S <sup>-1</sup>			
10 <sup>3</sup> [SDS]/M	10 <sup>4</sup> [C <sub>A</sub> <sup>o</sup> -CMC]/M	0.1M NaCl		0.2M NaCl	
		AO <sup>+</sup>	PF <sup>+</sup>	10 <sup>4</sup> [C <sub>A</sub> <sup>o</sup> -CMC]/M	AO <sup>+</sup>
1.2	-			3.0	9.5 ± 1
1.4	1.0			5.0	12.5 ± 1.3
1.6	3.0	21 ± 2.1	18.2 ± 1.1	7.0	14.5 ± 1.6
1.8	5.0	35 ± 2.1	22.2 ±	9.0	20.0 ± 1.6
1.9	6.0	-	-	10.0	-
2.0	7.0	41.7 ± 3.1	29.4 ± 1.9	11.0	-
2.1	8.0	-	-	12.0	22.6 ± 1.3
2.25	9.5	55.6 ± 4.3	33.0 ± 2.6	-	-
2.5	12.0	76.9 ± 5.1	40.0 ± 3.1	-	-

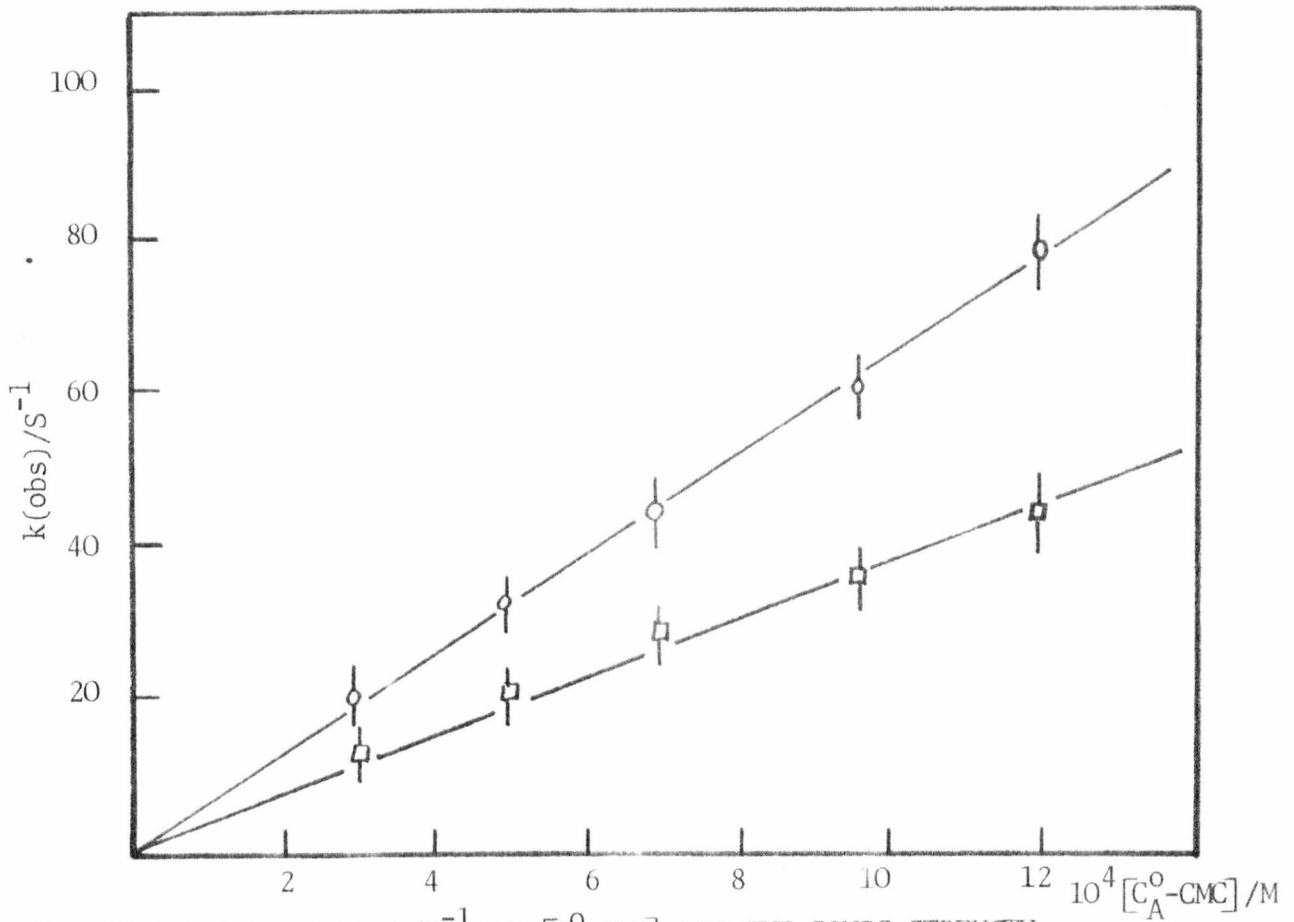


FIGURE 6.4.1.1 :  $k(\text{obs})/S^{-1}$  VS  $[C_A^O - CMC]$  FOR THE IONIC STRENGTH-JUMP FOR AO<sup>+</sup>/SDS AND PF<sup>+</sup>/SDS

- □ - PF<sup>+</sup>, - o - AO<sup>+</sup>, 0.1 NaCl, Temp. 298.2K

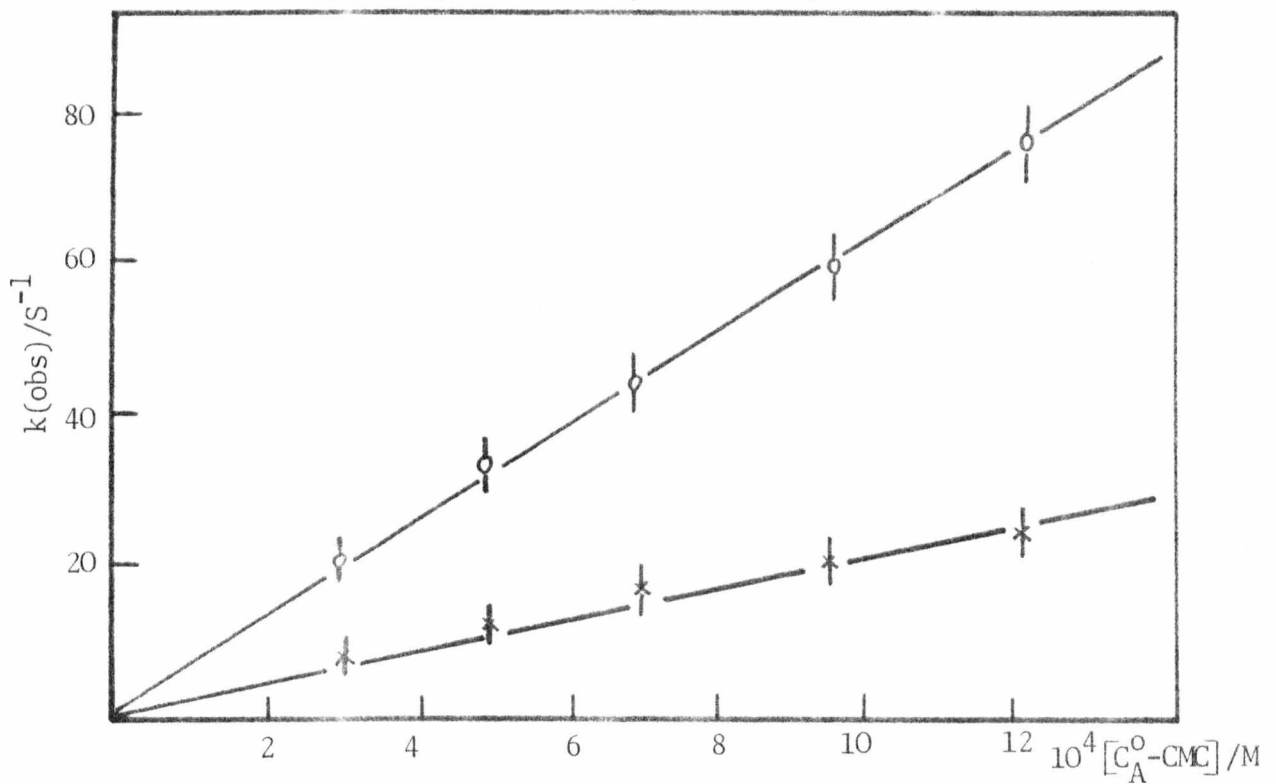


FIGURE 6.4.1.2 :  $k(\text{obs})/S^{-1}$  VS  $[C_A^O - CMC]$  FOR THE IONIC STRENGTH-JUMP FOR

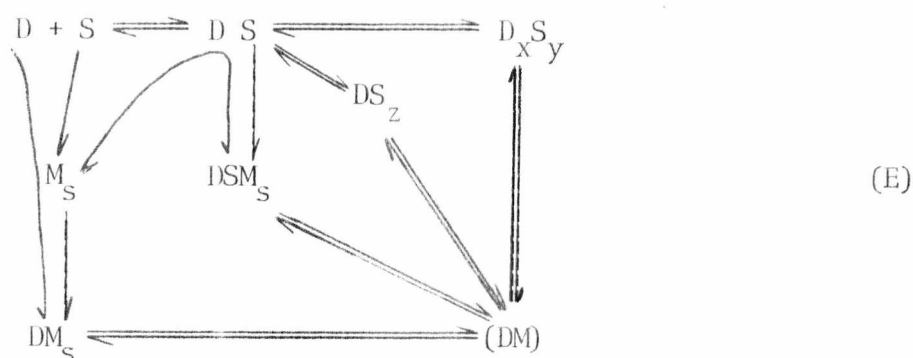
AO<sup>+</sup>/SDS - x - 0.2M NaCl, - o - 0.1M NaCl, Temp.298.2K

### 6.4.2 Mechanism

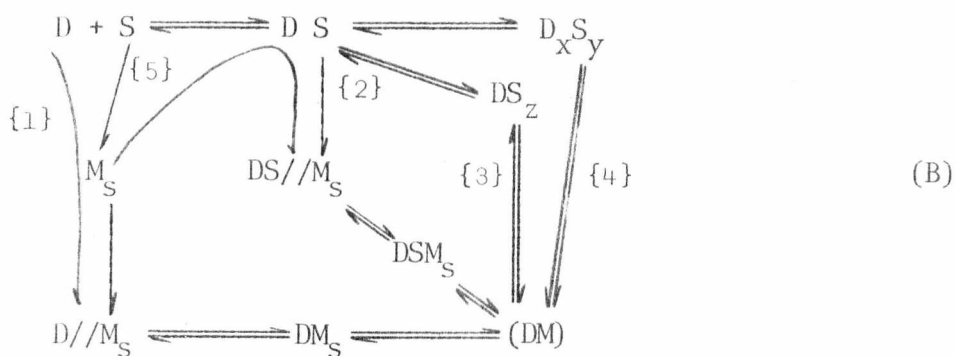
The proposed mechanism must be consistent with the following experimental observations:

- (i) linear dependence on surfactant concentration;
- (ii) small dependence on the type of dye (provided they are the same charge);
- (iii) small dependence on the added salt concentration;
- (iv) an amplitude much smaller than the calculated value.

The possible routes are shown in scheme (E), section 6.3.7.



Hence, as before:



Route {1} is the direct absorption pathway,

{2} is the absorption in a dye-surfactant monomer unit,

{3} is the dye-induced micelle mechanism,

{4} corresponds to the absorption of a dye from a large dye-surfactant aggregate,

{5} is pure micelle formation.

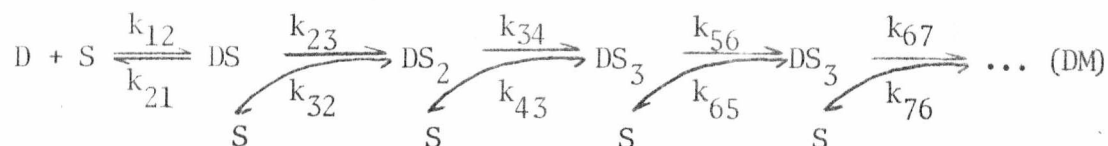
The experimental observations do not conform to pathway {1}. Direct dye absorption cannot therefore be the major mechanism in the ionic strength-jump experiment.

Pathway {4} in which a large dye-surfactant aggregate is broken down to release dye which is then available for absorption is unlikely to be rapid. Also, the rate of build-up of the large dye-surfactant aggregates is very slow hence it is unlikely that they would be sufficient concentration to provide a viable pathway.

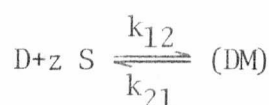
The two most likely pathways are {2} and {3} and these will be considered in more detail.

#### 6.4.2.1 The Dye-induced Micelle Mechanism

This scheme may be written



To simplify the mechanism we can make all the forward rate constants equal and the backward rate constants much smaller. We may then write the mechanism as



It is, of course, unclear at which point in such a mechanism when the dye may be considered to be in the hydrophobic environment of the

micelle. The surfactant monomers may orient themselves in such a way that the absorption and fluorescence changes occur at much lower aggregation numbers than in a true micelle. Because the surfactant monomers build up around the dye the absorption and fluorescence spectra may be changing all the time. (This is in contrast to the direct absorption mechanism where the spectral changes are associated with a definite movement of the dye).

By the method of Castellani<sup>(58)</sup> we may derive the relaxation time

$$g_{11} = 1/[\bar{D}] + z/[\bar{S}] + 1/[\bar{DM}]$$

$$r_{11} = k_{12}|\bar{D}||\bar{S}|^z = k_{21}|\bar{DM}|$$

hence  $\tau_I^{-1} = k_{12}([\bar{S}]^z + [\bar{D}][\bar{S}]^{z-1}) + k_{21}$  (6.4.2.1.1)

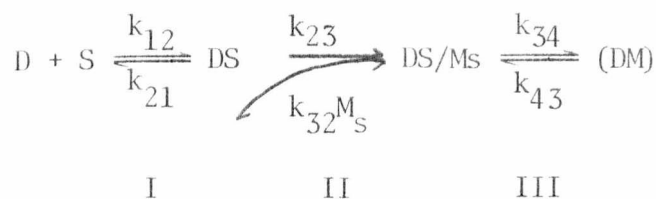
If the rate determining process is the formation of a small nucleus of surfactant monomers (as in pure micelle formation) and  $z \approx 2-6$ , then for  $[\bar{D}] < [\bar{S}]$ ,  $[\bar{S}]^z \gg [\bar{D}][\bar{S}]^{z-1}$  and equation (6.4.2.1.1) reduces to equation (6.4.2.1.2)

$$\tau_I^{-1} = k_{12}[\bar{S}]^z + k_{21} \quad (6.4.2.1.2)$$

The experimental observations do not conform to this equation and the mechanism can be discarded.

#### 6.4.2.2 Absorption of a Dye-Surfactant Monomer

Consider route {3} where DS is formed in a diffusion-controlled process



The respective relaxation times are<sup>(59)</sup>

$$\tau_{\text{I}}^{-1} = k_{12}([\overline{\text{D}}] + [\overline{\text{S}}]) + k_{21} \quad (6.4.2.2.1)$$

$$\tau_{\text{II}}^{-1} = \frac{k_{23}K_{12}([\overline{\text{DS}}] + [\overline{M}_s])}{1 + K_{12}([\overline{\text{DS}}] + [\overline{M}_s])} + k_{32} \quad (6.4.2.2.2)$$

$$\tau_{\text{III}}^{-1} = k_{34} \left( 1 + K_{34} \left( \frac{1}{(1 + K_{12}([\overline{\text{D}}] + [\overline{\text{S}}])^{-1})^{-1} [\overline{M}_s] + [\overline{\text{DS}}]} \right) \right)^{-1} + k_{43} \quad (6.4.2.2.3)$$

where  $K_{34} = [\overline{\text{DS}/M_s}] / [\overline{\text{DS}}] [\overline{M}_s] \approx 10^2 M^{-1}$  (from the surfactant exchange rate<sup>(28)</sup>)  $K_{12} = [\overline{\text{DS}}] / [\overline{\text{D}}] [\overline{\text{S}}] \approx 10 M^{-1}$ .

We only observe one relaxation process and the spectral evidence is that it is associated with the transfer of the dye from an aqueous to hydrophobic environment i.e. process III.

Hence,

$$k(\text{obs}) = k_{34} \left( 1 + K_{34} \left( \frac{1}{(1 + K_{12}([\overline{\text{D}}] + [\overline{\text{S}}])^{-1})^{-1} [\overline{M}_s] + [\overline{\text{DS}}]} \right) \right)^{-1} + k_{43} \quad (6.4.2.2.4)$$

we may make the following simplifications

$$[\bar{S}] > [\bar{D}] = 1.4 \times 10^{-3} M = \text{CMC}$$

$$[\bar{M}_S] > [\bar{DS}]$$

$$K_{34} \approx 10^2 M^{-1}, K_{12} \approx 1-10 M^{-1}$$

taking  $K_{12} \approx 1 M^{-1}$

equation (6.4.2.2.4) then becomes

$$k(\text{obs}) = k_{34} \left( 1 + 10^2 \left( \frac{1}{(1 + (1.4 \times 10^{-3})^{-1})^{-1} M_S} \right) \right)^{-1} + k_{43} \quad (6.4.2.2.5)$$

$$k(\text{obs}) = k_{34} \left( 1 + 10^2 \left( \frac{1}{(1 + 7.1 \times 10^2)^{-1} [\bar{M}_S]} \right) \right)^{-1} + k_{43} \quad (6.4.2.2.6)$$

$$= k_{34} \left( 1 + 10^2 \left( \frac{1}{1.4 \times 10^{-3} [\bar{M}_S]} \right) \right)^{-1} + k_{43} \quad (6.4.2.2.7)$$

$$= k_{34} \left( 1 + \frac{10^2 \cdot 7.1 \times 10^2}{[\bar{M}_S]} \right)^{-1} + k_{43} \quad (6.4.2.2.8)$$

$$k(\text{obs}) = k_{34} ([\bar{M}_S] / 7.1 \times 10^4) + k_{34} \quad (6.4.2.2.9)$$

Hence, a plot of  $k(\text{obs})$  against  $[\bar{M}_S]$  will give a slope of  $k_{34}/7.1 \times 10^4$  and an intercept of  $k_{34}$ .

The values obtained by this procedure will only be approximate

since  $K_{12}$  and  $K_{34}$  are only estimated.

The plots of  $k(\text{obs})$  against  $[M_s]$  are linear, figure 6.4.2.1,2.  $k_{43}$  is zero in all cases, the values of  $k_{34}$  are to an order of magnitude

$8 \times 10^9 \text{ M}^{-1} \text{ S}^{-1}$   $\text{AO}^+/\text{SDS}/0.1 \text{ NaCl}$

$4 \times 10^9 \text{ M}^{-1} \text{ S}^{-1}$   $\text{PF}^+/\text{SDS}/0.1 \text{ NaCl}$

$2 \times 10^9 \text{ M}^{-1} \text{ S}^{-1}$   $\text{AO}^+/\text{SDS}/0.2 \text{ NaCl}$

These values are very close to the diffusion-controlled limit but they cannot be considered to be more than an indication of the order of magnitude of the rate constant for the absorption of a DS monomer unit. Having said this, the values are what would be predicted taking into account the rate of exchange of a charged surfactant monomer. The neutral DS unit may be absorbed more rapidly (the entering surfactant portion preparing a "hole" in the micelle surface to facilitate entry of the dye).

The mechanism for dye absorption therefore appears to be composed of at least two routes: (i) the absorption of a dye-surfactant monomer which dominates at low surfactant concentration very close to the CMC and (ii) the direct absorption route which dominates at high surfactant concentrations.

### 6.4.3 Dye Concentration Dependence

The dependence of  $k(\text{obs})$  for a given surfactant concentration ( $1.5 \times 10^{-3} \text{ M}$ ) on the concentration of the dye is dramatic. For concentrations up to  $1.9 \times 10^{-5} \text{ M}$   $\text{AO}^+$   $k(\text{obs})$  is constant at  $19 \pm 1 \text{ s}^{-1}$ . Over a very narrow dye concentration range the rate decreases and then levels off at  $\sim 0.5 \text{ s}^{-1}$ . This effect has not been studied in detail and only the one surfactant concentration close to the CMC has been investigated. To date, no explanation has been attempted. Considerably more work

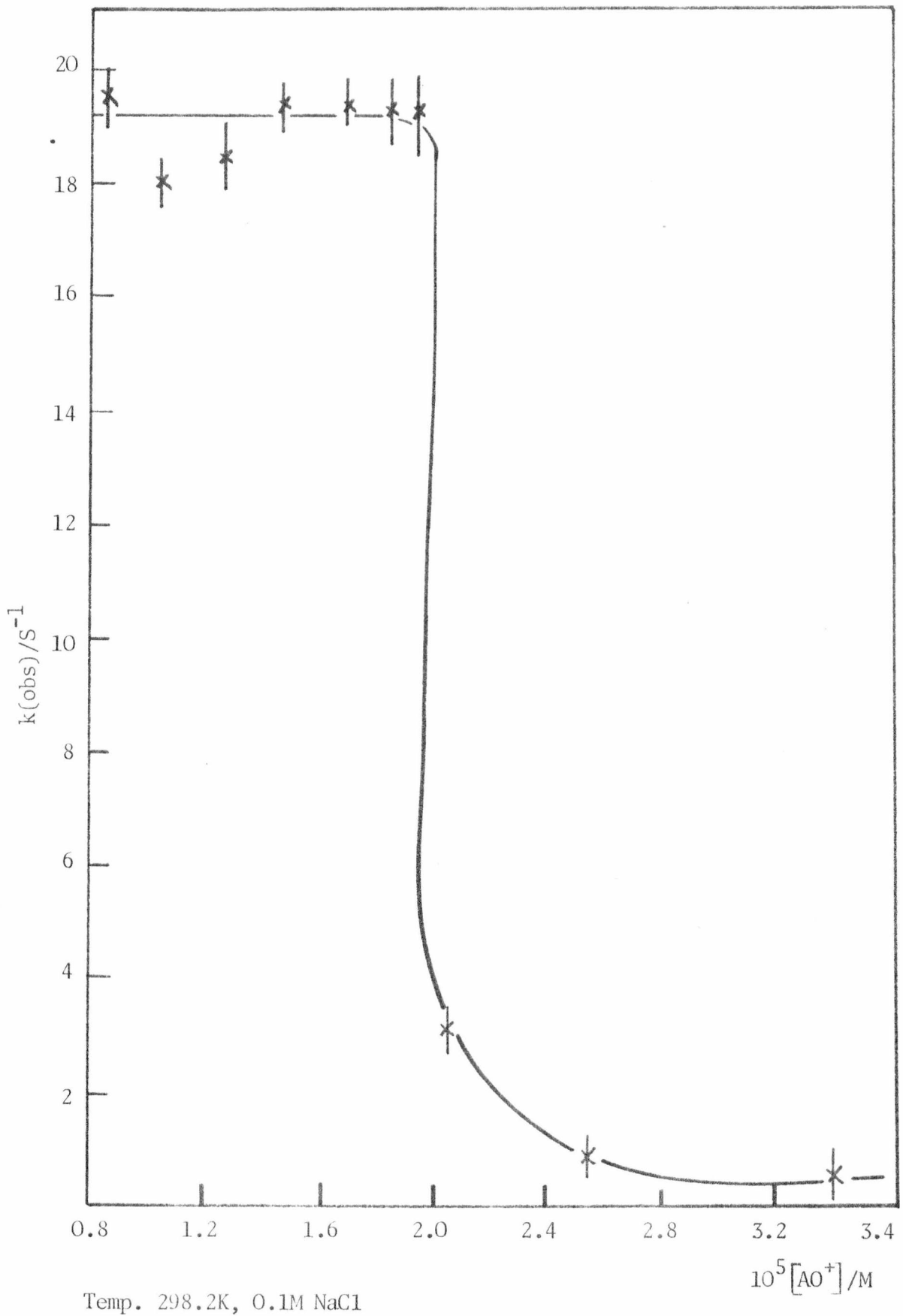


FIGURE 6.4.3.1

IONIC-STRENGTH JUMP [DYE] DEPENDENCE [SDS] =  $1.5 \times 10^{-3} M$

needs to be done on this type of dye dependence i.e. other surfactant concentrations, different surfactant chain-lengths and different dyes before any mechanism may be postulated for what is obviously a very complex phenomena. The results are shown in figure 6.4.3.1.

## 6.5 Temperature-Jump Experiments

### 6.5.1 Results

Preliminary temperature-jump measurements have been carried out on dye-micelle systems. Two relaxation times are observed for low dye concentration  $\sim 10^{-5}$  M, high ionic strength  $\sim 0.1$  and surfactant concentrations close to the CMC; (i) a fast process in the  $\mu$ sec time range and (ii) a slow process in the msec time range. The amplitude of both processes (monitored at 498nm  $AO^+$ , 448nm  $PF^+$ ) is more toward free dye in solution, i.e. decreasing absorbance.

The fast relaxation time ( $\sim 10\mu$ sec) is approximately constant for both dyes and is unaffected by the concentration of micelles in the system. For the concentration of dye used free  $AO^+$  exhibits a fast relaxation process (increasing absorbance at 498nm) whereas  $PF^+$  does not exhibit a detectable relaxation. Proflavine does undergo a dimerisation reaction but at the concentration used here, it is very fast ( $< 200$ nsec) and the concentration of  $PF_2^+$  is  $< 1\%$  of total dye.

There may be free dye in solution but since the dimerisation reaction is in the same time range and of opposite amplitude, it cannot be detected.

The slow relaxation time is independent of the dye ( $AO^+$  and  $PF^+$  give the same relaxation time). The slow relaxation time is, however, dependent on the dye concentration. The relaxation time decreases with increasing dye concentration (table 6.5.1.1). The slow relaxation

TABLE 6.5.1.1

DEPENDENCE OF RELAXATION TIMES ON  $[AO^+]$  FOR  $AO^+$ /SDS SYSTEM

$[SDS] = 1.5 \times 10^{-3} M$ ,  $0.1M NaCl$ , Temp.  $308.2K$ ,  $V^0 = 4.3$  Volts,  $\lambda_{obs} = 498nm$   
 $CMC = 1.3 \times 10^{-3} M$

$10^5 [AO^+]/M$	$\tau/msec$	$k(obs)/S^{-1}$	$10^2 \Delta A/mV$
1.5	$55 \pm 5$	$18 \pm 2$	1.0
1.75	$52 \pm 4.1$	$19.5 \pm 1.6$	1.05
2.0	$49.1 \pm 3$	$20.4 \pm 0.8$	1.15
2.25	$38.0 \pm 3.5$	$26.3 \pm 2$	1.30
2.50	$29.5 \pm 2.6$	$33.9 \pm 2.6$	1.50
3.0	$23.5 \pm 1.9$	$42.5 \pm 3$	1.75

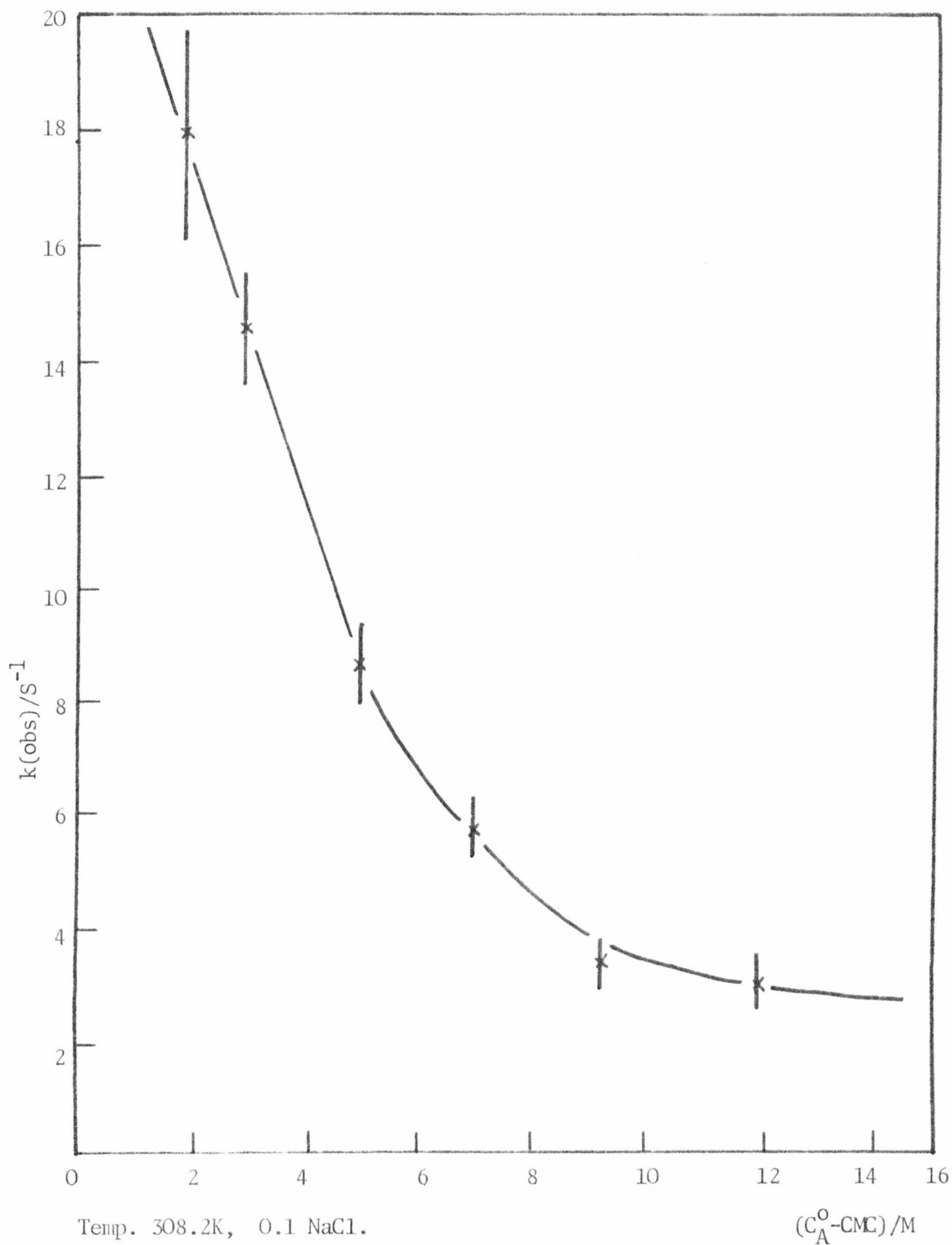


FIGURE 6.5.1.1

DEPENDENCE OF  $k(\text{obs})$  ON MICELLE CONCENTRATION FOR  $AO^+/SDS$

TABLE 6.5.1.2

DEPENDENCE OF k(obs) ON SDS CONCENTRATION

$[AO^+]$   $1.5 \times 10^{-5} M$ , 0.1M NaCl, Temp. 308.2K,  $V^0 = 4.3$  Volts,  $\lambda_{obs} = 498nm$

$$CMC = 1.3 \times 10^{-3} M$$

$10^3 [SDS] / M$	$\tau / msec$	$k(obs) / S^{-1}$	$10^2 \Delta A / mV$
1.5	$55 \pm 5$	$18.2 \pm 2$	1.0
1.6	$69 \pm 5$	$14.5 \pm 1$	1.0
1.8	$116 \pm 10$	$8.6 \pm 0.7$	0.8
2.0	$170 \pm 9.8$	$5.8 \pm 0.5$	0.65
2.25	$307 \pm 40$	$3.25 \pm 0.4$	0.6
2.50	$330 \pm 50$	$3.0 \pm 0.5$	0.5

time is also dependent on the micelle concentration and increases with increasing surfactant concentration for a given dye concentration (table 6.5.1.2 and figure 6.5.1.1).

### 6.5.2 Discussion

The fast relaxation time and the decrease in absorbance may be due to the movement of dye from the strong hydrophobic binding site to the outer weak binding site. The absorbance change is in the wrong direction for the dye dimerisation in the bulk solution.

The slow relaxation time may be due to the final release of dye and breakdown of the micelle. This may be slow since the evidence from the stopped-flow dissolution kinetics shows that the dye may stabilise the micelle somewhat.

Tondre et al<sup>(60)</sup> have studied the effects of dyes on the dissolution of micelles at low ionic strength and high surfactant concentrations. The results have been confirmed during the course of this work. Tondre et al find two relaxations which have opposing amplitudes<sup>(61)</sup>.

## 6.6 General Conclusions and Suggestions for Further Work

We may draw a number of general conclusions from the work presented in this thesis:

(i) the planar acridine (and related) dyes are useful for the CMC determination of anionic surfactants,

(ii) acridine dyes aggregate with anionic surfactants at much lower concentrations than in free solution, i.e. "mutually induced" aggregation,

(iii) this aggregation takes two forms,

(a) aggregation of dye and surfactant to form single units,

- (b) aggregation of these units to form much larger insoluble species,
- (iv) the rate of the dimerisation of dye in the initial aggregate is almost diffusion-controlled and is kinetically unaffected by the surfactant,
- (v) the build-up of the large insoluble aggregates is slow,
- (vi) above the CMC the dyes are absorbed by the micelles in a two step process,
  - (a) a weak electrostatic binding site (adsorption) followed by,
  - (b) movement into a stronger, hydrophobically stabilised binding site,
- (vii) the influence of dye size, charge, surfactant chain-length, surface pH and surface charge of the micelle play important roles in the determination of the rate of absorption of the dye, briefly the rate increases with
  - (a) decreasing dye size,
  - (b) increasing surface pH (deprotonation of the dye at the surface),
  - (c) decreasing surface charge,
  - (d) decreasing surfactant chain-length ,
- (viii) close to the CMC the mechanism appears to be different, the dye enters the micelle "tagged" to a surfactant monomer at the exchange rate of the surfactant monomer.

Areas of research which may be usefully expanded or initiated include:

- (i) an investigation of the absorption process in the complex transition region around the CMC,
- (ii) further temperature-jump measurements on pre and post-CMC solutions,

(iii) investigation of other dye surfactant systems e.g. cationic micelles/anionic dyes and non-ionic micelles,

(iv) study of biologically important micelles and small molecules e.g. bile salt micelles,

(v) an extension to lipid bilayer vesicles and the transport of small molecules through them.

## REFERENCES

- (1) P. Ekwall, H. Eikrem and L. Mandell, *Acta, Chem. Scand.*, 1963, 17, 111.
- (2) H.B. Klevens, *Chem. Rev.*, 1950, 47, 1.
- (3) H. Schott, *J. Phys. Chem.*, 1966, 70, 2966.
- (4) P.H. Elworthy, A.T. Florence and C.B. MacFarlane, *Solubilisation by Surface-Active Substances and Its Application in Chemical and Biological Sciences* (Chapman and Hall, London, 1968).
- (5) C. Neuberg, *Biochem. Z.*, 1930, 229, 467.
- (6) H. Freundlich and G.V. Slottman, *Biochem. Z.*, 1927, 188, 101.
- (7) R.H. Mckee, *Ind. Eng. Chem.*, 1946, 38, 382.
- (8) J.W. McBain, *Adv. in Colloid Science*, Vol.I, (Interscience, New York, 1942).
- (9) H.B. Klevens, *J. Phys. Colloid Chem.*, 1950, 54, 283.
- (10) S.R. Palit and J.W. McBain, *Ind. Eng. Chem.*, 1946, 38, 741.
- (11) J. Weichherz, *Kolloid-Z.*, 1929, 49, 158.
- (12) S.R. Palit, *Oil and Soap*, 1946, 23, 72.
- (13) H. Weil-Mahlrebe, *Biochem. J.*, 1946, 40, 363.
- (14) D. Attwood, L.R.J. Currie and P.H. Elworthy, *J. Colloid Interface Sci.*, 1974, 46, 249.
- (15) P. Ekwell, L. Mandell and K. Fontell, *Mol. Cryst. Liq. Cryst.*, 1969, 8, 157.
- (16) H. Schott, *J. Phys. Chem.*, 1966, 70, 2966.
- (17) G. Némethy and A. Ray, *J. Phys. Chem.*, 1973, 77, 64.
- (18) A.S. Waggoner, O.H. Griffith and C.R. Christensen, *Proc. Nat. Acad. Soc.*, 1967, 57, 1198.
- (19) K.K. Fox, I.D. Robb and R. Smith, *J. Chem. Soc. Faraday I*, 1972, 68, 445.
- (20) T. Nakagawa and H. Tizomoto, *Kolloid-Z. Polym.*, 1972, 250, 594.

- (21) J. Oakes, J. Chem. Soc. Faraday II, 1972, 68, 1464.
- (22) J.C. Ericksson and G. Gillberg, Acta. Chem. Scand., 1966, 20, 2019.
- (23) K. Takeda, N. Tatsamoto and T. Yasunaga, J. Colloid Interface Sci., 1974, 47.
- (24) G.L. Choules, R.C. Sandberg, M. Steggall and E.M. Eyring, Biochem., 1973, 12, 4544.
- (25) K. Akasaku, M. Sakoda and K. Hiromi, Biochem. Biophys. Res. Comm., 1970, 40, 1239.
- (26) H.J. Li and D.M. Crothers, J. Mol. Biol., 1969, 39, 461.
- (27) T.Y. Tsong, Biochemistry, 1975, 14, 5409.
- (28) E.A.G. Aniansson, S.N. Wall, H. Hoffmann, J. Kielmann, W. Ulbricht, R. Zana, J. Long and C. Tondre, J. Phys. Chem., 1976, 80, 905.
- (29) D. Eagland and F. Franks, Chem. Phys. Appl. Surface Active Subst., Proc. Int. Congr. 1964 (Pub. 1967), 2, 535.
- (30) J.E. Crooks, P.A. Tregloan and M.S. Zetter, J. Phys. E., 1970, 3, 73.
- (31) B.H. Robinson, N.C. White and C.M. Mateo, Adv. Molecular Relax. Processes, 1975, 7, 321.
- (32) A.D. James, B.H. Robinson and N.C. White, J. Colloid Interface Sci., To be published.
- (33) A. Ray and P. Mukerjee, J. Phys. Chem., 1966, 70, 2144.
- (34) B.H. Robinson, A. Löffler and G. Schwarz, J. Chem. Soc. Faraday I. 1973, 69, 56.
- (35) P. Mukerjee and A.K. Ghosh, J. Amer. Chem. Soc., 1970, 92, 6403.
- (36) L.P. Gianneschi and T. Kurucsev, J. Chem. Soc. Faraday II, 1974, 6, 1334.
- (37) S. Massari, P. Dell'Antone, R. Colonna and G.F. Azzone, Biochem., 1974, 13, 1038.
- (38) G.R. Haugen and W.H. Melhuish, Trans. Faraday Soc., 1964, 60, 386.
- (39) Estimated in the course of this work.
- (40) G.S. Hartley and J.W. Roe, Trans. Faraday Soc., 1940, 36, 101.

- (41) P. Mukerjee and K. Banerjee, *J. Phys. Chem.*, 1964, 68, 3567.
- (42) V. Zanker, *Z. Phys. Chem.*, 1952, 199, 225.
- (43) J.M. Irvin and E.N. Irvin, *J. Amer. Chem. Soc.*, 1950, 72, 2745.
- (44) M.M. Davis and H.B. Hetzer, *Anal. Chem.*, 1966, 38, 451.
- (45) A.D. James and B.H. Robinson, *Adv. Molecular Relax. Processes*, 1976,  
8, 287.
- (46) M.F. Emerson and A. Holtzer, *J. Phys. Chem.*, 1965, 69, 3718.
- (47) C. Tanford, *The Hydrophobic Effect* (Wiley-Interscience, New York, 1973).
- (48) P. Mukerjee and K.J. Mysels, "Critical Micelle Concentrations of  
Aqueous Surfactant Solutions", National Bureau of Standards,  
Washington, 1971.
- (49) D. Stigter and K.J. Mysels, *J. Phys. Chem.*, 1955, 59, 45.
- (50) K. Shirahama and T. Kashiwabara, *J. Colloid Interface Sci.*, 1971, 36,  
65.
- (51) B.D. Flockhart, *J. Colloid Sci.*, 1957, 12, 557.
- (52) P. Seeman, R.I. Sha'afi, W.R. Galey and A.K. Solomon, *Biochem.  
Biophys. Acta*, 1970, 211, 365.
- (53) E.E. Dreger, *Ind. Eng. Chem.*, 1944, 36, 610.
- (54) J.L. Kurz, *J. Phys. Chem.*, 1962, 66, 2239.
- (55) D.N. Hague, *Fast Reactions* (Wiley 1971).
- (56) D.J. Barnes, Personal Communication.
- (57) K.J. Timmins, N.C. White and B.H. Robinson, unpublished results.
- (58) G.W. Castellan, *Ber. Bunsenges.*, 1963, 67, 898.
- (59) G. Czerlinski, *Chemical Relaxation*, (Mored Dekker Inc., New York, 1966).
- (60) C. Tondre, J. Long and R. Zana, *J. Colloid Interface Sci.*, 1975, 52,  
327.
- (61) C. Tondre, personal communication.

APPENDIX I.

Computer Programme for the evaluation of Surfactant Aggregate Concentrations based on the Cooperative Model for Micelle Formation.

Input identifiers

R nucleation equilibrium constant  
K growth equilibrium constant  
T phase transition equilibrium constant  
C cooperative binding parameter  
N micelle aggregation number

Output

CAO weighed-in concentration of surfactant  
 $C_1, C_2$  concentration of monomer and dimer  
 $C_3, C_4, \dots, C_N$  concentration of species from aggregation number 3, 4 to N  
CM INF concentration of species from N to infinity  
CMIC concentration of micelles  
CMM concentration of micelles expressed in monomer  
M mean aggregation number

CH/F042/HC

SWGJ

BATCH

REAL GCL;

LIBRARY

ALGOL

DLIST;

SLINES;2500;

STIME;4;

```
1 RELATION OF SURFACTANT WEIGHING IN CONC AND AGGREGATE CONC DETERMINATION OF
2 CMC AND MEAN AGGREGATION NUMBER MODEL 3 ALL KS EQUAL;
3 "COMMENT" THE FOLLOWING TERMS ARE USED IN THE PROGRAM
4 R IS THE EQUIL CONST FOR NUCLEATION
5 K IS THE EQUIL CONST FOR GROWTH
6 T IS THE PHASE TRANS CONST
7 C IS THE COORDINATING PARAMETER
8 N IS THE MICELLE NUMBER
9 M IS THE MEAN AGGREGATION NUMBER
10 S=K*C
11 DS IS THE IMPERIMENTAL CHANGE IN S
12 CAO IS THE WEIGHING IN CONCENTRATION OF SURFACTANT
13 C1 IS THE CONC OF MONOMER
14 C2 IS THE CONCENTRATION OF DIMERS
15 CMINF IS THE CONC OF ALL AGG FROM M TO INFINITY
16 C3N IS THE CONC OF ALL AGG FROM C3 TO N
```

```
17 C4N IS THE CONC OF ALL AGG FROM C4 TO N
18 C4N IS THE CONC OF AGG FROM M TO INFINITY
19 ALL CONCs ARE IN TERMS OF MONOMER
20 CMIC IS THE CONC OF MICELLE
21 CMM IS THE CONC OF MICELLE IN TERMS OF MONOMER;
22 "BEGIN"
23 "REAL" R, M, T, S1, DS, S2;
24 "REAL" C, P;
25 "INTEGER" C;
26 "REAL" "ARRAY" C(0, C1, C2, C3), C4N, CMINF, CMIC, CMM, S, N[1:300];
27 "INTEGER" D;
28 "READ" R, M, T, S1, DS, S2, P;
29 "BEGIN"
30 K:=0*R;
31 "PRINT" ("13"), "EQUILIBRIUM CONSTANT=", SAMELINE, SCALED(6), K, ("L2");
32 "PRINT" ("12"), "COORDINATING PARAM=", SAMELINE, SCALED(3), C.
```

```

23  'S8'PHASE TOA'S CONST=' ,SAMELINE,SCALED(3),T,'L2';
24  "BEGIN"
25  "PRINT" 'L2', 'S1' NICELLE NUMBER=' ,SAMELINE,SCALED(3),N,'L1';
26  "PRINT" 'L2', 'S3'CA0'S9'C1'S8'C2'S6'C3N'S8'C4N'S9'CMIC'S8',
27  'CMM'S9'N'S9'O', 'L1';
28  C:=0;
29  "FOR" I:=S1 "STEP" IS "UNTIL" S2 "DO"
30  "BEGIN"
31  C:=C+1;
32  CNINF[C]:=(I/(Q*(1-I))) * (((I)^(N-1)) * ((N*(1-I)+1)/(1-I)^2));
33  P:=(I/((1-I)^(N-1)+1+1)) + (I*(Q-1)/(Q*K)) + (T*N*(I+N)/(Q*K)) - (CNINF[C]);
34  C1[C]:=I/I;
35  C2[C]:=(I/Q) + (C1[C]) * 2;
36  C3N[C]:=( (1-I) + (-2) - (1+2*I) ) * (C1[C]/Q) - CNINF[C];
37  C4N[C]:=( (1-I) + (-2) - (1+2*I+3*I^2) ) * (C1[C]/Q) - CNINF[C];
38  CMIC[C]:=(T*(1-I))/(R*Q);
39  CMM[C]:=H*CMIC[C];
40  M[C]:=P / ( (I/((1-I)*Q)) + 1 + ((T*(I)+(N-1))/Q) - (I)^(N)/(Q*(1-I)) ) * C1[C];
41  CA0[C]:=P;
42  S[C]:=I;
43  "PRINT" SCALED(3),CA0[C],PREFIX('S2'),C1[C],C2[C],C3N[C],C4N[C],
44  CNINF[C],CMIC[C],CMM[C],M[C],S[C], 'L1';
45  "END";
46  "END";
47  "END";
48  "END";
49  "END";
50  314 MC
51  518 CODE
52  382 TCTAL

```

APPENDIX I

- Computer Programme for the Evaluation of Rate Constants from Punched Tape. (Based on the Guggenheim method).

Input identifiers

D the number of points recorded  
C1 the starting point  
INC the interval between computations  
C2 the finishing point  
Z the sampling time

Output

K the rate constant  
ERRK error in rate constant  
PERRK % error in rate constant  
HALIFE number of half lives covered

&JOB CHR042;

&TIME;4;

&LINES; 2000;

&ALGOL;L;

LIBRARY  
ALGOL

```

1  CALCULATION OF RATE CONSTANTS FROM VOLTAGES SINGLE BINPUT METHOD;
2  "COMMENT" THE FOLLOWING TERMS ARE USED IN THIS PROG
3  TEMP IS THE TEMPERATURE OF THE RUN
4  AC IS ACRIDINE ORANGE
5  SDS IS SODIUM DODECYL SULPHATE
6  J IS THE NUMBER OF RUNS
7  SX IS THE SUM OF ALL X
8  SY IS THE SUM OF ALL Y
9  SXY IS THE SUM OF ALL XY PAIRS
10 S2X IS THE SUM OF ALL X *2
11 S2D IS THE SUM OF ALL
12 K IS THE RATE CONSTANT
13 INT IS THE INTERCEPT
14 ERRK IS THE ERROR IN K
15 ERRINT IS THE ERROR IN THE INTERCEPT
16 PERRK IS THE PERCENTAGE ERROR IN K
17 AMP IS THE AMPLITUDE
18 HALIFE IS THE NUMBER OF HALF LIVES COVERED
19 Z IS THE SAMPLING TIME;
20 "BEGIN"
21 "REAL" T, SX, S2X, SY, SXY, S2D, K, K1, INT, DENOM;

22 "REAL" ERRE, ERINT, PERRK, Z, AMP, M, HALIFE;
23 "REAL" AC, SDS, LAMBDA, R;
24 "REAL" PX, PY;
25 "INTEGER" D, C, H, G1, IJC, C2, I, J;
26 "REAL" J, AC, SDS, U;
27 "PRINT" '(L2)', '(S43) FINAL SDS CONCENTRATION=', SAMELINE, SCALED(6),
28 SDS, '(L1)';
29 '(S42)*****', '(L2)';
30 "PRINT" '(L2)', '(S43) FINAL AC CONCENTRATION=', SAMELINE, SCALED(6),
31 AC, '(L1)';
32 '(S42)*****', '(L2)';

```

```

33 "FOR" I:=1 "STEP" 1 "UNTIL" J "DO"
34 "BEGIN"
35 NEWSET:
36 "READ" T,D,Z,C1,INC,C2,LAMDA;
37 "BEGIN"
38 "REAL" "ARRAY" VT[C1:D];
39 "REAL" "ARRAY" A.Y,X[C1:D];
40 "BEGIN"
41 "FOR" C:=1 "STEP" 1 "UNTIL" D "DO"
42 "READ" READER(31), VT[C];
43 "PRINT" //L2,NAVELENGTH#,SAMELINE,ALIGNED(3,0),LAMDA,INM,
44 //S10,TEMP(CENTIGRADE)#,SAMELINE,ALIGNED(2,4),T,//L1,
45 "PRINT" //L3,NUMBER OF POINTS RECORDED#,SAMELINE,SCALED(4),D,
46 //S10,SAMPLING TIME (MILLISECONDS)#,SAMELINE,SCALED(4),Z,//L2,
47 "PRINT" //STEPPING FROM POINTS,SAMELINE,C1,//S5,TO,SAMELINE,C2,
48 //S5,COMPUTING EVERY,SAMELINE,INC,//S2,POINT(S),//L2,
49 "PRINT" //S2,VT[C],//L2,
50 "FOR" C:=1 "STEP" 1 "UNTIL" D "DO"
51 "BEGIN"
52 "PRINT" SAMELINE,SCALED(6),VT[C],//S2,
53 "END";
54 "FOR" C:=C1 "STEP" INC "UNTIL" (C2+C1-1)/2 "DO"
55 "BEGIN"
56 A[C]:=VT[C]-VT[C+(C2-C1+1)/2];
57 Y[C]:=FN(A[C]);
58 X[C]:= (C-1)*Z+1.0*10*(=3);
59 "BEGIN"
60 SX:=SY+SXY:=S2X:=S2D:=0;
61 "FOR" C:=C1 "STEP" INC "UNTIL" (C2+C1-1)/2 "DO"
62 "BEGIN"
63 SX:=SX+X[C];
64 SY:=SY+Y[C];
65 S2X:=S2X+X[C]^2;
66 SXY:=SXY+X[C]*Y[C];
67 "END";
68 M:=(C2-C1-1)/2+INC;
69 DENOM:=M*S2X-SX^2;
70 K1:=(M*SXY-SX*SY)/DENOM;
71 K1:=K1;
72 INT:=(SY*S2X-SXY*SY)/DENOM;
73 AMP:=EXP(INT);
74 "FOR" C:=C1 "STEP" INC "UNTIL" (C2+C1-1)/2 "DO"
75 S2D:=S2D+(Y[C]-K*X[C]-INT)^2;
76 ERRK:=SQRT((M*S2D)/((M-2)*DENOM));
77 PERRF:=1/10*ERRK/K;
78

```

```

ERRINT:=SQRT((S2A*S2B)/((M-2)*DENOM));
HALIFE:=( (C2-01+1)/2)*Z*K1/(0.7*1000);
"PRINT"//L5, RATE CONSTANT(1/SEC)#', SAMELINE, SCALED(6), #K,
//S10, ERROR IN RATE CONSTANT#, SAMELINE, SCALED(4), ERRK,
//L4, PERCENTAGE ERROR IN RATE CONSTANT#, SAMELINE, SCALED(4), PERRK,
//S10, NUMBER OF HALF LIVES COVERED#, SAMELINE, SCALED(2), HALIFE, //L5\';
"PRINT"//S24\';
SAMELINE, *****\';

```

```

"IF" W#0 "THEN" "GOTO" NEWSET;
"END";
"END";
"END";
"END";
"END";

```

584 MC  
820 CODE  
1204 TOTAL

END;  
116 LINES USED  
TIME = 0000 10.263  
ALTIME = 00 00 15  
A

